CHARACTERIZATION OF AGING AND FOAMING PROPERTIES FOR ASPHALT MIXTURES

A Dissertation

by

FAN YIN

Submitted to the Office of Graduate and Professional Studies of
Texas A&M University
in partial fulfillment of the requirements for the degree of

DOCTOR OF PHILOSOPHY

Chair of Committee,	Amy Epps Martin
Committee Members,	Jon A. Epps
	Robert L. Lytton
	Charles J. Glover
	David E. Newcomb
Head of Department,	Robin Autenrieth

December 2015

Major Subject: Civil Engineering

ABSTRACT

Economic, environmental, and engineering benefits have motivated the implementation of warm mix asphalt (WMA) in the United States. While asphalt foaming has become the most popular method for producing WMA, concerns remain about the performance of foamed asphalt mixtures due to the use of water in the foaming process. Along with the advent of WMA, recent changes in asphalt mixture components and production parameters have raised the need to review the current design practices and evaluation methods for asphalt mixtures, including the effects of aging. Therefore, the main objectives of this study were to evaluate the aging characteristics of asphalt mixtures and to explore asphalt foaming technology for WMA applications.

Aging of asphalt mixtures occurs during production and construction and continues throughout the service life of pavements. In this study, laboratory short-term aging protocols were evaluated in terms of simulating the asphalt aging and aggregate absorption that occurs during plant production and pavement construction. In addition, the concepts of cumulative degree-days and mixture property ratios were proposed to quantify field aging and to explore its correlation with laboratory long-term aging protocols in terms of mixture properties. Furthermore, the effects of various mixture components and production parameters on the aging characteristics of asphalt mixtures were investigated. Finally, post-construction cores obtained from several field projects were measured to explore mixture stiffness and binder property gradients in order to characterize the non-uniform field aging of asphalt pavements with depth.

Asphalt foaming technology was also explored in this study via a comprehensive laboratory experiment. A non-contact test method consisting of a laser device and a digital camera was developed to measure the asphalt foaming process in terms of volume expansion and collapse and evolution of asphalt foam bubbles. In addition, novel test methods were proposed to evaluate the workability and coatability for foamed asphalt mixtures. The proposed test methods were then utilized to investigate the effects of foaming water content and laboratory foamer type on asphalt foaming characteristics and foamed mixture properties. Finally, a mix design procedure for foamed asphalt mixtures was proposed and validated with field and laboratory data.

DEDICATION

To my beloved parents and wife

ACKNOWLEDGEMENTS

I would like to express my deepest appreciation to my committee chair, Dr. Amy Epps Martin, for her dedicated guidance, support, patience, and encouragement. I am so grateful for being her student and being part of the research team. My appreciation also goes to Dr. Jon A. Epps, Dr. Robert L. Lytton, Dr. Charles J. Glover, and Dr. David E. Newcomb, for serving as my committee members and for sharing their extensive knowledge and valuable experience. I acknowledge the National Cooperative Highway Research Program and the Texas A&M Transportation Institute for supporting this study.

I would like to thank Dr. Edith Arambula for her advice, support, friendship, and the valuable time she offered me to share and discuss research ideas. Thanks also go to Rick Canatella, Jeff Perry, Tony Barbosa, and Lee Gustavo from the Texas A&M Transportation Institute, and Stephen Johnson, Daniel Furdock, Guillermo Gomez Salas, Adolfo Portilla, Javier De La Cerda, and Jonathan Chiou from Texas A&M University for their help in laboratory-related activities. Thanks to my friends and colleagues for making my time at Texas A&M University a great experience.

Finally, I owe thanks to my parents, Peihai Yin and Shurong Yu, for their infinite love and support. Thanks to my lovely wife, Mengzhu Lu, for standing by my side throughout the process.

NOMENCLATURE

AC	Water Absorption Capacity
AMPT	Asphalt Mixture Performance Tester
ANACOVA	Analysis of Covariance
ANOVA	Analysis of Variance
AV	Air Void Content
BMP	Batch Mix Plant
CA	Carbonyl Area
CAM	Christensen-Anderson-Marasteanu
CDD	Cumulative Degree-Days
CI	Coatability Index
DMP	Drum Mix Plant
DOT	Department of Transportation
DSR	Dynamic Shear Rheometer
ER	Expansion Ratio
ER_{max}	Maximum Expansion Ratio
E*	Dynamic Modulus
FI	Foamability Index
FT_{be}	Effective Binder Film Thickness
FT-IR	Fourier Transform Infrared Spectroscopy
G_{mm}	Theoretical Maximum Specific Gravity

G-R Parameter	Glover-Rowe Parameter
G*	Complex Shear Modulus
HMA	Hot Mix Asphalt
HL	Half-Life
HWTT	Hamburg Wheel Tracking Test
IDT	Indirect Tensile
LC_{SN}	Stripping Number
LC_{ST}	Stripping Life
LVDT	Linear Variable Differential Transducers
LMLC	Laboratory-Mixed Laboratory-Compacted
LSV	Low Shear Viscosity
LTOA	Long-Term Oven Aging
M_R	Resilient Modulus
NMAS	Nominal Maximum Aggregate Size
OT	Overlay Test
P_{ba}	Percentage of Absorbed Asphalt
P_{be}	Percentage of Effective Asphalt
PG	Performance Grade
PMLC	Plant-Mixed Laboratory-Compacted
RAP	Reclaimed Asphalt Pavement
RAS	Recycled Asphalt Shingle
RRP	Rutting Resistance Parameter

SAI	Surface Area Index
SGC	Superpave Gyratory Compactor
SIP	Stripping Inflection Point
SSD	Saturated-Surface Dry
STOA	Short-Term Oven Aging
T_c	Compaction Temperature
TSR	Tensile Strength Ratio
TTI	Texas A&M Transportation Institute
Tukey's HSD	Tukey-Kramer Honestly Significant Difference
TxDOT	Texas Department of Transportation
VEC-DT	Viscoelastic Characterization Direct Tension
WMA	Warm Mix Asphalt
W_{opt}	Optimum Foaming Water Content
τ_{max}	Maximum Shear Stress
δ	Phase Angle
$\Delta\varepsilon^{vp}$	Viscoplastic Strain Increment

TABLE OF CONTENTS

Page

LIST OF FIGURES

Page

LIST OF TABLES

Page

CHAPTER I

INTRODUCTION

Overview

Asphalt mixtures are well-established paving materials with proven performance used on 94 percent of paved roads in the United States. They are produced by mixing asphalt binder and aggregate at an elevated temperature in either batch mix plants (BMP) or drum mix plants (DMP) and then compacted at temperatures ranging from 220°F (104°C) to 325°F (163°C) (Kuennen 2004; Newcomb 2007). The goal of asphalt mixture production is to ensure complete drying of the aggregate, proper coating and bonding of the aggregate with asphalt binder, and adequate workability for handling and compaction. All of these processes contribute substantially to good pavement performance in terms of durability and resistance to rutting, cracking, and moisture damage.

Economic, environmental, and engineering benefits motivate the reduction of production and construction temperatures for asphalt mixtures. The latest technology that has been adopted for this purpose is warm mix asphalt (WMA), which was first introduced in Europe in the mid-1990s, and transferred to the United States in the early 2000s. WMA is defined as an asphalt mixture that includes WMA additives (wax, surfactants, etc.) or is produced using the mechanical foaming process. Oftentimes, WMA is produced at temperatures approximately 50°F (28°C) cooler than those used for hot mix asphalt (HMA); the significant temperature reduction is achieved primarily by reducing the viscosity of the asphalt binder through various mechanisms.

WMA technologies offer a number of benefits, including decreased energy consumption, reduced emissions and fumes at the plant, extended haul distances, longer pavement construction season and reduced construction days, improved workability and compactability, reduced aging, and better resistance to cracking and raveling. However, barriers to the widespread implementation of WMA include the potentially increased susceptibility to rutting and moisture damage due to the incomplete drying of the aggregates and the reduced asphalt aging and absorption at lower production temperatures, and the imprecise correlation between the laboratory and field performance of these technologies. Additionally, there have been a number of questions surrounding the use of water in the mechanical foaming process, which has become the most popular method for producing WMA in the United States. For instance: Will the presence of water have detrimental effects on mixture performance? What are the factors that affect the asphalt foaming process and foamed mixture properties? Will mix design and evaluation procedures need to be modified to accommodate the foaming process?

Due to the use of WMA additives and asphalt foaming technology and the reduction in production temperatures, WMA is likely to have different aging characteristics as compared to HMA. Aging refers to the stiffening of asphalt binders and mixtures with time due to volatization, oxidation, and other chemical processes. It occurs due to the heating of the binder during production and construction in the short term and due to oxidation with time over the long term during its service life. It has been widely acknowledged that aging of asphalt mixtures has a significant effect on pavement performance in terms of improving resistance to rutting and moisture susceptibility, but

reducing cracking resistance and durability. Considering that WMA has lower stiffness and higher susceptibility to rutting and moisture damage than HMA during the initial in-service periods, there is a need to evaluate the performance evolution of WMA with aging, and more importantly, to determine when (or if) the properties of WMA and HMA converge.

The aging characteristics of asphalt mixtures have been studied extensively over the last few decades, and laboratory procedures to simulate aging of asphalt mixtures have been adopted for use in binder specifications and mix design. For instance, the rolling thin-film oven and the pressure aging vessel on asphalt binders are used to simulate the short-term aging occurred during plant production and construction and in-service aging over an approximately seven to ten-year period, respectively. In addition, laboratory short-term oven aging (STOA) protocols on asphalt loose mixes prior to compaction and long-term oven aging (LTOA) protocols on compacted asphalt mixtures are used for the same purposes. These procedures worked well in an environment in which the amount of recycled materials was relatively low, WMA was not common, and production temperatures were fairly consistent.

In the last few decades, changes have occurred in asphalt mixture components and production parameters, including increased use of polymer modifiers and recycled materials, the advent of WMA technologies, and DMPs replacing BMPs. Although these changes are beneficial to the asphalt industry, they have raised the need to further evaluate the aging characteristics of asphalt mixtures to consider the impacts of climate,

binder source, aggregate type, recycled materials, WMA technology, plant type, and production temperature.

Research Objectives and Methodology

A laboratory experiment was first performed to evaluate the performance evolution of WMA versus HMA with aging, and more importantly, to determine when (of if) the properties of these two mixture types converged. Based on the preliminary experiment, two main objectives were set for this study: 1) to evaluate the aging characteristics of asphalt mixtures and 2) to explore asphalt foaming technology for WMA applications. Figure 1 presents the research methodology used herein.

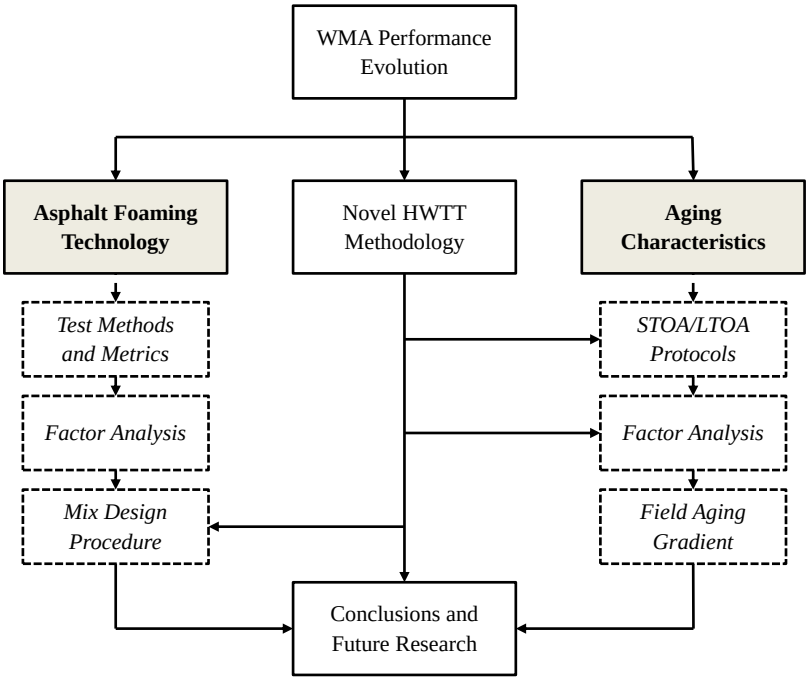

Figure 1. Research methodology.

Research efforts were devoted towards exploring asphalt foaming technology for WMA applications, including development of test methods and metrics to characterize asphalt foaming and foamed mixtures, identification of factors affecting the asphalt foaming characteristics and foamed mixture properties, and development of a mix design procedure for foamed asphalt mixtures.

The aging characteristics of asphalt mixtures in general were also evaluated in this study. Laboratory STOA and LTOA protocols were developed and (or) validated to simulate the asphalt aging and absorption during plant production and construction and through the initial period of performance (one to two years after construction). Additionally, efforts were made to identify mixtures components and production parameters with significant effects on the aging characteristics of asphalt mixtures and to characterize the non-uniform field aging of asphalt pavements with depth.

In addition, a novel methodology was introduced to analyze the Hamburg wheel tracking test (HWTT) results, which was used as a tool for evaluating the moisture susceptibility and rutting resistance of asphalt mixtures with various aging and foaming properties. Finally, conclusions and recommendations for future research were made based on the results of this study.

Dissertation Outline

This dissertation consists of eight chapters. The present chapter (Chapter I) demonstrates the significance of the research topic, describes the research objectives and methodology, and provides the dissertation outline.

Chapter II provides details about the WMA performance evolution experiment, including literature review, experimental design, and test results and data analysis. The contents are reprinted with minor revisions from a paper published in the *Journal of the Association of Asphalt Paving Technologists* (2013).

Chapter III discusses the shortcomings of the HWTT test that were recognized while performing the laboratory experiment described in Chapter II, and introduces a novel analysis methodology for evaluating moisture susceptibility and rutting resistance of asphalt mixtures. The contents are reprinted with minor revisions from a paper published in the *Transportation Research Record: Journal of the Transportation Research Board* (2014).

Chapter IV explores the asphalt foaming technology for WMA applications, including test methods and metrics developed to characterize asphalt foaming and foamed mixtures, effects of water content and laboratory foamer type on asphalt foaming technology, and the proposed mix design procedure. The contents are reprinted with minor revisions from two papers published in the *Transportation Research Record: Journal of the Transportation Research Board* (2015) and *Proceedings of the 12th International Society for Asphalt Pavements Conference* (2014), and two papers submitted for publication in the *International Journal of Pavement Engineering* (2015) and *Road Materials and Pavement Design* (2015).

Chapter V presents the validation of a laboratory STOA protocol to simulate the short-term aging of asphalt mixtures that occurs during plant production and construction. In addition, the effects of various mixture components and production

parameters on the short-term aging characteristics of asphalt mixtures are investigated. The contents are reprinted with minor revisions from a paper published in the *Journal of the Association of Asphalt Paving Technologists* (2015).

Chapter VI introduces a novel metric to quantify the field aging of asphalt mixtures and determine its correlation with laboratory LTOA protocols. The evaluation of those factors studied in Chapter V on the long-term aging characteristics of asphalt mixtures is also included. The contents are reprinted with minor revisions from a paper submitted for publication in the *Journal of the Association of Asphalt Paving Technologists* (2016).

Chapter VII provides information with regard to characterizing non-uniform field aging in asphalt pavements with depth. Laboratory test results in terms of mixture stiffness gradient and binder property gradient for aged field cores (i.e., post-construction cores) obtained from several field projects are presented and discussed.

Chapter VIII summarizes the main findings and conclusions of this study. In addition, recommendations for future research are provided.

CHAPTER II

PERFORMANCE EVOLUTION OF ASPHALT MIXTURES WITH AGING*

Overview

Economic, environmental, and engineering benefits motivate the reduction of production and placement temperatures for asphalt concrete paving materials that are used on the majority of paved roads in the United States. The latest technology that has been adopted for this purpose is WMA, which is asphalt concrete paving material produced and placed at temperatures approximately 50°F (28°C) cooler than those used for HMA. WMA was first introduced in Europe in the mid-1990s as a way to reduce greenhouse gas emissions and then transferred to the United States in the early 2000s largely through the joint efforts of the National Asphalt Paving Association and the Federal Highway Administration.

WMA is able to provide a number of benefits, including decreased energy consumption, reduced emissions and fumes at the plant, improved working conditions at the construction site, extended haul distances, longer pavement construction season, improved workability and compactability, reduced aging, and better resistance to cracking. However, there are several barriers to the widespread implementation, such as the wide variety of WMA technologies and the imprecise correlation between laboratory and field performance. Also, WMA could be more susceptible to rutting and moisture-

* Reprinted (with minor revisions) with permission from "Performance Evolution of Hot-Mix and Warm-Mix Asphalt with Field and Laboratory Aging" by Fan Yin, Lorena Garcia Cucalon, Amy Epps Martin, Edith Arambula, and Eun Sug Park, 2013, *Journal of the Association of Asphalt Paving Technologists*, Vol. 83, pp. 109-142, Copyright [2013] by AAPT.

related pavement distresses (especially in the early life of the pavement) due to the lower production temperature and the additional moisture introduced by some WMA technologies. The majorities of previous studies on performance evaluation of WMA as compared to HMA have observed reduced mixture stiffness, strength, and rutting resistance at the initial stage, but the difference for WMA versus HMA reduced with elapsed time in the field and long-term aging in the laboratory. However, it has not been determined when (or if) equivalent stiffness and moisture susceptibility between WMA versus HMA is achieved.

Therefore, the objectives of this research study are to: 1) evaluate the evolution of WMA stiffness with field and laboratory aging to determine when (or if) the stiffness of WMA and HMA converge, and 2) evaluate the moisture susceptibility of WMA after field and laboratory aging as compared to the performance of HMA.

Background

In the past few years, studies have quantified the performance evolution of WMA in terms of moisture susceptibility and rutting resistance. This is particularly important since WMA in laboratory tests generally shows greater rutting and moisture susceptibility as compared to HMA. This discrepancy could be due to the lower WMA production temperature and/or the additional moisture introduced by some WMA technologies. These same studies have also demonstrated that moisture susceptibility and rutting resistance of WMA mixtures improve significantly after mixture aging in the laboratory or in the field.

Several researchers have measured the effect of different laboratory LTOA protocols on WMA mixtures. Mogawer et al. (2011) evaluated WMA mixtures prepared using Advera® and SonneWarmix™, conditioned for four hours at 235°F (113°C), allowed to cool at room temperature for six hours, and then long-term aged for 14 hours at 140°F (60°C). The HWTT results (AASHTO T 324) of these long-term aged mixtures were compared against the corresponding WMA mixtures conditioned for only four hours at 235°F (113°C), 265°F (129°C), or 295°F (146°C). For SonneWarmix™, the number of load cycles to reach the stripping inflection point (SIP) for the longer aging protocol with cooling was 4,200 passes, and the mixtures with only four hours conditioning at 235°F (113°C) required very similar number of passes to reach the SIP (i.e., 4,300 passes). For Advera®, the number of load cycles to reach the SIP for the longer aging protocol with cooling (i.e., 4,000 passes) was between the values obtained for those with only four hours conditioning at 235°F (113°C) (i.e., 3,400 passes) and four hours at 265°F (129°C) (5,500 passes). Thus, the results indicated that laboratory LTOA protocols improved WMA HWTT performance in terms of moisture susceptibility.

Other studies have assessed the effect of LTOA on mixture indirect tensile (IDT) strength in the laboratory by aging the specimens in a forced draft oven at 185°F (85°C) in accordance with AASHTO R 30. Brown and Scholz (2000) evaluated the aging characteristics of HMA mixtures with different binders and aggregates by determining IDT strength using the Nottingham Asphalt Tester (BS DD213) with and without LTOA. A significant increase in IDT strength of mixtures with LTOA was shown. In another

study, WMA mixtures were prepared with Aspha-min®, Sasobit®, and Evotherm DAT™ using two aggregate sources and various amounts of coal ash and shingles (Xiao et al. 2012). The dry IDT strength values of the unaged specimens and those LTOA at 185°F (85°C) for the standard five days were very similar. However, a significant difference was observed for moisture-conditioned specimens per the South Carolina SC T70 moisture conditioning procedure, with the wet IDT strength being significantly higher for long-term aged specimens versus the unaged counterparts (except for Aspha-min®). The study concluded that the LTOA protocol of five days at 185°F (85°C) improved the moisture susceptibility of WMA mixtures. Another study by Diefenderfer and Hearon (2008) also used the IDT strength test (AASHTO T283) on long-term aged specimens with LTOA protocols of four and eight days at 185°F (85°C) to evaluate the performance of WMA mixtures prepared with Sasobit®. Test results indicated that the tensile strength ratio (TSR) of WMA mixtures produced at 266°F (130°C) and 230°F (110°C) increased after four-day LTOA prior to testing, while no difference was observed for mixtures produced at 302°F (150°C). Additionally, an increase in TSR was only shown by WMA mixtures produced at 230°F (110°C) as LTOA time extended from four days to eight days. The authors concluded that the moisture resistance of WMA mixtures with Sasobit® improved significantly with LTOA. While IDT strength test is the most common laboratory test used for evaluating moisture susceptibility, sources of variability have been recently identified, and concern remains regarding the poor correlation with field performance (Azari 2010).

The effect of field aging on WMA performance evolution has also been evaluated through laboratory tests performed on WMA with Evotherm ET field cores after one month and one year in-service (Estakhri et al. 2009). According to the HWTT rut depth results, the one-month WMA field cores showed no improvement in rutting resistance with respect to the plant-mixed laboratory-compacted (PMLC) specimens, but the one-year WMA field cores showed a significant improvement in performance, with rut depths similar to those obtained for the one-year HMA field cores. Similar trends were also observed for the IDT strength results. Another study by Estakhri (2012) evaluated the field performance of WMA at different in-service times as compared to HMA. Ten field projects in Texas were evaluated in the study. Mixture properties in terms of rutting, cracking, and moisture susceptibility were evaluated in laboratory tests including the HWTT (AASHTO T 324), the Overlay test (OT) (Tex-248-F), and the dry and wet IDT strength test (AASHTO T 283). For the majority of the field projects, WMA showed comparable performance to HMA. In addition, WMA field cores at one year in-service indicated significant stiffening as compared to those obtained at construction. These results suggest that there is likely an aging period in the field required to achieve equivalent performance for WMA as compared to HMA.

The majority of previous studies on evaluating performance evolution of WMA with aging have recognized that field and laboratory aging had a significant effect on improving mixture stiffness, rutting resistance, and moisture susceptibility, and that the improvement was more pronounced for WMA than HMA. However, the time required

in the field or laboratory aging conditions required to achieve equivalent performance between WMA and HMA have not been explored.

Experimental Design

Materials and Specimen Fabrication

Materials used in this research study are from two field projects located in Iowa and Texas. The Iowa field project is near Adams County on U.S. Route 34. Five different fractions of quartzite, limestone aggregates, and river sands from four different producers, and 17 percent reclaimed asphalt pavement (RAP) were used. The mixture used is a coarse graded 9.5mm nominal maximum aggregate size (NMAS) mix, with the combined aggregate gradation presented in Figure 2. The type of asphalt binder was a performance grade (PG) 58-28 binder with a specific gravity of 1.03. The design optimum binder content was 5.4 percent (by weight of the total mixture). Besides HMA, Evotherm® 3G and Sasobit® were used as the WMA technologies in this field project. Both WMA additives were blended at 0.4 percent by weight of binder at the contractor's asphalt plant. Construction was completed in September 2011, and field cores at construction, after winter at six months in-service, and after summer at 12 months in-service were obtained.

The Texas field project is on FM 973, near the Austin Bergstrom International Airport. Three types of limestone aggregates and two sands were used in this field project. The mixture used is a coarse graded 12.5mm NMAS mix, with the combined aggregate gradation presented in Figure 2. A PG 70-22 binder with a specific gravity of 1.03 was used with a design optimum binder content of 5.2 percent (by weight of the

total mixture). Besides HMA, Evotherm DAT™ and a foaming process were used as the WMA technologies. In order to treat the binder with Evotherm DAT™, the binder was heated at the contractor's asphalt plant or in the laboratory to the mixing temperature and five percent of the additive by weight of the binder was blended. The foamed asphalt was also produced on-site by injecting a five percent water and air to the heated binder inside a special expansion chamber. In the laboratory, a foaming device that simulates the air-atomized mixing at the plant was used to produce foamed asphalt/mixtures with five percent water. The construction of this field project was completed in January 2012, and field cores at construction, after summer at eight months in-service, and after winter at 14 months in-service were obtained.

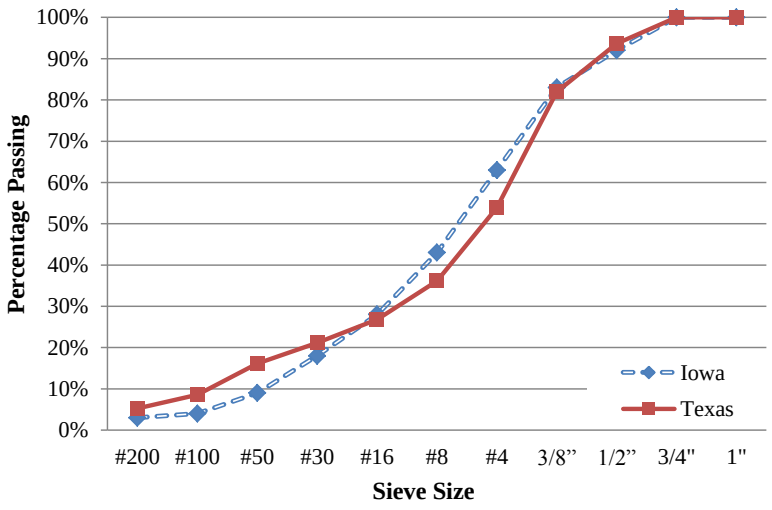

Figure 2. Combined aggregate gradations for the Iowa and Texas field projects.

To fabricate laboratory-mixed laboratory-compacted (LMLC) specimens, aggregates and binders were heated to the specified mixing temperature independently

and then mixed with a portable bucket mixer. Afterward, following the recommendation by Yin et al. (2013), WMA and HMA loose mixes were conditioned in the oven for two hours at 240°F (116°C) and 275°F (135°C), respectively, prior to compaction with the Superpave gyratory compactor (SGC). Trial specimens were fabricated to assure specimens were obtained with air void contents (AV) of 7±0.5 percent (AASHTO T166). To simulate the long-term aging in the field, SGC compacted specimens were further aged according to the proposed research methodology in an environmental room or oven prior to being characterized with laboratory tests. Most LMLC specimens were tested approximately one week after LTOA.

Laboratory Tests

The resilient modulus (M_R) test was conducted through repetitive applications of a compressive haversine load along the vertical diametral plane of cylindrical asphalt concrete specimens. The resulting horizontal deformations of the specimen were measured by two linear variable differential transducers (LVDT) aligned along the horizontal diametral plane. An environmentally controlled room at 77°F (25°C) was used for temperature conditioning and testing. The test equipment used to perform the measurements and the specimen setup are shown in Figure 3. M_R stiffness was measured per ASTM D7369 with external LVDTs aligned along the horizontal diametral plane (i.e., gauge length as a fraction of diameter of the specimen = 1.00). As expressed in Equation 1, the M_R stiffness was calculated based on vertical load, horizontal deformation, and the asphalt mixture's Poisson ratio.

$$M_R = \frac{P(\nu + 0.2732)}{t\Delta}$$ Equation 1

where:

M_R = M_R stiffness of asphalt mixture;

p = vertical load;

υ = Poisson's ratio;

t = specimen thickness; and

Δ = horizontal deformation measured by LVDTs.

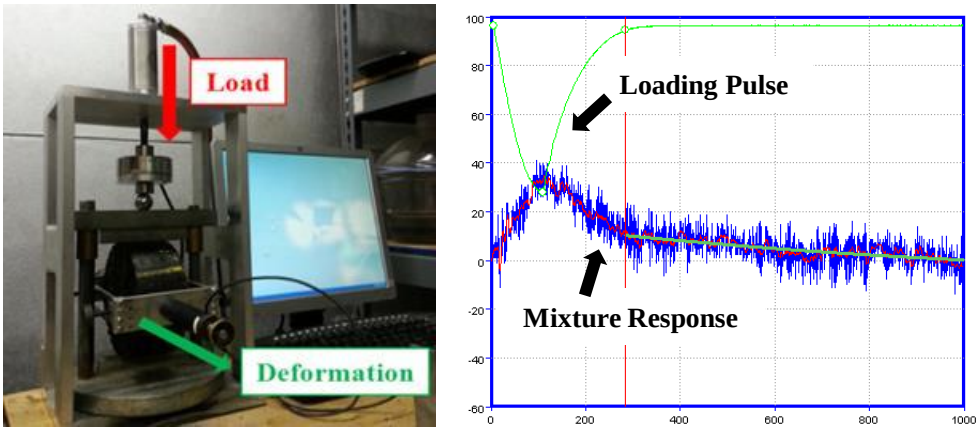

(a) (b)

Figure 3. M_R test; (a) sample setup in loading frame, (b) data acquisition system.

The IDT strength test is the most common national standard test to evaluate moisture susceptibility of asphalt mixtures. IDT strength at 77°F (25°C) was determined for both dry specimens and for wet specimens moisture conditioned in accordance with the modified Lottman procedure per AASHTO T 283 with partial vacuum saturation, one freeze-thaw cycle, and soaking in warm water. All laboratory-compacted specimens were fabricated to a diameter of 6 inches (150 mm) and a height of 3.75 inches (95 mm) in the SGC to target AV contents of 7±0.5 percent. The TSR was determined as the ratio

of the average IDT strength results obtained from three moisture conditioned specimens to the average IDT strength results from three dry control specimens. The wet IDT strengths and TSR values were used as moisture susceptibility parameters to compare the performance of WMA versus HMA. As only one replicate TSR value was produced from each set of six specimens, the TSR results for different specimen or mixture types were compared based on the precision and bias statement that indicated a d2s acceptable range of two results with more than a 95 percent confidence level of 9.3 percent (Azari 2010).

The HWTT test per AASHTO T 324 is a laboratory procedure that utilizes repetitive loading in the presence of water and measures the rut depth induced in an asphalt mixture with increasing load cycles. It has been recently adopted by several states to simultaneously evaluate rutting resistance and moisture susceptibility of asphalt mixtures. As shown in Figure 4, two SGC cylindrical specimens with a diameter of 6 inches (150mm) and a thickness of 2.4 inches (61 mm) are placed side-by-side, submerged in warm water at 122°F (50°C) in accordance with Tex-242-F, and subjected to approximately 52 passes of a steel wheel per minute. Each set of specimens is loaded for a maximum of 20,000 load cycles or until the center of the specimen deforms by 0.5 inch (12.5 mm).

During testing, rut depths at different positions along the specimens are recorded with each load cycle. Typical parameters obtained from the HWTT test include creep slope, stripping slope, and SIP, as shown in Figure 5. In this research study, the SIP and stripping slope were used as two moisture susceptibility parameters, and 2,000 load

cycles (SIP) and 0.2 µm/cycle (stripping slope) were used as d2s values in the analysis, as reported by Epps Martin et al. (2014).

Figure 4. HWTT equipment with loaded specimens.

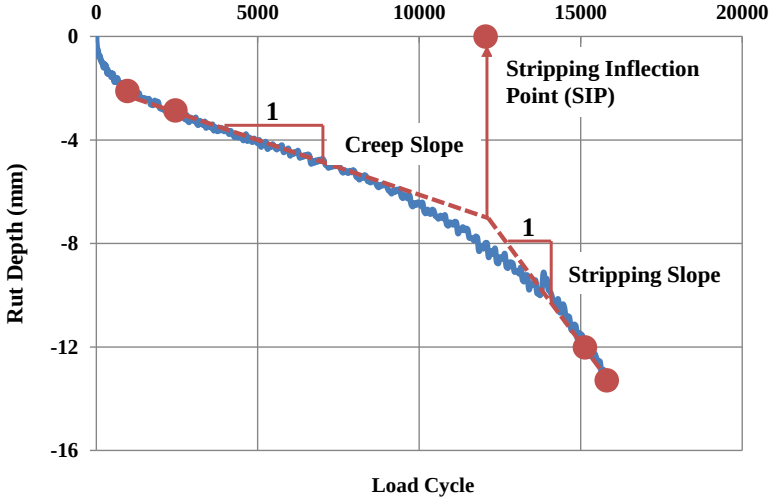

Figure 5. HWTT results in terms of rut depth versus load cycles.

Research Methodology

Figure 6 illustrates the research methodology followed in this research study. The aging period to equivalent stiffness for WMA versus HMA in its early life was first evaluated. field cores at different in-service times from the Iowa and Texas field projects were tested in the M_R test to measure the change in mixture stiffness with field aging and to determine the critical time at which the field stiffness of HMA and WMA converged. Meanwhile, the M_R testing was performed on LMLC specimens aged at 140°F (60°C) over a series of different time periods (1, 2, 4, 8, and 16 weeks). Reduced testing variability was achieved by using the same set of LMLC specimens throughout the experiment. The LTOA protocols were selected based on a previous study by Glover et al. (2005), which indicated four weeks of aging at 140°F (60°C) produced mixtures with similar aging levels to pavements with approximately one year in-service under Texas climate conditions. Thus, the selected LTOA protocols might reflect approximately 0-4 years under Texas climate conditions and likely 2-8 years under milder climates in the United States. The M_R stiffness results were also used to determine the correlation between mixture stiffness in the field and in the laboratory.

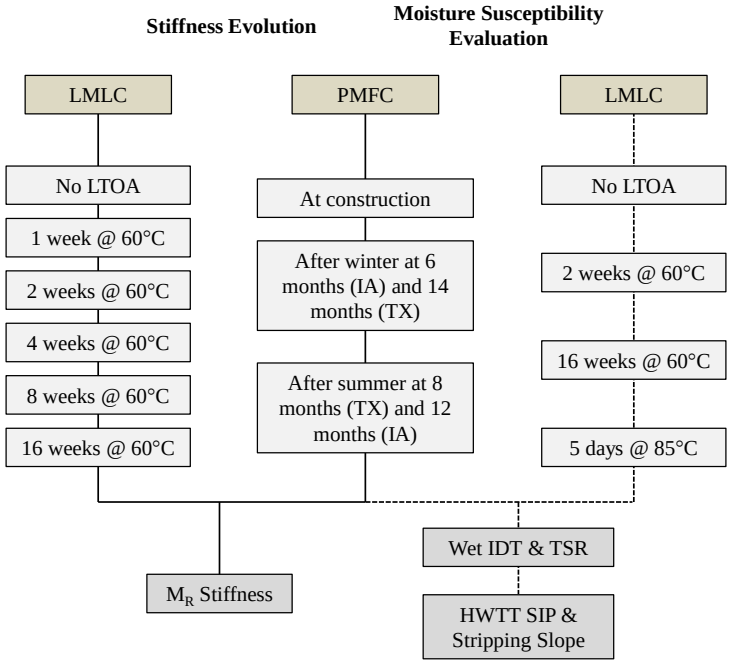

Figure 6. Research methodology for the performance evolution experiment.

Afterwards, the moisture susceptibility of WMA was evaluated in the IDT strength and HWTT tests after field aging and various LTOA protocols, including two and 16 weeks at 140°F (60°C) and five days at 185°F (85°C) in accordance with AASHTO R 30. Due to the limited amount of Iowa aggregates available, only LMLC specimens with LTOA protocol of 16 weeks at 140°F (60°C) were included for moisture susceptibility evaluation, while those specimens with LTOA protocols of two weeks at 140°F (60°C) and five days at 185°F (85°C) were not available.

Test Results and Data Analysis

Stiffness Evolution with Aging

Field cores at different in-service times and LMLC specimens with LTOA protocols from the Iowa and Texas field projects were tested to determine M_R stiffness and the results were used to evaluate stiffness evolution with field and laboratory aging.

Field Aging

Figure 7 and Figure 8 present the M_R stiffness results of field cores at different in-service times from the Iowa and Texas field projects, respectively. Each bar in these figures represents the average value of three replicate specimens, and the error bars represent ± one standard deviation from the average value. The Analysis of Variance (ANOVA) followed by Tukey-Kramer Honestly Significant Difference (Tukey's HSD) tests were conducted with a five percent significance level (i.e., alpha = 0.05) to verify the difference in M_R stiffness for various field aging stages. The ANOVA result indicated that field aging was significant for all mixtures with p-values smaller than 0.05, and the Tukey's HSD results are shown with different letters shown in the center of the bars. The M_R stiffness decreases as letters change from A to C, and field cores with different letters have M_R values that are statistically different from each other.

As illustrated in Figure 7 for the Iowa field project, the stiffness of HMA and WMA with Evotherm® 3G field cores increased slightly after winter at six months in-service, while field cores of WMA with Sasobit® increased significantly. In addition, a statistically significant increase in stiffness of field cores from six months to 12 months in-service was noted for all mixtures. The placement of pavement sections for the Iowa

field project was completed in September 2011, so pavements were subjected to the winter climatic conditions for the first six months in service and summer climatic conditions from six months to 12 months in-service. Therefore, it is expected that the accelerated aging of pavements in the field from six to 12 months in-service was related to the high in-service temperature experienced by the pavement during the summer.

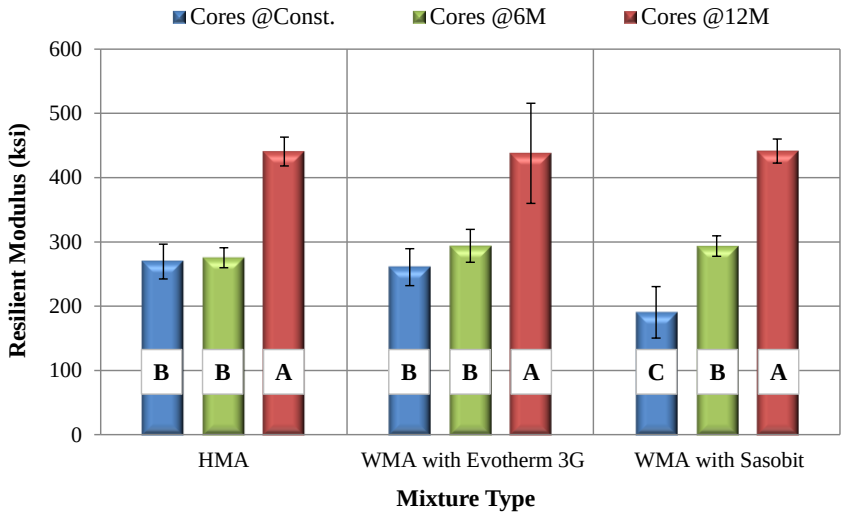

Figure 7. Comparison of M_R stiffness results for field cores with different in-service times from the Iowa field project.

The M_R stiffness of field cores for both HMA and WMAs for the Texas field project increased significantly from at construction to after summer at eight months in-service, as shown in Figure 8. The placement of pavement sections for the Texas field project was completed in January 2012, and so the pavement was subjected to summer climatic conditions prior to the second set of cores being taken and tested for M_R stiffness. Therefore, the expectation that pavements experience considerable aging in the

summer was verified by the increase in M_R stiffness for the Texas field project. Also, no statistically significant increase in mixture stiffness was shown for WMA field cores after winter at 14 months in-service, as compared to those after summer at eight months in-service, while field cores of HMA experienced a significant increase from eight to 14 months in-service.

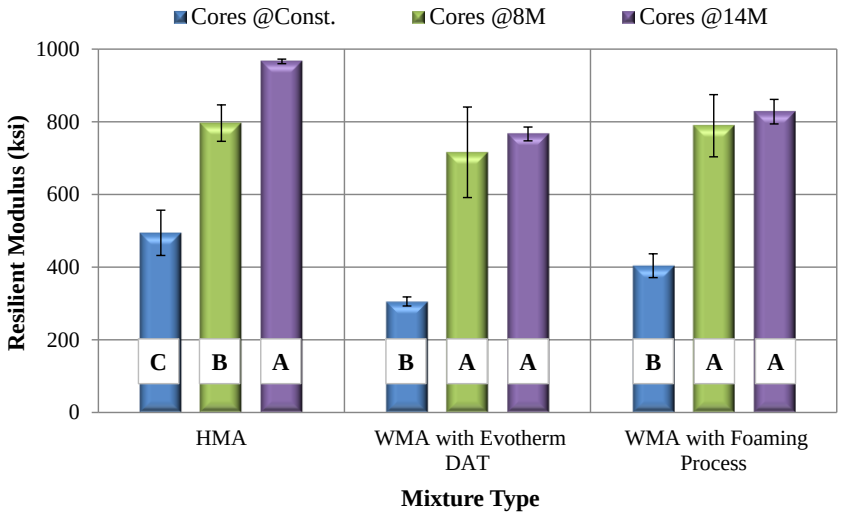

Figure 8. Comparison of M_R stiffness results for field cores with different in-service times from the Texas field project.

The aging period in the field to equivalent stiffness for WMA versus HMA for the Iowa and Texas field projects was determined as shown in Figure 9 and Figure 10, respectively. The ANOVA followed by Tukey's HSD tests were conducted with a 5 percent significance level (i.e., alpha = 0.05) to verify the difference in M_R stiffness of field cores of WMA versus HMA for each field in-service time. The ANOVA result indicated that mixture type was significant for Iowa and Texas cores at construction and

Texas cores after winter at 14 months in-service with p-values smaller than 0.05, and the Tukey's HSD results are shown with different capital letters shown in the center of the bars.

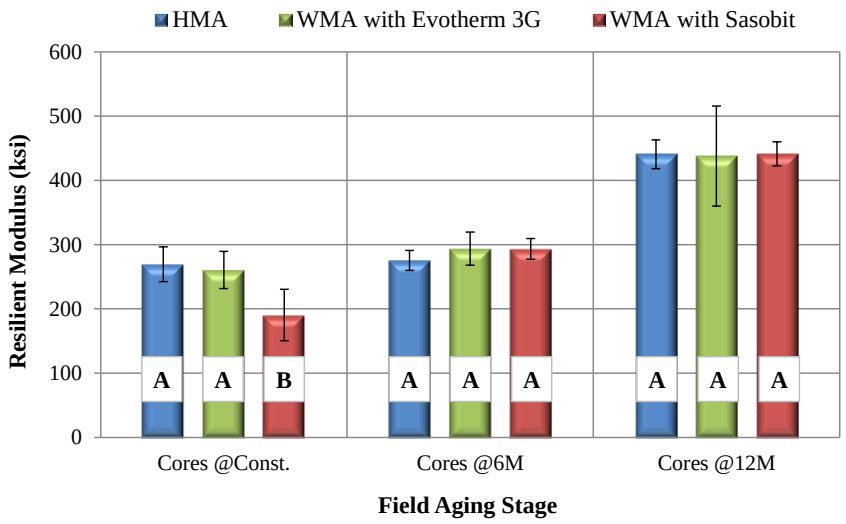

Figure 9. Comparison of M_R stiffness results for WMA versus HMA field cores from the Iowa field project.

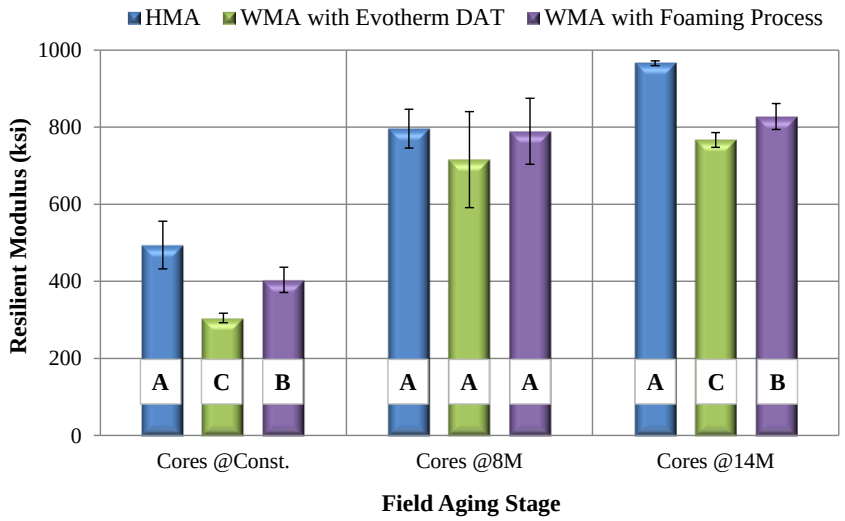

Figure 10. Comparison of M_R stiffness results for WMA versus HMA field cores from the Texas field project.

For the Iowa field project (Figure 9), the initial stiffness of field cores for HMA was higher than that for WMA with Sasobit® and equivalent to that for WMA with Evotherm® 3G. For field cores after winter at six months in-service and after summer at 12 months in-service, equivalent stiffness between HMA and both WMAs was achieved. Figure 10 presents the comparison of M_R stiffness results for WMA versus HMA from the Texas field project. As illustrated, the stiffness of field cores at construction for HMA was higher than those of two WMA mixtures, with the stiffness of WMA with foaming process was also higher than that of WMA with Evotherm DAT™. After summer at eight months in-service, equivalent stiffness was achieved by all mixtures. However, for field cores after winter at 14 months in-service, the stiffness of HMA was again higher than the two WMA mixtures.

Thus, it can be inferred from the M_R stiffness results presented in Figure 7 through Figure 10 that HMA and WMAs field cores from both field projects had experienced a significant increase in stiffness with field aging since construction. The increase in stiffness in the summer was more significant than that in winter, which is likely due to the high in-service temperature experienced by the pavement in the summer. Equivalent stiffness between HMA and both WMAs were achieved for field cores after winter at six months in-service and after summer at 12 months in-service for the Iowa field project and field cores after summer at eight months in-service for the Texas field project.

Laboratory Aging

Figure 11 and Figure 12 present the M_R stiffness for LMLC specimens aged at 140°F (60°C) over a series of time periods for the Iowa and Texas field projects, respectively. To evaluate the mixture stiffness evolution, curve fitting using an exponential function, as shown in Equation 2, was employed on the M_R stiffness results. The markers in the figures represent the measured average M_R stiffness from three replicates, and the dashed lines indicate the fitted M_R stiffness results.

$$E_{(t)} = E_0 + (E_{max} - E_0) * e^{-(\frac{\rho}{t})^{\beta}} \quad \text{Equation 2}$$

where:

$E_{(t)}$ = mixture stiffness with laboratory aging at time t;

E_{max} = maximum mixture stiffness;

E_0 = initial mixture stiffness;

t = laboratory aging time; and

ρ and β = curve fitting coefficients.

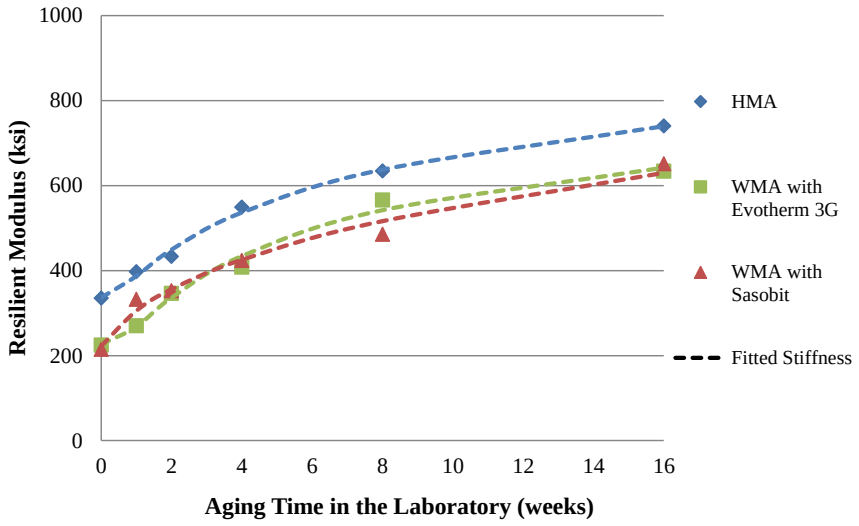

Figure 11. Measured and fitted M_R stiffness with laboratory aging for the Iowa field project.

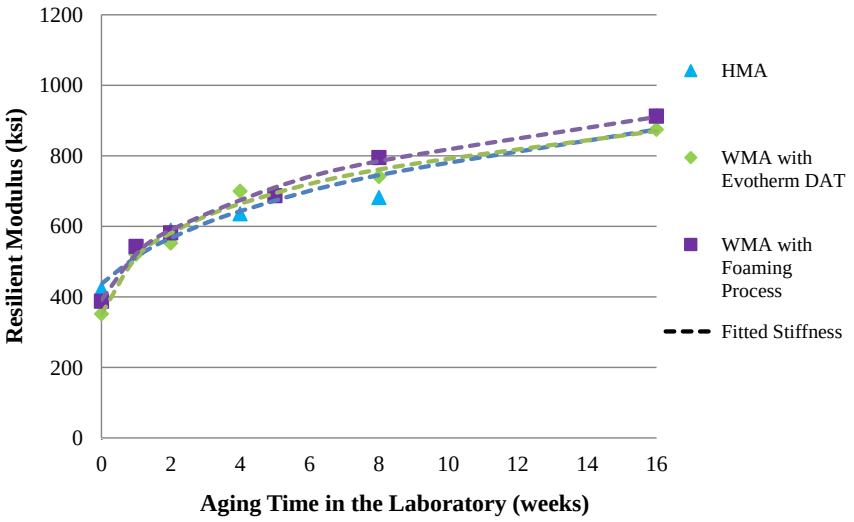

Figure 12. Measured and fitted M_R stiffness with laboratory aging for the Texas field project.

As illustrated in Figure 11, the stiffness of Iowa HMA was higher than the stiffness of WMA with Evotherm® 3G and WMA with Sasobit® for all laboratory LTOA times. Thus, the equivalent stiffness between HMA and WMA mixtures was not likely to be achieved in the laboratory within a reasonable time period. The fitted stiffness of the WMA mixtures after two weeks of laboratory aging was similar to the initial stiffness of HMA, as shown in Figure 11. Predicted stiffness of mixtures from the Texas field project shown in Figure 12 indicated that the stiffness of HMA was equivalent to those of two WMA mixtures for all LTOA periods at 140°F (60°C).

Based on the M_R stiffness results presented in Figure 11 and Figure 12, the LTOA protocol of two weeks at 140°F (60°C) was selected for the moisture susceptibility evaluation. This aging period at 140°F (60°C) represented the time at which the stiffness of WMA was similar to the initial stiffness of HMA (Iowa field project) and the stiffness of HMA and WMA converged (Texas field project). In addition, additional LTOA protocols of 16 weeks at 140°F (60°C) and five days at 185°F (85°C) were included in the moisture susceptibility experiment.

Moisture Susceptibility after Aging

WMA mixtures from the Iowa and Texas field projects were tested in the IDT strength and HWTT tests, and the results were compared against the corresponding HMA mixtures, for each field and laboratory aging stage. The objective was to determine if equivalent moisture susceptibility between WMA and HMA was achieved after field aging or laboratory LTOA.

IDT Strength Results

The wet IDT strengths and TSR values were used as moisture susceptibility parameters to compare the performance of WMA versus HMA after field and laboratory aging. ANOVA followed by Tukey's HSD tests were performed on the wet IDT strengths with a five percent significance level (i.e., alpha = 0.05) to discriminate asphalt mixtures with different moisture susceptibility. The analysis was done independently for each field and laboratory aging stage (i.e., field cores at construction, LMLC specimens with LTOA of two weeks at 140°F, etc).

Figure 13 and Figure 14 present the wet IDT strengths and TSR results for the Iowa and Texas mixtures, respectively, with HMA compared against both WMAs for each field and laboratory aging stage. Each bar represents the average wet IDT strength of three replicate specimens and the error bars represent ± one standard deviation from the average value. The ANOVA result confirmed that mixture type was significant for most Iowa and Texas mixtures with p-values smaller than 0.05. The results of the Tukey's HSD tests to compare WMAs versus HMA for each field and laboratory aging stage are shown with letters in the center of the bars. The wet IDT strengths decrease as letters change from A to C, and mixtures with different letters have wet IDT strengths that are statistically different from each other.

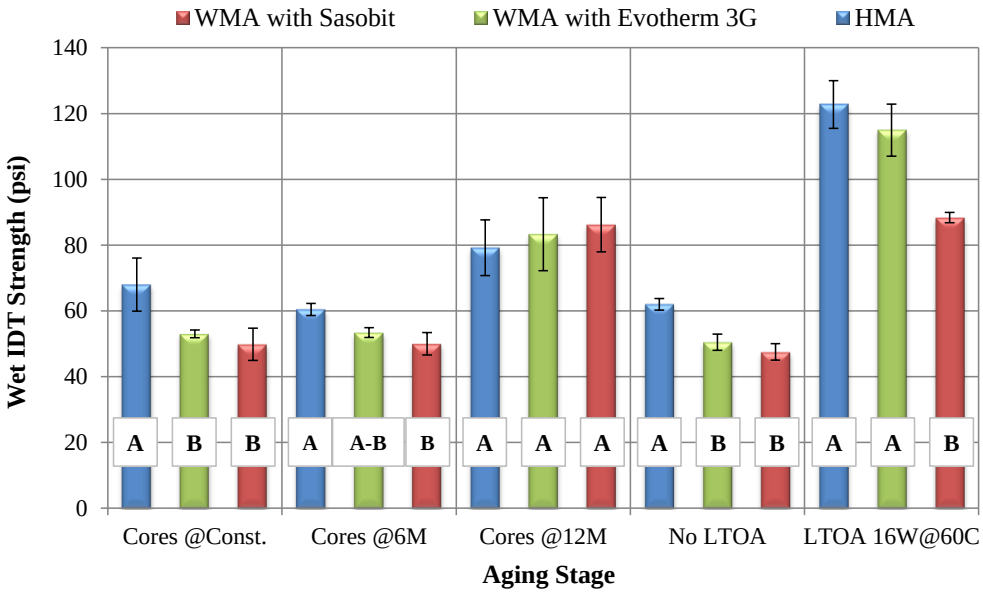

(a)

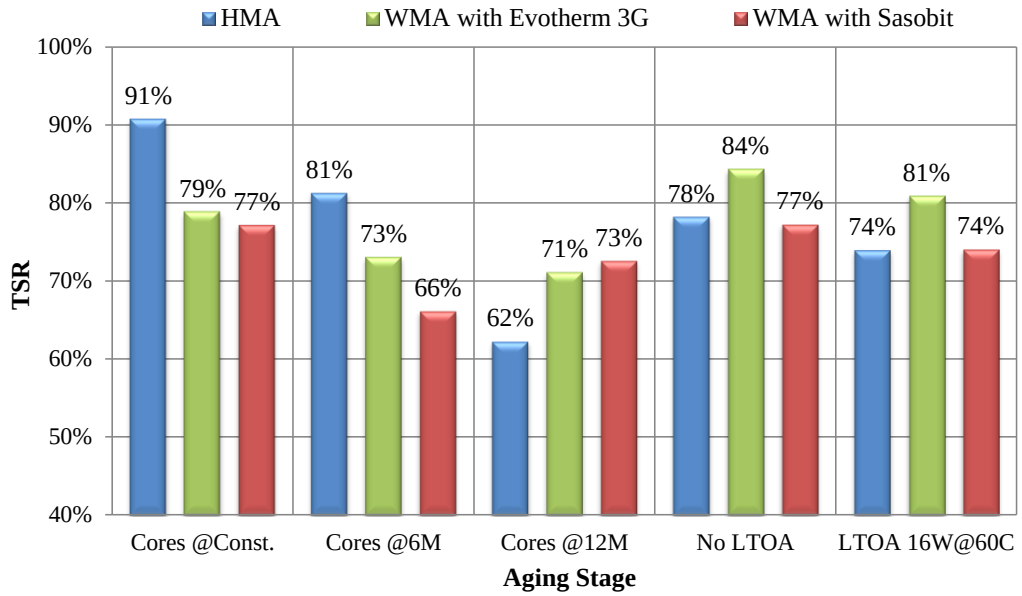

(b)

Figure 13. IDT strength test results for the Iowa field project; (a) wet IDT strength, (b) TSR.

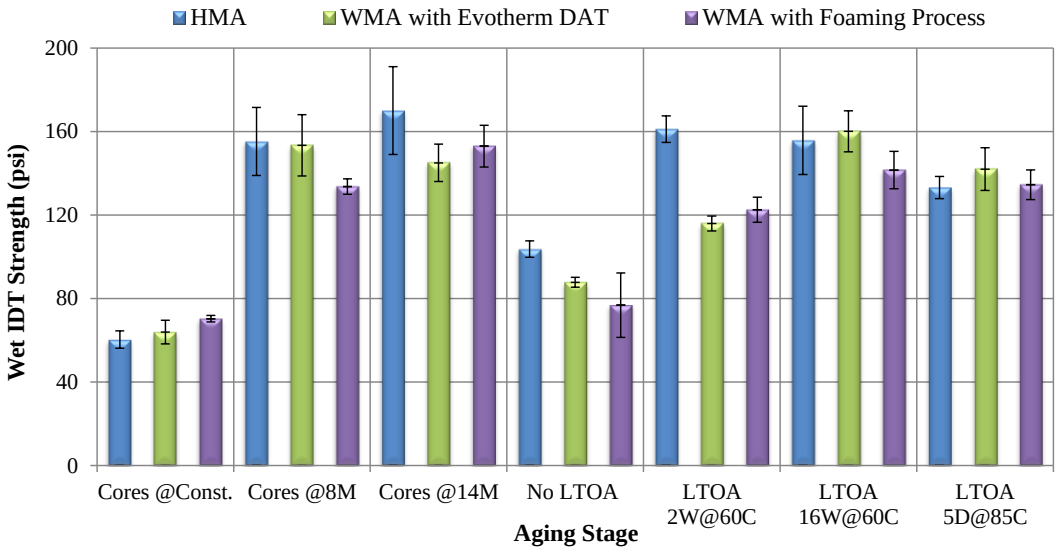

(a)

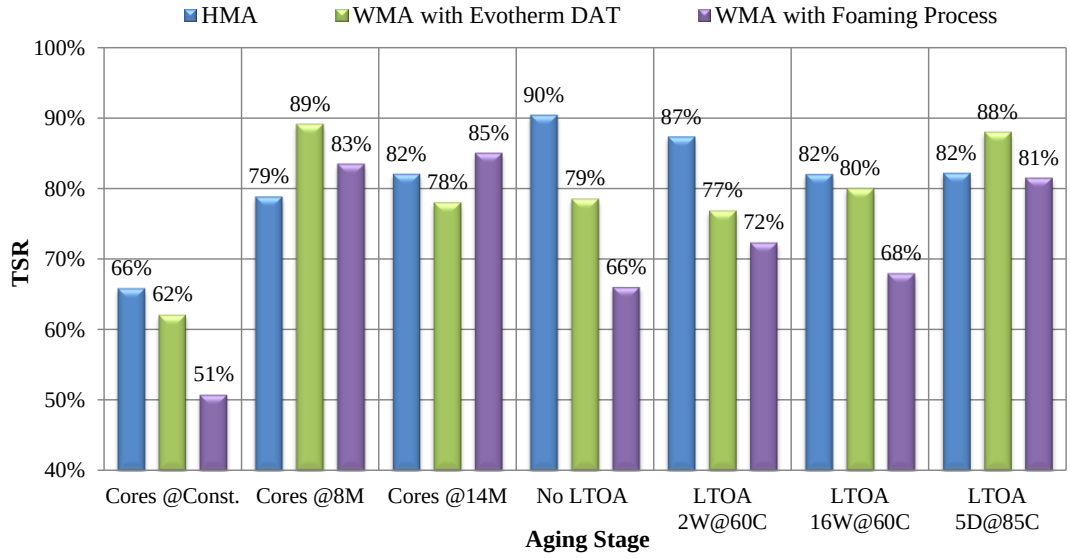

(b)

Figure 14. IDT strength test results for the Texas field project; (a) wet IDT strength, (b) TSR.

As illustrated in Figure 13(a) for the Iowa field project, HMA field cores at construction and after winter at six months in-service had statistically higher wet IDT strengths as compared to those of WMA with Evotherm® 3G and field cores at construction of WMA with Sasobit®. However, equivalent wet IDT strength was achieved between HMA and both WMAs for the field cores after summer at 12 months in-service. Wet IDT strengths of WMA LMLC specimens without LTOA protocol were statistically lower than those of their HMA counterpart. As for LMLC specimens with LTOA protocol of 16 weeks at 140°F (60°C), equivalent wet IDT strengths were achieved by HMA and WMA with Evotherm® 3G, but the wet IDT strength of WMA with Sasobit® was statistically lower. Figure 13(b) shows that all TSR values of field coress except WMA with Sasobit® field cores after winter at six months in-service and HMA field cores after summer at 12 months in-service were higher than 70 percent. In the case of field cores at construction and after winter at six months in-service, the TSR values of HMA were higher than those of WMA mixtures. However, the opposite trend was shown for field cores after summer at 12 months in-service. Based on the d2s value of 9.3 percent for TSR (Azari 2010), equivalent TSR values were obtained between HMA and WMA LMLC specimens.

As illustrated in Figure 14(a) for the Texas field project, in all cases of field cores except those at construction, the wet IDT strengths of HMA were statistically higher or equivalent to WMA mixtures. For LMLC specimens without LTOA and with LTOA protocol of two weeks at 140°F (60°C), HMA had statistically higher wet IDT strengths than both WMA mixtures except LMLC specimens without LTOA of WMA with

Evotherm DAT™, where an equivalent wet IDT strength was shown. In the case of LMLC specimens with LTOA protocols of 16 weeks at 140°F (60°C) and five days at 185°F (85°C), equivalent wet IDT strengths were achieved by HMA and both WMA mixtures. Figure 14(b) shows that in the case of field cores at construction, HMA and WMA with Evotherm DAT™ had equivalent TSR values (based on the d2s value of 9.3 percent), with both higher than that for WMA with foaming process. However, higher and equivalent TSR values of field cores after summer at eight months in-service were shown for WMA with Evotherm DAT™ and WMA with foaming process, respectively, as compared to HMA. For field cores after winter at 14 months in-service, equal TSR values were shown for HMA and both WMAs based on the 9.3 percent d2s value. All WMA with foaming process LMLC specimens except those subjected to the LTOA protocol of five days at 185°F (85°C) had lower TSR values as compared to their HMA counterparts, and lower than the minimum threshold of 80 percent suggested by AASHTO T 283. Higher TSR values for HMA versus both WMAs were shown for LMLC specimens without LTOA and those with LTOA protocol of two weeks at 140°F (60°C). However, in the cases of LMLC specimens with longer LTOA time or higher LTOA temperature, equivalent TSR values were obtained for HMA and WMA with Evotherm DAT™.

HWTT Results

Figure 15 and Figure 16 present the SIP and stripping slope results for the Iowa and Texas field projects, respectively, with HMA compared against WMAs for each field and laboratory aging stage. D2s values of 2,000 load cycles for the SIP and

0.2µm/cycle for the stripping slope were used to discriminate asphalt mixtures with different performances in the HWTT test.

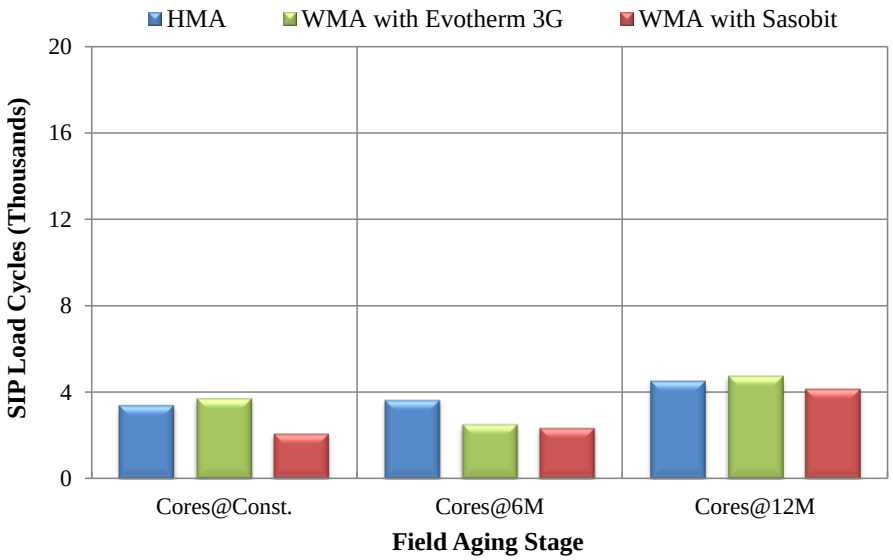

(a)

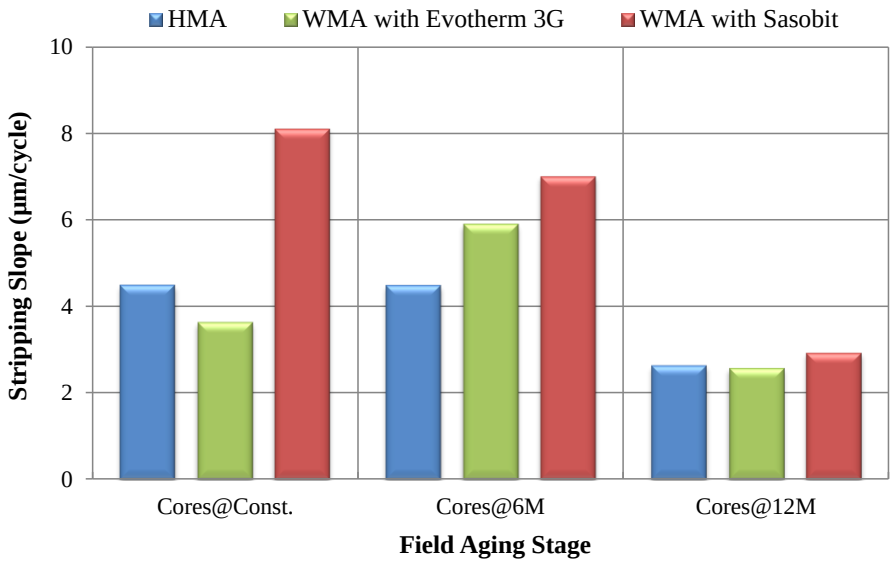

(b)

Figure 15. HWTT test results for the Iowa field project; (a) SIP, (b) stripping slope.

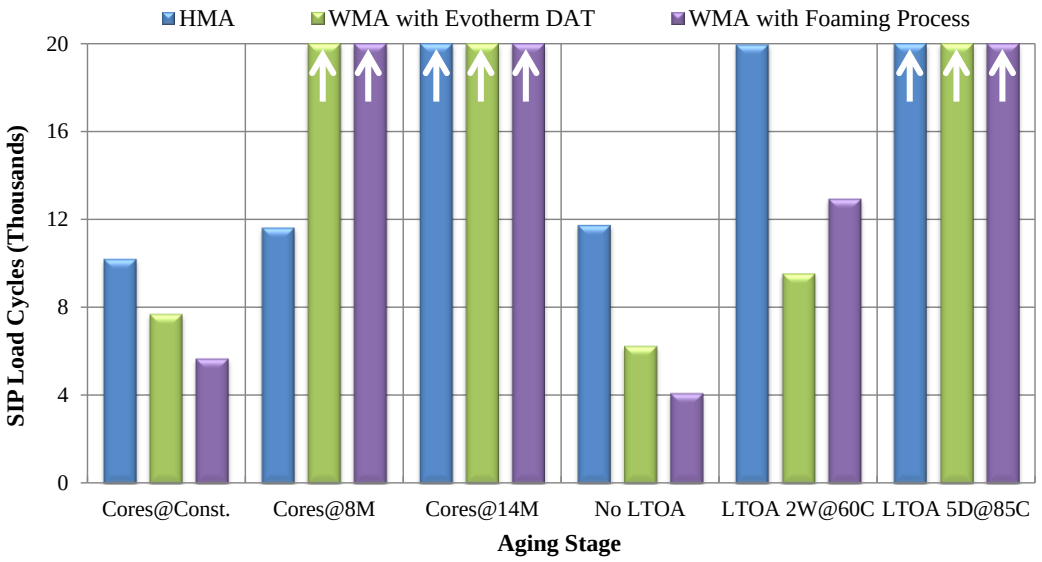

(a)

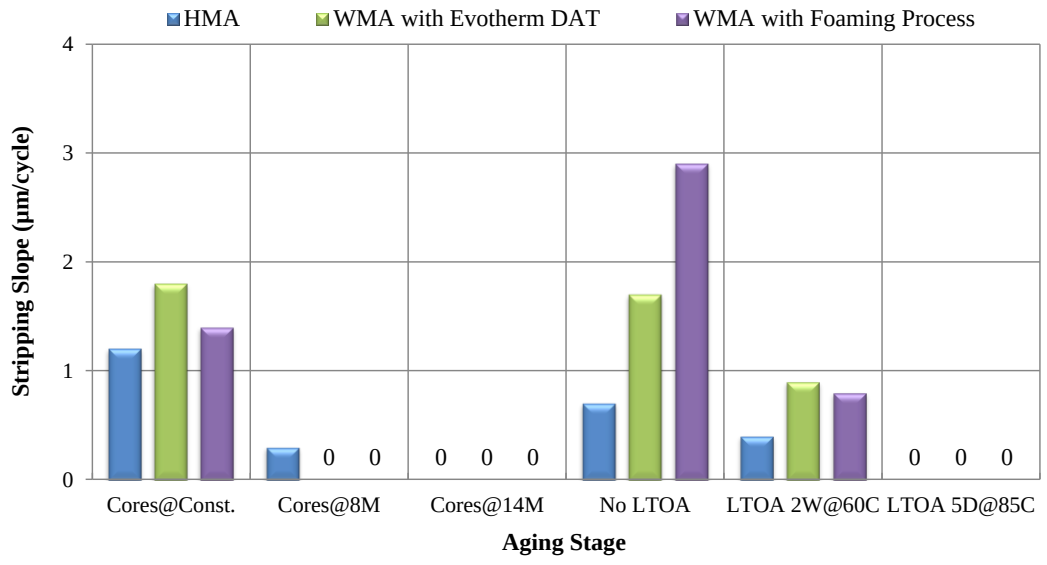

(b)

Figure 16. HWTT test results for the Texas field project; (a) SIP, (b) stripping slope.

As illustrated in Figure 15(a), the SIP values for all Iowa field cores at different in-service times are low, less than 5,000 load cycles. Considering the d2s threshold of

2,000 load cycles, the WMA mixtures were considered equivalent to their HMA counterparts for each field aging stage. For the stripping slope results shown in Figure 15(b), the performance of HMA was better than that of WMA with Sasobit®, but worse than that of WMA with Evotherm® 3G. HMA field cores after winter at six months in-service exhibited better moisture resistance than both WMA mixtures, as indicated by a significantly lower stripping slope. However, after summer at 12 months in-service, the difference in moisture susceptibility between both WMAs and HMA was reduced. Additionally, equal stripping slopes were shown by HMA and WMA with Evotherm® 3G, which was slightly lower than that of WMA with Sasobit®.

According to the HWTT results for the Texas field project (Figure 16), the moisture susceptibility of short-term aged specimens (i.e., field cores at construction, LMLC specimens without LTOA, and LMLC specimens with LTOA of two weeks at 140°F [60°C]) was better for HMA as compared to both WMA mixtures, as indicated by higher SIP values and lower stripping slopes. The results of field cores after summer at eight months in-service indicated that HMA had a lower SIP value and a higher stripping slope than the WMA mixtures, although the stripping slope for the HMA was insignificant. In the case of field cores after winter at 14 months in-service and LMLC specimens with LTOA protocol of five days at 185°F (85°C), no stripping was shown by either HMA or WMA mixtures, and therefore, equivalent performance in terms of moisture susceptibility was expected for these mixtures.

CHAPTER III

NOVEL METHOD FOR MOISTURE SUSCEPTIBILITY AND RUTTING EVALUATION USING HWTT*

Overview

The HWTT test is a laboratory procedure that utilizes repetitive loading in the presence of water and measures the rut depth induced in an asphalt mixture with increasing load cycles. During testing, rut depths at different positions along the specimens are recorded with each load cycle. The average rut depth of the center measurements is then plotted and presented as the output of the test. As shown in Figure 5, the resulting HWTT curves (i.e., rut depth at the center of the specimen versus load cycle) can be divided into the following three main phases: 1) post compaction phase, 2) creep phase, and 3) stripping phase (Solaimanian et al. 2003).

The post compaction phase consists of the consolidation of the specimen that occurs as the wheel load densifies the mixture and AV contents decrease significantly. This phase usually occurs within the first 1,000 load cycles. The creep phase is the deformation that occurs primarily due to the viscous flow of the asphalt mixture and is represented by an approximately constant rate of increase in rut depth with load cycle. The stripping phase starts once the bond between the asphalt binder and the aggregate starts degrading, causing visible damage such as stripping or raveling with additional

* Reprinted (with minor revisions) with permission from "Novel Method for Moisture Susceptibility and Rutting Evaluation Using Hamburg Wheel Tracking Test" by Fan Yin, Edith Arambula, Robert Lytton, Amy Epps Martin, and Lorena Garcia Cucalon, Washington, D.C., 2014, *Transportation Research Record: Journal of the Transportation Research Board*, No. 2446, pp. 1-7, Copyright [2014] by TRB.

load cycles. The SIP represents the number of load cycles on the HWTT curve where a sudden increase in rut depth occurs, mainly due to the stripping of the asphalt binder from the aggregate (Aschenbrener and Currier 1993). The SIP is graphically represented at the intersection of the fitted lines that characterize the creep phase and the stripping phase.

As discussed in Chapter II, the SIP and stripping slope, and rut depth at a certain number of load cycles are widely used as the main HWTT parameters to evaluate mixture moisture susceptibility and rutting resistance, respectively. Asphalt mixtures with higher SIP values and lower stripping slopes and rut depths are considered to have good performance in the HWTT. However, laboratory experience had indicated that these HWTT parameters were not always able to accurately evaluate mixture properties. For instance, mixture resistance to rutting could not be precisely characterized by rut depth at a certain number of load cycles due to the interacting effects on rut depth from both loading and stripping, especially for mixtures that were prone to stripping in the presence of water. Additionally, fitting two straight lines for the creep phase and the stripping phase was likely to introduce a significant bias to the evaluation of moisture susceptibility using the SIP because the post compaction phase was assumed to be the first 1,000 cycles and a one-mm rut depth was used to estimate the slope of the creep and striping phases.

In this research study, a novel methodology to analyze HWTT results was provided by curve fitting the entire output of rut depth versus load cycle. Three new parameters were proposed to evaluate mixture moisture susceptibility and rutting

resistance separately and with significantly improved accuracy. A detailed discussion of the new analysis methodology is presented in the following section.

Data Analysis Methodology

The rut depth versus load cycle HWTT output data is first plotted to obtain a typical curve for the test as shown in Figure 17. Then, Equation 3 is used to model the results.

$$RD_{LC} = \rho * \left[ln\left(\frac{LC_{ult}}{LC}\right)\right]^{-\frac{1}{\beta}} \quad \text{Equation 3}$$

where:

LC = number of load cycles;

RD_{LC} = rut depth at a certain number of load cycles (mm); and

LC_{ult}, ρ, and β = model coefficients.

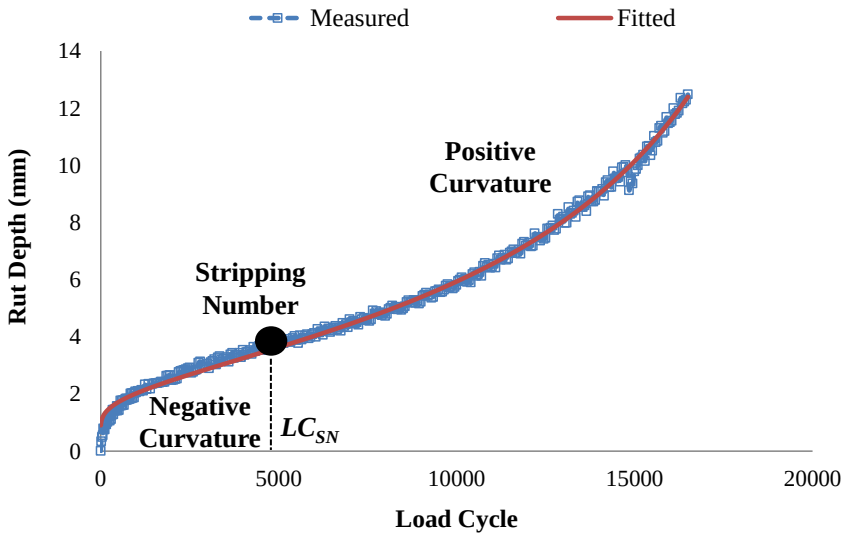

Figure 17. HWTT LC_{SN} determination.

The fitted curve is composed of one part with negative curvature followed by another part with positive curvature. In the part of the fitted curve with negative curvature, the mixture is expected to be stiffening by the action of the repeated wheel load and the rut depth is increasing due to the viscoplastic deformation of the asphalt mixture. Thus, this part of the curve can be used to evaluate mixture resistance to rutting in the presence of water. In the part of the fitted curve with positive curvature, the mixture is expected to be softening due to the stripping of the asphalt binder from the aggregate after water penetrates through the interface between the two components. The increasing rut depth in this part is more related to the stripping of the asphalt binder from the aggregate than the viscoplastic deformation of the mixture; and therefore, this part of the curve can be used to evaluate the mixture moisture susceptibility.

Moisture Susceptibility

The critical point of the HWTT results is where the curvature of the rut depth versus load cycle curve changes from negative to positive (i.e., inflection point). As shown in Figure 17, this point, referred to as the stripping number (LC_{SN}), is proposed as a parameter to quantify moisture susceptibility.

To determine the LC_{SN}, the second derivative of Equation 3 is set to zero. The derivation is determined as shown in Equation 4:

$$\frac{\partial^2 RD}{\partial LC^2} = \frac{\rho}{\beta * LC^2} * \left\{ \left(\frac{1}{\beta} + 1\right) * \left[ln\left(\frac{LC_{ult}}{LC}\right)\right]^{-\left(\frac{1}{\beta}+2\right)} - \left[ln\left(\frac{LC_{ult}}{LC}\right)\right]^{-\left(\frac{1}{\beta}+1\right)} \right\} \quad \text{Equation 4}$$

Setting Equation 4 to zero, the LC_{SN} is found as expressed in Equation 5:

$$LC_{SN} = LC_{ult} exp\left(-\frac{\beta + 1}{\beta}\right) \quad \text{Equation 5}$$

LC_{SN} represents the maximum number of load cycles that the asphalt mixture can resist in the HWTT before the adhesive fracture between the asphalt binder and the aggregate occurs. Mixtures with higher LC_{SN} values are expected to be less moisture susceptible as compared to those with lower LC_{SN} values. Mixtures that do not show a stripping phase in the HWTT are considered to have a robust resistance to moisture damage, with LC_{SN} values larger than the number of load cycles applied during the test (i.e., 20,000).

As previously mentioned, the rut depth accumulated before the SN is primarily related to the viscoplastic deformation of the asphalt mixture under loading. For the HWTT results, the viscoplastic strain in the specimen can be calculated as the ratio of the rut depth to the specimen thickness at any given number of load cycles up to LC_{SN}. A typical viscoplastic strain versus load cycle HWTT curve including the post compaction phase and part of the creep phase is presented in Figure 18(a). The Tseng-Lytton model (Tseng and Lytton 1989) employed to fit this part of the curve is shown in Equation 6:

$$\varepsilon^{vp} = \varepsilon_{\infty}^{vp} exp\left[-\left(\frac{\alpha}{LC}\right)^{\lambda}\right] \quad \text{Equation 6}$$

where:

$\varepsilon_{\infty}^{vp}$ = saturated viscoplastic strain in the HWTT specimen; and

α and λ = model coefficients.

The total rut depth of the HWTT specimen in the stripping phase has two components: the contribution from stripping and that due to further viscoplastic deformation under loading. Once $\varepsilon_{\infty}^{vp}$, α, and λ are determined from a non-linear regression analysis, the viscoplastic strain of the specimen can be projected into the stripping phase using Equation 6, as shown by the extended fitted curve in Figure 18(b). Therefore, the permanent strain induced by stripping (i.e., stripping strain) can be calculated by the difference between the total permanent strain and the projected viscoplastic strain in the stripping phase. The total permanent strain of the HWTT specimen is determined using Equation 7:

$$\varepsilon^{p} = \frac{RD_{(LC)}}{T} \qquad \text{Equation 7}$$

where:

ε^{p} = permanent strain; and

T = HWTT specimen thickness (mm).

Subtracting Equation 6 from Equation 7, the stripping strain of the HWTT specimen is calculated as described in Equation 8:

$$\varepsilon^{st} = \frac{RD_{(LC)}}{T} - \varepsilon_{\infty}^{vp} exp\left[-\left(\frac{\alpha}{LC}\right)^{\lambda}\right] \qquad \text{Equation 8}$$

where:

ε^{st} = stripping strain.

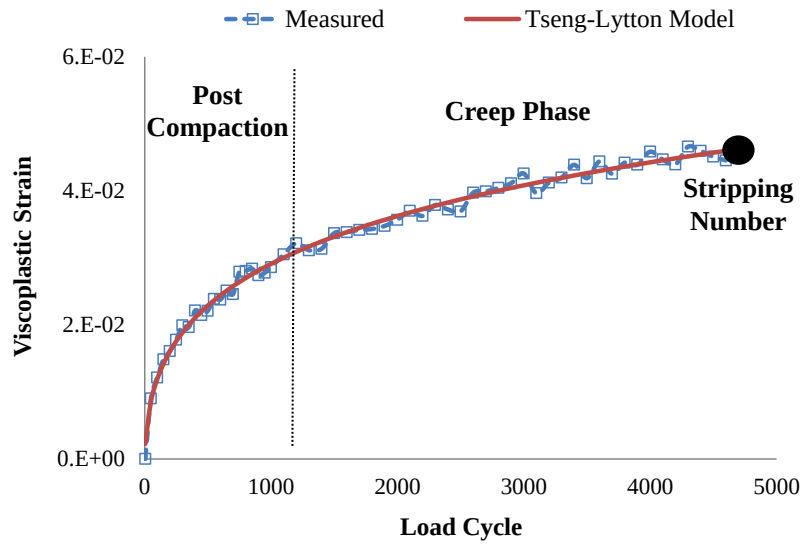

(a)

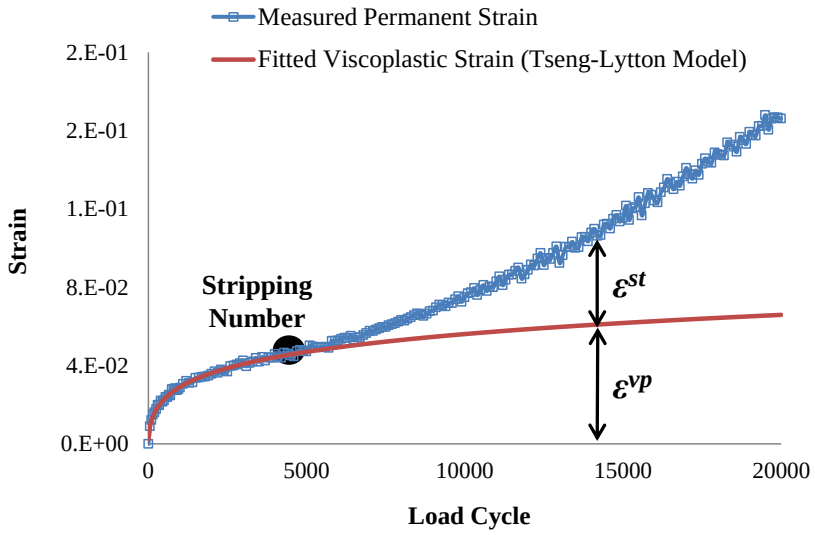

(b)

Figure 18. Typical viscoplastic strain behavior versus load cycle in HWTT; (a) fitted viscoplastic strain in post compaction and creep phases, (b) projected viscoplastic strain in strain phase.

A typical stripping strain versus load cycle HWTT curve is presented in Figure 19. As shown, the stripping strain is zero at load cycles up to LC_{SN}, and afterwards, it increases rapidly. A step function as expressed in Equation 9 is then used to model the stripping strain of the specimen:

$$\varepsilon^{st} = \varepsilon_0^{st}\{exp[\theta(LC - LC_{SN})] - 1\}, \; if LC - LC_{SN} \geq 0$$

$$\varepsilon^{st} = 0, \text{ if } LC - LC_{SN} \leq 0 \qquad \text{Equation 9}$$

where:

ε_0^{st} and θ = model coefficients.

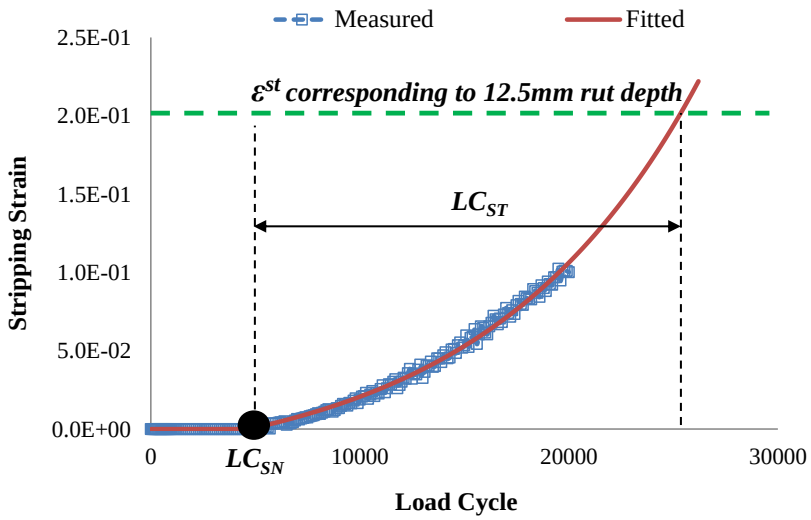

Figure 19. Typical stripping strain versus load cycle in HWTT.

To quantify rut depth accumulation due to stripping, the parameter stripping life (LC_{ST}) is proposed. As shown in Figure 19, it represents the number of additional load cycles after LC_{SN} needed for the rut depth accumulated by the predicted stripping strain to reach 0.5 inch (12.5 mm), which is the common HWTT failure criterion adopted by

several agencies. The stripping strain corresponding to 0.5 inch (12.5 mm) rut depth is calculated using Equation 10:

$$\varepsilon_{RD-12.5mm}^{st} = \frac{12.5}{T} \quad \text{Equation 10}$$

Making Equation 9 and Equation 10 equal, LC_{ST} is found as described in Equation 11:

$$LC_{ST} = \frac{1}{\theta}\ln\left(\frac{12.5}{T * \varepsilon_0^{st}} + 1\right) \quad \text{Equation 11}$$

Mixtures with higher LC_{ST} values are expected to be less moisture susceptible after the SN as compared to those with lower LC_{ST} values. LC_{ST} cannot be determined for mixtures that do not exhibit a stripping phase during the test.

Rutting Resistance

To quantify mixture resistance to rutting in the HWTT and compare different mixtures, the parameter viscoplastic strain increment ($\Delta\varepsilon^{vp}$) is proposed. This parameter is calculated as the slope of the projected viscoplastic strain by Tseng-Lytton model at a certain number of load cycles (i.e., 10,000 load cycles or LC_{SN}), as described in Equation 12:

$$\Delta\varepsilon^{vp} = \alpha^{\lambda}\lambda\varepsilon_{\infty}^{vp}\exp\left[-(\frac{\alpha}{LC})^{\lambda}\right](LC)^{-(\lambda+1)} \quad \text{Equation 12}$$

The determination of this HWTT rutting resistance parameter isolates the viscoplastic strain during the creep phase and does not include contributions from the post compaction phase due to different specimen AV or after the SN due to stripping of

asphalt binder from the aggregates. Asphalt mixtures with higher $\Delta\varepsilon^{vp}$ values are expected to be more susceptible to rutting than those with lower $\Delta\varepsilon^{vp}$ values.

Comparison of Test Parameters

Actual HWTT results for three different field mixtures (i.e., mixtures A, B, and C) were analyzed in this section using the new parameters. Comparisons of the $\Delta\varepsilon^{vp}$ value at 10,000 load cycles (i.e., $\Delta\varepsilon^{vp}_{10,000}$) versus rut depth at a certain number of load cycles and LC_{SN} and LC_{ST} versus SIP were performed to illustrate the capability of these parameters to characterize mixture rutting resistance and moisture susceptibility, respectively.

The HWTT results of rut depth versus load cycle for Mixture A and Mixture B are shown in Figure 20, together with rut depths at 5,000, 10,000, 15,000, and 20,000 load cycles. As illustrated, the rut depth of Mixture A was higher than that of Mixture B for the first 15,000 load cycles, while the opposite trend was shown with increasing load cycles. Therefore, an inconsistent conclusion in terms of evaluating rutting resistance of Mixture A versus Mixture B could be obtained based on the number of load cycles selected for the rut depth evaluation. Based on the shape of the HWTT test result for Mixture B, the mixture likely experienced the post compaction phase, creep phase, and stripping phase during the test. In other words, stripping occurred within the mixture before reaching 20,000 load cycles. Therefore, the accumulated rut depth of Mixture B after the SN resulted from both stripping and viscoplastic deformation. Additionally, a significant difference in rut depth in the post compaction phase between Mixture A and Mixture B is shown in Figure 20, which was likely attributed to the difference in mixture AV. Consequently, the characterization of mixture resistance to rutting in the HWTT on

the basis of rut depth at a certain number of load cycles might not necessarily describe adequately the behavior of the mixture.

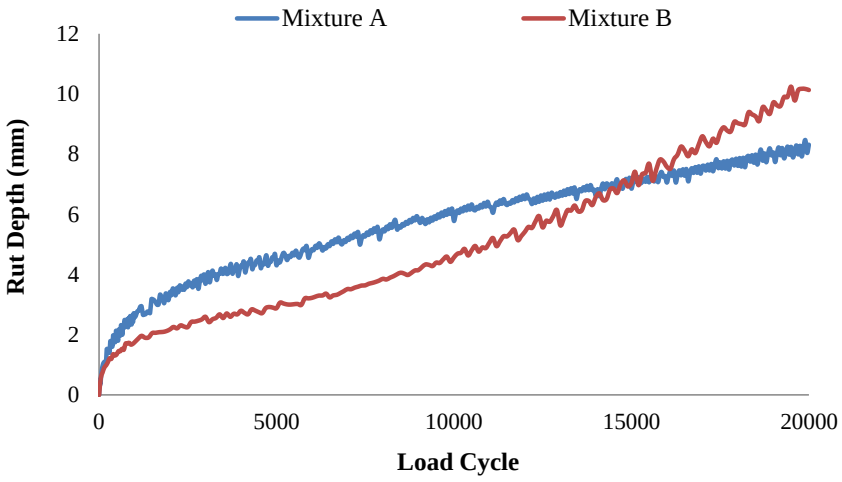

Mixture	Rut Depth at Certain Number of Load Cycle (mm)			
	5,000	10,000	15,000	20,000
Mixture A	4.3	5.8	6.9	8.3
Mixture B	2.9	4.6	7.0	10.1

Figure 20. HWTT results of rut depth at certain number of load cycles for Mixture A and Mixture B.

In order to better characterize mixture resistance to rutting, the point where stripping occurred were first determined. Additionally, the rut depths accumulated in the post compaction phase were discounted for an accurate rutting resistance analysis. LC_{SN} values for Mixture A and Mixture B were calculated to be 20,000 and 4,667 load cycles, respectively. Therefore, no stripping was exhibited by Mixture A, while stripping occurred at 4,667 load cycles for Mixture B. Figure 21 presents the permanent strain and the viscoplastic strain versus load cycles for Mixture A and Mixture B. As illustrated,

the fitted viscoplastic strain by the Tseng-Lytton model for Mixture A was higher than that for Mixture B, and additionally, a significantly different viscoplastic strain was shown in the post compaction phase between the two mixtures. In the creep phase, Mixture A was expected to be more susceptible to rutting than Mixture B, as shown by higher viscoplastic strain values. The new rutting resistance parameter $\Delta\varepsilon_{10,000}^{vp}$ for Mixture A and Mixture B was calculated to be 3.78 and 1.37 microstrain per load cycle, respectively, which verified the expectation that Mixture A was more susceptible to rutting as compared to Mixture B.

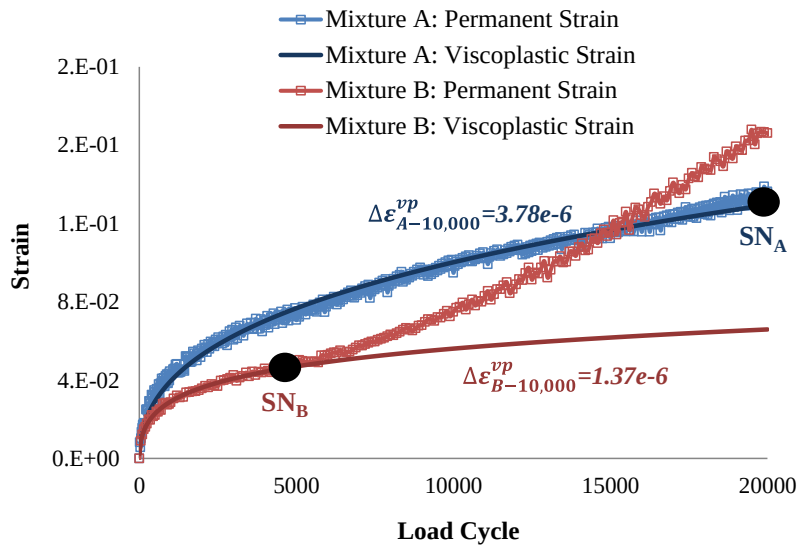

Figure 21. HWTT $\Delta\varepsilon_{10,000}^{vp}$ results for Mixture A versus Mixture B

The HWTT result of Mixture C as shown in Figure 22 was used to compare LC_{SN} and LC_{ST} versus *SIP* in terms of characterizing mixture moisture susceptibility. During the test, the mixture was continuously loaded for 20,000 load cycles regardless of if the

rut depth at the center of the specimen reached 0.5 inch (12.5 mm). The HWTT result of Mixture C was analyzed in two different ways: (1) with an ending point of a maximum of 20,000 load cycles [Figure 22(a)] and (2) with an ending point of a maximum rut depth of 0.5 inch (12.5 mm) [Figure 22(b)]. Two straight lines were used to fit the creep phase and the stripping phase and to calculate the SIP value for each case. As shown in Figure 22, the calculated SIP values were 16,199 and 14,113 depending on the ending point of the test. Thus for the same asphalt mixture (Mixture C) and the same test results, the SIP values were significantly different based on a d2s value of 2,000 load cycles (Epps Martin et al., 2014). Therefore, it was demonstrated with this example that using the SIP to characterize mixture moisture susceptibility is highly dependent on the ending point of the test, which could lead to biased results.

The new moisture susceptibility parameter LC_{SN} calculated for Mixture C with the two different ending points resulted in values of 4,032 and 4,051 for the long and short tests, respectively. This indicated that LC_{SN} was much less dependent on the ending point of the test and that the calculation avoided the bias resulting from data interpolation when fitting two straight lines for the creep phase and the stripping phase.

The other moisture susceptibility parameter LC_{ST} for Mixture C was calculated to be 15,690 and 15,860, for the long and short tests, respectively. In addition to the parameter of LC_{SN} for characterizing mixture moisture susceptibility before the SN, LC_{ST} was able to illustrate mixture performance in the HWTT after the SN. To summarize, the new parameters LC_{SN} and LC_{ST} were able to better characterize mixture moisture susceptibility in the HWTT as compared to the current SIP parameter.

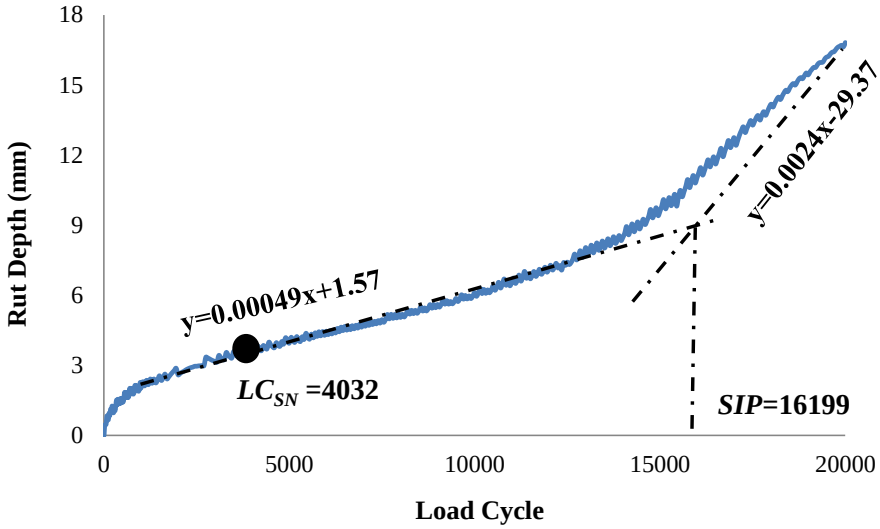

(a)

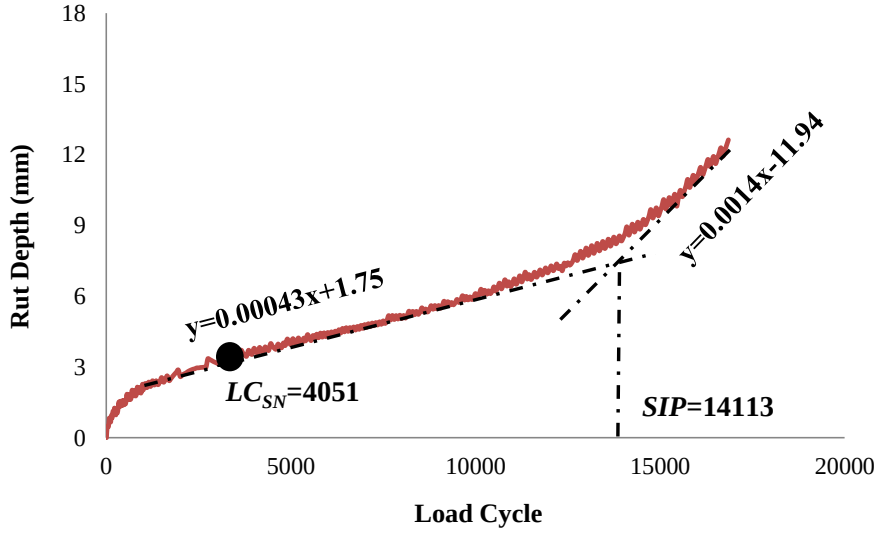

(b)

Figure 22. HWTT results of LC_{SN} and LC_{ST} versus SIP for Mixture C; (a) ending point of maximum of 20,000 load cycles, (b) ending point of maximum of 0.5 inch (12.5 mm) rut depth.

CHAPTER IV

ASPHALT FOAMING FOR WMA APPLICATIONS*

Overview

The use of WMA technology results in reduced production and paving temperatures without sacrificing the quality of the final product. There have been a number of products and processes introduced to produce WMA since 2005, including waxes, surfactants, mineral additives, and mechanical foaming process. This research study focused on exploring asphalt foaming technology for WMA applications since mechanical foaming process is currently the largest segment of the WMA market.

In the mechanical foaming process, small amounts of cold water are injected into a stream of binder heated to temperatures ranging between 320°F (160°C) and 360°F (182°C). The mixing of cold water and hot binder causes steam to form, resulting in volume expansion and subsequent viscosity reduction of the binder, and therefore, a better coating of the aggregate particles along with improved mixture workability.

While the mechanical foaming process is currently being widely used, there have been a number of questions surrounding the incorporation of water in the asphalt mixture production process. The main concern is whether the presence of water will have detrimental effects on mixture properties in terms of workability, coatability, or

---

* Reprinted (with minor revisions) with permissions from "Effect of Water Content on Binder Foaming Characteristics and Foamed Mixture Properties" by Fan Yin, Edith Arambula, and David Newcomb, Washington, D.C., 2015, *Transportation Research Record: Journal of the Transportation Research Board*, No. 2506, pp. 1-7, Copyright [2015] by TRB, and "Workability and Coatability of Foamed Warm-Mix Asphalt" by Fan Yin, Edith Arambula, David Newcomb, and Amit Bhasin, 2014, *Proceedings of the 12th International Society for Asphalt Pavements Conference*, pp. 721-730, Copyright [2014] by ISAP.

performance. Additionally, laboratory test methods for measuring the asphalt foaming process have several limitations, as will be discussed later, and the effects from various foaming components on asphalt foaming characteristics have not been fully explored. Finally, foamed asphalt mixtures have been currently designed in accordance with the traditional HMA procedure, which is not able to ensure foamed mixtures with desirable performances.

Therefore, the objectives of this research study to: 1) develop test methods and metrics to characterize asphalt foaming and foamed mixture, 2) evaluate the effects of foaming water content and laboratory foamer type on asphalt foaming characteristics and foamed mixture properties, and 3) develop a mix design procedure for foamed asphalt mixtures.

Test Methods and Metrics to Characterize Asphalt Foaming

A review of literature on previous studies shows that a graduate dipstick is commonly used to characterize asphalt foaming in terms of the maximum expansion ratio (ER_{max}) and half-life (HL) (Abel 1978; Brennen et al. 1983; He and Wong 2006; Jenkins 2000; Namutebi 2011). The ER_{max} is defined as the ratio of the maximum volume of foamed asphalt binder to the volume occupied by the same mass of the binder without any water or foam in it; the HL is defined as the time required for the foamed asphalt binder to collapse to half of its maximum volume. The general trend is that ER_{max} increases and HL decreases with higher foaming water contents (within the range of 1 percent to 6 percent). However, the measurements of ER_{max} and HL using the dipstick method has some of the limitations including: 1) visual observation of the foam height

and time which is subjective and could potentially bias the test results and 2) using only two instantaneous parameters to describe the entire asphalt foaming process.

A non-contact test method was proposed in this research study for measuring the entire asphalt foaming process, and the test setup is shown in Figure 23. A laser device consisting of an emitter and a detector to measure the distance from the device to a reflecting surface based on the phase-shift principle and a digital camera were mounted on two tripods aligned vertically and perpendicularly to the ground. Both the laser device and the camera were connected to a laptop for remote control and data acquisition. The laser device was able to collect a distance reading every one second based on the difference in time between when the laser light is emitted and received. The digital camera was set in continuous shooting mode with a one-second delay between each image.

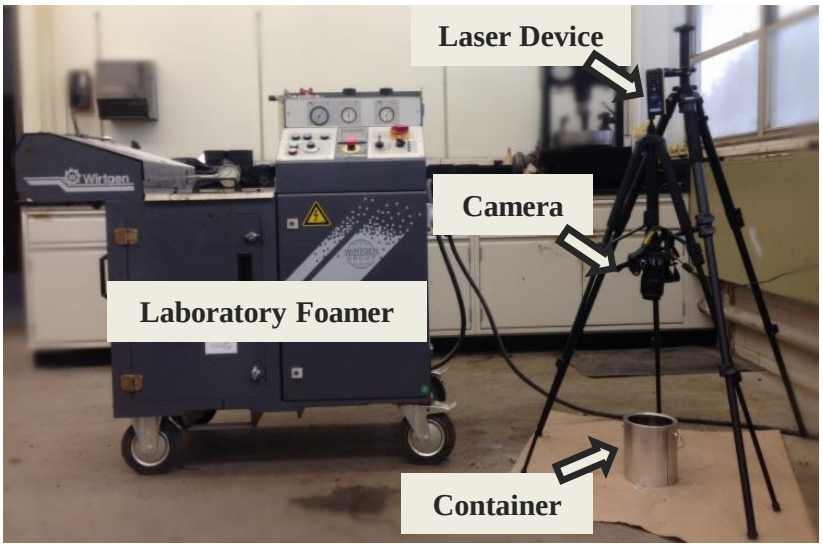

Figure 23. Laboratory test setup for measuring asphalt foaming.

To capture the entire dynamic foam expansion and collapse process, a certain amount of foamed asphalt at a specific foaming water content was produced in the laboratory foamer, and then dispensed into a container. Afterward, the container filled with the foamed asphalt sample was positioned under the tripods for data acquisition. Distance data was measured from the laser device to the surface of the foamed asphalt sample, while digital images of the surface foam bubbles were continuously captured until no significant changes in foam height could be visually observed.

The expansion ratio (*ER*) was calculated with distance data measured by the laser device and the final height of the foamed asphalt. A typical plot of *ER* over time is presented in Figure 24. Then, an exponential function was used to fit the *ER* results, as expressed in Equation 13.

$$ER(t) = 1 + ae^{-bt} + (ER_{max} - a - 1)e^{-ct} \quad \text{Equation 13}$$

where:

ER(t) = *ER* at time *t*; and

a, b, and c = fitting coefficients.

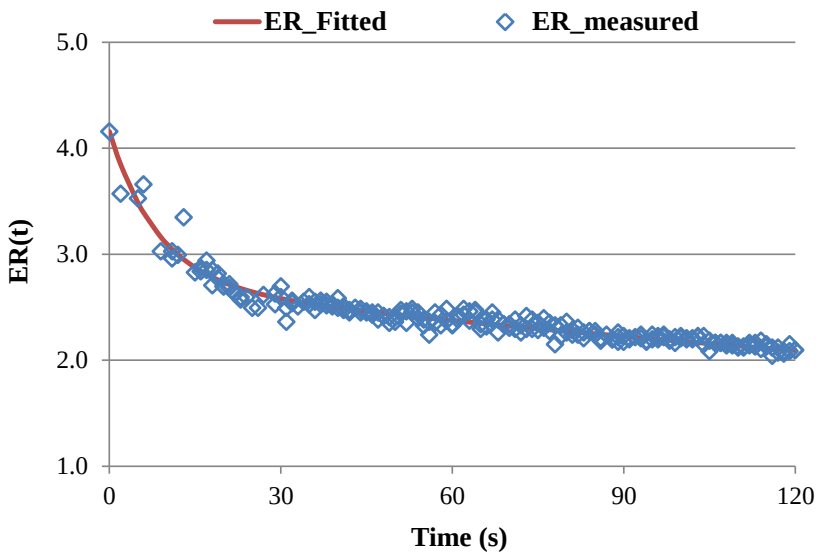

Figure 24. A typical plot of asphalt foaming *ER* with time.

In this study, ER_{max} was used as a asphalt foaming parameter to quantify the maximum volume expansion created by the foaming process. In addition, the foamability index (*FI*), which was defined as the area under the *ER* curve at a selected time, was proposed as another parameter for evaluating binder foam expansion and collapse over time. The determination of *FI* was expressed in Equation 14. Foamed asphalts with higher ER_{max} and *FI* values were expected to have higher expansion and better stability than those with lower values.

$$FI(t) = \int_0^t ER(t)\, d(t) \qquad \text{Equation 14}$$

Figure 25 presents the digital images of surface foam bubbles captured at 30, 60, and 90 seconds after the start of the foaming process. As can be observed, the surface foam bubbles decreased in size with elapsed time and became more homogeneous in terms of size distribution. Assuming that the binder volume expansion was created by

sphere-shaped foam bubbles and that the size distribution of foam bubbles observed at the surface was the same throughout the sample depth, the total number of volume foam bubbles in the foamed asphalt sample at a specific time could be estimated using Equation 15 through Equation 19.

Figure 25. Digital images of surface foam bubbles at various times.

$$V_f(t) = \frac{\pi {D_0}^2 h_f(t)}{4} \quad \text{Equation 15}$$

where:

$V_f(t)$ = the volume of foamed asphalt at time t;

D_0 = the diameter of the sampling container for foamed asphalt; and

$h_f(t)$ = the height of foamed asphalt at time t.

$$V_{af}(t) = \frac{\pi {D_0}^2 h_{af}}{4} \quad \text{Equation 16}$$

where:

$V_{af}(t)$ = the volume of asphalt after foaming; and

h_{af} = the height of asphalt after foaming.

$$h_f(t) = h_{af} ER(t) \quad \text{Equation 17}$$

$$V_{fb}(t) = V_f(t) - V_{af}(t) \quad \text{Equation 18}$$

where:

$V_{fb}(t)$ = the volume of foam bubbles at time *t*.

$$N_{fb}(t) = \frac{\pi\left(\frac{D_0}{2}\right)^2 h_{af}[ER(t)-1]}{\sum_1^{N_{sfb}(t)} \frac{\pi\left[D_{sfb-i}(t)\right]^3}{6}} N_{sfb}(t) \quad \text{Equation 19}$$

where:

$N_{fb}(t)$ = number of volume foam bubbles at time *t*;

$N_{sfb}(t)$ = number of surface foam bubbles at time *t* (obtained from counting foam bubbles using digital images); and

$D_{sfb\text{-}i}(t)$ = diameter of the i^{th} surface foam bubble at time *t*.

Knowing the total number and size distribution, the total surface area of all volume foam bubbles could be calculated as described in Equation 20, of which a high value was desirable as more asphalt surfaces would be available for coating the aggregate particles during mixing. In addition, the surface area of the asphalt prior to foaming was calculated using Equation 21.

$$SA_{fb}(t) = \frac{N_{fb}(t)}{N_{sfb}(t)} \sum_1^{N_{sfb}(t)} \pi\left[D_{sfb-i}(t)\right]^3 \quad \text{Equation 20}$$

where:

$SA_{fb}(t)$ = the total surface area of volume foam bubbles at time *t*.

$$SA_{ufb} = \pi D_0\left(\frac{D_0}{2} + h_{af}\right) \quad \text{Equation 21}$$

where:

SAu_{fb} = the surface area of the asphalt prior to foaming.

Finally, the surface area index (*SAI*) was proposed as another asphalt foaming parameter to quantify the surface area evolution of foam bubbles over time. As

expressed in Equation 22, the *SAI* value referred to the ratio of the total surface area of all foam bubbles over the surface area of the asphalt prior to foaming. Foamed asphalts with higher *SAI* values were expected to have more asphalt surfaces available and therefore, a better aggregate coating ability.

$$SAI(t) = \frac{SA_{fb}(t)}{SA_{ufb}} \quad \text{Equation 22}$$

To sum up, three parameters of ER_{max}, *FI*, and *SAI* were proposed in this study for characterizing the entire asphalt foaming process in terms of volume expansion and collapse and foam bubble evolution. Foamed asphalts with higher ER_{max}, *FI*, and *SAI* values were expected to have better foaming characteristics in terms of volume expansion, stability, and aggregate coatability during mixing.

Test Methods and Metrics to Characterize Foamed Mixtures

One of the major unknowns in the application of asphalt foaming for WMA is that, to date, there have been no established relationships between asphalt foaming characteristics to foamed mixture workability, coatability, or performance. Foaming is intended to improve mixture workability and coatability from reduction in binder viscosity due to the binder volume expansion. Therefore, it is important to evaluate the workability and coatability of foamed asphalt mixtures.

Workability of asphalt mixtures is a property that describes the ease with which the mixture can be placed, worked by hand, and compacted. It is a function of temperature, binder properties (e.g., viscosity, grade, polymer modification, etc.), aggregate properties (e.g. size, angularity, etc.), among other factors. Coatability of

asphalt mixtures is defined as the degree of coating of the aggregates by the asphalt binder. This parameter is important to the performance of asphalt mixtures, since well-coated aggregates are likely to have a stronger bond between the particle and the binder, and thus a better resistance to moisture damage and other distresses.

In this research study, a novel test method was proposed to evaluate the workability of foamed asphalt mixtures using SGC compaction date (i.e., shear stress versus number of gyrations). In addition, a test method based on the aggregate absorption method originally developed by Velasquez et al. (2012) was develop to characterize the coatability of foamed asphalt mixtures. Detailed information regarding the workability and coatability test methods and metrics are introduced in the following sections.

Workability

A SGC was used for the workability evaluation, which was operated based on a "shear-compaction" principle. During compaction, the loose mix particles reoriented under the vertical and shear pressure for a target number of gyrations (i.e., 300) to ensure that a maximum shear stress (τ_{max}) was achieved (DeSombre et al. 1998).

After sieving, the aggregates were combined into individual batches according to the volumetric mix design and pre-heated in the oven to the mixing temperature. The asphalt binders were heated in the oven for two to three hours prior to transfer to the laboratory foamer. The laboratory foamer (i.e., Wirtgen WLB 10S) was calibrated according to the manufacturer's recommendation. The pre-heated aggregate batch was introduced into the mixer bucket and the portable mixer was placed under the laboratory

foamer, as shown in Figure 26. The specific amount of foamed asphalt was dispensed into the bucket mixer as it was running. The mixer was stopped after 60 seconds and the loose mix was placed back into the oven for two hours at 275°F (135°C) for HMA and 240°F (116°C) for foamed WMA to achieve the proper short-term aging (Yin et al., 2013).

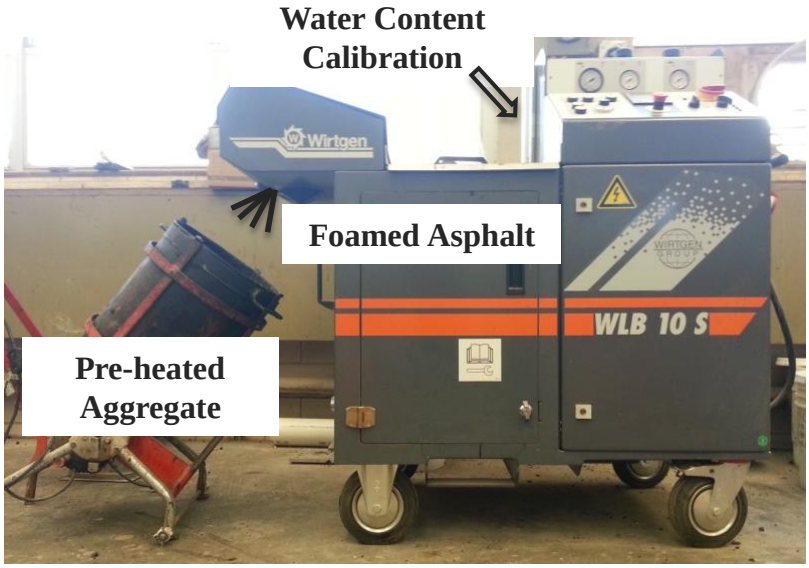

Figure 26. Mixing aggregates with foamed asphalts.

The loose mix was divided into individual specimen size batches (4,700g per batch) after the short-term aging and then compacted. During compaction, the shear stress was continually monitored and plotted for each gyration. As shown in Figure 27, compaction was stopped after a significant reduction in shear stress was observed, which usually occurred between 200 and 300 gyrations.

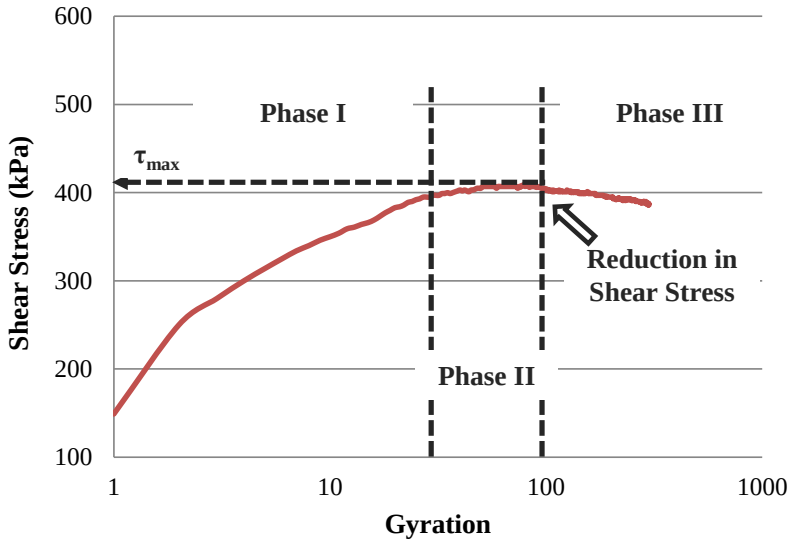

Figure 27. Typical shear stress versus number of SGC gyrations curve.

Figure 27 presents a typical curve of the shear stress versus number of SGC gyrations during compaction. As illustrated, the curve could be divided in three phases. In the first phase, the slope of the shear stress curve was steep. The loose mix particles were being reoriented due to the initial compaction, and there was a significant increase in the internal friction within the mixture due to the stone-on-stone contact resulting from loose mix particles reorientation. The shear stress started to level off in the second phase. The density of the mixture was expected to be near or at the target value somewhere in this phase. The third phase started when a decrease in shear stress was observed. The reduction in shear stress was partially attributed to the dominant effect of pore pressure. For practical applications, the third phase in the compaction process was avoided to prevent aggregate crushing after the maximum density was achieved.

According to DeSombre et al. (1998), the shear stress versus SGC gyration curve could be used to determine the compaction characteristics of asphalt mixtures. Specifically, asphalt mixtures which compacted more rapidly (steeper slope in loose mix height versus number of gyration curve) in the first few gyrations were expected to have a higher shear stress level afterwards, due to increased internal friction within the mix. In addition, mixtures with a lower shear stress levels were expected to have better workability than those with a higher shear stress level. Therefore, the τ_{max} value measured in the SGC compaction curve was proposed as the parameter to evaluate mixture workability.

Coatability

The method used for evaluating the coatability of foamed asphalt mixtures was primarily based on the aggregate absorption method originally developed by Velasquez et al. (2012). The method was based on the assumption that a completely coated aggregate had no access to water absorption when submerged in water for a short period (i.e., one hour), as water could not penetrate through the asphalt film surrounding the aggregate surface. Conversely, a partially coated aggregate was expected to have detectable water absorption, as water was able to penetrate and be absorbed by the uncoated particle. The following procedure was used to determine coatability of the asphalt mixtures.

After sieving, coarse aggregate fractions retained on the 3/8-inch sieve were combined into two individual batches (4,000g per batch) following mix design, with one batch pre-heated in the oven at the mixing temperature while the other was stored at the

room temperature. The amount of binder for the coarse aggregate fraction batch was determined based on the total binder content specified in the mix design and the surface area distribution of the coarse aggregate fraction. The amount of binder for mixing with the 4,000g coarse aggregate fraction batch was calculated using Equation 23.

$$W_b = 4{,}000 * \frac{P_b}{1 - P_b} * \frac{SA_{coarse}}{SST} * \frac{1}{P_{s-coarse}} \qquad \text{Equation 23}$$

where:

W_b = amount of foamed asphalt for mixing with a 4,000g coarse aggregate batch;

P_b = mix design asphalt binder content;

SA_{coarse} = surface area of the coarse aggregate fraction;

SST = total surface area of the mix design combined aggregates; and

$P_{s\text{-}coarse}$ = percentage of coarse aggregates by the combined aggregates.

The same mixing and short-term aging procedure as those used in the workability evaluation were used to mix the coarse aggregate fraction batch with foamed asphalt and to short-term age the loose mix. The loose mix was taken out of the oven after short-term aging and cooled down to room temperature. The loose mix batch and the coarse aggregate fraction were each submerged under water for one hour. Afterwards, these two batches were damp-dried with a terry cloth to achieve the saturated-surface dry (SSD) condition. The SSD weights of the loose mix batch and coarse aggregate fraction batch were recorded as $W_{loose\text{-}SSD}$ and $W_{agg\text{-}SSD}$, respectively. The water absorption for the loose mix batch and the coarse aggregate fraction batch were determined using Equation 24 and Equation 25, respectively.

$$Abs\ percent_{loose} = \frac{W_{loose-SSD} - (4{,}000 + W_b)}{4{,}000 + W_b} * 100\% \qquad \text{Equation 24}$$

$$Abs\ percent_{agg} = \frac{W_{agg-SSD} - 4{,}000}{4{,}000} * 100\% \quad \text{Equation 25}$$

The coatability index (*CI*), as expressed in Equation 26, was proposed as the parameter for evaluating mixture coatability. Asphalt mixtures with higher *CI* values were expected to have a better aggregate coating by the asphalt binder than those with lower *CI* values.

$$CI = \frac{Abs\%_{agg} - Abs\%_{loose}}{Abs\%_{agg}} * 100\% \quad \text{Equation 26}$$

Effect of Selected Variables on Asphalt Foaming Characteristics and Foamed Mixture Properties

Foaming Water Content

Materials used in this research study were procured from an asphalt plant located in Huntsville, Texas. The plant was an Astec Double Barrel with a shear/colloid mill foaming unit located approximately 15-ft. away and 3-ft higher than the inlet to the drum. The asphalt binder used was a PG 64-22 and the optimum binder content per mix design was 4.5 percent. Limestone was the primary aggregate used in the mixture along with sandstone and 20 percent RAP. The mixture used was a Type C mix per Texas Department of Transportation (TxDOT) specification with a 19.0-mm NMAS.

Figure 28 presents the experimental design followed in this section. During the first plant visit on November 29, 2013, the plant was producing foamed mixtures with 5.5 percent water content at approximately 300°F (149°C). Asphalt foaming characteristics produced by the plant foaming unit were measured on-site using the laser device and the digital camera on a side platform. Foamed loose mix produced at the

plant was sampled from the trucks after being loaded from the silo and then transported back to the laboratory (approximately 60 miles away from the plant) for fabricating PMLC specimens and evaluated for their workability. Raw materials including virgin asphalt binder, aggregates, and RAP were also sampled during the visit.

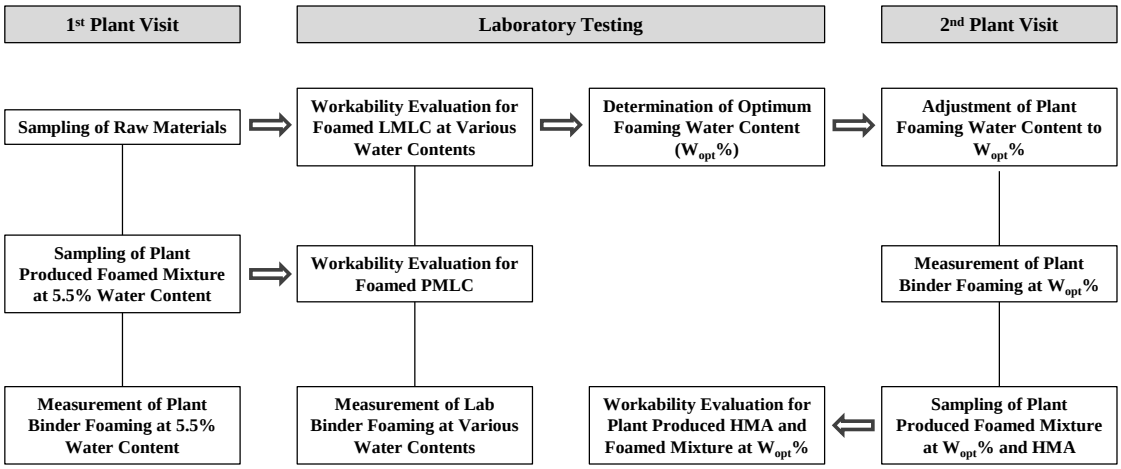

Figure 28. Experimental design for evaluating the effect of foaming water content

In the laboratory, asphalt was foamed using a laboratory foamer at the following water contents: 0.7 percent (which was the minimum water content the equipment was able to output), 1.0 percent, 1.5 percent, 2.0 percent, 3.0 percent, and 5.5 percent. Evaluation of asphalt foaming characteristics and foamed mixture workability were performed to determine an optimum foaming water content (W_{opt}), referring to the specific water content at which the laboratory foamed mixture had the best workability. Afterwards, foamed LMLC specimens were fabricated at the W_{opt} for performance evaluation and comparison to the performance of the HMA counterpart.

Asphalt Foaming Characteristics

Figure 29 presents the ER_{max} and *FI* values at 60 seconds results of the on-site and laboratory asphalt foaming measurements. The dots and bars represent the average ER_{max} and *FI* value of three replicate measurements, respectively.

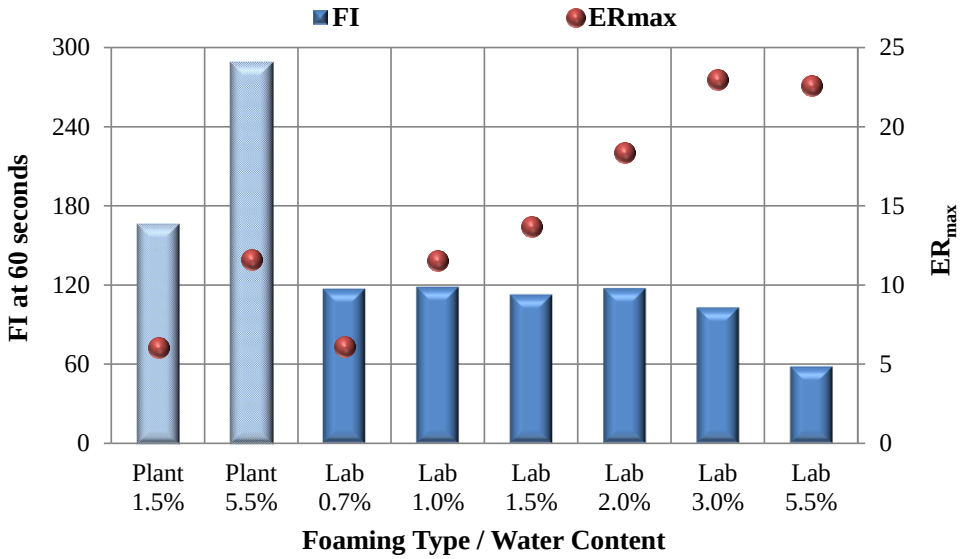

Figure 29. ER_{max} and *FI* results of plant and laboratory asphalt foaming measurements at various foaming water contents.

As illustrated, a direct correlation was observed for both plant and laboratory asphalt foaming measurements between ER_{max} and water content, with ER_{max} increasing with higher water contents. As compared to the laboratory asphalt foaming measurement, the on-site plant measurement showed significantly lower ER_{max} values at the same foaming water contents of 1.5 percent and 5.5 percent. However, an equivalent increase

in ER_{max} value proportional to the amount of water used in the foaming process was presented for plant and laboratory asphalt foaming measurements.

Equivalent *FI* values were achieved for laboratory asphalt foaming measurements at 0.7 percent, 1.0 percent, 1.5 percent, and 2.0 percent, while reduced values were shown for higher foaming water contents of 3.0 percent and 5.5 percent. Therefore, as more water was used in the foaming process, the asphalt foaming achieved a higher volume expansion but also a faster foam collapse rate, which ultimately led to lower stability. However, an opposite trend was observed for plant asphalt foaming measurements, where foamed asphalt at 1.5 percent water content exhibited lower stability as indicated by a lower *FI* value than that at a higher water content of 5.5 percent. In addition, the comparison between plant asphalt foaming versus laboratory asphalt foaming showed that plant asphalt foaming had a significant higher *FI* value at 60 seconds than the laboratory-foamed sample at the same water contents.

The *SAI* values at 60 seconds obtained from the analysis of the digital images acquired during the foaming process are illustrated in Figure 30. The results showed a distinctive trend of *SAI* values increasing with water content up to a certain value of about 2.0 percent, after which the *SAI* value decreased significantly. Similar with the *FI* results, the significant reduction in *SAI* values at higher foaming water contents was likely attributed to the dominant effect of the foam collapse rate. As compared to the laboratory asphalt foaming measurement, the plant asphalt foaming measurement showed a significantly higher *SAI* value at the same water content of 1.5 percent. The determination of the *SAI* value for plant asphalt foaming at 5.5 percent was not available

since no distinguishable surface bubbles were observed from the digital images acquired during the on-site foaming process although foaming did occur.

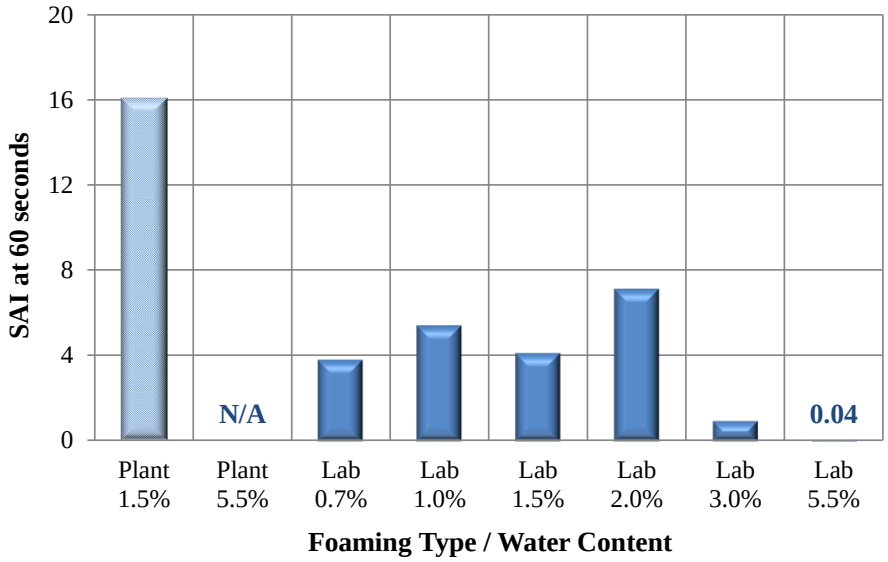

Figure 30. *SAI* results of plant and laboratory asphalt foaming measurements at various foaming water contents.

In general, the amount of water used in the foaming process had a significant effect on asphalt foaming characteristics. Higher water contents produced higher foamed asphalt volume expansion but also lower stability due to faster collapse rate, as indicated by the higher ER_{max} and lower *FI* values. A positive correlation between *SAI* and water content was observed at low water contents (i.e., 0.7 percent to 2.0 percent) while the opposite trend was shown for higher water contents. The magnitude of *SAI* value was dependent on the competing mechanisms between the quantity and size of foam bubbles in the asphalt volume. A significant difference in asphalt foaming characteristics at the

same water content was observed for plant produced asphalt foaming versus laboratory produced asphalt foaming, and the difference was likely attributed to the different foaming mechanisms involved in the plant foaming unit versus the laboratory foamer.

Foamed Mixture Properties

The workability results in terms of τ_{max} values obtained for HMA and foamed LMLC specimens produced at various foaming water contents in the laboratory foamer are shown in Figure 31(a). As can be observed in the figure, the τ_{max} value for the foamed specimens decreased as foaming water content increased from 0.7 percent to 1.5 percent while the opposite trend was observed when the water contents was higher than 1.5 percent. Therefore, 1.5 percent was considered the W_{opt}, able to yield the best workability characteristic (i.e., the lowest τ_{max} value). In addition, an equivalent τ_{max} value was observed for control HMA and the foamed mixtures at 1.0 percent and 1.5 percent foaming water contents, while higher τ_{max} values were shown by foamed mixtures produced at the other foaming water contents.

After the W_{opt} was determined, water content for the plant foaming unit was adjusted from 5.5 percent to 1.5 percent during the second visit to the asphalt plant. The workability results for PMLC specimens at adjusted foaming water content of 1.5 percent was compared to those of plant produced HMA and foamed mixture at 5.5 percent foaming water content acquired during the first plant visit and shown in Figure 31(b). The plant produced foamed mixture at 1.5 percent foaming water content had a better workability as indicated by a lower τ_{max} value than both HMA and foamed mixture with 5.5 percent water content, which was consistent with the workability results

obtained for the foamed LMLC mixtures. Therefore, the W_{opt} obtained via workability evaluation for foamed LMLC specimens was verified by plant foaming.

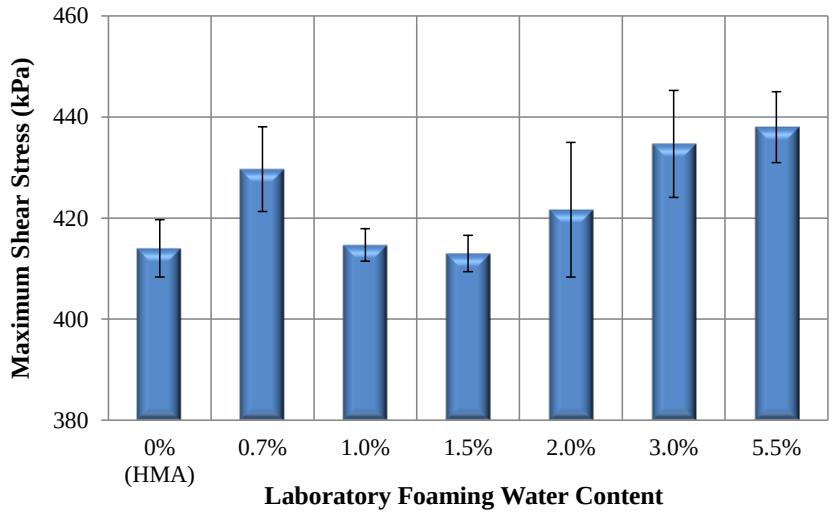

(a)

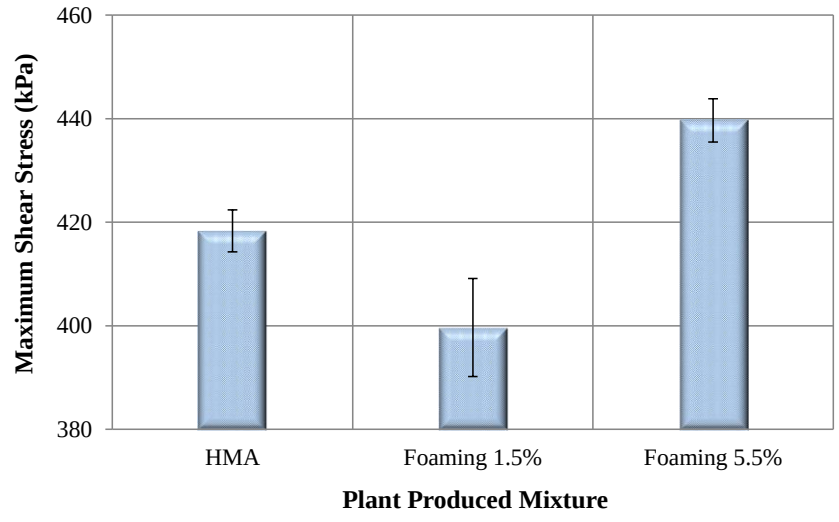

(b)

Figure 31. Workability results for various foaming water contents; (a) laboratory produced foamed mixture, (b) plant produced foamed mixture.

Laboratory Foamer

Figure 32 presents three commonly used commercially available laboratory foamers; the Wirtgen WLB 10S (Wirtgen foamer), the InstroTek Accufoamer (InstroTek foamer), and the Pavement Technology Inc. Foamer (PTI foamer).

(a) (b) (c)

Figure 32. Laboratory foamers; (a) Wirtgen foamer, (b) InstroTek foamer, (c) PTI foamer.

The Wirtgen foamer is designed to regulate a specific amount of dispensed asphalt and water by mass flow meters. The asphalt is heated to a temperature ranging from 284°F (140°C) to 392°F (200°C) and circulated inside the foamer. The foamed asphalt is produced by combining specific quantities of water, compressed air, and asphalt inside an expansion chamber. During the process, the added water vaporizes and causes the asphalt to foam. Afterwards, the foamed asphalt is dispensed directly from the nozzle into the mixer, where it is combined with the preheated aggregates. The Wirtgen

foamer is able to dispense about 0.4 lb. (200 grams) of asphalt in 2 seconds due to the high pressure at which the water and air are injected (approximately 72 psi).

The InstroTek foamer is designed to deliver a specific amount of asphalt and water by regulating the overhead pressure. It is recommended by the manufacturer to calibrate the foamer prior to use by a trial-and-error process in order to determine the time required to deliver a specific amount of hot asphalt and water at a fixed driving pressure and at various pressures, respectively. The InstroTek foamer comes with an Excel spreadsheet programmed with the relationship between the foaming water content and the overhead pressure for a given flow rate. Once the calibration parameters are set in the spreadsheet, it can be used to determine the flow time required to produce the desired amount of foamed asphalts at any given foaming water content and overhead pressure.

The PTI foamer is designed to regulate a specific amount of dispensed asphalt by a load cell. An air pipe charged with a pressure ranging from 80 psi (552 kPa) to 110 psi (758 kPa) is connected to the main regulator to actuate the foamer and to charge a water reservoir. A small amount of air is used to atomize the water to fine water droplets, which are expected to promote the asphalt volume expansion. During the foaming process, the asphalt is discharged from the reservoir by actuating a pneumatic cylinder. Then, the pneumatic cylinder closes and the flow of asphalt is pinched. The PTI foamer is able to accommodate up to 14 lb. (6.4 kg) of asphalt in the chamber. In addition, the position of the chamber can be adjusted along the frame to meet the height requirements for different laboratory mixers.

Table 1 summarizes the main features and parameters of the three laboratory foamers investigated in this study. Notable differences are shown while comparing the three foamers, mainly with regard to: 1) the type of nozzle that sprays the asphalt and water and 2) the pressure charged on the asphalt, water, and air to mix in the expansion chamber. Therefore, the three laboratory foamers may produce significantly different asphalt foaming characteristics and foamed mixture properties.

Table 1. Summary of Laboratory Foamer Characteristics

Characteristic	Wirtgen foamer	InstroTek foamer	PTI foamer
Air flow pressure	Min. 15 psi (100 kPa)Max. 145 psi (1000 kPa)	Min. 75 psi (517 kPa), Max. 150 psi (1034 kPa)	Min. 80 psi (552 kPa) Max. 110 psi (758 kPa)
Water flow pressure	Max. 145 psi (1000 kPa)	Max. 30 psi (207 kPa)	33 psi (230 kPa)
Asphalt flow pressure	Max. 145 psi (1000 kPa)	Max. 60 psi (413 kPa)	The asphalt is dispensed by gravity
Reaction chamber	Water and compressed air are injected into the hot asphalt.	Pressurized asphalt and water meet at a single junction.	A small amount of air is used to atomize the water to a fine droplet.
Asphalt temperature	284–392°F (140–200°C)	320-390°F (160-200°C)	Max 350°F (177°C)
Discharge time	100 g/s	16-20 g/s	14-20 g/s
Mass control	Mass flow control	Overhead pressure control	Scale control
Asphalt chamber size	5.3 gallon (20.0 L)	1.7 gallon (6.6 L)	1.6 gallon (6.4 L)
Foaming water content	0 percent–5 percent	0 percent–9 percent	1 percent–7 percent
Water temperature	No heat	Max. 180°F (82°C)	No heat

According to Newcomb et al. (2015), asphalt mixture components such as asphalt source, asphalt grade, aggregate source, etc. have a significant effect on asphalt foaming characteristics and foamed mixture properties, and therefore, the laboratory

foamer type was included as the only variable in this research study, while others factors were kept constant. Materials used in this research study were provided by Pavers Supply Company from their plant located in Huntsville, Texas. The asphalt binder was a PG 64-22, and the optimum asphalt binder content per mix design was 4.5 percent. Limestone was the primary aggregate used in the mixture along with manufactured sand and washed sand. The mixture was a Type C mix per TxDOT specification with 9.5-mm NMAS.

Foamed asphalts were produced at various foaming water contents ranging from 1 percent to 3 percent by the Wirtgen foamer, the InstroTek foamer, and the PTI foamer. The asphalt foaming characteristics were measured by the non-contact test method described previously. The results were used to identify the effects of the laboratory foamer on asphalt foaming characteristics. In addition, the workability and coatability of foamed mixtures produced at various foaming water contents by the three laboratory foamers were also evaluated. The W_{opt} for each laboratory foamer was determined based on the τ_{max} and *CI* results, where W_{opt} was defined as the specific water content at which the foamed mixture had the lowest τ_{max} value and a *CI* value greater than the conventional HMA.

Table 2 summarizes the operational parameters for the three laboratory foamers used in the experiment. To produce foamed mixtures in the laboratory, the asphalt binder was preheated in the oven at 320°F (160°C) for two hours prior to being transferred to the foamers. The aggregate, pre-heated to 275°F (135°C), was introduced into the portable bucket mixer. Then, a specific amount of foamed asphalt at given foaming

water content was dispensed into the bucket mixer as it rotated. Afterwards, the foamed loose mix was short-term aged in an oven for two hours at 240°F (116°C) prior to compaction. The control HMA was mixed at 295°F (143°C) and then short-term aged for two hours at 275°F (135°C).

Table 2. Summary of the Operational Parameters for Laboratory Foamers

Parameter	Wirtgen foamer	InstroTek foamer	PTI foamer
Air flow pressure	73 psi (500 kPa)	75 psi (517 kPa)	110 psi (758 kPa)
Water flow pressure	73 psi (500 kPa)	Depended upon foaming water content	33 psi (230 kPa)
Asphalt flow pressure	73 psi (500 kPa)	30 psi (207 kPa)	Dispensed by gravity
Asphalt temperature	320°F (160°C)	320°F (160°C)	320°F (160°C)
Water temperature	Room temperature (Approx. 25°C)	Room temperature (Approx. 25°C)	Room temperature (Approx. 25°C)
Foaming water content	1%, 2%, 3%	1%, 2%, 3%	1%, 2%, 3%

Asphalt Foaming Characteristics

Figure 33 presents the ER_{max} values obtained for the foamed asphalts from the Wirtgen foamer, the InstroTek foamer, and the PTI foamer. The dots represent the average ER_{max} values of three replicate measurements and the error bars span ± 1 standard deviation from the average value. As illustrated, at all foaming water contents ranging from 1 percent to 3 percent, foamed asphalts produced by the Wirtgen foamer had the largest ER_{max} values, followed by those produced in the InstroTek foamer and then the PTI foamer. In addition, the increase in ER_{max} values for the Wirtgen foamer and the InstroTek foamer was proportional to increasing foaming water contents, while no significant effect of the foaming water content was observed for the PTI foamer. The

difference in ER_{max} values observed for the three laboratory foamers was likely due to the way the foam was produced in the units. In the Wirtgen foamer, the foam was expelled under pressure once the water and the asphalt were combined. However in the InstroTek foamer, the foam travelled through a 10-inch (254-mm) tube prior to being dispensed, which restricted the flow rate of the foamed asphalt coming out of the expansion chamber. The PTI foamer allowed the foamed asphalt to be drawn out of the expansion chamber by gravity, which produced an even slower flow rate. Therefore, it was indicated that the rate of the foamed asphalt dispensed out from the laboratory foamer had a significant effect on its volume expansion.

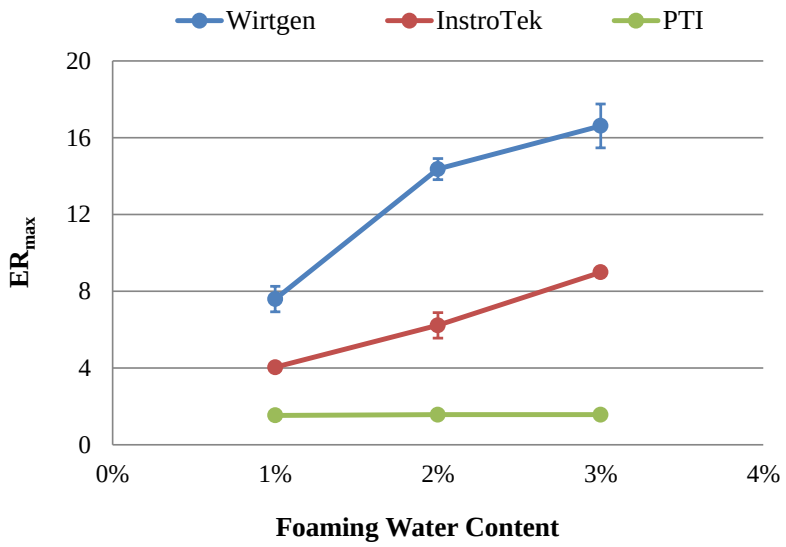

Figure 33. ER_{max} results of foamed asphalts produced by various laboratory foamers.

Figure 34 presents the *FI* values of foamed asphalts produced at various foaming water contents by the Wirtgen foamer and the InstroTek foamer. The *FI* values for the

PTI foamer were not calculated as no significant change in volume was observed during the foaming process. As illustrated in Figure 34, at 1.0 percent and 2.0 percent foaming water contents, the foamed asphalts produced in the Wirtgen foamer had higher *FI* values at 60 seconds than those produced in the InstroTek foamer, indicating a greater volume of foam remaining. However, an equivalent *FI* value was achieved by the two foamers at 3.0 percent water content.

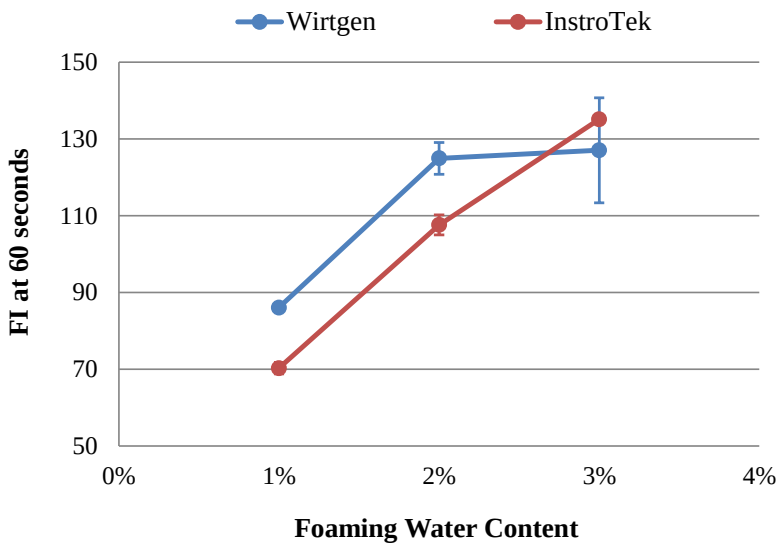

Figure 34. *FI* results of foamed asphalts produced by the Wirtgen foamer and the InstroTek foamer.

Figure 35 illustrates the *SAI* values of the foamed asphalts produced by the Wirtgen foamer and the InstroTek foamer. The determination of *SAI* values for foamed asphalts produced at 3.0 percent foaming water content and those produced by the PTI foamer was not available since only a limited amount of surface foam bubbles were

captured by the digital camera 60 seconds after the foaming process. As shown in Figure 35, an increase in *SAI* values at 60 seconds was observed for the InstroTek foamer as the water content increased from 1.0 percent to 3.0 percent. However, the opposite trend was shown for the Wirtgen foamer; the reduction in *SAI* values with increasing foaming water contents was likely due to the faster foam collapse rate. Additionally, higher *SAI* values at 60 seconds were presented for foamed asphalts produced by the Wirtgen foamer than those produced by the InstroTek foamer. Therefore, it was indicated that the Wirtgen foamer was able to produce more semi-stable foam bubbles, which were smaller in size but having larger surface areas.

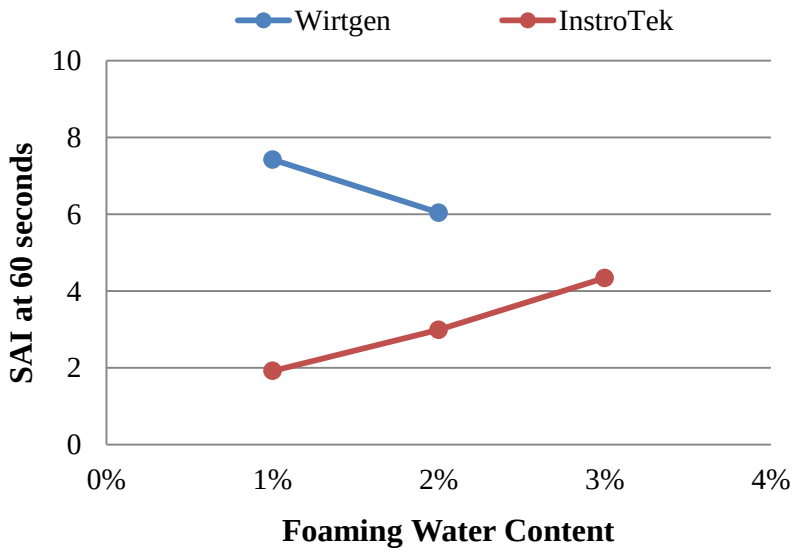

Figure 35. *SAI* results of foamed asphalts produced by the Wirtgen foamer and the InstroTek foamer.

Foamed Mixture Properties

Figure 36 and Figure 37 present the workability and coatability results for the conventional HMA versus foamed mixtures produced by the Wirtgen foamer at 1.0 percent, 2.0 percent, and 3.0 percent foaming water contents, respectively. Considering that no significant volume expansion was observed for the foamed asphalts produced by the PTI foamer (Figure 33), foamed mixtures were produced with a higher foaming water content range of 1.0 percent to 5.0 percent, and their workability and coatability results are shown in Figure 38. Due to equipment availability, the workability evaluation for foamed mixtures produced by the Wirtgen foamer and the InstroTek foamer was performed by an IPC compactor while those produced by the PTI foamer was evaluated using a Pine compactor. Although these two compactors are not likely to have identical compaction characteristics in terms of τ_{max} values, the evaluation of mixture workability and the identification of W_{opt}, as will be discussed subsequently, were performed separately for each laboratory foamer. In the figures, the bars represent the average τ_{max} value of three replicate measurements, and the error bars span ± 1 standard deviation from the average value. The dots represent the *CI* values for the foamed mixtures and the conventional HMA.

As illustrated in Figure 36, foamed mixtures produced at various water contents by the Wirtgen foamer exhibited higher or equivalent τ_{max} values than the control HMA, indicating worse or equivalent workability characteristics. The coatability results in terms of *CI* values indicated that compared to the control HMA, equivalent or better coatability was achieved by foamed mixtures produced at 2.0 percent and 3.0 percent

water contents. According to the results shown in Figure 36, 2.0 percent was selected as the W_{opt} for the foamed mixtures produced by the Wirtgen foamer.

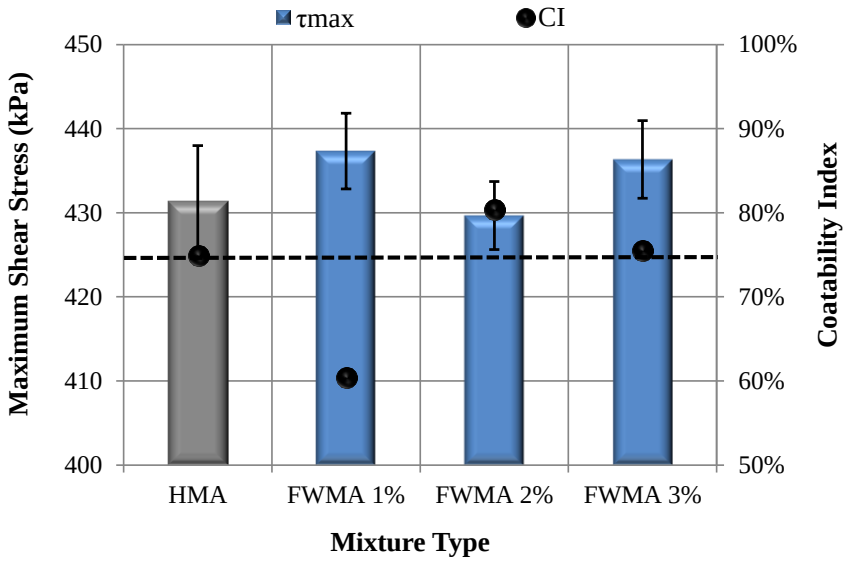

Figure 36. τ_{max} and *CI* results for foamed mixtures produced by the Wirtgen foamer.

The results presented in Figure 37 indicated that for the InstroTek foamer, better mixture workability and coatability characteristics in terms of lower τ_{max} and higher *CI* values were observed for foamed mixtures at three various water contents as compared to the control HMA. The W_{opt} for the foamed mixtures produced by the InstroTek foamer was 2.0 percent, which produced the mixture with the lowest τ_{max} value and a higher *CI* value as compared to the conventional HMA.

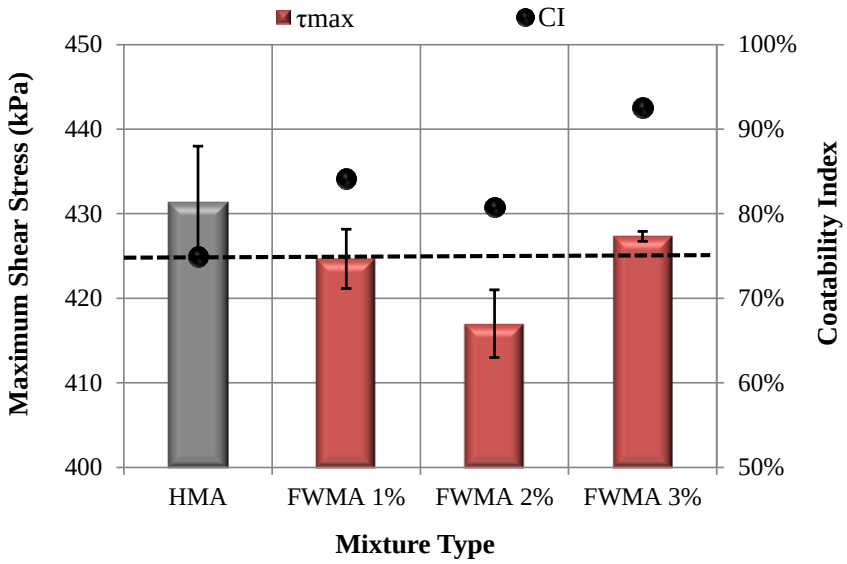

Figure 37. τ_{max} and *CI* results for foamed mixtures produced by the InstroTek foamer.

Figure 38 shows foamed mixtures produced at 1.0 percent, 3.0 percent, and 5.0 percent foaming water contents by the PTI foamer exhibited better workability characteristics than the control HMA, as indicated by the lower τ_{max} values. The trend was observed despite the fact that the foamed asphalt produced in the PTI foamer exhibited insignificant volume expansion as previously shown in Figure 33. A different trend was shown for the coatability results for the mixtures produced in the PTI foamer where higher *CI* values were obtained for foamed mixtures at 3.0 percent and 5.0 percent foaming water contents than the conventional HMA while the opposite trend was shown for the 1.0 percent foaming water content. Considering that 5.0 percent water content exhibited a *CI* value slightly higher than 3.0 percent water content, it was considered the optimum for the foamed mixtures produced by the PTI foamer.

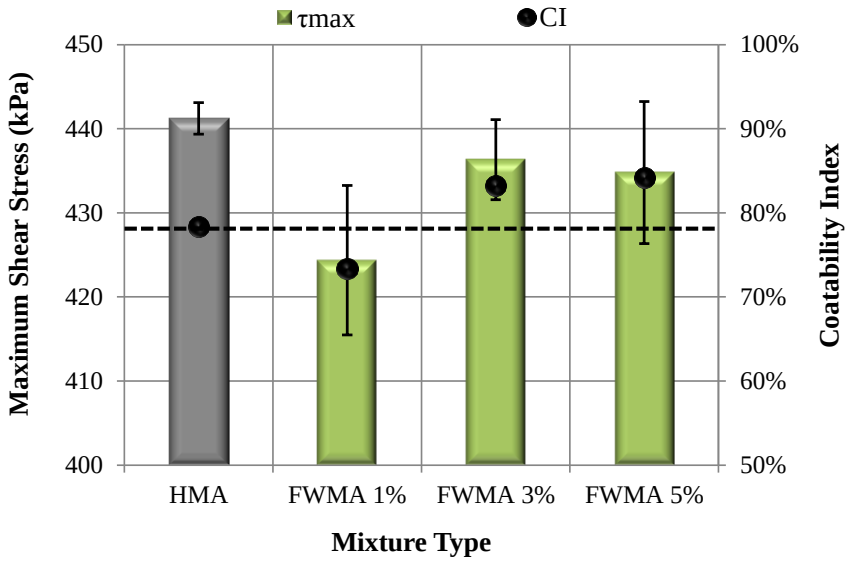

Figure 38. τ_{max} and *CI* results for foamed mixtures produced by the PTI foamer.

Development of a Mix Design Procedure for Foamed Asphalt Mixtures

While foamed asphalt mixtures have been extensively produced and implemented, a standard mix design procedure has not been established yet. Currently, the design of foamed asphalt mixtures is based on the traditional HMA design procedure in accordance with AASHTO R 35 to determine the optimum binder content, followed by an estimate of the foaming water content based on the foaming equipment manufacturer's recommendations, engineering judgement, or previous experience. However, laboratory foaming experiments indicate that certain asphalt binders have negligible foaming ability possible due to the presence of anti-foaming agents, while for other binders a considerable difference in foamed mixture workability and coatability can be attained by minor changes in the foaming water content. Therefore, the current

mix design procedure may not ensure foamed asphalt mixtures have the optimum performance.

The objective of this research study is to develop a mix design procedure for foamed asphalt mixtures that includes the consideration of asphalt foaming ability, the optimization of foaming water contents for achieving the desirable workability and coatability, and evaluation of mixture properties.

Factors for Consideration

Asphalt foaming ability is the primary factor to be considered when developing a mix design procedure for foamed asphalt mixtures. Laboratory foaming experiments indicate that certain binders have negligible foaming ability possibly due to the presence of anti-foaming agents introduced through the crude refining or binder production processes (Fu 2011; Kekevi et al. 2012). These binders are not expected to demonstrate volume expansion or formation of foam bubbles during the foaming process, and therefore, may not be suited for producing foamed asphalt mixtures.

Another factor to consider is the effect of foaming on mixture workability and coatability. Foamed asphalt mixtures are expected to have better aggregate coating and improved mixture workability due to the volume expansion and the formation of bubbles during the foaming process, even when produced at reduced temperatures. Laboratory foaming experience indicates that a considerable difference in mixture workability and coatability can result from minor changes in the foaming water content (i.e., 0.5 percent by weight of binder). Therefore, it is important in the mix design procedure to determine

the W_{opt} that yields foamed asphalt mixtures with optimum workability and coatability characteristics.

Finally, performance evaluation should also be considered as part of the mix design procedure, in order to ensure adequate performance throughout the service life of the pavement. There has always been a concern regarding the moisture susceptibility of foamed mixtures due to the incorporation of water in the mixture. In addition, the lower production temperature used in the production of foamed WMA mixtures could result in reduced stiffness and rutting resistance. Therefore, the performance parameters of the foamed asphalt mixtures should comply with established standards.

Foamed Mix Design Procedure

Figure 39 presents the proposed mix design procedure for foamed asphalt mixtures. The determination of asphalt foaming ability was initially considered since the asphalt foaming experiment indicated some binders had little foaming ability. However, according to the results measured for various laboratory foamers described previously, the same binders may or not expand in different foamers, but in all cases improved mixture workability and coatability characteristics were observed. Therefore, the determination of asphalt foaming ability was not included in the foamed mix design procedure as shown in Figure 39, but it could still be performed at discretion of the agency or organization conducting the mix design.

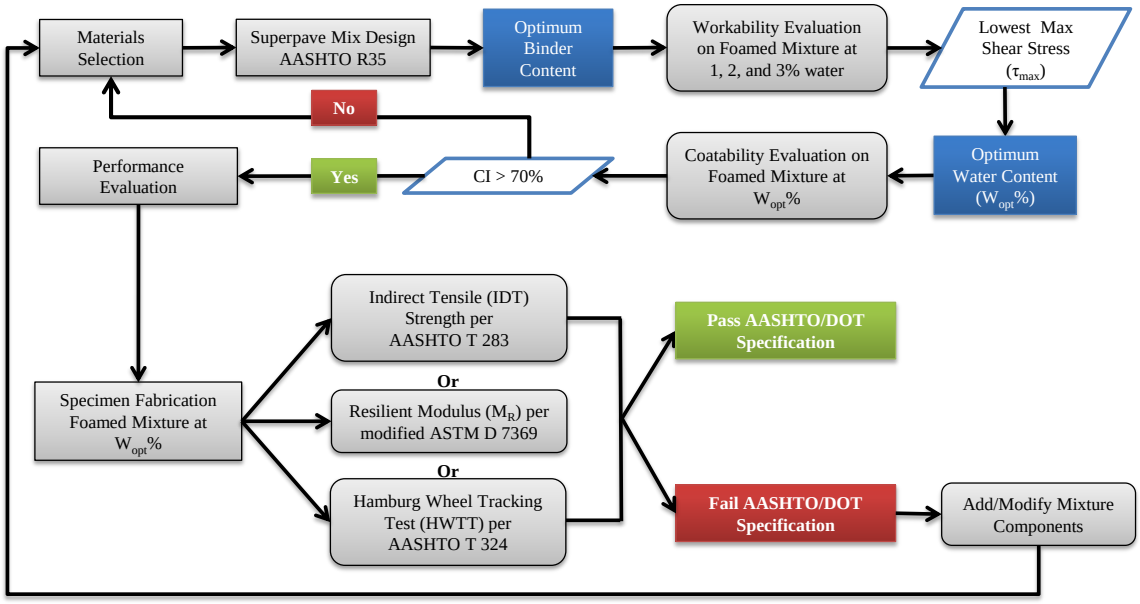

Figure 39. Proposed mix design procedure for foamed asphalt mixtures.

As illustrated, the mix design procedure started with materials selection for the development of a traditional mix design procedure in accordance with AASHTO Superpave R 35 to determine the optimum binder content. Afterwards, a set of foamed mixtures were produced by a laboratory foamer at 1.0 percent, 2.0 percent, and 3.0 percent water contents for workability evaluation. The foaming water content that yielded the lowest τ_{max} value was considered the optimum.

Then, the coatability of the foamed mixture at the W_{opt} was evaluated as compared against the minimum threshold value of 70 percent proposed by Newcomb et al. (2015). If the foamed mixture had a *CI* value higher than 70 percent, it was expected to have adequate aggregate coatability. Otherwise, sufficient asphalt volume expansion and formation of foam bubbles might not be achieved in the foaming process, and therefore, the binder was not suitable for producing foamed mixtures. Adjustments in

terms of modifying the binder source, adding or modifying foaming additives, or other modifications were then proposed prior to a subsequent evaluation for the foamed mixture against the same criteria.

The final step in the proposed mix design procedure was performance evaluation of the foamed mixture at W_{opt}. Standard laboratory tests including the M_R test per ASTM D7369, IDT strength test per AASHTO T 283, and HWTT test per AASHTO T 324 were recommended to ensure the designed mixture have adequate stiffness, rutting resistance, and moisture resistance. If the performance parameters of the foamed mixture complied with established AASHTO or Department of Transportation (DOT) specifications, the foamed mixture was accepted. Otherwise, changes in mixture components would be considered and the mixture retested.

Field Validation

The proposed mix design procedure was validated using materials from an asphalt plant located in Cleves, Ohio. The plant was a counter flow plant with a Gencor foamer. The asphalt binder used was a PG 64-22 and the optimum binder content per mix design was 5.6 percent. Local gravel was the primary aggregate used in the mixture along with natural sand and fractioned RAP. The mixture had a 9.5-mm NMAS.

During the plant visit, the foamed asphalt mixture was produced with 1.5 percent water content at approximate 300°F (149°C). Plant loose mix and raw materials including asphalt binders, aggregates, and RAP were sampled and then shipped to Texas A&M Transportation Institute (TTI) for specimen fabrication. The PMLC specimens were fabricated by reheating the loose mix in an oven at 275°F (135°C) for

approximately four hours prior to being compacted in the SGC. In the TTI laboratory, the Wirtgen foamer was used to produce foamed mixtures at various foaming water contents. The LMLC specimens were mixed at 300°F (149°C) and then short-term aged for two hours at 275°F (135°C) prior to compaction. In addition, a set of control specimens (i.e., non-foamed) was also fabricated and tested for performance evaluation as compared to the foamed specimens.

Figure 40 presents the workability results for foamed mixtures at 1.0 percent, 2.0 percent, and 3.0 percent foaming water contents versus the control mixture. Each bar represents the average τ_{max} value of three replicates, and the error bars represent one standard deviation from the average value. As illustrated, a comparable τ_{max} value was achieved among all mixtures, indicating equivalent workability. Therefore, the lowest foaming water content of 1.0 percent was selected as the optimum and then evaluated for mixture coatability.

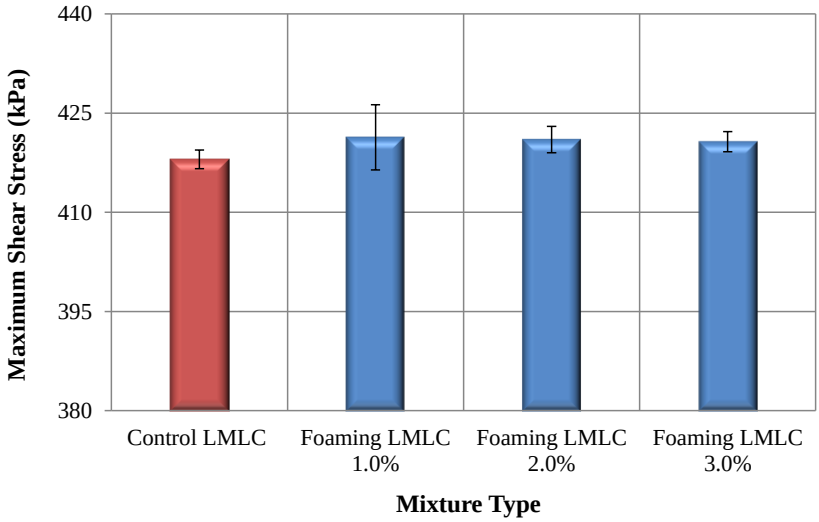

Figure 40. Workability results for foamed versus control mixtures.

Figure 41 presents the coatability results for the foamed mixture at the W_{opt} of 1.0 percent versus the control mixture. Both mixtures had *CI* values significantly higher than the minimum proposed threshold of 70 percent, indicating adequate aggregate coatability. In addition, the designed foamed mixture had a higher *CI* value than the control mixture, which was likely due to the enhanced binder volume and surface area during the foaming process. According to the workability and coatability results presented in Figure 40 and Figure 41, the designed foamed mixture at the W_{opt} exhibited adequate mixture workability and coatability characteristics.

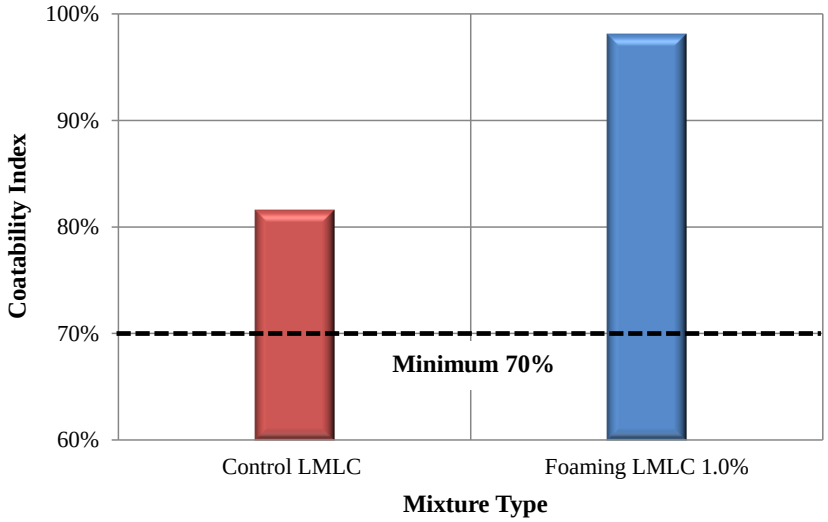

Figure 41. Coatability results for foamed versus control mixtures.

After determining the W_{opt} from workability and coatability evaluation, a new set of foamed LMLC specimens were produced at 1.0 percent water to evaluate their performance. The laboratory test results were compared against the established AASHTO or DOT specifications to ensure the designed foamed mixture had adequate stiffness, rutting resistance, and moisture resistance. In addition, the control mixture LMLC specimens and the reheated foamed PMLC specimens were also included for performance evaluation.

The M_R test was performed in accordance with ASTM D7369 at 77°F (25°C), and the stiffness results for foamed and control mixtures are presented in Figure 42. Each bar represents the average M_R stiffness of three replicates, and the error bars represent one standard deviation from the average value. As illustrated, an equivalent M_R stiffness value was achieved by LMLC specimens of foamed and control mixtures, which indicated that the inclusion of water as part of the foaming process was not

detrimental to mixture stiffness. As compared to the foamed LMLC specimens, the foamed PMLC specimens at 1.5 percent foaming water content exhibited a significantly higher M_R stiffness, which was likely due to mixture stiffening effect that occurred during the reheating process (Al-Qadi et al. 2010; Epps Martin et al. 2014).

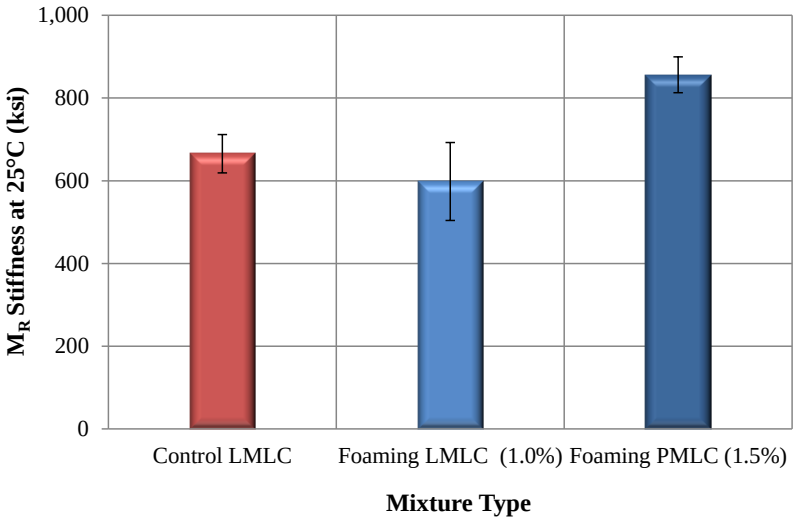

Figure 42. M_R stiffness results for foamed versus control mixtures.

The IDT strength test was performed in accordance with AASHTO T283, and the results for the foamed and control mixtures are shown in Figure 43. For each pair, the bar on the left and the bar on the right represent the average dry IDT strength and wet IDT strength after moisture conditioning with partial vacuum saturation, one freeze-thaw cycle, and hot water contents of three replicates. The error bars represent one standard deviation from the average value, and the TSR values are shown above the IDT strength bars.

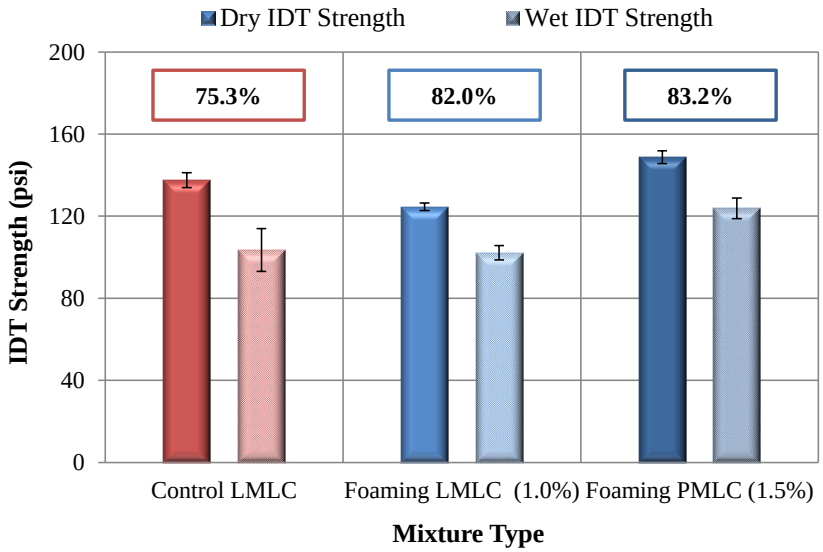

Figure 43. IDT strength test results for foamed versus control mixtures.

As illustrated in Figure 43, a slightly higher dry IDT strength was observed for the control mixture as compared to the foamed LMLC specimen at the W_{opt} of 1.0 percent. However, an equivalent wet IDT strength, and subsequently, a higher TSR value was shown by the foamed mixture as compared to the control mixture. In addition, the TSR value for the foamed LMLC specimen was higher than the minimum threshold of 80 percent specified by AASHTO T 283. Therefore, the designed foamed mixture at the W_{opt} exhibited adequate resistance to moisture damage in the IDT strength test. As compared to the foamed LMLC specimens, the foamed PMLC specimens at 1.5 percent foaming water content exhibited higher IDT strengths possibly due to the mixture stiffening effect mentioned previously, although an equivalent TSR value to the foamed LMLC specimens at W_{opt} was obtained.

The HWTT test was performed at 122°F (50°C) in accordance with TxDOT specification Tex-242-F, and test parameters including LC_{SN}, LC_{ST}, and $\Delta\varepsilon_{10,000}^{vp}$ values were used to evaluate mixture moisture susceptibility and rutting resistance, respectively. Figure 44 presents the HWTT rut depth results for the foamed and control mixtures. For both LMLC specimens of foamed and control mixtures, the HWTT curves showed an apparent stripping phase, which indicated that stripping occurred during the test. However, the HWTT curve of foamed PMLC specimens showed a different trend, where only post compaction and creep phases were observed. In addition, all three mixtures passed the failure criteria of 20,000 load cycles with less than 0.5 in. (12.5mm) rut depth per TxDOT specification, indicating adequate resistance to rutting and moisture susceptibility in the HWTT test.

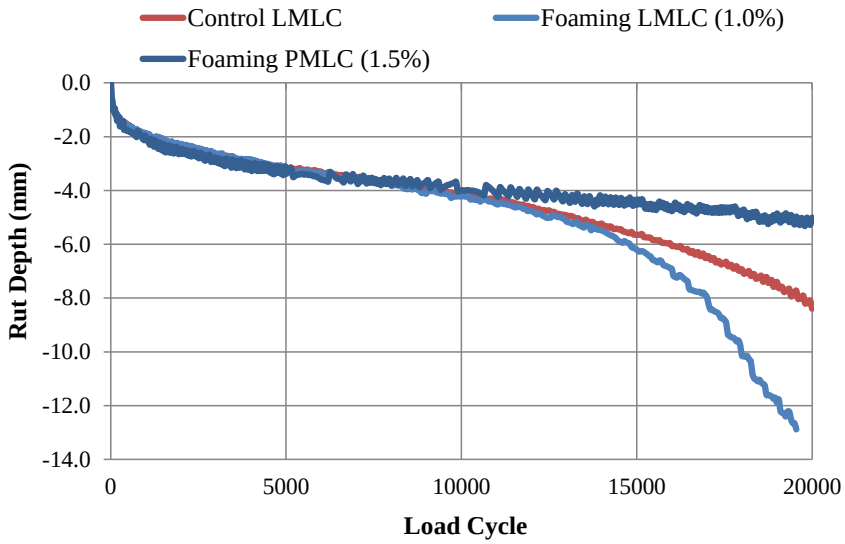

Figure 44. HWTT rut depth results for foamed versus control mixtures.

Figure 45 presents the comparison in LC_{SN}, LC_{ST}, and $\Delta\varepsilon_{10,000}^{vp}$results for foamed and control mixtures. As illustrated in Figure 45(a), slightly higher LC_{SN} and LC_{ST} values were shown for the control LMLC specimens than the foamed LMLC specimens at 1.0 percent water content, indicating better resistance of the control mixture to moisture damage in the HWTT. As discussed previously, the foamed PMLC specimens did not experience the stripping phase during the test, and therefore, a LC_{SN} value of 20,000 load cycles was obtained. The HWTT results presented in Figure 45(b) illustrated that all three asphalt mixtures had an equivalent $\Delta\varepsilon_{10,000}^{vp}$value, indicating comparable rutting resistance. According to the results presented in Figure 44 and Figure 45, the HWTT performance of the designed foamed mixture at W_{opt} complied with the TxDOT specification, despite showing slightly higher moisture susceptibility as compared to the control mixture.

The proposed mix design procedure was also validated with materials obtained from a plant in Texas; the detailed results of the validation are documented elsewhere

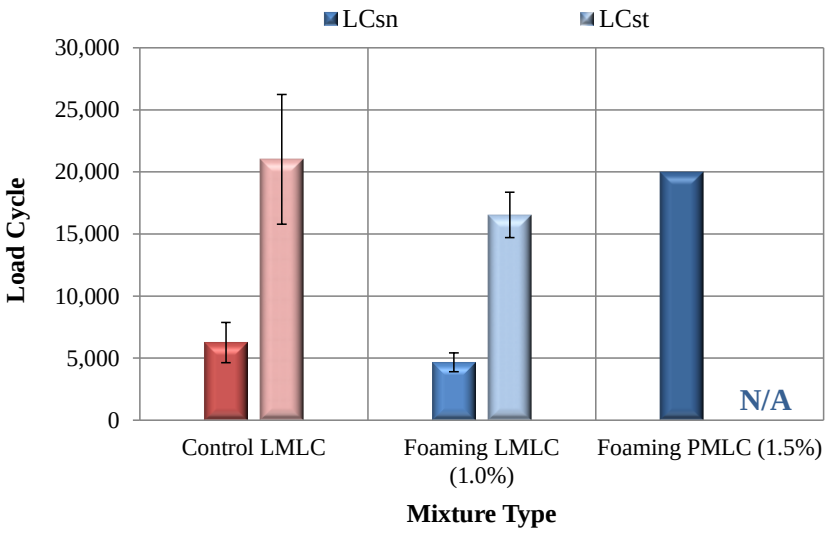

(a)

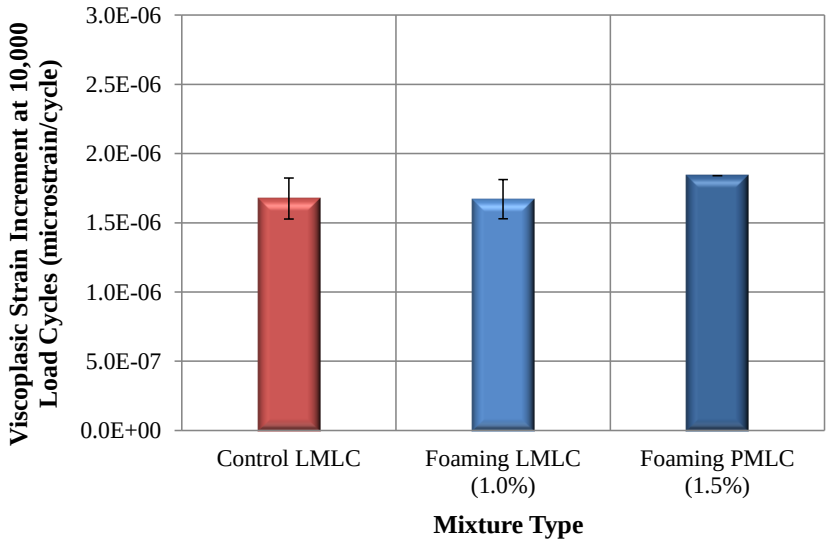

(b)

Figure 45. HWTT test results for foamed versus control mixtures; (a) moisture susceptibility parameters LC_{SN} and LC_{ST}, (b) rutting resistance parameter $\Delta\varepsilon_{10,000}^{vp}$

(Yin et al. 2015). The plant was an Astec Double Barrel with a shear/colloid mill foaming unit. Raw materials including a PG 64-22 binder, limestone and sandstone, and fractioned RAP were sampled for fabricating laboratory foamed specimens with the Wirtgen foamer. The workability results indicated that the τ_{max} value decreased as foaming water content increased from 0.7 to 1.5 percent while the opposite trend was observed for higher water contents (i.e., 1.5 to 5.5 percent). Therefore, 1.5 percent was considered the W_{opt}, which was also verified by measuring the workability of the plant produced foamed mixture using the Astec foaming unit. Further, the laboratory foamed mixture at the W_{opt} was tested for M_R stiffness, IDT strength, and HWTT moisture susceptibility and rutting resistance. Test results indicated that the designed foamed mixture had superior performance as compared to the control (i.e., non-foamed) mixture, with all performance parameters satisfying established AASHTO and DOT specifications.

CHAPTER V

SHORT-TERM AGING OF ASPHALT MIXTURES*

Overview

Asphalt mixtures may be produced in either BMPs or DMPs and then compacted at temperatures ranging from 220°F (104°C) to 325°F (163°C) (Kuennen 2004; Newcomb 2007). The goal of asphalt mixture production is to ensure complete drying of the aggregate, proper coating and bonding of the aggregate with the binder, and adequate mixture workability for handling and compaction. These processes are important to the mixture's durability and resistance to permanent deformation, moisture susceptibility, and cracking. Advances in asphalt technology, including the use of polymer modified binders and use of more angular aggregate resulted in increased mixing and compaction temperatures up to a limit of approximately 350°F (177°C) where polymer breakdown in the binder can occur. Conversely, the use of WMA technology led to reduced production and paving temperatures without sacrificing the quality of the final product. The result is a wider range of available production temperatures for asphalt mixtures.

Traditionally, asphalt mixtures have been designed on the basis of volumetric parameters (Asphalt Institue 1984; Asphalt Institute 1995). Laboratory mixing and compaction temperatures were dependent upon the stiffness or viscosity of the asphalt binder. This system was refined with time, first for the Marshall and Hveem procedures,

---

* Reprinted (with minor revisions) with permission from "Short-Term Aging of Asphalt Mixtures" by Fan Yin, Amy Epps Martin, Edith Arambula, and David Newcomb, 2015, *Journal of the Association of Asphalt Paving Technologists*, Vol. 84, Copyright [2015] by AAPT.

and then for Superpave. In the last two decades, changes have occurred in asphalt mixture components which are beneficial, but pose challenges in terms of how mixtures are designed and evaluated. Increased use of polymer modifiers, incorporation of recycled asphalt materials including RAP and recycled asphalt shingles (RAS), and the advent of WMA are departures from the norm under which the current volumetric mix design was developed.

Compounding this complexity is the evolution in asphalt plant design. The 1970s saw a rapid and persistent increase in the number of continuous plants, as DMPs replaced BMPs. In a BMP, the aggregates are dried prior to being loaded into hot bins in a batching tower. Gates on the hot bins are opened, allowing for the proper proportion of aggregates to be weighed in a bin prior to dropping into the pugmill, where the asphalt binder is introduced and mixed with the aggregates. A DMP differs from a BMP in that cold aggregates are fed onto a weigh belt in the proper proportions prior to entering the elevated end of the drum for drying. The aggregates are dried as they tumble through the drum toward the lower end, where they are mixed with the asphalt binder prior to exiting to a slat conveyor for loading into a silo.

As discussed, the changes in asphalt mixture components, production parameters, and plant design have raised the question of the accuracy of the current mix design procedures in assessing the volumetric needs of asphalt mixtures and the physical characteristics required to meet performance expectations. Therefore, there is a need to address many of these issues, considering the impact of binder source, aggregate absorption, WMA technology, inclusion of recycled materials, plant type, and

production temperature on the volumetric and performance characteristics of asphalt mixtures during production and construction.

The objectives of this research study are to: 1) validate a laboratory STOA protocol for asphalt loose mix prior to compaction in simulating the asphalt aging and absorption of asphalt mixtures produced in a plant and then loaded into a truck for transport, and 2) identify mixture components and production parameters with significant effects on the performance of short-term aged asphalt mixtures.

Background

The aging of asphalt binders in mixtures has long been a concern to those in the pavement field. The standard practice for laboratory mix design of asphalt mixtures is to simulate the asphalt aging and absorption that occurs during production and construction by conditioning the loose mix prior to compaction for a specific amount of time at a specific temperature. For HMA, the recommended loose mix aging procedure per AASHTO R 30 for preparing specimens for volumetric mix design is two hours at the compaction temperature and four hours at 275°F (135°C) for preparing performance testing specimens. The implementation of WMA raised the question of the impact of lower plant production temperatures on the aging characteristics and absorption of asphalt by aggregates in the WMA mixtures and how to adequately simulate the differences in the laboratory.

A number of studies have been performed focusing on short-term aging characteristics of asphalt mixtures and simulation of plant aging by laboratory STOA protocols; a brief summary is presented in Table 3. In general, these studies have

concluded that most short-term aging of asphalt mixtures occurs during production through placement and compaction and does not stop at plant load-out, and that binder source and type including the presence of polymers, WMA technology, and plant type have substantial effects on short-term aging characteristics of asphalt mixtures. Additionally, a variety of laboratory STOA protocols have been evaluated to simulate short-term aging and asphalt absorption during plant production and construction when fabricating LMLC specimens for volumetric analysis and performance testing. A general trend has been observed that an increase in laboratory STOA temperature and/or time leads to more aging and asphalt absorption in asphalt mixtures. However, the validity of the standard short-term aging procedure per AASHTO R 30 in simulating aging during plant production and construction has been questioned because it produces a more significant level of binder/mixture aging. Also, a comprehensive study to establish a standard laboratory STOA protocol that encompasses the effects of binder source, aggregate absorption, WMA technology, inclusion of recycled materials, plant type, and production temperature has not been undertaken.

Table 3. Previous Research on Short-Term Aging of Asphalt Mixtures

Reference	Short-Term Aging	Major Finding
Heithaus and Johnson (1958)	• Field Aging	Most aging during production and construction through compaction
Traxler (1961)		
Chipperfield and Welch (1967)		
Aschenbrener and Far (1994)		
Traxler (1961)	Factor on Aging	Binder chemistry and aggregate absorption major effects
Chipperfield and Welch (1967)		Aggregate gradation no effect
Terrel and Holen (1976)		Plant type significant effect; DMP < BMP due to lower temperature and less moisture
Lund and Wilson (1984); Lund and Wilson (1986)		Binder type and binder source significant effects
Chollar et al. (1989)		Slightly more aging from DMP than BMP
Aschenbrener and Far (1994)		Aggregate absorption important effect
Topal and Sengoz (2008)		• Binder type and binder source significant effects • Reduced aging with polymers
Zhao et al. (2009)		
Morian et al. (2011)		• Binder type and binder source significant effects • Reduced aging with polymers • Aggregate absorption and gradation important effects
Mogawer et al. (2012)		• Production temperature, silo storage, inclusion of recycled materials, and reheating significant effects • Softer binder with RAP = harder binder without RAP
Daniel et al. (2014)		• Production temperature and silo storage significant effects • Reduced difference in virgin vs. RAP mixtures after reheating
Aschenbrener and Far (1994)	• 2 hours at compaction temperature (T_c)	• Reheating significant effect on HWTT results • Recommend 2h @ T_c
Estakhri et al. (2010)	4 hours at 135°C	• WMA 4h @ 135°C comparable to HMA 4h @ 121°C • Recommend 4h @ 135°C for WMA

Table 3. Continued

Reference	Short-Term Aging	Major Finding
Rashwan and Williams (2011)	2 hours at 150°C (HMA) 2 and 4 hours at 110°C (WMA)	Dynamic modulus (E*) and flow number (FN) higher for HMA with different temperature and for mixtures with RAP
Jones et al. (2011)	• 4 hours at T_c	• Equivalent HWTT results and HVS rutting for HMA and WMA • More HWTT rutting in WMA without short-term aging
Bonaquist (2011)	• 2 hours at T_c • 4 hours at T_c	• G_{mm} (aggregate absorption) and IDT strength comparable to cores at construction • Recommend 2h @ T_c for WMA and suggested additional longer aging period for evaluating rutting and moisture susceptibility
Hajj et al. (2011)	• 4 to 15 hours at 121°C	• Recommend compaction of WMA Foaming within 4h • Foaming effects lost @ 4-15h @ 121°C
Clements et al. (2012)	• 1/2, 2, 4, and 8 hours at 135°C (HMA) • 1/2, 2, 4, and 8 hours at 114°C (WMA)	• Equivalent DCT results for WMA vs. HMA • Reduced E* and FN and increased rutting for WMA vs. HMA
Estakhri (2012)	• 2 hours at 135°C • 4 hours at 135°C	• Equivalent HWTT for WMA vs. HMA • Aging time and temperature effect on HWTT and OT results
Sharp and Malone (2013)	1 hour at 150°C	Recommend 1h @150°C for WMA
Epps Martin et al. (2014)	2 and 4 hours at T_c • 2 and 4 hours at 135°C • 2 hour at T_c + 16 hours at 60°C + 2 hours at T_c	• Effect on aging: STOA temperature > STOA time • Recommend 2h @135°C for HMA and 2h @ 116°C for WMA

A previous study focusing on evaluation of laboratory STOA protocols for WMA provided preliminary results toward understanding short-term aging through the plant and its simulation by laboratory STOA protocols (Yin et al. 2013). Various STOA protocols were selected based on available literature for fabricating HMA and WMA

LMLC specimens from two field projects, and these specimens were tested to determine the effect of each STOA protocol on mixture stiffness. Cores at construction and plant-mixed plant-compacted (PMPC) specimens were also incorporated in the study to represent asphalt mixtures experiencing short-term aging and asphalt absorption during production through compaction. Table 4 summarizes the M_R stiffness results for LMLC specimens with different STOA protocols compared through statistical analysis of Tukey's HSD test at a 95 percent confidence level. In Table 4, solid shading indicates statistically higher M_R stiffness values for LMLC specimens as compared to either cores at construction or PMPC specimens, no shading/hatching indicates statistically equivalent performance for these specimen comparisons, and vertical hatching indicates that LMLC specimens exhibited statistically lower M_R stiffness values for the same comparisons. In summary, M_R stiffness results showed that mixture stiffness increased with higher temperature and longer time in the STOA protocol. Among the five selected STOA protocols for producing LMLC specimens, two hours at 275°F (135°C) and two hours at T_c were more representative in terms of stiffness of HMA and WMA mixtures with plant aging, respectively. Considering the difficulty in accurately defining T_c in the field and the common range of T_c for WMA, two hours at 240°F (116°C) instead of two hours at T_c was recommended as the standard laboratory conditioning protocol for WMA LMLC specimens. For HMA LMLC specimens, two hours at 275°F (135°C) was recommended prior to compaction.

Table 4. Summary Trends of Laboratory STOA Protocols (Yin et al. 2013)

STOA Protocol	2h@Tc		4h@Tc		2+16+2h@Tc		2h@275°F		4h@275°F	
Asphalt Mixture	Core	PMPC	Core	PMPC	Core	PMPC	Core	PMPC	Core	PMPC
Iowa HMA										
Iowa WMA I										
Iowa WMA II										
Texas HMA					N/A					
Texas WMA I										
Texas WMA II										

Therefore, the STOA protocols of two hours at 275°F (135°C) for HMA and two hours at 240°F (116°C) for WMA were evaluated in this research study for simulating asphalt aging and absorption during plant production and construction, with a further validation by asphalt mixtures with a wider range of asphalt mixture components and production parameters.

Experimental Design

Figure 46 presents the research methodology used in this research study. First, the laboratory test results of LMLC specimens fabricated using the selected STOA protocols were compared against those of corresponding PMPC specimens and cores at construction. A second set of comparisons was also performed to evaluate the effect of each factor (asphalt mixture components or production parameters) on short-term aging of asphalt mixtures for each type of early-life specimens (i.e., LMLC specimens, PMPC specimens, and cores at construction).

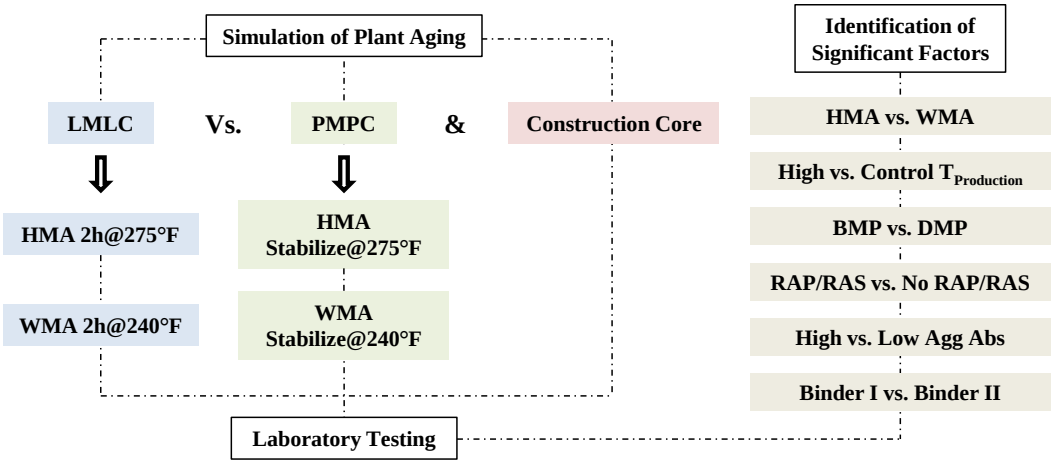

Figure 46. Research methodology for evaluating short-term aging of asphalt mixtures.

Field Projects and Materials

Materials used in this research study were from nine field projects located in the states of Texas, New Mexico, Connecticut, Wyoming, South Dakota, Iowa, Indiana, and Florida. The following factors were considered in order to include a wide spectrum of materials and production parameters: binder source, aggregate absorption, WMA technology, inclusion of recycled materials, plant type, and production temperature. During construction of these field projects, PMPC specimens were fabricated on-site in conjunction with acquisition of raw materials and cores at construction. Table 5 provides a summary of these field projects in terms of mixture components and production parameters.

Table 5. Summary of Field Projects

Project	Asphalt	Aggregate	Mixture	% RAP	% RAS	$T_{production}$	Factor
Texas I	70-22 64-22	Limestone	HMA	-	-	325°F	WMA Technology Recycled Material
			HMA	15	3	325°F	
			Foaming	-	-	275°F	
			Evotherm	-	-	275°F	
			Evotherm	15	3	270°F	
New Mexico	76-28 64-28	Siliceous Gravel	HMA	-	-	345°F	WMA Technology Recycled Material
			HMA	35	-	315°F	
			Foaming	35	-	285°F	
			Evotherm	35	-	275°F	
Connecticut	76-22	Basalt	HMA	20	-	322°F	WMA Technology
			Foaming	20	-	312°F	
Wyoming	64-28	Limestone	HMA	-	-	315°F	WMA Technology Production Temperature
			Foaming	-	-	275&295°F	
			Evotherm	-	-	255&275°F	
South Dakota	58-34	Quartize	HMA	20	-	310°F	WMA Technology
			Foaming	20	-	275°F	
			Evotherm	20	-	270°F	
			Advera	20	-	280°F	
Iowa	58-28	Limestone (0.9&3.2 percent Water Absorption Capacity [AC]) Field Sand	HMA (0.9%AC)	20	-	295&325°F	WMA Technology Production Temperature Aggregate Absorption
			HMA (3.2%AC)	20	-	295&310°F	
			Foaming (0.9%AC)	20	-	265&295°F	
			Foaming (3.2%AC)	20	-	260&290°F	

Table 5. Continued

Project	Asphalt	Aggregate	Mixture	% RAP	% RAS	$T_{production}$	Factor
Indiana	64-22	Limestone	HMA (BMP)	25	-	305°F	WMA Technology Plant Type
			HMA (DMP)	25	-	300°F	
			Advera (BMP)	25	-	273°F	
			Foaming (DMP)	25	-	271°F	
Florida	58-28	Granite (0.6%AC) Limestone (3.7%AC)	HMA (0.6%AC)	25	-	306°F	WMA Technology Aggregate Absorption
			HMA (3.7%AC)	25	-	308°F	
			Foaming (0.6%AC)	25	-	272°F	
			Foaming (3.7%AC)	25	-	267°F	
Texas II	64-22	Limestone	HMA (BMP Binder A)	-	-	325°F	Plant Type Binder Source
			HMA (BMP Binder V)	-	-	325°F	
			HMA (DMP Binder A)	-	-	325°F	
			HMA (DMP Binder V)	-	-	325°F	

Specimen Fabrication and STOA Protocol

To fabricate LMLC specimens, aggregates and binders were heated to the specific plant production temperature independently and then mixed with a portable mixer. Afterwards, loose mix was short-term aged in the oven following the selected laboratory STOA protocols of two hours at 275°F (135°C) for HMA and two hours at 240°F (116°C) for WMA prior to compaction in the SGC. Trial specimens were fabricated to assure specimens were obtained with AV contents of 7±0.5 percent.

Cores were obtained from all field projects soon after construction, and the AV contents of the cores are summarized in Table 6. To fabricate PMPC specimens, plant produced loose mix was taken from the trucks before leaving the plant or at the paving site, if necessary, transported to an on-site laboratory and maintained in an oven for one to two hours at the field compaction temperature prior to compaction to stabilize the temperature of the mix. Trial specimens were fabricated to assure PMPC specimens achieved a target AV content of 7±0.5 percent. In this study, PMPC specimens and cores at construction were included as representative of plant produced asphalt mixtures experiencing asphalt aging and absorption during production and construction.

Table 6. Summary of AV Contents for Cores at Construction

Field Project	AV Range
Texas I	6.5% - 7.7%
New Mexico	3.6% – 8.3%
Connecticut	4.3% - 6.3%
Wyoming	5.1% - 9.3%
South Dakota	6.9% - 10.0%
Iowa	5.8% – 12.0%
Indiana	6.3% - 11.2%
Florida	5.2% - 9.4%
Texas II	4.7% - 10.4%

Laboratory Tests

Based on previous experience, M_R, E*, and HWTT tests were selected for comparing the performance of asphalt mixtures fabricated following the selected

laboratory STOA protocols versus the corresponding PMPC specimens and cores at construction and also to investigate the effects of mixture components and production parameters on the performance of short-term aged asphalt mixtures. The M_R test was performed in accordance with ASTM D7369, and M_R stiffness at 77°F (25°C) was used as the mixture stiffness parameter. The HWTT test (AASHTO T 324) was included in the experiment to discriminate short-term aged asphalt mixtures with distinct rutting resistance. Data analysis was performed using the novel methodology described in Chapter III, and the $\Delta\varepsilon^{vp}$ value at LC_{SN} (i.e., $\Delta\varepsilon_{SN}^{vp}$) was utilized as the mixture rutting resistance parameter.

The E* test was conducted under unconfined conditions using the Asphalt Mixture Performance Tester (AMPT) shown in Figure 47, following the test procedure specified in AASHTO TP 79-13. SGC compacted specimens were compacted to a height of 6.7 inches (170 mm), and then cored and trimmed to obtain test specimens with a diameter of 4 inches (100 mm) and a height of 6 inches (150 mm).

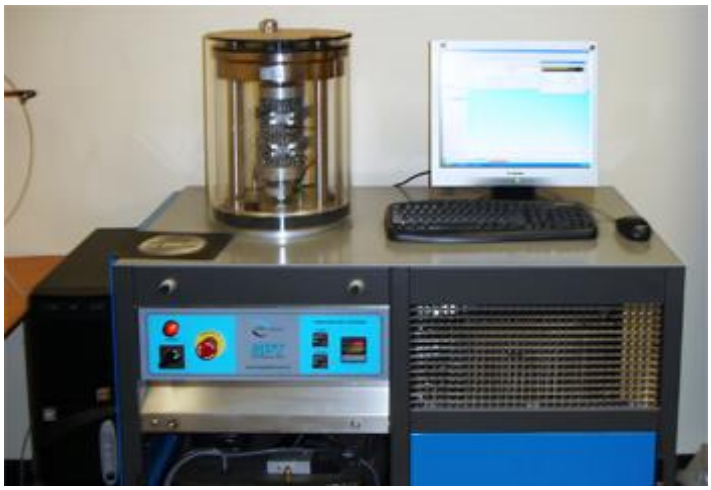

Figure 47. AMPT for E* testing.

The testing was conducted at three temperatures of (39, 68, and 104°F) 4, 20, and 40°C and three frequencies of 0.1, 1, and 10 Hz for each temperature. Load levels were determined by a trial and error process to assure the amplitude of measured vertical strains was in the range of 50 to 75 microstrains, in order to prevent damage to the test specimen. The E* master curve was constructed by fitting the E* values at each temperature/frequency condition to the sigmoidal function described in Equation 27, followed by horizontally shifting according to the time-temperature shift factor function expressed in Equation 28. To further discriminate E* stiffness of asphalt mixtures due to different binder/mixture aging levels, the E* stiffness at 68°F (20°C) and 10 Hz was used as another indicator for asphalt mixture stiffness in addition to the E* master curve.

$$log|E^*| = a + \frac{b}{1 + \frac{1}{e^{d+g*log(f_R)}}} \quad \text{Equation 27}$$

where:

f_R = reduced frequency; and

a, b, d, and g = fitting coefficients of the sigmoidal function.

$$log a_T = \alpha_1 T^2 + \alpha_2 T + \alpha_3 \quad \text{Equation 28}$$

where:

a_T = time-temperature shift factor; and

α_1, α_2, and α_3 = fitting coefficients of the time-temperature shift factor function.

Test Results and Data Analysis

This section provides the mixture test results for LMLC specimens fabricated following the selected laboratory STOA protocols of two hours at 275°F (135°C) for HMA and two hours at 240°F (116°C) for WMA, PMPC specimens, and cores at construction. Mixture volumetrics, M_R stiffness, E* stiffness, and HWTT rutting resistance results were analyzed toward simulating asphalt aging and absorption during plant production and construction by the selected laboratory STOA protocols, and identifying mixture components and production parameters with significant effects on the performance of short-term aged asphalt mixtures.

Mixture Volumetrics

Table 7 presents the comparison of volumetrics of LMLC specimens fabricated following the selected laboratory STOA protocols and PMPC specimens in terms of theoretical maximum specific gravity (G_{mm}), percentage of absorbed asphalt (P_{ba}), percentage of effective asphalt (P_{be}), and effective binder film thickness (FT_{be}). The volumetrics were calculated using the mix design aggregate gradation and asphalt content per *Superpave Mix Design* (Asphalt Institute 2001).

Table 7. Mixture Volumetrics for LMLC versus PMPC Specimens

Field Project	Mixture Type	PMPC				LMLC			
		G_{mm}	P_{ba}	P_{be}	FT	G_{mm}	P_{ba}	P_{be}	FT
Texas I	HMA	2.420	0.53	4.70	9.09	2.397	0.10	5.11	9.88
	Evotherm	2.408	0.30	4.91	9.50	2.399	0.13	5.07	9.81
	Foaming	2.400	0.15	5.06	9.77	2.407	0.28	4.93	9.53
	HMA+RAP/RAS	2.410	0.83	4.42	7.89	2.418	0.98	4.27	7.64
	Evotherm+RAP/RAS	2.420	1.02	4.24	7.58	2.417	0.96	4.29	7.67
New Mexico	HMA	2.342	0.41	5.01	10.21	2.329	0.16	5.25	10.70
	HMA+RAP	2.340	0.66	4.78	9.66	2.339	0.64	4.79	9.70
	Evotherm+RAP	2.343	0.72	4.72	9.55	2.333	0.52	4.91	9.93
	Foaming+RAP	2.335	0.56	4.87	9.85	2.349	0.84	4.61	9.32
Connecticut	HMA+RAP	2.676	1.26	3.71	8.55	2.652	0.90	4.04	9.33
	Foaming+RAP	2.675	1.24	3.72	8.59	2.658	0.99	3.96	9.14
Wyoming	HMA	2.470	0.76	4.28	8.81	2.491	1.13	3.93	8.09
	Evotherm High T	2.479	0.92	4.13	8.50	2.494	1.18	3.88	7.98
	Evotherm Ctrl T	2.487	1.06	3.99	8.22	2.501	1.30	3.76	7.75
	Foaming High T	2.485	1.03	4.03	8.29	2.497	1.24	3.83	7.88
	Foaming Ctrl T	2.470	0.76	4.28	8.81	2.505	1.37	3.70	7.61
South Dakota	HMA+RAP	2.441	0.58	4.75	7.28	2.441	0.58	4.75	7.28
	Evotherm+RAP	2.440	0.56	4.77	7.31	2.440	0.56	4.77	7.31
	Foaming+RAP	2.428	0.35	4.97	7.62	2.440	0.56	4.77	7.31
	Advera+RAP	2.432	0.42	4.90	7.51	2.432	0.42	4.90	7.51

Table 7. Continued

Field Project	Mixture Type	PMPC				LMLC			
		G_{mm}	P_{ba}	P_{be}	FT	G_{mm}	P_{ba}	P_{be}	FT
Iowa	High Abs HMA+RAP High T	2.425	2.35	4.82	10.18	2.373	1.35	5.75	12.14
	High Abs HMA+RAP Ctrl T	2.439	2.61	4.57	9.67	2.373	1.35	5.75	12.14
	High Abs Foaming+RAP High T	2.435	2.54	4.64	9.81	2.365	1.19	5.89	12.45
	High Abs Foaming+RAP Ctrl T	2.437	2.57	4.61	9.74	2.373	1.35	5.75	12.14
	Low Abs HMA+RAP High T	2.481	0.61	4.42	9.28	2.482	0.63	4.40	9.25
	Low Abs HMA+RAP Ctrl T	2.476	0.52	4.50	9.46	2.479	0.58	4.45	9.35
	Low Abs Foaming+RAP High T	2.477	0.54	4.49	9.42	2.488	0.73	4.30	9.04
	Low Abs Foaming+RAP Ctrl T	2.474	0.49	4.54	9.53	2.489	0.75	4.29	9.00
Indiana	HMA+RAP BMP	2.451	1.31	4.77	8.12	2.458	1.32	4.65	7.92
	HMA+RAP DMP	2.446	1.48	5.00	8.55	2.443	1.43	5.05	8.64
	Advera+RAP BMP	2.448	1.29	4.84	8.24	2.456	1.43	4.71	8.02
	Foaming+RAP DMP	2.455	1.43	4.73	8.06	2.440	1.16	4.98	8.49
Florida	High Abs HMA+RAP	2.350	2.03	4.66	6.93	2.341	1.86	4.83	7.17
	High Abs Foaming+RAP	2.363	2.18	4.37	6.48	2.365	2.22	4.33	6.43
	Low Abs HMA+RAP	2.537	0.79	3.74	5.61	2.540	0.84	3.70	5.54
	Low Abs Foaming+RAP	2.548	1.09	3.64	5.46	2.540	0.96	3.76	5.65
Texas II	HMA BMP Alon	2.402	1.39	5.06	7.97	2.393	1.11	5.11	8.10
	HMA DMP Alon	2.415	1.34	4.65	7.28	2.393	1.11	5.11	8.10
	HMA BMP Valero	2.395	1.26	5.19	8.17	2.392	1.16	5.21	8.20
	HMA DMP Valero	2.411	1.26	4.71	7.38	2.392	1.16	5.21	8.20

Figure 48 and Figure 49 present the correlations for LMLC specimens versus PMPC specimens in terms of G_{mm} and P_{ba} values. As illustrated in Figure 49, most of the data points fell on the line of equality indicating equivalent G_{mm} values were achieved by PMPC specimens and LMLC specimens. The exceptions were mixtures from the Iowa field project that were produced as HMA and foamed WMA with high absorptive aggregates (3.2 percent AC). A reasonable correlation in terms of P_{ba} values was also observed in Figure 48 when comparing the two specimen types, with the exception of the same subset of the Iowa mixtures. Based on mixture volumetrics summarized in Table 7, Figure 48, and Figure 49, practically equivalent mixture volumetrics were observed for PMPC specimens and LMLC specimens for a wide range of asphalt mixtures. Therefore, the selected laboratory STOA protocols of two hours at 275°F (135°C) for HMA and 240°F (116°C) for WMA were considered suitable to simulate the asphalt absorption during plant production and construction.

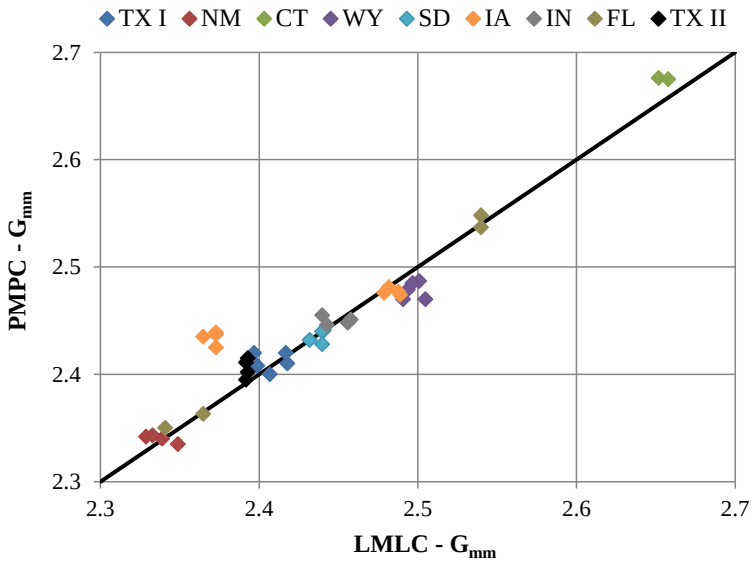

Figure 48. G_{mm} correlation for LMLC versus PMPC specimens.

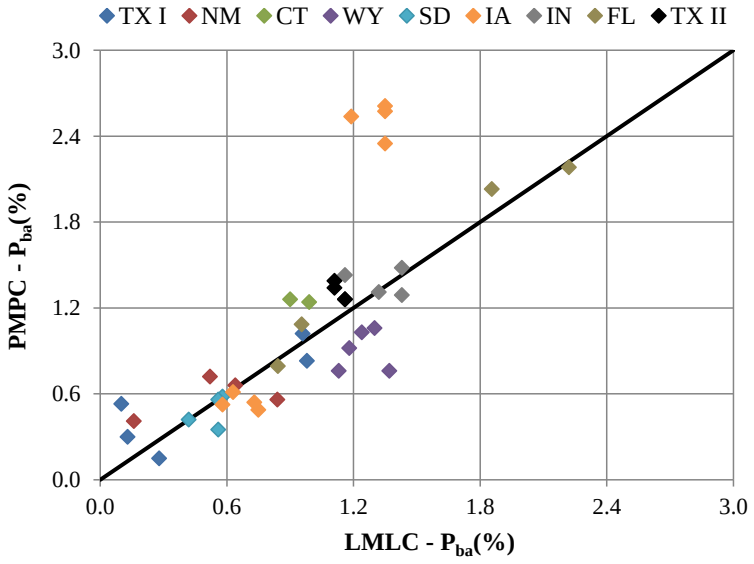

Figure 49. P_{ba} correlation for LMLC versus PMPC specimens.

Simulation of Plant Aging

As mentioned previously, the laboratory STOA protocols of two hours at 275°F (135°C) for HMA and two hours at 240°F (116°C) for WMA were used to simulate asphalt aging during plant production and construction. In order to explore the correlation in asphalt mixture aging induced by the selected laboratory STOA protocols versus that occurred during plant production, M_R stiffness, E* stiffness, and HWTT rutting resistance parameter for LMLC specimens from nine field projects were plotted against the corresponding results obtained for PMPC specimens and cores at construction. A detailed discussion of the results is presented in the following sections.

M_R Test Results

Figure 50 and Figure 51 present the M_R stiffness correlation of LMLC specimens versus PMPC specimens and cores at construction, respectively. As illustrated, most of the data points fell on the line of equality, which indicated that M_R stiffness for LMLC specimens with the selected laboratory STOA protocols of two hours at 275°F (135°C) for HMA and two hours at 240°F (116°C) for WMA closely mimicked the M_R stiffness of the PMPC specimens and cores at construction. In addition, there was a remarkable similarity in the pattern of M_R stiffness results for PMPC specimens and cores at construction indicating an insignificant difference between these two types of specimens.

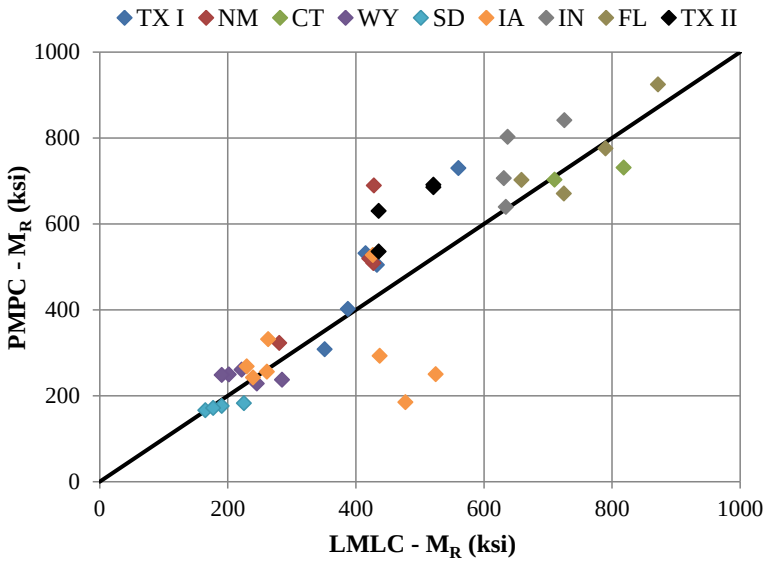

Figure 50. M_R stiffness correlation for LMLC versus PMPC specimens.

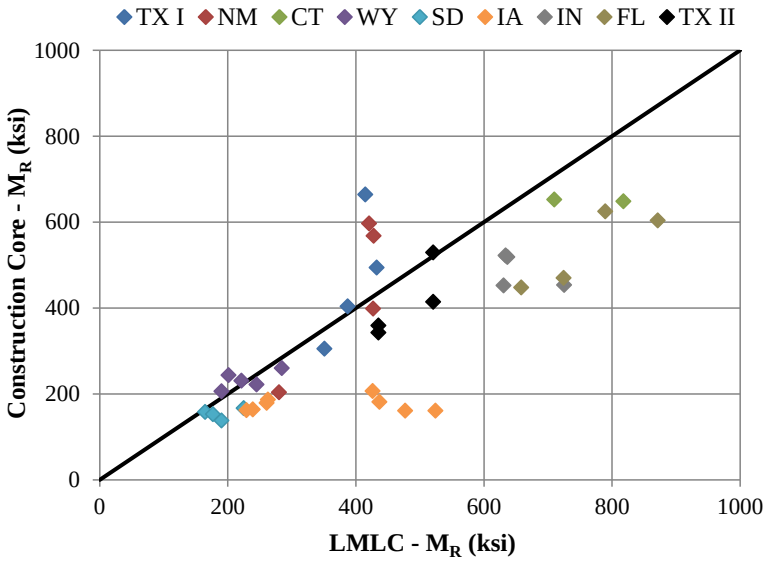

Figure 51. M_R stiffness correlation for LMLC specimen versus cores at construction.

E Test Results*

Figure 52 presents the correlation of E* stiffness results at 68°F (20°C) and 10Hz for LMLC specimens versus PMPC specimens of asphalt mixtures from Connecticut, Indiana, and Texas II field projects. Consistent with results shown in Figure 50, a good correlation in E* stiffness was observed for LMLC specimens versus PMPC specimens in Figure 52. Therefore, the laboratory STOA protocols of two hours at 275°F (135°C) for HMA and two hours at 240°F (116°C) for WMA were able to produce laboratory asphalt mixtures with an equivalent E* stiffness as compared to plant produced asphalt mixtures. The outlier shown in Figure 52 was the BMP PMPC specimen of HMA from the Indiana field project, which showed a significantly lower E* stiffness as compared to its corresponding LMLC counterpart.

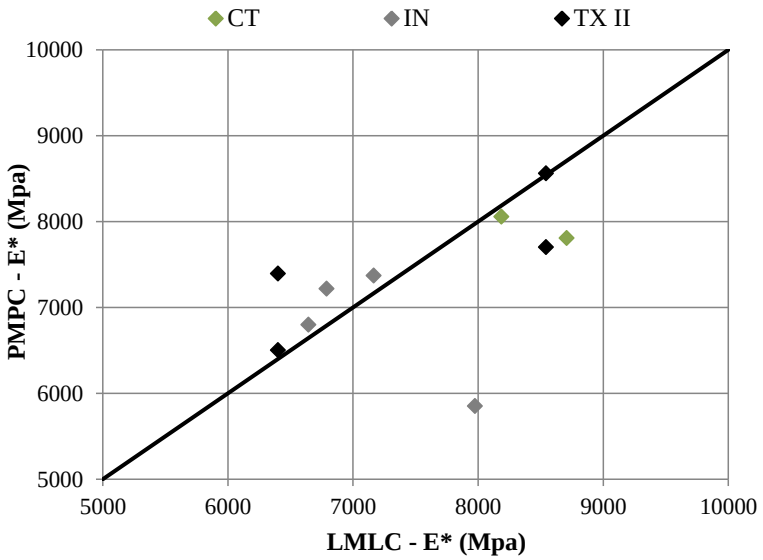

Figure 52. E* stiffness correlation for LMLC versus PMPC specimens.

HWTT Test Results

Figure 53 and Figure 54 present the HWTT $\Delta\varepsilon_{SN}^{vp}$ results for LMLC specimens versus PMPC specimens and cores at construction, respectively. The asphalt mixtures included in this evaluation did not show early stripping during the tests and had LC_{SN} values greater than 3,000 load cycles. As illustrated in Figure 53, a reasonable correlation in $\Delta\varepsilon_{SN}^{vp}$ values between LMLC specimens and PMPC specimens was obtained, indicating the selected LTOA protocols were able to produce laboratory asphalt mixtures with an equivalent rutting resistance in the HWTT as compared to the mixture produced in the plant. However, a distinct trend was shown in Figure 54, where almost all of the data points were above the line of equality. Thus, cores at construction exhibited a higher rutting susceptibility in the HWTT as compared to their corresponding LMLC specimens. The degradation and debonding of the plaster needed to fit the cores into the testing mold was likely a significant contributor to higher rut depths for cores at constructions and a consequent poor correlation with the LMLC results. Therefore, there is a need for appropriate modifications to the HWTT procedure for testing field cores in the future.

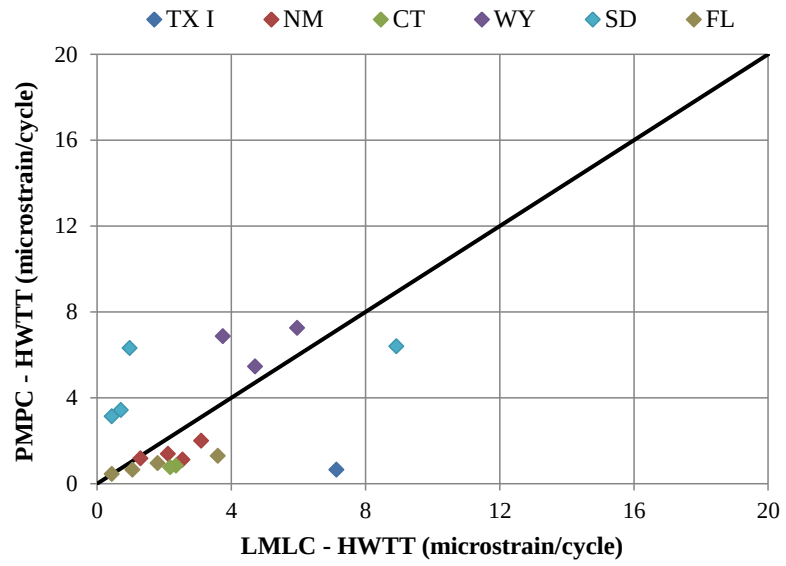

Figure 53. HWTT $\Delta\varepsilon_{SN}^{vp}$ correlation for LMLC versus PMPC specimens.

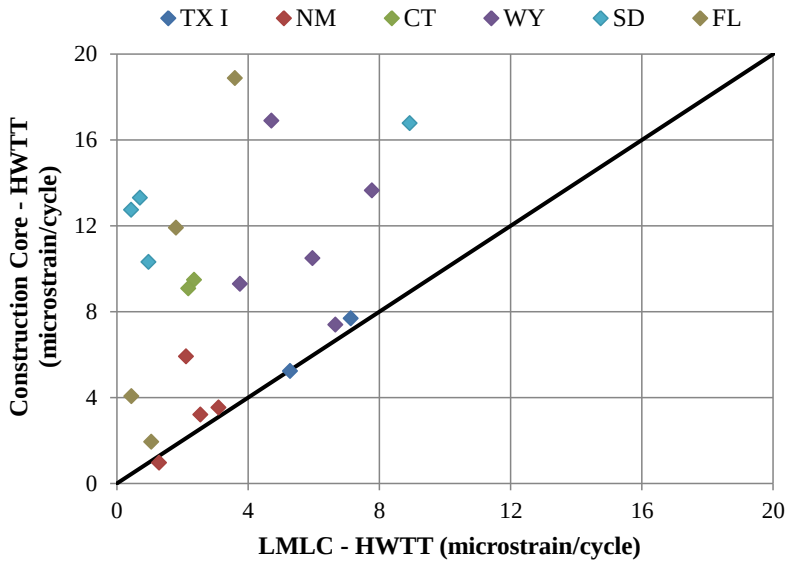

Figure 54. HWTT $\Delta\varepsilon_{SN}^{vp}$ correlation for LMLC specimens versus cores at construction.

In addition to the HWTT $\Delta\varepsilon_{SN}^{vp}$ results, the traditional rutting resistance parameter of rut depth at 5,000 load cycles was also used to evaluate the simulation of plant aging by the selected laboratory STOA protocols. The results for LMLC specimens versus PMPC specimens and cores at construction are presented in Figure 55 and Figure 56, respectively. Although a substantial variability in the rut depth measurements was exhibited in Figure 55, there was a reasonable correlation in terms of rutting resistance between LMLC specimens and their corresponding PMPC specimens. Similar to the test results shown in Figure 54, a higher rutting susceptibility as indicated by higher rut depths at 5,000 load cycles for cores at construction versus their corresponding LMLC specimens was also observed in Figure 56. Again, HWTT results for cores at construction were possibly biased due to the disintegration and debonding of the plaster needed to properly fit the cores into the molds during the test.

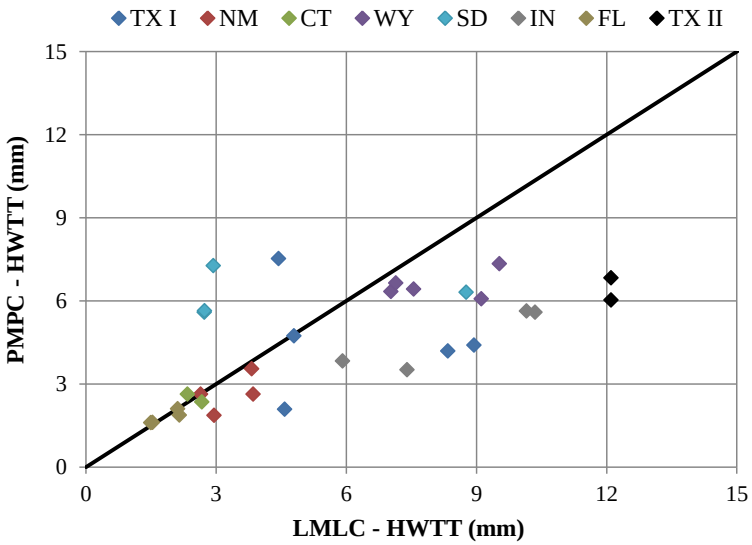

Figure 55. HWTT rut depth at 5,000 load cycles correlation for LMLC versus PMPC specimens.

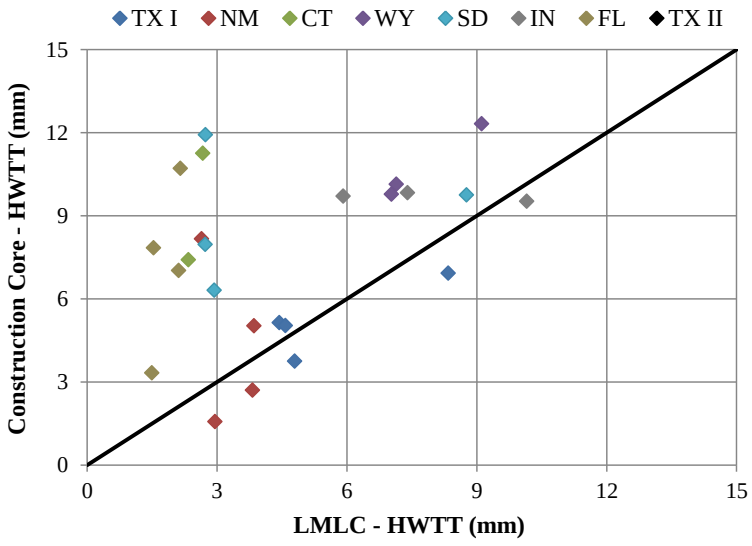

Figure 56. HWTT rut depth at 5,000 load cycles correlation for LMLC specimens versus cores at construction.

Summary

According to the M_R and E* test results, good correlations in mixture stiffness between LMLC specimens with the selected laboratory STOA protocols and PMPC specimens and cores at construction were obtained for a wide range of asphalt mixtures from nine field projects. In addition, an approximately equivalent rutting resistance was also observed for LMLC specimens and PMPC specimens in terms of HWTT $\Delta\varepsilon_{SN}^{vp}$ values and rut depths at 5,000 load cycles. A higher rutting susceptibility in the HWTT was shown for cores at construction than the corresponding LMLC specimens, which was possibly caused by the need to plaster the cores to fit the height of the HWTT molds. Thus, the simulation of binder/mixture aging during plant production and construction by the laboratory STOA protocols of two hours at 275°F (135°C) for HMA and 240°F (116°C) for WMA was verified in this research study for a wider range of asphalt mixtures.

Factors Affecting Short-Term Aging Characteristics

This section presents the results of the laboratory experiments to identify mixture components and production parameters (i.e., factors) with significant effects on the performance of short-term aged asphalt mixtures. These factors include binder source, aggregate absorption, WMA technology, inclusion of recycled materials, plant type, and production temperature. Detailed discussions for each factor are presented in the following sections.

A statistical analysis was also performed to identify which factors had a significant effect on the M_R stiffness results. Separate statistical experiments and

analyses were performed to assess the effects of each of the six factors of interest while incorporating information on field project, specimen type (i.e., cores at construction, PMPC specimens, and LMLC specimens), and NMAS (i.e., 9.5mm, 12.5mm, and 19 mm), and AV as variables.

WMA Technology (HMA vs. WMA)

The M_R and HWTT results for LMLC specimens, PMPC specimens, and cores at construction from eight field projects are shown in Figure 57 through Figure 59, with M_R stiffness and HWTT rutting resistance parameters of $\Delta\varepsilon_{SN}^{vp}$ values and rut depth at 5,000 load cycles for HMA mixtures plotted against those of corresponding WMA mixtures. The x-axis coordinate represents HMA test results, and the y-axis coordinate represents the corresponding WMA test results. The black solid line is the line of equality, and the red dashed line illustrates the shift from the line of equality for M_R stiffness or rutting resistance parameters in the HWTT.

The M_R stiffness comparison for HMA versus WMA shown in Figure 57 illustrated that most of the data points were below the line of equality, indicating a higher M_R stiffness for HMA as compared WMA. Figure 58 and Figure 59 presents the HWTT $\Delta\varepsilon_{SN}^{vp}$ and rut depth at 5,000 load cycles comparison for HMA versus WMA, respectively. As illustrated, most of the data points were above the line of equality, indicating a better rutting resistance in the HWTT for HMA than WMA. Thus, the inclusion of WMA technology was likely to produce asphalt mixtures with lower stiffness and higher rutting susceptibility.

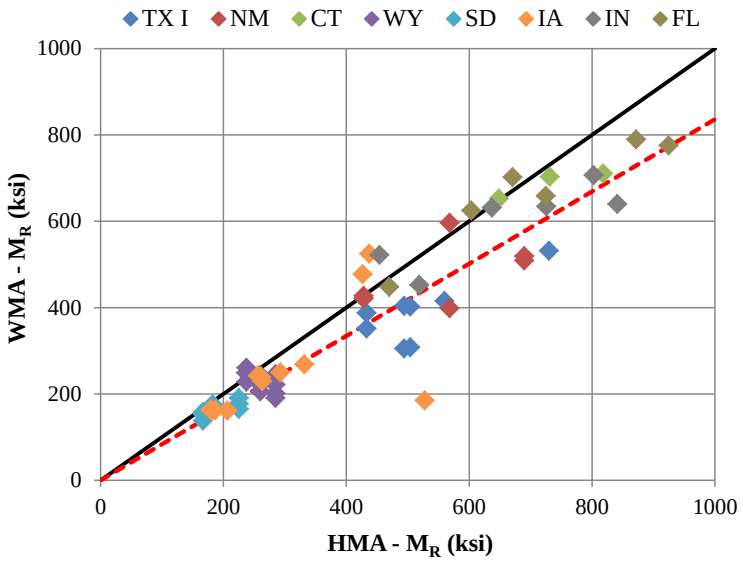

Figure 57. M_R stiffness comparison for HMA versus WMA.

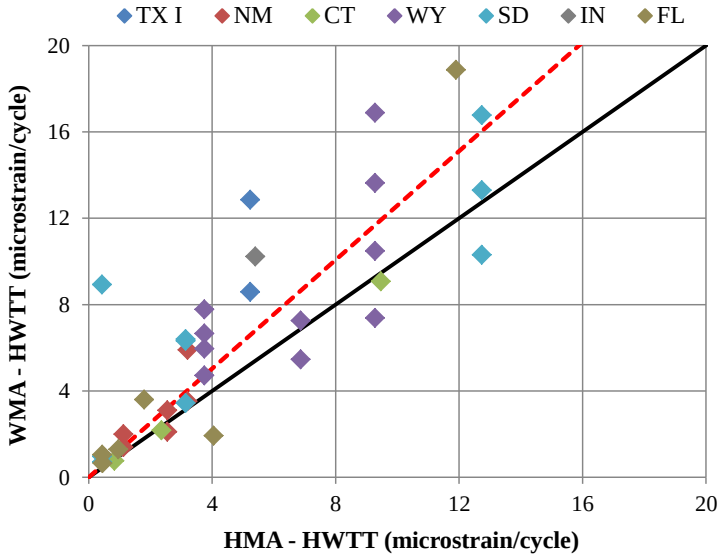

Figure 58. HWTT $\Delta\varepsilon_{SN}^{vp}$ comparison for HMA versus WMA.

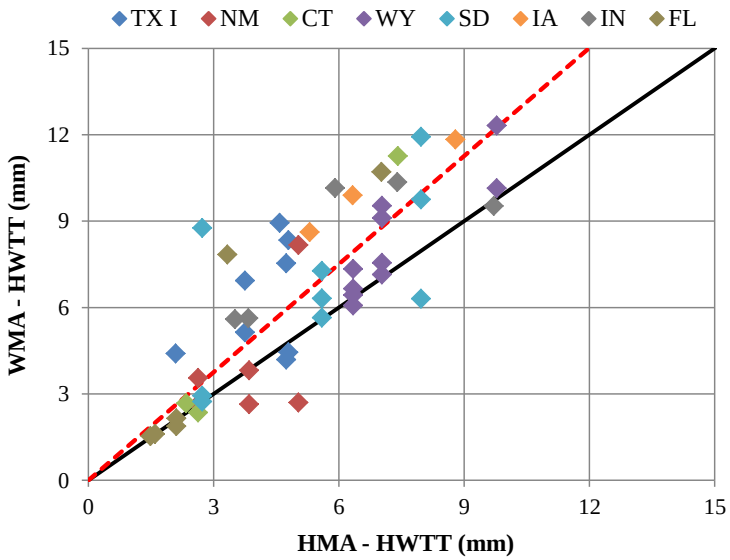

Figure 59. HWTT rut depth at 5,000 load cycles comparison for HMA versus WMA.

Figure 60 and Figure 61 present the E* master curve comparisons for HMA versus WMA from the Connecticut and Indiana field projects, respectively. The comparison was performed for each specimen type (i.e., BMP PMPC specimen, DMP PMPC specimen, and LMLC specimen). For all comparisons in terms of E* stiffness for HMA versus WMA (except for BMP PMPC specimens from the Indiana field project), the E* master curves for HMA mixtures were above or overlapping with those for WMA counterpart mixtures indicating higher or equivalent E* stiffness values over a wide range of testing temperatures and frequencies. For the exceptional case, slightly lower E* stiffness values were observed for HMA mixtures as compared to their WMA counterparts.

For the statistical analysis, M_R stiffness measurements obtained from eight field projects (Connecticut, Florida, Indiana, Iowa, New Mexico, South Dakota, Texas I, and

Wyoming), with information about specimen type, WMA technology, NMAS, and AV were used. The analysis of covariance (ANACOVA), having WMA technology and specimen type as main effects along with a two-way interaction effect between them (specimen type * WMA technology), NMAS and AV as covariates, and field project as a random effect, was fitted to the data. The fixed test results indicated that specimen type, WMA technology, AV, and specimen type * WMA technology were statistically significant at $\alpha = 0.05$, while the effect of NMAS was not significant. When there is a significant interaction effect, the effect of each factor involved in the interaction needs to be assessed against the levels of the other factor because the effect might be different for each level of the other factor. Therefore, the effect of WMA technology was assessed for each level of specimen type. According to the analysis results, except for cores at construction, the predicted M_R stiffness was lower for WMA than for HMA.

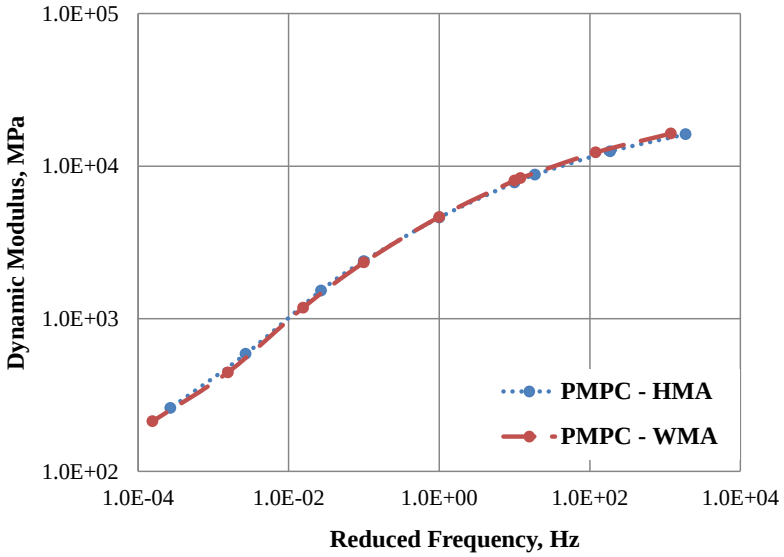

(a)

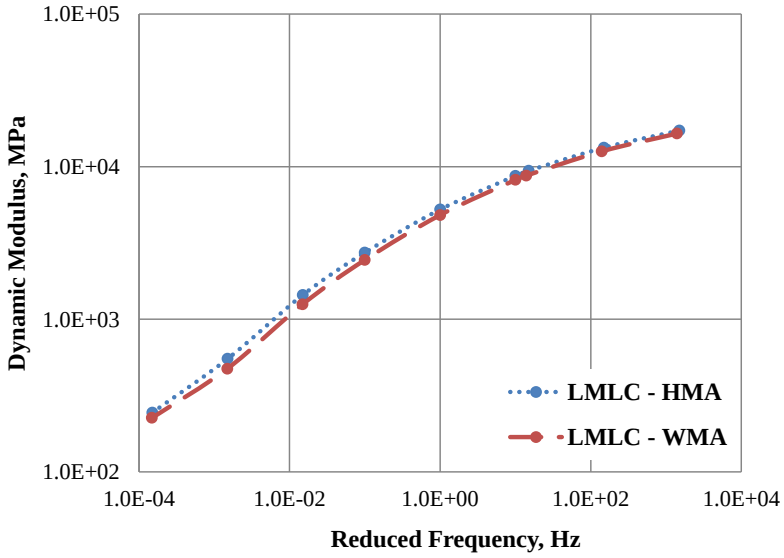

(b)

Figure 60. E* master curve comparison for HMA versus WMA for the Connecticut field project; (a) PMPC specimens, (b) LMLC specimens.

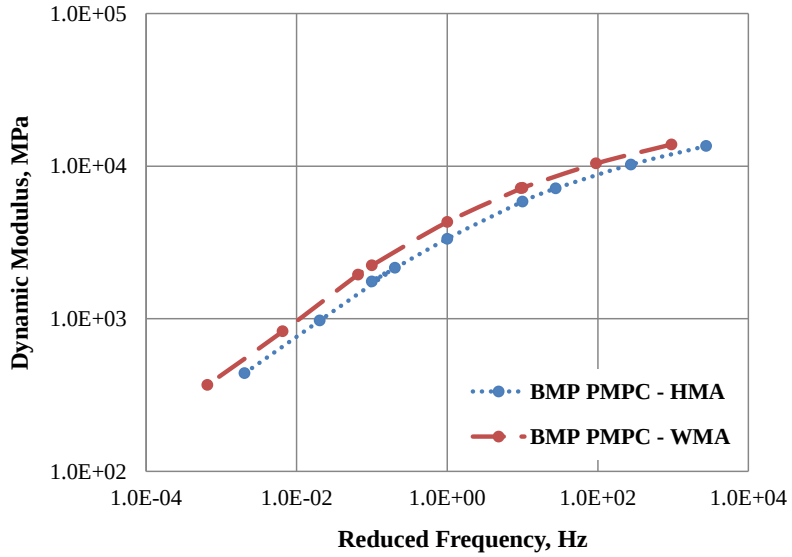

(a)

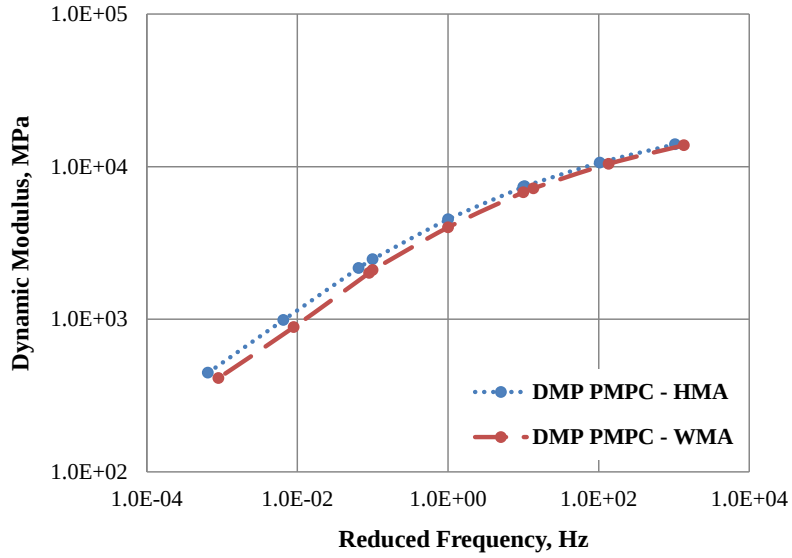

(b)

Figure 61. E* master curve comparison for HMA versus WMA for the Indiana field project; (a) BMP PMPC specimens, (b) DMP PMPC specimens, (c) BMP LMLC specimens, (d) DMP LMLC specimens.

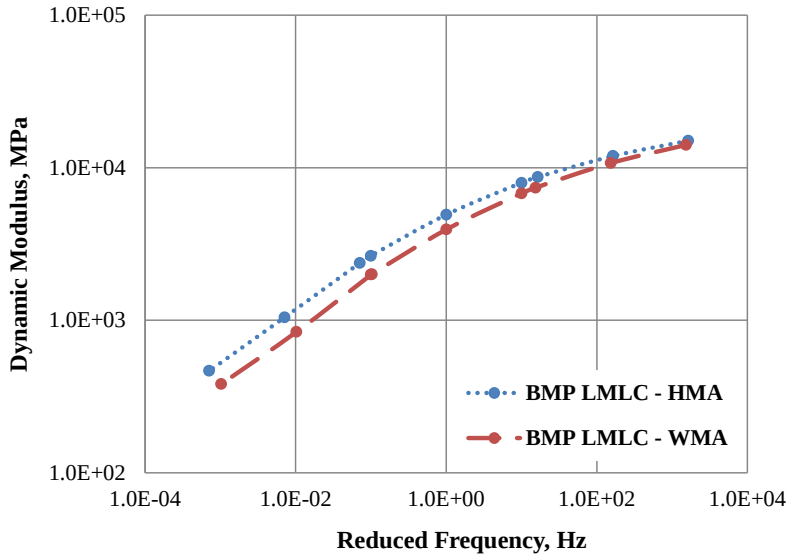

(c)

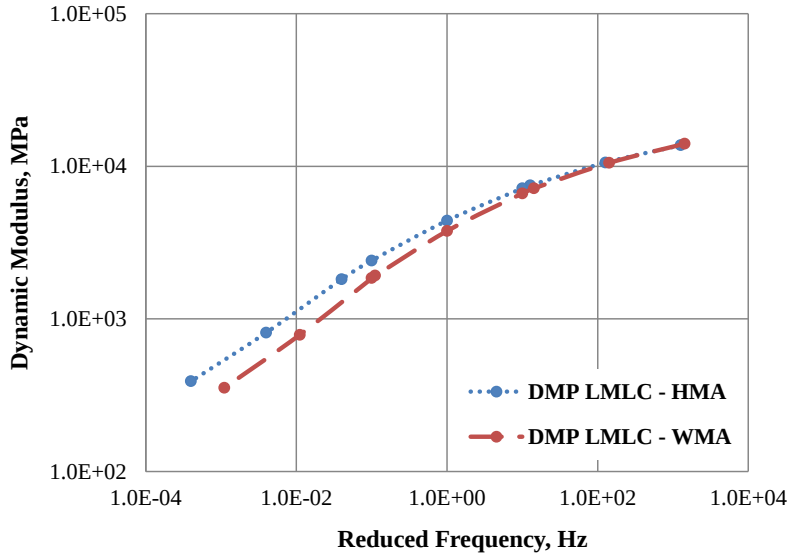

(d)

Figure 61. Continued.

Production Temperature (High vs. Control)

The M_R results for LMLC specimens, PMPC specimens, and cores at construction from the Wyoming and Iowa field projects are presented in Figure 62, with M_R stiffness for mixtures produced at high temperatures and those at control temperatures plotted against each other. The evaluation of rutting resistance in the HWTT by $\Delta\varepsilon_{SN}^{vp}$ value and rut depth at 5,000 load cycles was not available for this factor since early stripping was observed for the majority of Iowa mixtures, with LC_{SN} values less than 3,000 load cycles and rut depths greater than the failure criteria of 12.5mm at 5,000 load cycles. The x-axis coordinate represents the M_R stiffness for mixtures produced at control temperatures, and the y-axis coordinate represents M_R stiffness for mixtures produced at high temperatures. The black solid line is the line of equality, and the red dashed line illustrates the shift from the line of equality for M_R stiffness.

As illustrated in Figure 62, most of the data points fell on the line of equality, indicating equivalent M_R stiffness for those asphalt mixtures. Therefore, an increase in production temperature (20 to 30°F) during mixing followed by the same short-term aging protocols had no significant effect on mixture stiffness.

For the statistical analysis, the ANACOVA model, including production temperature, WMA technology, and specimen type as main effects along with all possible two-way interactions, AV as a covariate, and field project as a random effect, was first fitted to the data, but none of the two-way interaction effects were statistically significant. Thus, the two-way interaction effects were removed from the model, and the ANACOVA model was fitted again to the data. The results showed that the effects of

specimen type and WMA technology were statistically significant at $\alpha = 0.05$, while the effect of production temperature and AV were not.

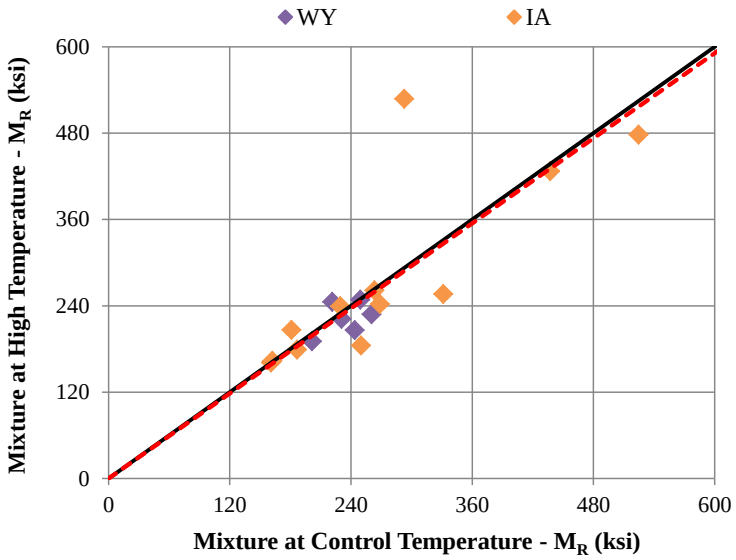

Figure 62. M_R stiffness comparison for asphalt mixtures produced at high versus control temperatures.

Plant Type (BMP vs. DMP)

The M_R and HWTT test results for LMLC specimens, PMPC specimens, and cores at construction from the Indiana and Texas II field projects are presented in Figure 63 and Figure 64, with M_R stiffness and the HWTT rutting resistance parameter of rut depth at 5,000 load cycles for BMP produced mixtures and DMP produced mixtures plotted against each other. The evaluation of rutting resistance in the HWTT by $\Delta\varepsilon_{SN}^{vp}$ value was not available for this factor since early stripping was observed for the majority of Indiana and Texas II asphalt mixtures. The x-axis coordinate represents the test results

for BMP produced mixtures, and the y-axis coordinate represents corresponding test results for DMP produced mixtures. The black solid line is the line of equality, and the red dashed line illustrates the shift from the line of equality for M_R stiffness or rut depth measurements in the HWTT.

The M_R results in Figure 63 illustrated that most of the data points were on the line of equality, indicating equivalent mixtures stiffness was achieved by asphalt mixtures produced in a BMP and the corresponding mixtures produced in a DMP. Figure 64 presents the traditional HWTT rutting resistance parameter of rut depth at 5,000 load cycles for the comparison of BMP produced mixtures versus DMP produced mixtures. Similar to Figure 63, most of the data points fell on the line of equality. Therefore, equivalent mixture stiffness and rutting resistance was observed for asphalt mixtures produced in a BMP and a DMP.

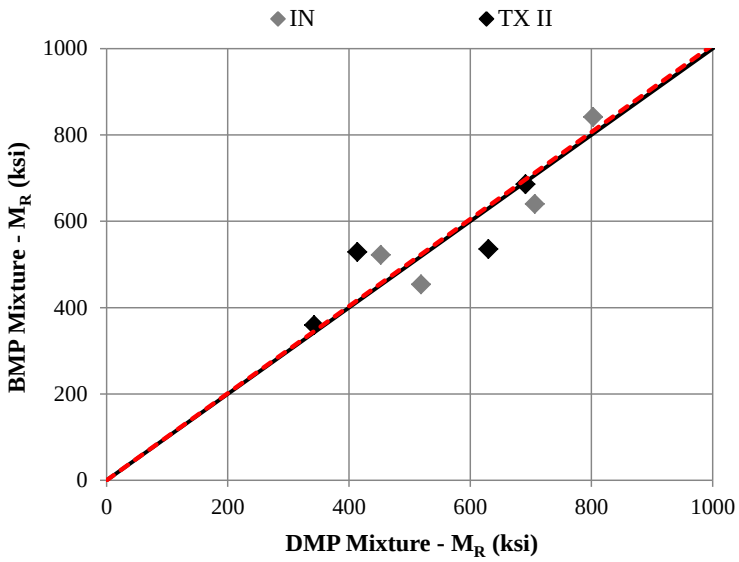

Figure 63. M_R stiffness comparison for asphalt mixtures produced at BMP versus DMP.

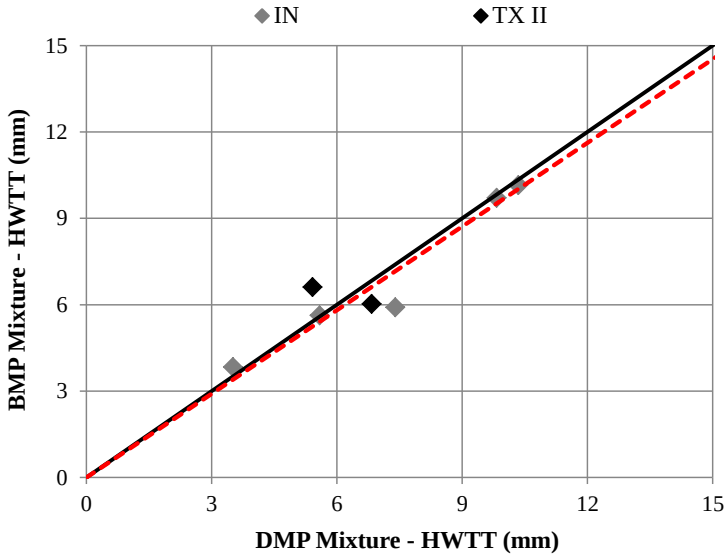

Figure 64. HWTT rut depth at 5,000 load cycles comparison for asphalt mixtures produced at BMP versus DMP.

For the statistical analysis, the ANACOVA model including plant type and specimen type as main effects, plant type * specimen type as a two-way interaction effect, AV as a covariate, and field project as a random effect, was first fitted to the data. However, the two-way interaction effect was not statistically significant, and the ANACOVA model without the two-way interaction effect was fitted again to the data. The results showed that the effects of specimen type and AV were statistically significant at $\alpha = 0.05$, while the effect of plant type was not.

Inclusion of Recycled Materials (RAP/RAS vs. No RAP/RAS)

The M_R and HWTT test results for LMLC specimens, PMPC specimens, and cores at construction from the Texas I and New Mexico field projects are presented in Figure 65 through Figure 67, with M_R stiffness and HWTT rutting resistance parameters of $\Delta\varepsilon_{SN}^{vp}$ values and rut depth at 5,000 load cycles for control mixtures without recycled mixtures and RAP/RAS mixtures plotted against each other. The control mixtures from the Texas I field project were produced using a PG 70-22 binder while the RAP/RAS mixtures were produced using a softer PG 64-22 binder in conjunction with 15 percent RAP and 3 percent RAS; the control mixtures from the New Mexico mixtures were produced using a PG 76-28 binder while the RAP mixtures were produced using a softer PG 64-28 binder in conjunction with 35 percent RAP. The x-axis coordinate represents test results for the control mixtures, and the y-axis coordinate represents corresponding test results for RAP/RAS mixtures. The black solid line is the line of equality, and the red dashed line illustrates the shift from the line of equality for M_R stiffness or HWTT rutting resistance parameters.

The M_R stiffness results shown in Figure 65 illustrated that most of the data points were above the line of equality, indicating significantly higher stiffness for RAP/RAS mixtures as compared to the control mixtures. The shifted line of equality presents a relatively weak correlation (R^2 value of 0.33), which indicated that the increase in mixture stiffness induced by adding recycled materials was inconsistent. Therefore, recycled materials (i.e. RAP and RAS) from different sources utilized in different field projects should be treated as unique materials whose properties are related to the original asphalt mixtures and in-service times and climatic conditions.

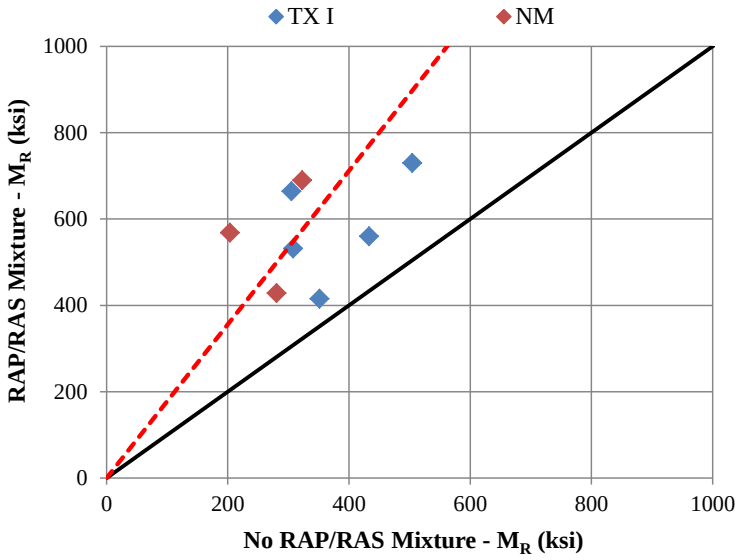

Figure 65. M_R stiffness comparison for asphalt mixtures with versus without RAP and RAS.

Figure 66 presents the HWTT $\Delta\varepsilon_{SN}^{vp}$ comparison for RAP/RAS mixtures versus control mixtures. As illustrated, most points were above the line of equality, indicating

decreased rutting resistance in the HWTT for RAP/RAS mixtures as compared to the control counterpart mixtures. Figure 67 presents the traditional HWTT rutting resistance parameter of rut depth at 5,000 load cycles. No consistent trend in the comparison of RAP/RAS mixtures versus control mixtures was observed for this parameter.

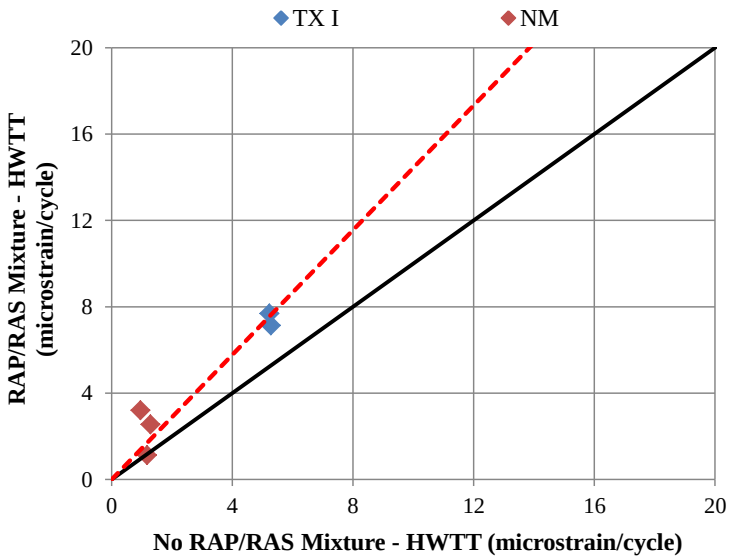

Figure 66. HWTT $\Delta\varepsilon_{SN}^{vp}$ comparison for asphalt mixtures with versus without RAP and RAS.

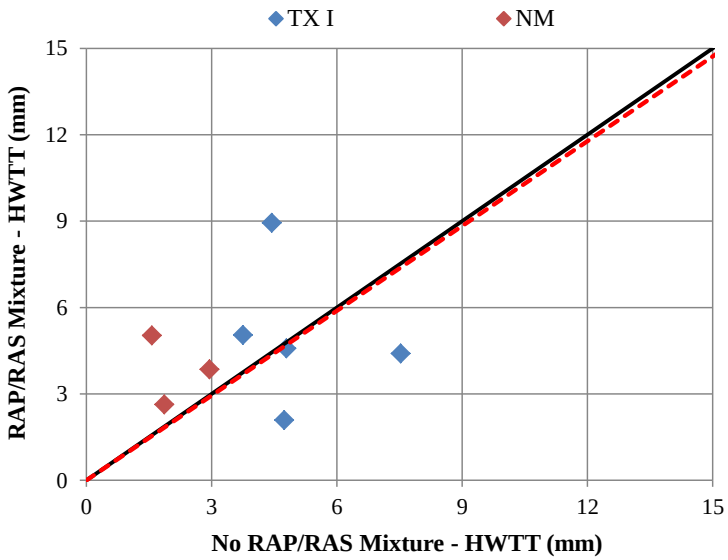

Figure 67. HWTT rut depth at 5,000 load cycles comparison for asphalt mixtures with versus without RAP and RAS.

For the statistical analysis, the ANACOVA model including recycled materials, specimen type, and WMA technology as main effects along with all possible two-way interaction effects among them, AV as a covariate, and field project as a random effect, was first fitted to the data. Because the WMA technology * recycled materials interaction effect was not statistically significant at $\alpha = 0.05$, it was removed, and the ANACOVA model was fitted again to the data. The results showed that the only effect that was not statistically significant at $\alpha = 0.05$ was AV. A multiple comparison procedure of the Tukey's HSD test showed that the difference between no RAP/RAS and RAP/RAS mixtures was statistically significant for cores at construction, PMPC specimens, and LMLC specimens, although the difference varied with specimen type. The conclusion from the statistical analysis was that, in general, mixtures with

RAP/RAS had higher M_R stiffness than mixtures with no RAP/RAS although there is considerable variability due to the origin, age and nature of the recycled materials.

Aggregate Absorption (High vs. Low Absorptive Aggregate)

The M_R and HWTT test results for LMLC specimens, PMPC specimens, and cores at construction from the Iowa and Florida field projects are presented in Figure 68 and Figure 69, with M_R stiffness and the HWTT rutting resistance parameter of rut depth at 5,000 load cycles for asphalt mixtures using high absorptive aggregates versus low absorptive aggregates plotted against each other. The evaluation of rutting resistance in the HWTT by $\Delta\varepsilon_{SN}^{vp}$ value was not available for this factor since early stripping was observed for the majority of Iowa and Florida asphalt mixtures, with LC_{SN} values less than 3,000 load cycles. The x-axis coordinate represents test results for mixtures using high absorptive aggregates, and the y-axis coordinate represents corresponding test results for mixtures using low absorptive aggregates. The black solid line is the line of equality, and the red dashed line illustrates the shift from the line of equality for M_R stiffness or HWTT rut depth measurements.

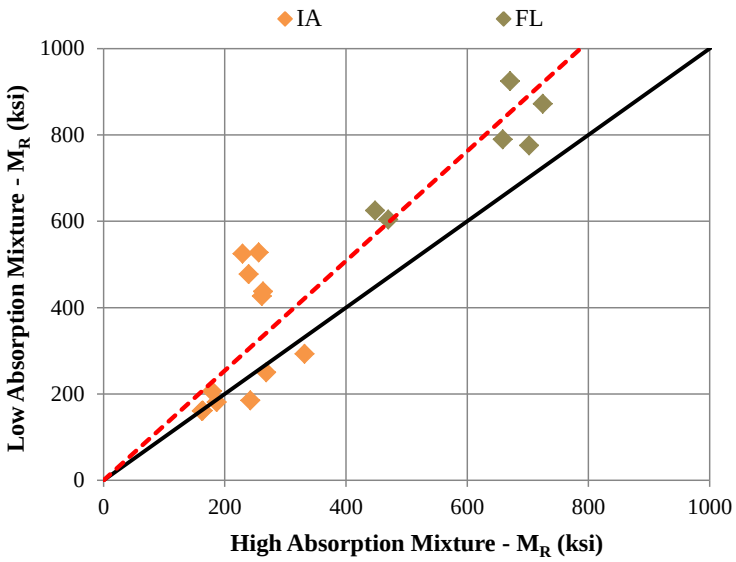

Figure 68. M_R stiffness comparison for asphalt mixtures using high versus low absorptive aggregates.

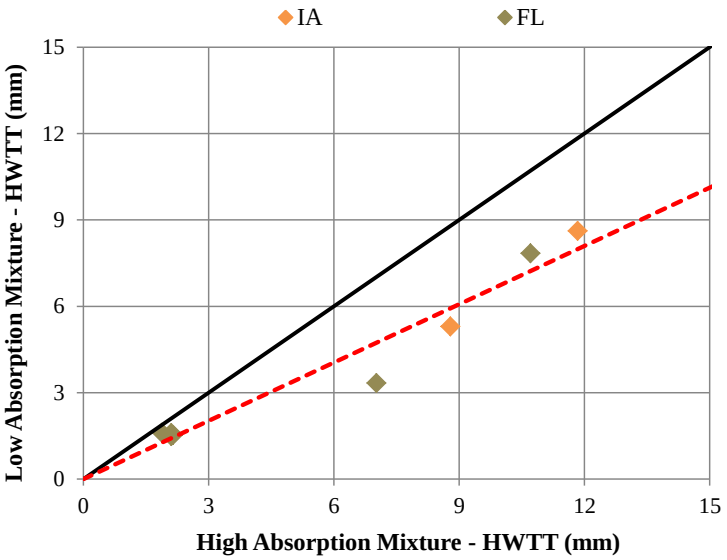

Figure 69. HWTT rut depth at 5,000 load cycles comparison for asphalt mixtures using high versus low absorptive aggregates.

The M_R stiffness comparison for mixtures using high versus low absorptive aggregates shown in Figure 68 illustrated that most of the data points were above the line of equality, indicating a higher M_R stiffness for mixtures using low absorptive aggregates as compared to the counterpart mixtures using high absorptive aggregates. Figure 69 presents the HWTT results in terms of rut depth at 5,000 load cycles. Similar to Figure 68, most of the data points in Figure 69 were below the line of equality, indicating better rutting resistance in the HWTT for mixtures using low versus high absorptive aggregates. The better mixture performance in terms of stiffness and rutting resistance observed for mixtures using low absorptive aggregates as compared to those using high absorptive aggregates might be attributed to thinner effective binder film thicknesses in these mixtures as indicated by lower P_{be} and FT_{be} values in Table 7.

For the statistical analysis, the ANACOVA model, including aggregate absorption, specimen type, and WMA technology as main effects, AV as a covariate, and field project as a random effect, was fitted to the M_R stiffness measurements obtained from the Iowa and Florida field projects. The results showed that the effects of specimen type, WMA technology, and aggregate absorption were statistically significant at $\alpha = 0.05$, while the effect of AV was not.

Binder Source (Binder I vs. Binder II)

The M_R results for LMLC specimens, PMPC specimens, and cores at construction from the Texas II field project are presented in Figure 70, with M_R stiffness for mixtures using binder A plotted against those of corresponding mixtures using binder V. The evaluation of rutting resistance in the HWTT by $\Delta\varepsilon_{SN}^{vp}$ value and rut depth at

5,000 load cycles was not available for this factor since early stripping was observed for all Texas II mixtures with LC_{SN} values less than 3,000 load cycles and rut depths greater than the failure criteria of 12.5mm at 5,000 load cycles. The x-axis coordinate represents M_R stiffness for mixtures using binder A, and the y-axis coordinate represents M_R stiffness for mixtures using binder V. The black solid line is the line of equality, and the red dashed line illustrates the shift from the line of equality for M_R stiffness.

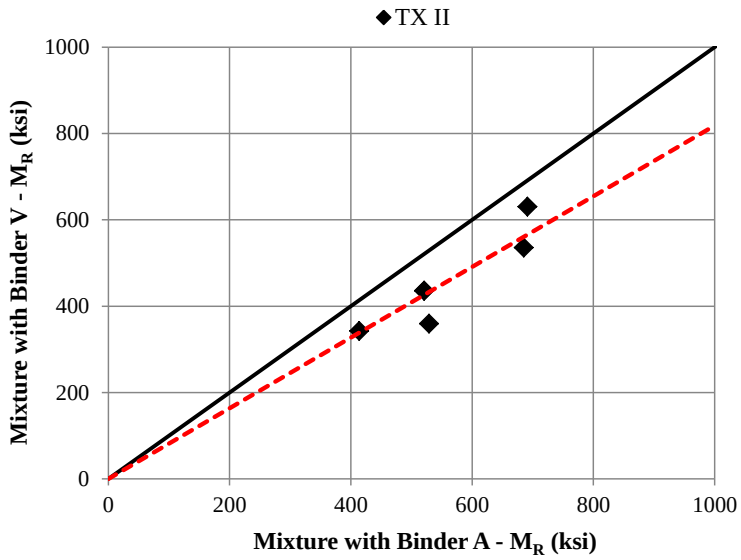

Figure 70. M_R stiffness comparison for asphalt mixtures using different binder sources.

As shown in Figure 70 for the M_R stiffness comparison for asphalt mixtures using two different binder sources, most of the data points were below the line of equality, indicating a higher M_R stiffness for asphalt mixtures using binder A than the counterpart mixtures using binder V.

Figure 71 presents the E* master curve comparisons for PMPC specimens and LMLC specimens of asphalt mixtures with binder A versus binder V. The comparison was performed for each specimen type (i.e., BMP PMPC specimen, DMP PMPC specimen, and LMLC specimen). As illustrated, the E* master curves for mixtures with binder A were consistently above the curves obtained for mixtures with binder V. Therefore, binder source exhibited a significant effect on the performance of short-term aged asphalt mixtures, and consequently, asphalt mixtures using the same PG graded binders from different sources would exhibit substantially different mixture performance in terms of stiffness and rutting resistance.

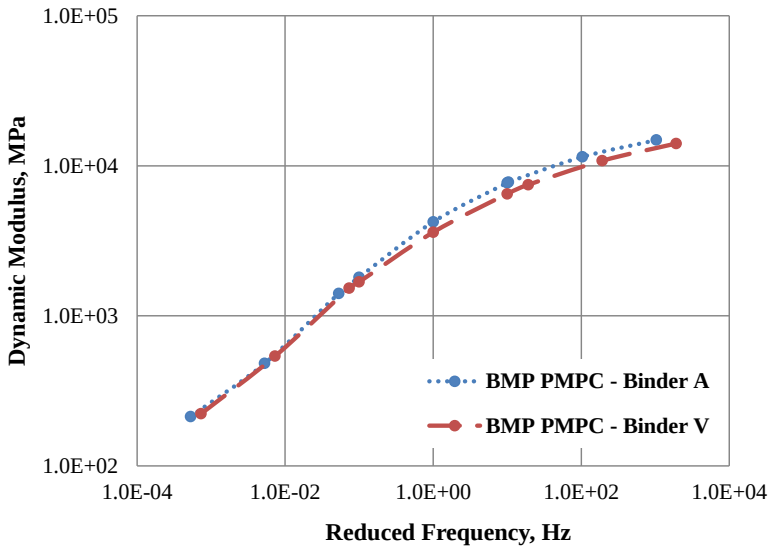

(a)

Figure 71. E* master curve comparison for asphalt mixtures using different binder sources for the Texas II field project; (a) BMP PMPC specimens, (b) DMP PMPC specimens, (c) LMLC specimens.

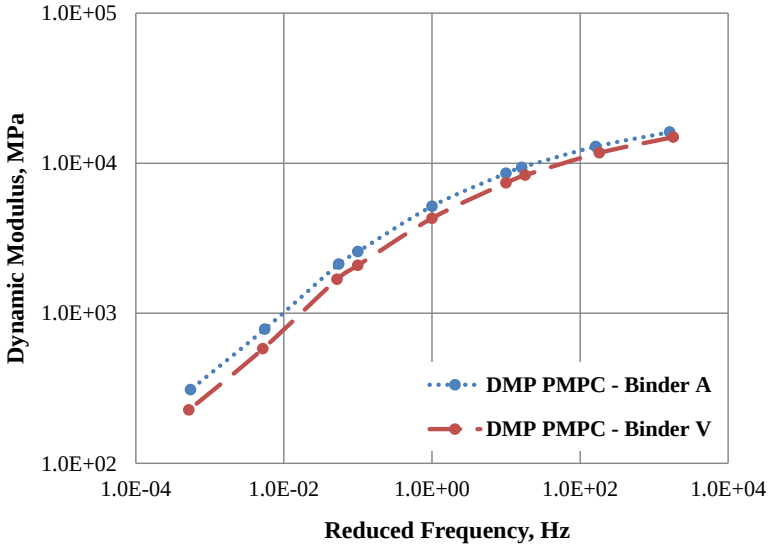

(b)

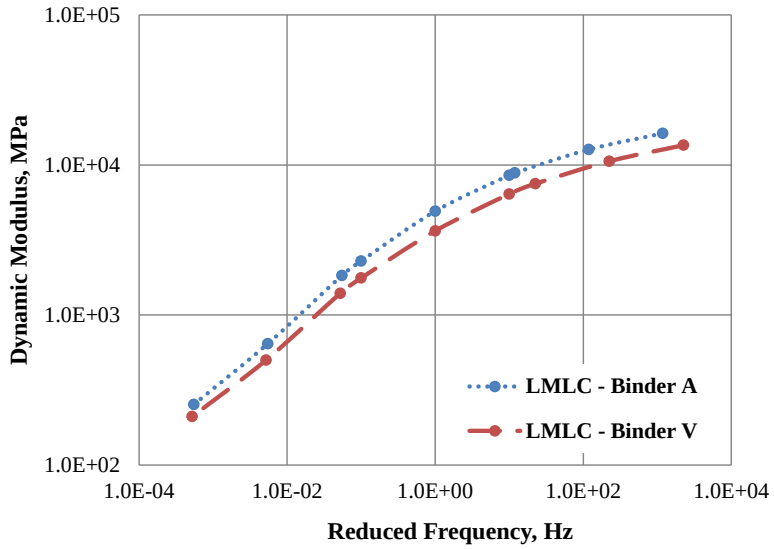

(c)

Figure 71. Continued.

For the statistical analysis, the ANACOVA model included binder source and specimen type as main effects and AV as a covariate; originally, a model including the two-way interaction of binder source * specimen type was used, but the interaction

effect was not statistically significant, and therefore removed. The results showed that the effects of binder source, specimen type, and AV were all statistically significant at $\alpha = 0.05$. Specifically, Binder A yielded significantly higher M_R stiffness than Binder V.

Summary

In this section, the effects of various mixture components and production parameters including WMA technology, production temperature, plant type, inclusion of recycled materials, aggregate absorption, and binder source on the performance of short-term aged asphalt mixtures were evaluated. The correlations in terms of M_R stiffness and HWTT rutting resistance parameters were performed for each factor, and the results are summarized in Table 8. Those mixture components and production parameters with significant effects were identified based on the magnitude of the slope for the shifted lines of equality being greater than 1.05 or smaller than 0.95 (i.e., 5 percent off from the line of equality) and were corroborated via statistical analysis.

As shown in Table 8, binder source, aggregate absorption, WMA technology, and inclusion of recycled materials had significant effects on stiffness and rutting resistance of short-term aged asphalt mixtures. However, no significant effect from plant type and production temperature was observed.

Table 8. Summary of the Effects of Mixture Components and Production Parameters on the Performance of Short-Term Aged Asphalt Mixtures

Factor	M_R Stiffness			HWTT $\Delta\varepsilon_{SN}^{vp}$		HWTT Rut Depth	
	Slope Magnitude	Significant Effect	STAT Significant	Slope Magnitude	Significant Effect	Slope Magnitude	Significant Effect
WMA Technology	0.836	Yes	Yes	1.259	Yes	1.251	Yes
Production Temperature	0.985	No	No	-	-	-	-
Plant Type	1.008	No	No	-	-	0.968	No
Inclusion of Recycled Materials	1.779	Yes	Yes	1.444	Yes	0.983	No
Aggregate Absorption	1.271	Yes	Yes	-	-	0.675	Yes
Binder Source	0.818	Yes	Yes	-	-	-	-

CHAPTER VI

LONG-TERM AGING OF ASPHALT MIXTURES

Overview

Aging refers to the stiffening of asphalt mixtures with time due to volatilization, oxidation, and other chemical processes. It occurs due to the heating of the binder during production and construction in the short-term and due to oxidation with time over the long-term throughout the service life of the pavement. The ability to simulate field aging of asphalt binders and mixtures has been studied extensively, and laboratory aging procedures including the use of pressure aging vessel on asphalt binders and laboratory LTOA protocols on compacted asphalt mixtures have been adopted for use in binder specifications and mix design. Additionally, field aging of asphalt mixtures has been assumed to be relatively consistent in the past, and acceptable correlations have been established between field aging and laboratory LTOA protocols (Bell et al. 1994; Brown and Scholz 2000; Epps Martin et al. 2014; Glover et al. 2005; Houston et al. 2007). However, this occurred at a time when the amount of recycled materials was relatively low, WMA was not common, and plant production temperatures were fairly consistent.

In the last three decades, changes have occurred in asphalt mixture components, mixture processing, and plant design, including increased use of polymer modifiers, increased use of recycled materials, the advent of WMA, and DMPs replacing BMPs. Although these changes are beneficial for economic, environmental, and technical reasons, they have raised the need to review the practices on how asphalt mixtures are

designed and evaluated. Therefore, there is a need to further evaluate the long-term aging characteristics of asphalt mixtures that considers the impacts of climate, aggregate type, recycled materials, WMA technology, plant type, and production temperature.

The objectives of this research study are to: 1) develop a correlation between field aging (i.e., one to two years after construction) and laboratory LTOA protocols that accommodates various mixture components and production parameters, and 2) identify factors with significant effects on the long-term aging characteristics of asphalt mixtures.

Background

Aging of asphalt pavements continues throughout their in-service life, though at a lower rate compared to that occurring during production and construction. Therefore, it is important to account for the changes in asphalt mixture properties due to field aging when preparing laboratory samples for long-term performance testing. The standard practice for laboratory mix design of asphalt mixtures is to simulate field aging by conditioning compacted specimens for five days at 185°F (85°C) in accordance with AASHTO R 30. In the past few decades, studies have evaluated the effect of field and laboratory long-term aging on asphalt mixture properties and identified reasonable correlations between field aging and laboratory LTOA protocols. A brief summary of these studies is provided in Table 9.

Table 9. Previous Research on Long-Term Aging of Asphalt Mixtures

Reference	Long-Term Aging	Major Findings
Kemp and Predoehl (1981)	Field Aging	Air temperature, voids, and aggregate porosity significant effects
Kari (1982)		Pavement permeability and asphalt content significant effects
Rolt (2000)		• Exposure time and ambient temperature significant effects • Binder content, mixture air voids, and filler content no effect
Rondon et al. (2012)		• Increased mixture stiffness, rutting resistance, and fatigue resistance for first 29 months of environmental exposure • Opposite trend observed between 30 and 42 months
Farrar et al. (2013)		• Field aging not limited to the top 25mm of the pavement • Field aging gradient observed
West et al. (2014)		• WMA less aging than HMA during production • Reduced difference between WMA vs. HMA with field aging • Equivalent binder true grade and binder absorption for WMA vs. HMA after 2 years of field aging
Morian et al. (2011)	Lab Aging (3, 6, and 9 months at 60°C)	• Increased mixture E* and binder carbonyl area with LTOA • Binder source significant effect while aggregate source no effect
Azari and Mohseni (2013)	Lab Aging (2 days at 85°C 5 days at 85°C)	• Increased mixture resistance to permanent deformation with LTOA • Interdependence observed between STOA and LTOA
Tarbox and Daniel (2012)	Lab Aging (2 days at 85°C 4 days at 85°C 8 days at 85°C)	• Increased stiffness with LTOA • Stiffening effect from LTOA: virgin mixture > RAP mixture • Global Aging System model > LTOA
Safaei et al. (2014)	Lab Aging (2 days at 85°C 8 days at 85°C)	• Increased stiffness with LTOA • Reduced difference in stiffness for HMA vs. WMA with LTOA

Table 9. Continued

Reference	Long-Term Aging	Major Findings
Bell et al. (1994)Bell et al., 1994	Field vs. Lab Aging (4 days at 100°C 8 days at 85°C)	• STOA of 4 hours at 135°C = field aging during the construction process • Effect on mixture aging: LTOA temperature > LTOA time • STOA plus LTOA of 4 days at 100°C and 8 days at 85°C = 9-years of field aging in Washington State
Brown and Scholz (2000)	Field vs. Lab Aging (4 days at 85°C)	• Stiffness: LTOA of 4 days at 85°C = 15years of field aging in the United States
Houston et al. (2007)	Field vs. Lab Aging (5 days at 80°C 5 days at 85°C 5 days at 90°C)	• Significant field and laboratory aging • AV effect on field aging • AASHTO R35 LTOA (5D@85°C) vs. 7-10 Yrs field aging: lab > field when AV < 8 percent; lab < field when AV > 8 percent
Epps Martin et al. (2014)	Field vs. Lab Aging (1 to 16 weeks at 60°C)	• Increased stiffness with field aging and laboratory LTOA • Pavement in-service temperature effect on field aging • Stiffness: WMA = HMA, after 6-8 months of field aging • Stiffness: STOA of 2 hours at 135°C for HMA and 2 hours at 116°C for WMA plus LTOA of 4-8 weeks at 60°C = first summer of field aging

As summarized in Table 9, previous studies have documented that field aging had a significant effect on mixture properties, and a number of factors had been identified to have an influence on field aging characteristics of asphalt mixtures, including pavement in-service temperature and time, mixture AV and binder content, and aggregate absorption. Similar to field aging, laboratory LTOA protocols were able to produce asphalt mixtures with significantly increased mixture stiffness and rutting resistance as compared to that for unaged mixtures. In addition, the aging characteristics of asphalt mixtures were more sensitive to LTOA temperature than LTOA time. Finally,

a variety of correlations between field aging and laboratory LTOA protocols had been proposed, and the differences among those correlations were likely due to the different binder or mixture properties investigated.

Despite the previous research efforts on long-term aging of asphalt mixtures, there are still several aspects that need to be fully addressed. For example, the quantification of field aging using pavement in-service time failed to account for the differences in construction dates and climates for various field projects; therefore, a better field aging metric is needed considering both pavement in-service temperature and time. Furthermore, it is essential to develop a correlation between field aging and laboratory LTOA protocols that encompasses the effects of aggregate absorption, recycled materials, WMA technology, plant type, and production temperature.

Experimental Design

Field Projects and Materials

Seven of the field projects introduced in Chapter V were included in this research study; the Connecticut and Texas II field projects were not used here since no post-construction cores were obtained due to the traffic concerns of the agency or time constraints of the study. For each of the seven field projects, cores at construction and at least one set of post-construction cores were acquired to represent field aging. In addition, raw materials including asphalt binders, aggregates, and recycled materials were collected for fabricating LMLC specimens.

Specimen Fabrication and LTOA Protocols

To fabricate LMLC specimens, aggregates and binders were heated to the specified plant mixing temperature and then mixed using a portable mixer. Afterwards, the loose mix was conditioned in the oven following the laboratory STOA protocol of two hours at 275°F (135°C) for HMA and 240°F (116°C) for WMA prior to compaction in the SGC. As discussed previously in Chapter V, the selected STOA protocol was able to simulate the mixture volumetrics, stiffness, and rutting resistance for cores at construction. Trial specimens were fabricated to ensure specimens were obtained with AV contents of 7.0±0.5 percent. To simulate long-term aging in the field, the short-term aged LMLC specimens were further aged after compaction in accordance with laboratory LTOA protocols of two weeks at 140°F (60°C), three days at 185°F (85°C) (only for two field projects), and five days at 185°F (85°C) prior to being tested for performance evaluation.

Laboratory Tests

M_R and HWTT tests were used in this research study to evaluate the stiffness and rutting resistance of long-term aged asphalt mixtures (i.e., post-construction cores and LMLC specimens with STOA plus LTOA protocols) from various field projects. The M_R test was performed in accordance with ASTM D7369, and M_R stiffness at 77°F (25°C) was used as the mixture stiffness parameter. The HWTT test was performed at 122°F (50°C) per TxDOT specification Tex-242-F. Data analysis was performed using the novel methodology described in Chapter III, and the $\Delta\varepsilon_{SN}^{vp}$ value was used as the mixture rutting resistance parameter.

Research Methodology

Figure 72 presents the research methodology used in this research study. Short-term and long-term aged asphalt mixtures (i.e., cores at various in-service times and LMLC specimens with different aging protocols) from seven field projects were tested to determine the M_R stiffness and HWTT $\Delta\varepsilon_{SN}^{vp}$ values. The test results were analyzed to quantify the evolution of mixture stiffness and rutting resistance with long-term aging in the field and establish a correlation between field aging and laboratory LTOA protocols. In addition, comparisons in terms of M_R stiffness results were also performed to evaluate the effects of mixture and production factors on the long-term aging characteristics of asphalt mixtures.

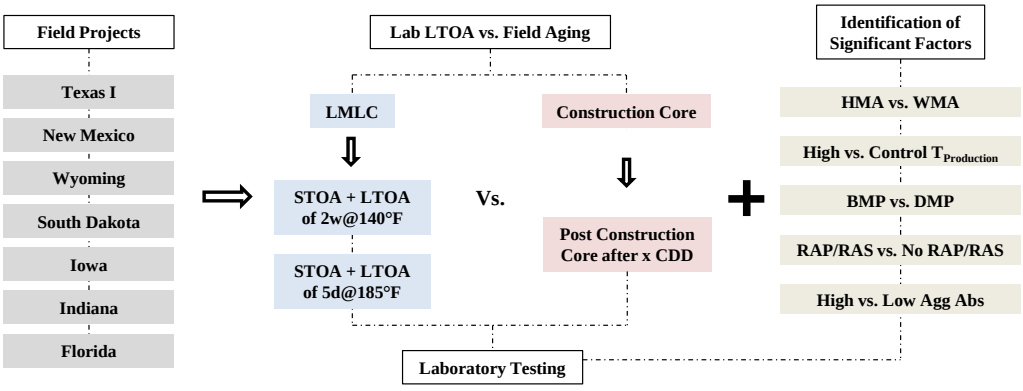

Figure 72. Research methodology for evaluating long-term aging of asphalt mixtures.

Previous literature indicated that field aging of asphalt mixtures had been commonly quantified by the in-service time of the pavement at the time of coring. However, this approach failed to differentiate field projects with different construction dates and climates. To address this shortcoming, the concept of cumulative degree-days

(CDD) (32°F [0°C] base) was proposed in this study, as expressed in Equation 29. Compared to the field in-service time, the CDD value provided a better measure of field aging when comparing field projects built in different climates and at various times of the year.

$$CDD = \sum (T_{dmax} - 32) \quad \text{Equation 29}$$

where:

T_{dmax} = daily maximum temperature, °F.

In order to quantify the evolution of mixture stiffness and rutting resistance with field and laboratory aging, two mixture property ratios—M_R ratio and HWTT rutting resistance parameter (RRP) ratio—were proposed. As expressed in Equation 30, the M_R ratio is defined as the fraction of the M_R stiffness of either field or laboratory long-term aged specimens over that of short-term aged specimens.

$$M_R\ Ratio = M_{R-LTA}/M_{R-STA} \quad \text{Equation 30}$$

where:

$M_{R\text{-}LTA}$ = M_R stiffness of long-term aged specimens including post-construction cores or LMLC specimens after STOA plus LTOA; and

$M_{R\text{-}STA}$ = M_R stiffness of short-term aged specimens including cores at construction or LMLC specimens after STOA.

Since field and laboratory aging produces asphalt mixtures with increased M_R stiffness, the M_R ratio was expected to be greater than 1.0. However, the HWTT RRP ratio exhibited the opposite trend with aging due to the mixture stiffening effect (i.e., less rutting with aging). Therefore, the HWTT RRP ratio was defined as the ratio of the $\Delta\varepsilon_{SN}^{vp}$

value of short-term aged specimens over the $\Delta\varepsilon_{SN}^{vp}$ value of long-term aged specimens, as expressed in Equation 31, in order to expect a ratio greater than 1.0 with aging.

$$HWTT\ RRP\ Ratio = \Delta\varepsilon_{SN}^{vp}{}_{STA} / \Delta\varepsilon_{SN}^{vp}{}_{LTA} \quad \text{Equation 31}$$

where:

$\Delta\varepsilon_{SN}^{vp}{}_{STA}$ = HWTT RRP of short-term aged specimens including cores at construction or LMLC specimens after STOA; and

$\Delta\varepsilon_{SN}^{vp}{}_{LTA}$ = HWTT RRP of long-term aged specimens including post-construction cores or LMLC specimens after LTOA plus STOA.

M_R ratio and HWTT RRP ratio values greater than 1.0 indicate an increase in mixture stiffness and rutting resistance after long-term aging. To discriminate asphalt mixtures with different aging characteristics, those with higher property ratios are considered more sensitive to aging and more likely to exhibit an increase in mixture stiffness and rutting resistance with time.

To further characterize the evolution of binder or mixture properties with field aging, the exponential function shown in Equation 32 was used to correlate the measured property ratio values of post-construction cores with their corresponding CDD values.

$$Mixture\ Property\ Ratio = 1 + \alpha * exp\left[-\left(\frac{\beta}{CDD}\right)^{\gamma}\right] \quad \text{Equation 32}$$

where:

α, β, and γ = fitting coefficients.

As previously mentioned, the selected laboratory STOA protocol was representative of cores at construction in terms of mixture volumetrics, stiffness, and

rutting resistance. Therefore, based on the definitions for mixture property ratios, the correlation between field aging and laboratory LTOA protocols could be made.

Test Results and Data Analysis

This section provides the mixture M_R and HWTT results for LMLC specimens fabricated following the selected STOA and LTOA protocols and cores at various in-service times from seven field projects. The test results were analyzed to establish a correlation between field aging and laboratory LTOA protocols, and to identify mixture components and production parameters with significant effects on the long-term aging characteristics of asphalt mixtures.

Quantification of Field Aging

CDD (32°F [0°C] base) was used to quantify field aging and to account for the differences in construction dates and climates for various field projects. The CDD values for the seven field projects obtained from weather stations near the construction sites are presented in Figure 73, with data points highlighted in black representing the time when field cores were acquired. As illustrated, the CDD curves were noticeably different for various field projects, and therefore, were able to provide a distinct indication of the individual climatic characteristics. Specifically, the average slopes (i.e., secant slopes) of the curves for the Texas, New Mexico, and Florida field projects were significantly steeper than those located in colder climatic zones, including Wyoming, South Dakota, Iowa, and Indiana, due to differences in ambient temperatures.

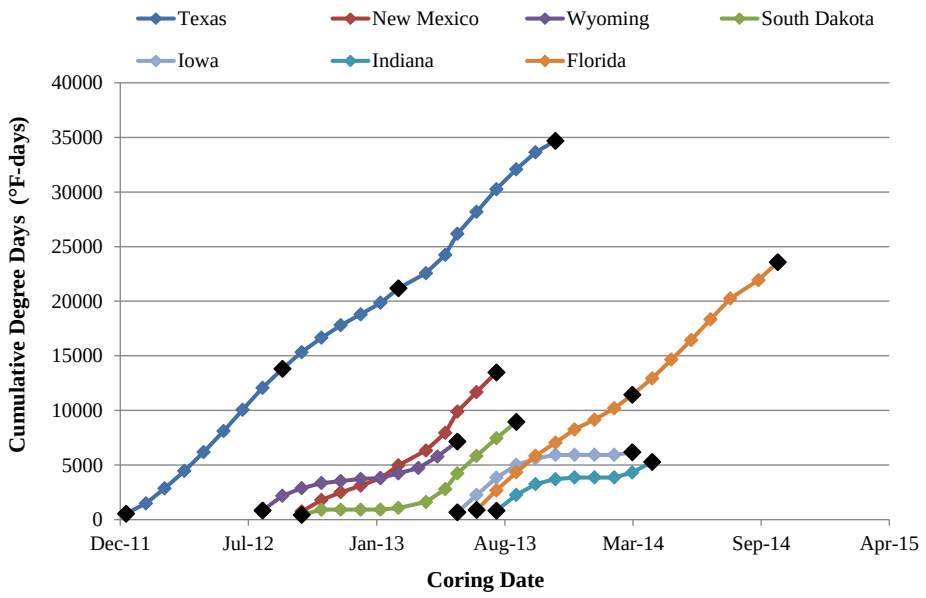

Figure 73. CDD values for various field projects.

Additionally, the construction date had a significant effect on the CDD values and subsequently on field aging of the asphalt mixture. For example, the South Dakota field project shown in Figure 73 was constructed in October 2012, and the pavement went through the 2012 winter prior to the 2013 summer. Consequently, the CDD curve was flat for the first several months (corresponding to the winter season); afterwards, the slope of the curve increased due to higher ambient temperatures during the summer. On the basis of these considerations, field projects with different construction dates and climates would have different CDD values for a given pavement in-service time. Specifically, field projects located in warmer climates and constructed in the spring or summer were likely to experience more severe initial field aging due to higher CDD values compared to those located in colder climates and constructed in the fall or winter.

Figure 74 and Figure 75 present the plots of the CDD values for post-construction cores versus their associated M_R ratios and HWTT RRP ratios, respectively; the data points represent the average property ratio values for each field project, and the adjusted line represents the exponential function noted in Equation 32. As illustrated, both the M_R ratio and the HWTT RRP ratio values exhibited a significant increase with CDD values. According to the coefficients of determination (i.e., R^2 values) shown in Figure 74 and Figure 75, it was feasible to use the property ratios as a function of CDD values to quantify mixture aging in the field.

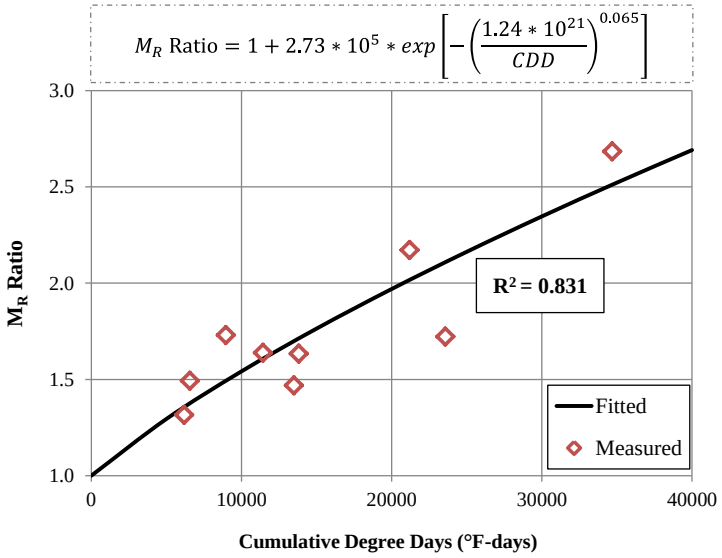

Figure 74. M_R ratio versus CDD values.

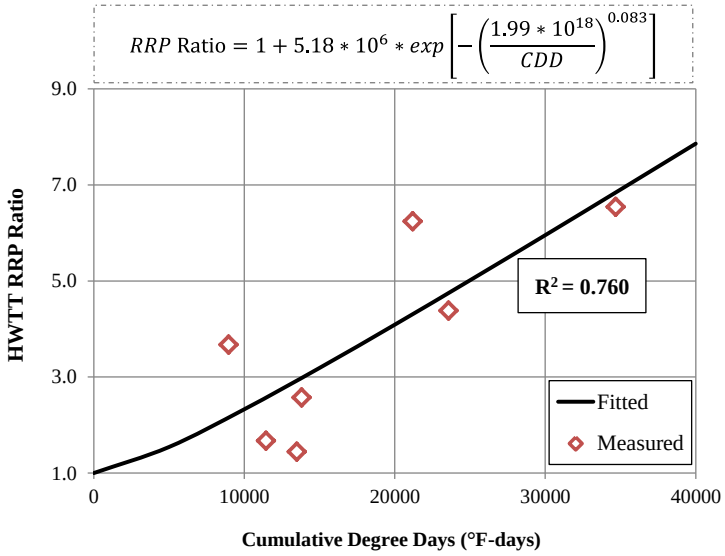

Figure 75. HWTT RRP ratio versus CDD values.

Correlation of Field Aging with LTOA Protocols

Mixture property ratios were used to quantify the increase in mixture stiffness and rutting resistance with field aging. For specimens fabricated in the laboratory, short-term aged mixtures correspond to LMLC specimens with the selected STOA protocol, and long-term aged mixtures refer to LMLC specimens with STOA plus LTOA protocols on compacted specimens of two weeks at 140°F (60°C), three days at 185°F (85°C), or five days at 185°F (85°C). For field specimens, short-term aged mixtures correspond to cores at construction, while long-term aged specimens refer to post-construction cores (i.e., acquired eight to 22 months after construction). Table 10 presents the M_R ratio and HWTT RRP ratio results for long-term aged LMLC specimens from the field projects included in the study. The average M_R ratio values for LTOA protocols of two weeks at 140°F (60°C) and five days at 185°F (85°C) were

approximately 1.48 and 1.78, respectively. The HWTT RRP ratio values obtained for the same set of LMLC specimens were 2.33 (two-week protocol) and 3.93 (five-day protocol). The higher M_R ratio and HWTT RRP ratio values indicated that the LTOA protocol at 185°F (85°C) produced a greater level of mixture aging compared to that at 140°F (60°C), though associated with a shorter aging time period (i.e., five days versus two weeks).

Table 10. M_R Ratio and HWTT RRP Ratio Results for Long-Term Aged LMLC Specimens

Field Project	Two Weeks at 140°F (60°C)		Five Days at 185°F (85°C)	
	M_R ratio	HWTT RRP ratio	M_R ratio	HWTT RRP ratio
Texas	1.603	2.270	1.940	5.437
New Mexico	1.889	1.991	2.205	2.643
Wyoming	1.441	-	1.803	-
South Dakota	1.583	-	1.946	-
Iowa	1.309	-	1.649	-
Indiana	1.304	-	1.542	-
Florida	1.216	2.721	1.380	3.718

Figure 76 and Figure 77 illustrate the correlation of field aging and laboratory LTOA protocols on M_R ratio and HWTT RRP ratio, respectively. The average mixture property ratio values for long-term aged LMLC specimens are plotted as markers by crossing the exponential curves shown in Figure 74 and Figure 75. The vertical and horizontal error bars represent one standard deviation from the average mixture property ratio values and their corresponding CDD values of the post-construction cores,

respectively. As illustrated, the laboratory LTOA protocol of two weeks at 140°F (60°C) was able to produce mixture aging equivalent to an average of 9,100 and 10,000 CDD values in terms of mixture stiffness and rutting resistance, respectively. Additionally, the laboratory LTOA protocol of five days at 185°F (85°C) per AASHTO R 30 produced mixture aging equivalent to an average of 16,000 CDD values for mixture stiffness and 19,000 CDD values for mixture rutting resistance.

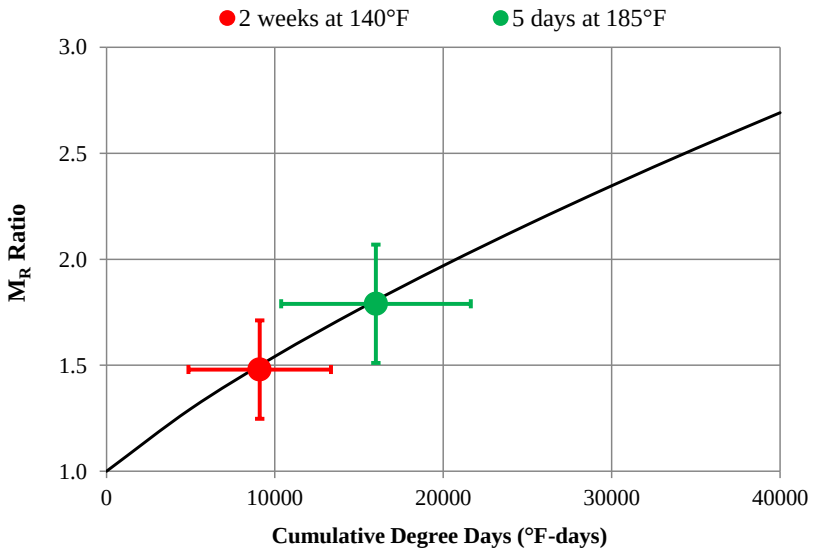

Figure 76. M_R ratio correlation of field aging with laboratory LTOA.

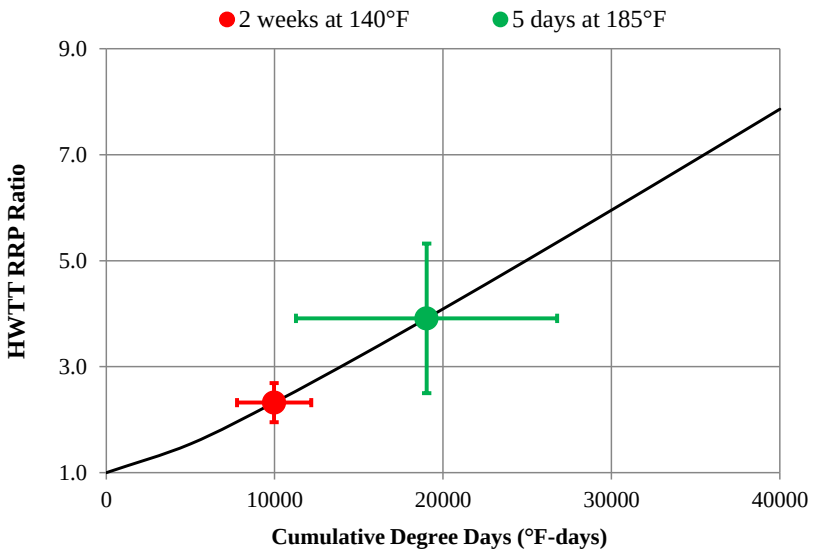

Figure 77. HWTT RRP ratio correlation of field aging with laboratory LTOA.

A subset of LMLC specimens from the Indiana and Florida field projects were aged using an additional LTOA protocol of three days at 185°F (85°C), given the fact that the mixture aging induced by the standard laboratory LTOA protocol of five days at 185°F (85°C) per AASHTO R 30 was more significant than that of two weeks at 140°F (60°C). The property ratios for the Indiana and Florida LMLC specimens with different LTOA protocols were compared against each other to determine if an equivalent level of laboratory aging could be produced by LTOA protocols of three days at 185°F (85°C) and two weeks at 140°F (60°C). Figure 78 shows the comparison of three laboratory LTOA protocols in terms of their corresponding CDD values after equating their M_R ratio values to the curve presented in Figure 74. For both the Indiana and Florida mixtures, approximately equivalent CDD values were observed for LTOA protocols of three days at 185°F (85°C) and two weeks at 140°F (60°C), which were significantly

lower than those from five days at 185°F (85°C). Therefore, the three-day protocol at 185°F (85°C) could be used as a practical alternative to two weeks at 140°F (60°C) in colder climates because of the shorter aging time span required.

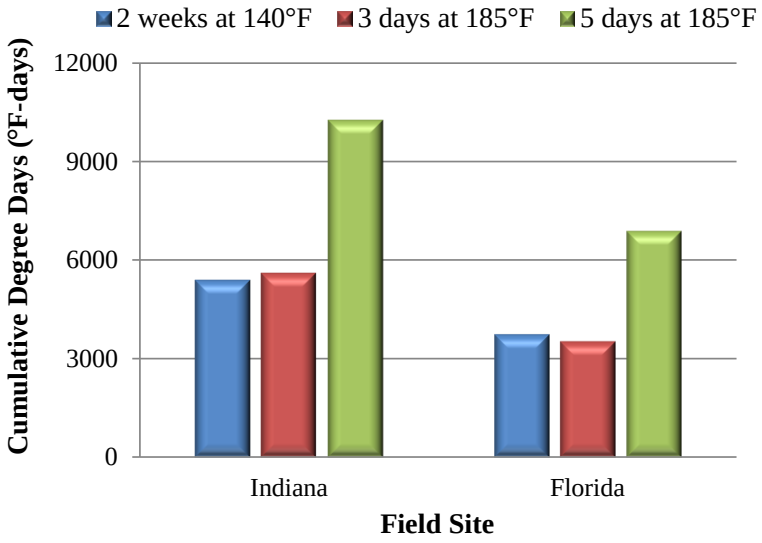

Figure 78. Comparison of CDD values achieved by various LTOA protocols for the Indiana and Florida field projects.

Based on the mixture stiffness and rutting resistance results discussed previously, LTOA protocols of three days at 185°F (85°C) or two weeks at 140°F (60°C) and five days at 185°F (85°C) were representative of field aging of approximately 9,600 (average of 9,100 [M_R ratio] and 10,000 [HWTT RRP ratio]) and 17,500 (average of 16,000 [M_R ratio] and 19,000 [HWTT RRP ratio]) CDD values, respectively. Using the information shown in Figure 73, the in-service time for each field project corresponding to the critical CDD values was determined and is summarized in Table 11. As shown, the

laboratory LTOA protocols of three days at 185°F (85°C) or two weeks at 140°F (60°C) were equivalent to approximately seven months in-service in warmer climates and 12 months in-service in colder climates. While the aging induced by the laboratory LTOA protocol of five days at 185°F (85°C) was approximately equivalent to 12 months and 23 months in-service for warmer climates and colder climates, respectively.

Table 11. Correlation of Field Aging with Laboratory LTOA

Field Project	Climate	Two Weeks at 140°F (60°C) or Three Days at 185°F (85°C)	Five Days at 185°F (85°C)
Texas	Warmer Climate	6 months	11 months
New Mexico		8 months	14 months
Florida		7 months	12 months
Average		7 months	12 months
Wyoming	Colder Climate	12 months	23 months
South Dakota		12 months	23 months
Iowa		12 months	23 months
Indiana		11 months	22 months*
Average		12 months	23 months

Factors Affecting Long-Term Aging Characteristics

This section presents the laboratory test results for identifying factors with significant effects on the long-term mixture aging characteristics of asphalt mixtures. These factors include WMA technology, production temperature, plant type, inclusion of recycled materials, and aggregate absorption. Detailed discussions for each factor are presented in the following sections.

A statistical analysis was also performed to identify which factors had a significant effect on the M_R ratio results. Separate statistical experiments and analyses were performed to assess the effects of each of the five factors of interest while incorporating the field project as a random variable.

WMA Technology (HMA vs. WMA)

The M_R ratio results for long-term aged mixtures including post-construction cores and LMLC specimens with LTOA from the seven field projects are shown in Figure 79. The x-axis represents HMA test results, and the y-axis represents the corresponding WMA test results. The solid line is the line of equality, and the dashed line illustrates the shift from the line of equality for the M_R ratio results.

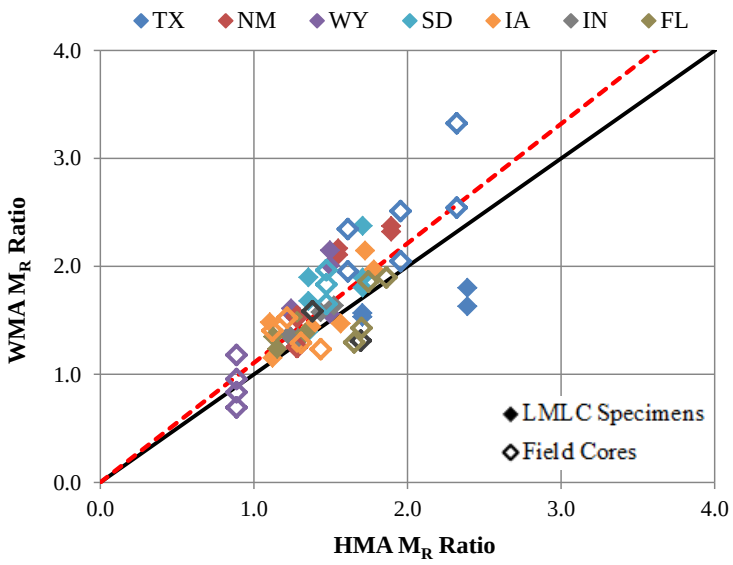

Figure 79. M_R ratio comparison for HMA versus WMA.

The M_R ratio comparison for HMA versus WMA illustrates that most of the data points aligned above the line of equality, indicating a greater increase in mixture stiffness after long-term aging for WMA compared to HMA. In order to determine the critical in-service time when WMA equals HMA in mixture stiffness, CDD values for WMA and HMA post-construction cores and their associated M_R ratios were fitted separately, as shown in Figure 80. The data points represent the average HMA and WMA M_R ratio values for each field project, and the curves represent the exponential functions as expressed in Equation 32 for the M_R ratio versus CDD values. As illustrated, the WMA curve aligned above the HMA curve, verifying a greater increase in mixture stiffness after long-term aging for WMA versus HMA.

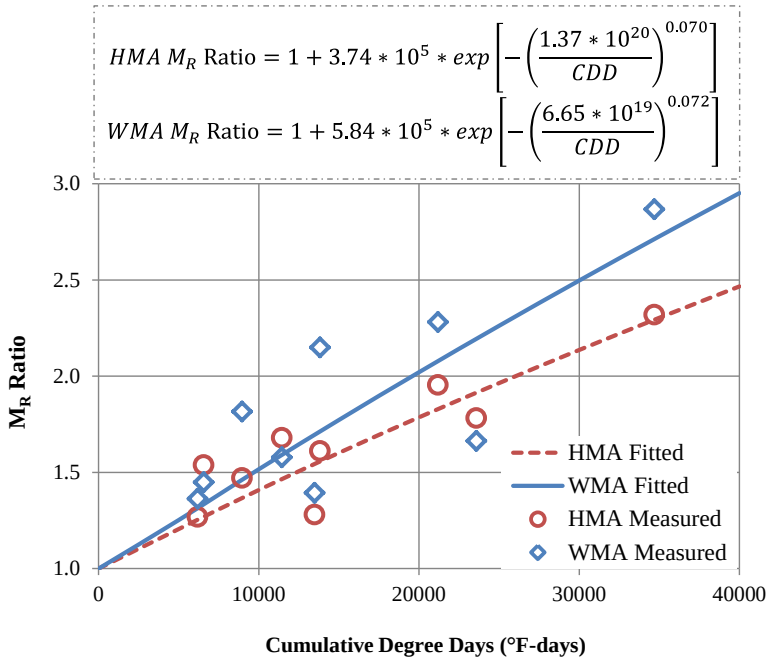

Figure 80. M_R ratio versus CDD for HMA and WMA post-construction cores.

Based on the definition of mixture M_R ratio (Equation 30), the M_R stiffness of WMA and HMA post-construction cores at a given CDD value can be determined using Equation 33 and Equation 34, respectively. The fitted exponential functions for HMA and WMA post-construction cores shown in Figure 80 are denoted as f_{HMA} and f_{WMA}.

$$M_{R-WMA} = M_{R-WMA0} * f_{WMA}$$

$$f_{WMA} = 1 + 5.84 * 10^5 * exp\left[-\left(\frac{6.65 * 10^{19}}{CDD}\right)^{0.072}\right] \quad \text{Equation 33}$$

where:

$M_{R\text{-}WMA}$ = M_R stiffness of WMA post-construction cores at a given CDD value; and

$M_{R\text{-}WMA0}$ = M_R stiffness of WMA cores at construction.

$$M_{R-HMA} = M_{R-HMA0} * f_{HMA}$$

$$f_{HMA} = 1 + 3.74 * 10^5 * exp\left[-\left(\frac{1.37 * 10^{20}}{CDD}\right)^{0.070}\right] \quad \text{Equation 34}$$

where:

$M_{R\text{-}HMA}$ = M_R stiffness of HMA post-construction cores at a given CDD value; and

$M_{R\text{-}HMA0}$ = M_R stiffness of HMA cores at construction.

By making Equation 33 and Equation 34 equal, the critical CDD value for achieving equivalent M_R stiffness by WMA and HMA ($CDD_{WMA=HMA}$) can be determined, as expressed in Equation 35.

$$\frac{M_{R-WMA0}}{M_{R-HMA0}} = \frac{1 + 3.74 * 10^5 * exp\left[-\left(\frac{1.37 * 10^{20}}{CDD}\right)^{0.070}\right]}{1 + 5.84 * 10^5 * exp\left[-\left(\frac{6.65 * 10^{19}}{CDD}\right)^{0.072}\right]} \quad \text{Equation 35}$$

In addition to $CDD_{WMA=HMA}$, the determination of the CDD value at which the M_R stiffness of WMA post-construction cores equaled that of HMA cores at construction ($CDD_{WMA=HMA0}$) was also essential in order to understand the performance evolution of WMA in the field compared to HMA. The determination of the $CDD_{WMA=HMA0}$ value is expressed in Equation 36.

$$\frac{M_{R-WMA0}}{M_{R-HMA0}} = \frac{1}{1 + 5.84 * 10^5 * exp\left[-\left(\frac{6.65 * 10^{19}}{CDD}\right)^{0.072}\right]} \quad \text{Equation 36}$$

Depending on the difference in the initial M_R stiffness for WMA and HMA cores at construction (i.e., $M_{R\text{-}WMA0}/M_{R\text{-}HMA0}$), the stiffness evolution of WMA and HMA with field aging can be categorized into three different scenarios, as shown in Figure 81. Continued. . Scenario I in Figure 81. Continued. (a) illustrates the case where the M_R stiffness of the HMA cores was consistently higher than their WMA counterparts, but the difference in stiffness between these two mixtures decreased with field aging. Scenario II in Figure 81. Continued. (b) indicates the case where HMA had higher mixture stiffness compared to WMA at the initial aging stage (i.e., cores at construction), while the opposite occurred after a time in the field. Scenario III represents the case where equivalent mixture stiffness was shown for HMA and WMA cores at construction, but higher stiffness for post-construction cores was observed for WMA versus HMA, as shown in Figure 81. Continued. (c).

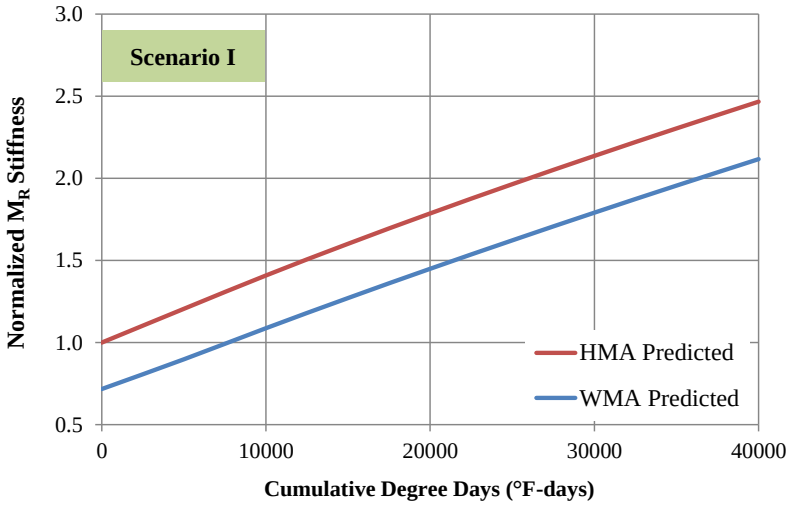

(a)

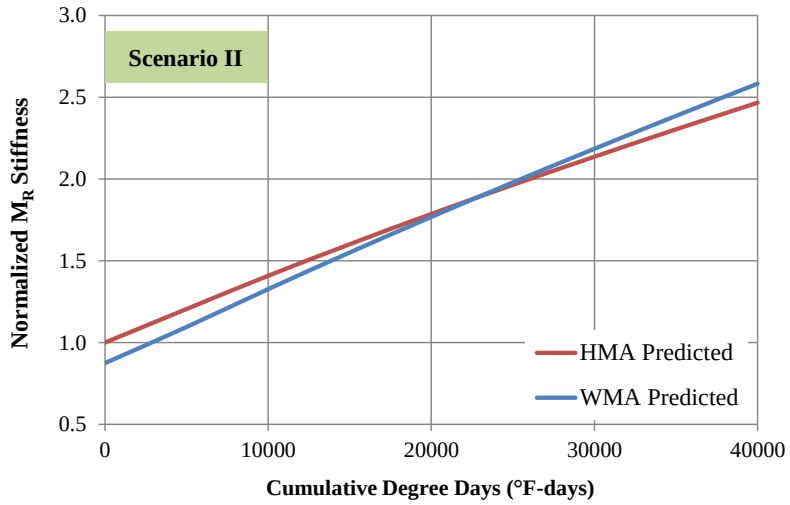

(b)

Figure 81. Normalized M_R stiffness evolution with field aging for HMA versus WMA; (a) Scenario I, (b) Scenario II, (c) Scenario III.

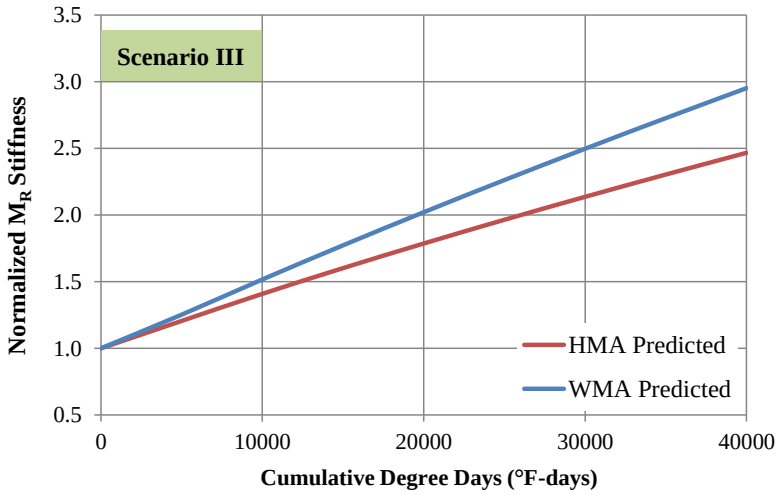

(c)

Figure 81. Continued.

Table 12 summarizes the $CDD_{WMA=HMA}$ and $CDD_{WMA=HMA0}$ values for each field project included in the experiment. For the majority of the cases (four out of seven), the M_R stiffness evolution with field aging followed the trend illustrated in Scenario II, indicating that the stiffness of WMA was initially lower than that of HMA but it was able to catch up to the stiffness of HMA after a certain amount of time in the field. The average $CDD_{WMA=HMA}$ and $CDD_{WMA=HMA0}$ values for those four field projects were approximately 23,000 and 3,000 CDD values, respectively. Thus, field aging of approximately 3,000 CDD values might be necessary for the stiffness of WMA to equal the initial stiffness of HMA, and equivalent WMA and HMA mixture stiffness was likely to be achieved after 23,000 CDD values of field aging.

Table 12. Summary of $CDD_{WMA=HMA}$ and $CDD_{WMA=HMA0}$ Values

Field Project	Scenario	WMA_0/HMA_0	CDD Values	
			WMA = HMA	WMA = HMA_0
Texas	I	0.717	-	7,700
New Mexico	II	0.876	22,400	2,900
Wyoming	II	0.867	25,500	3,200
South Dakota	II	0.897	16,500	2,400
Iowa	II	0.860	28,200	3,300
Indiana	III	1.002	0	0
Florida	III	0.999	0	0

Referring to Figure 73, the in-service time for each field project corresponding to 23,000 and 3,000 CDD values was determined and is summarized in Table 13. As shown, approximately 17 months in-service in warmer climates and 29 months in-service in colder climates were needed in order to achieve equivalent mixture stiffness for WMA versus HMA. As for the in-service time corresponding to $CDD_{WMA=HMA0}$ of 3,000 CDD values, approximately two months and three months were required in warmer climates and colder climates, respectively.

Table 13. Field In-Service Time Corresponding to $CDD_{WMA=HMA}$ and $CDD_{WMA=HMA0}$ Values for Various Field Projects

Field Project	Climate	CDD Values	
		WMA = HMA	WMA = HMA_0
Texas	Warmer Climate	16 months	2 months
New Mexico		19 months	3 months
Florida		15 months	1 months
Average		17 months	2 months
Wyoming	Colder Climate	31 months	2 months
South Dakota		32 months*	7 months
Iowa		28 months*	2 months
Indiana		26 months*	2 months
Average		29 months	3 months

** Projected in-service time based on historical climatic information.*

For the statistical analysis, an ANOVA model having WMA technology and aging level as main effects along with field project as a random effect was fitted to the data. The results showed that the effects of WMA technology and aging level were statistically significant at $\alpha = 0.05$. More specifically, WMA mixtures showed a higher predicted M_R ratio value than HMA mixtures.

Production Temperature (High vs. Control)

The M_R ratio results for long-term aged mixtures including post-construction cores and LMLC specimens with LTOA from the Wyoming and Iowa field projects are shown in Figure 82, with the M_R ratio for mixtures produced at high temperatures and those at control temperatures plotted against each other. The x-axis represents the test results for control temperature mixtures, and the y-axis represents the results for

mixtures produced at high temperature. The solid line is the line of equality, and the dashed line illustrates the shift from the line of equality for the M_R ratio results.

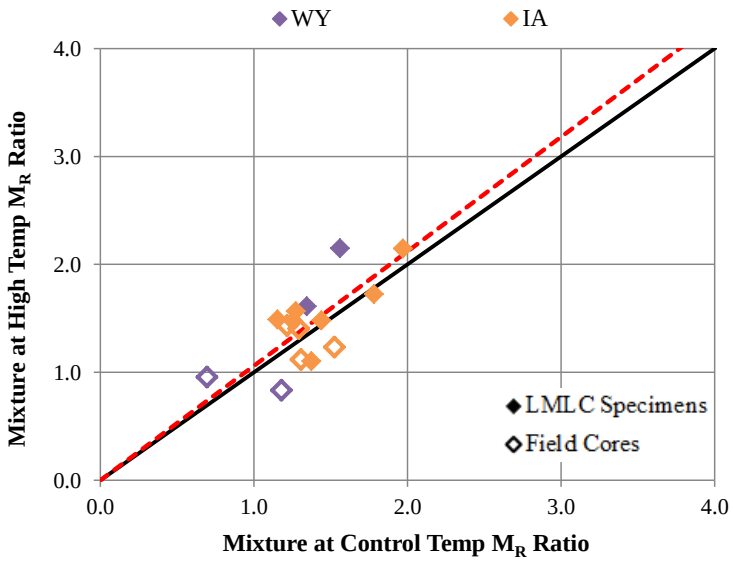

Figure 82. M_R ratio comparison for mixtures produced at high versus control temperatures.

The M_R ratio results shown in Figure 82 illustrate that most of the data points aligned along the line of equality, indicating an equivalent increase in M_R stiffness induced by the long-term aging of mixtures produced at high versus control temperatures. Therefore, production temperature differences of 20 to 30°F for these two field projects had no significant effect on the sensitivity of mixture stiffness to long-term aging.

For the statistical analysis, an ANOVA model including production temperature, WMA technology, and aging level as fixed effects and field project as a random effect

was fitted to the data. Results showed that the effect of the factor of interest, production temperature, was not statistically significant at $\alpha = 0.05$.

Plant Type (BMP vs. DMP)

The M_R ratio results for long-term aged mixtures including cores after 10 months in-service and LMLC specimens with LTOA of two weeks at 140°F (60°C) and five days at 185°F (85°C) from the Indiana field project are shown in Figure 83, with the M_R ratio for BMP-produced mixtures and DMP-produced mixtures plotted against each other. The x-axis represents the test results for BMP-produced mixtures, and the y-axis represents corresponding results for DMP-produced mixtures. The solid line is the line of equality, and the dashed line illustrates the shift from the line of equality for the M_R ratio results.

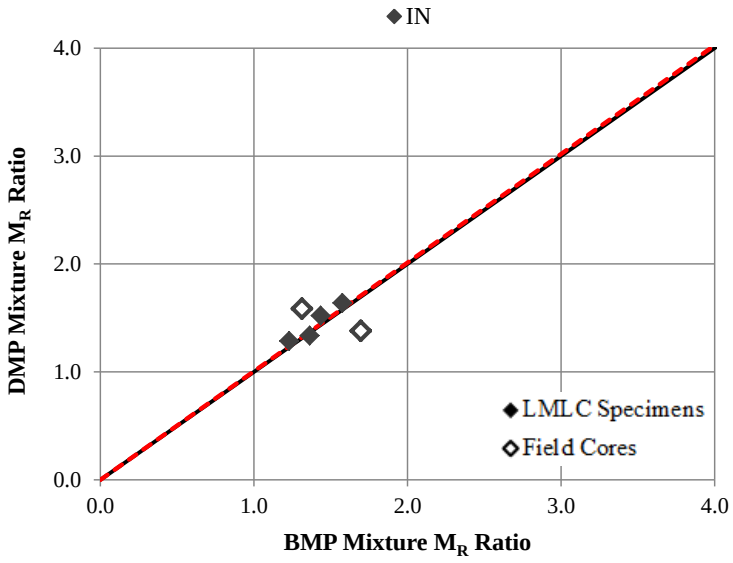

Figure 83. M_R ratio comparison for mixtures produced at BMP versus DMP.

The M_R ratio results shown in Figure 83 illustrate that most of the data points aligned along the line of equality, indicating an equivalent increase in M_R stiffness induced by long-term aging for the BMP- and DMP-produced mixtures. Therefore, plant type had no significant effect on the sensitivity of mixture stiffness to long-term aging.

For the statistical analysis, the ANOVA model including plant type, aging level, and WMA technology as main effects showed that none of the factor effects (as well as the factor of interest, plant type) was statistically significant at $\alpha = 0.05$.

Inclusion of Recycled Materials (RAP/RAS vs. No RAP/RAS)

The M_R ratio results for long-term aged mixtures including post-construction cores and LMLC specimens with LTOA protocols from the Texas and New Mexico field projects are shown in Figure 84, with the M_R ratio values for control mixtures without recycled materials and RAP/RAS mixtures plotted against each other. The x-axis represents the test results for the control mixtures, and the y-axis represents corresponding results for RAP/RAS mixtures. The solid line is the line of equality, and the dashed line illustrates the shift from the line of equality for the M_R ratio results.

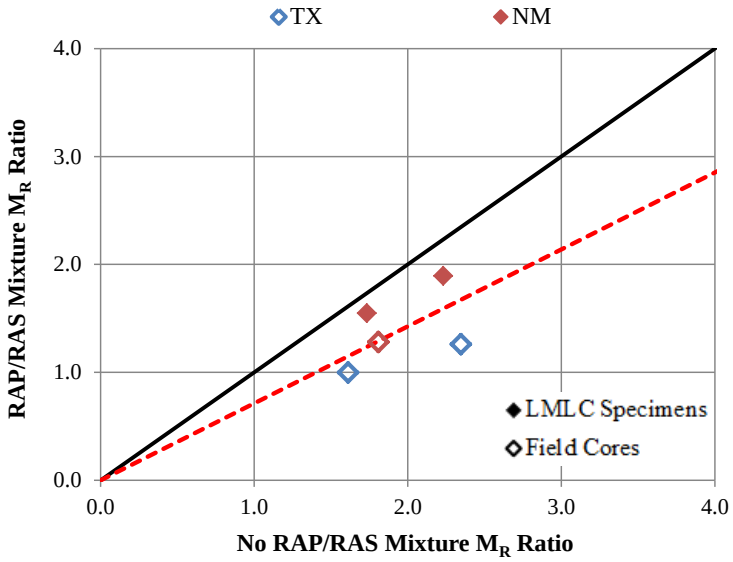

Figure 84. M_R ratio comparison for mixtures with versus without RAP/RAS.

The M_R ratio results shown in Figure 84 illustrate that the data points aligned below the line of equality, indicating a significantly higher increase in M_R stiffness after long-term aging for the control mixtures compared to the RAP/RAS mixtures. Considering the lower initial stiffness but higher M_R ratios for control mixtures versus the RAP/RAS mixtures (discussed previously in Chapter V), equivalent mixture stiffness between these two mixture types could be achieved after certain aging periods. The greater sensitivity to aging exhibited by the control mixtures might be attributed to the larger amount of virgin binder in the mixture, which had higher oxygen diffusivity and was more susceptible to aging than the recycled binder (Glover et al. 2014; Tarbox and Daniel 2012). Therefore, the inclusion of recycled materials had a significant effect on mixture aging characteristics in this research study.

For the statistical analysis, the ANOVA model included recycled materials, aging level, and WMA technology as main effects (since all possible two-way interactions were statistically insignificant at $\alpha = 0.05$). Since field project was confounded with aging level for this dataset, field project could not be included as a random effect in the ANOVA model. The results showed that the effects of recycled materials, aging level, and WMA technology were all statistically significant at $\alpha = 0.05$. The conclusion of the statistical analysis was that the control mixtures (i.e., no RAP/RAS) had a higher M_R ratio compared to mixtures with RAP/RAS.

Aggregate Absorption (High vs. Low Absorptive Aggregate)

The M_R ratio results for long-term aged mixtures including post-construction cores and LMLC specimens with LTOA protocols from the Iowa and Florida field projects are shown in Figure 85, with the mixture property ratio for mixtures using high absorptive aggregates versus low absorptive aggregates plotted against each other. The x-axis represents test results for mixtures using high absorptive aggregates, and the y-axis represents corresponding test results for mixtures using low absorptive aggregates. The solid line represents the line of equality, and the dashed line illustrates the shift from the line of equality for the M_R ratio results.

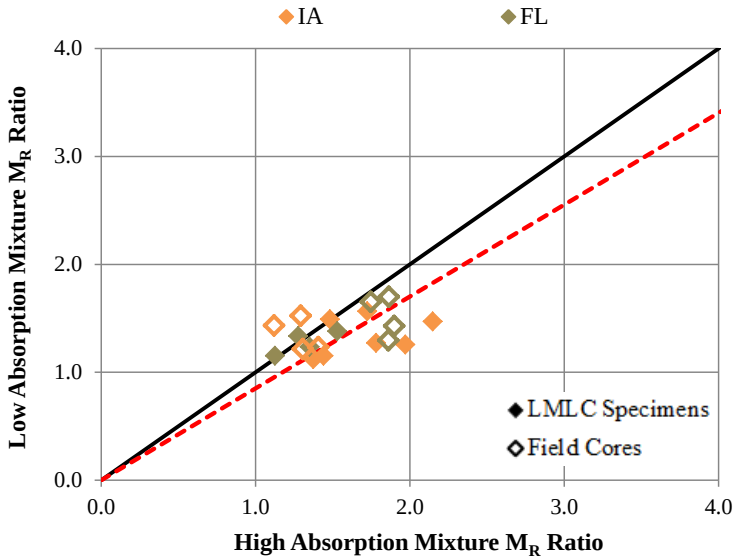

Figure 85. M_R ratio comparison for mixtures produced using high versus low absorptive aggregates.

The M_R ratio comparison for mixtures using high absorptive versus low absorptive aggregates shown in Figure 85 illustrated that most of the data points aligned below the line of equality, indicating a greater increase in M_R stiffness induced by long-term aging for mixtures using high absorptive aggregates compared to the mixtures using low absorptive aggregates. Considering the lower initial stiffness but higher M_R ratios for mixtures using high absorptive aggregates versus low absorptive aggregates (discussed previously in Chapter V), equivalent mixture stiffness between these two mixture types could be achieved after certain aging periods. The greater sensitivity of mixture stiffness to aging for mixtures using high absorptive aggregates was likely due to the higher volume of effective binder in these mixtures that was available for aging (i.e., higher P_{be} values from volumetrics calculation), and/or the continuous asphalt

absorption by the aggregates with time (West et al. 2014). Therefore, aggregate absorption and more specifically, the amount of effective binder had a significant effect on mixture aging characteristics in this research study.

For the statistical analysis, an ANOVA model including aggregate absorption, aging level, and WMA technology as main effects, aging level * aggregate absorption and WMA technology * aggregate absorption as two-way interaction effects (WMA technology * aging level interaction was not statistically significant), and field project as a random effect was fitted to the data. The results showed that the effects of aggregate absorption, aging level, aging level * aggregate absorption, and WMA technology * aggregate absorption were statistically significant at $\alpha = 0.05$. In addition, the difference between mixtures using high absorptive and low absorptive aggregates was statistically significant for WMA but not for HMA.

Summary

In this section, the effects of various mixture components and production parameters including WMA technology, production temperature, plant type, inclusion of recycled materials, and aggregate absorption on the mixture aging characteristics were evaluated based on the change in mixture stiffness after long-term aging. The comparisons in terms of M_R ratio were performed for each factor, and the results are summarized in Table 14. Factors with a significant effect on mixture aging characteristics were identified based on the magnitude of the slope for the shifted lines of equality being greater than 1.05 or smaller than 0.95 (i.e., 5 percent off the line of equality) and were corroborated via statistical analysis. According to Table 14, WMA

technology, inclusion of recycled materials, and aggregate absorption showed significant effects on mixture aging characteristics, while no significant effects from production temperature and plant type were observed.

Table 14. Summary of the Effects of Mixture Components and Production Parameters on Mixture Long-Term Aging Characteristics

Factor	M_R Ratio		
	Slope Magnitude	Significant Effect	Statistically Significant
WMA Technology	1.107	Yes	Yes
Production Temperature	1.060	Marginal Yes	No
Plant Type	1.006	No	No
Inclusion of Recycled Materials	0.713	Yes	Yes
Aggregate Absorption	0.851	Yes	Yes

CHAPTER VII

CHARACTERIZATION OF NON-UNIFORM FIELD AGING IN ASPHALT PAVEMENTS

Overview

Aging of asphalt mixtures occurs during plant production and construction and continues throughout the service life of the pavement. Although extensive work has been conducted to quantify field aging and evaluate its effect on asphalt mixtures (as discussed previously in Chapter VI), little effort has been devoted towards understanding the rate of field aging with pavement depth. Due to the non-uniform AV contents and temperature distribution in the pavement structure, the surface of the pavement will age faster than the bottom; thus a field aging gradient exists. As a consequence, the asphalt mixtures at the pavement surface tend to have higher stiffness and better rutting resistance but are more susceptible to fatigue and thermal cracking than those at the bottom of the pavement structure. The objective of this research study is to characterize the non-uniform field aging of asphalt pavements in terms of mixture stiffness and binder property gradients with pavement depth.

Experimental Design

Figure 86 presents the research methodology used in this research study. Field cores were obtained from four field projects listed in Table 5 (i.e., Texas I, Iowa, Indiana, and Florida) at various in-service times and then tested in the non-destructive viscoelastic characterization direct tension (VEC-DT) test to determine their mixture

stiffness gradient with depth. Afterwards, the samples were cut into two or three thin layers (approximately 10 mm thick), and the AV contents were measured for each layer in accordance with AASHTO T 166. Then, asphalt binders were extracted from each layer in accordance with ASTM D2172 using a solvent blend of 85 volume percent Toluene plus 15 volume percent ethanol, and recovered using a rotary evaporator per ASTM D5404. The extracted and recovered asphalt binders were then tested with the dynamic shear rheometer (DSR) and Fourier transform infrared spectroscopy (FT-IR) to determine their rheological and chemical properties. The results obtained herein provide a better understanding of the non-uniform field aging of asphalt pavements and their effects on asphalt binder and mixture properties.

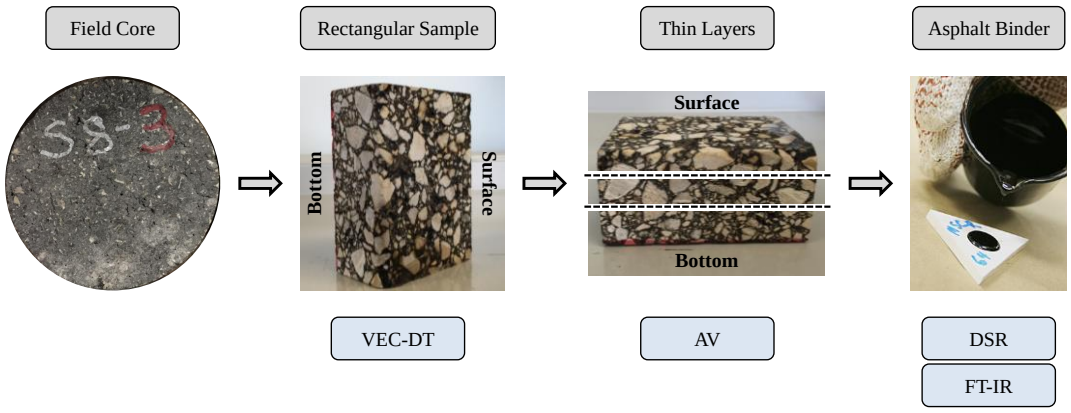

Figure 86. Research methodology for characterizing field aging gradient.

Viscoelastic Characterization Direct Tension Test (VEC-DT)

The VEC-DT test was developed by Luo and Lytton (2009) for determining the relaxation modulus and complex modulus of laboratory fabricated specimens. Afterwards, several modifications to the test procedure were proposed to make it

applicable for testing field cores (Koohi et al. 2011; Luo et al. 2015). The modified VEC-DT setup was used in this research study for determining the mixture stiffness gradient of field cores with various in-service times. Detailed information with regard to specimen preparation, test setup, and data analysis are described in the following sections.

Specimen Preparation

The cylindrical field core was first cut into a rectangular sample (length * width = 4.5 inches * 3.0 inches [114.3 mm * 76.2 mm]), with the thickness ranging from one to two inches (25.4 to 50.8 mm). Then, a pair of end caps was glued to the two ends of the specimen prior to being set in a magnetic gluing vice. Afterwards, four LVDTs were mounted to the specimen at the surface, bottom, and center, as shown in Figure 87, in order to measure the vertical deformations during the test.

Figure 87. VEC-DT test specimen mounted with two end caps and four LVDTs.

Test Setup

Before testing, the specimen was conditioned in a temperature chamber at the target test temperature of 50°F (10°C) for at least two hours to ensure temperature equilibrium. As shown in Figure 88, the VEC-DT specimen was set up in the MTS machine with one end attached to the dower bar and the other one fixed at the bottom plate through a ball joint. During the test, a monotonically increasing tensile load was applied at a rate of 0.001 inch per minute and continued until the strain of the specimen reached a maximum value of 75 microstrains to prevent crack initiation. For most cases, the test was more than 20 seconds in duration before reaching this strain level.

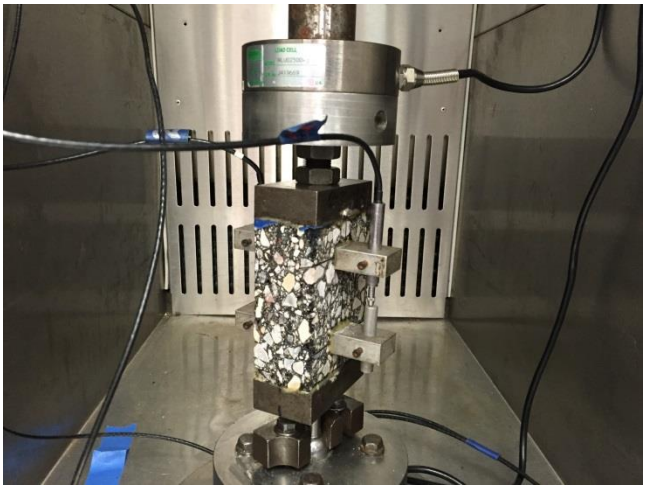

Figure 88. Specimen setup in the VEC-DT test.

Data Analysis

The strain distribution along the specimen thickness was assumed to follow a second polynomial function described in Equation 37. A power function proposed by

Koohi et al. (2011), as expressed in Equation 38, was used to illustrate the mixture stiffness profile of the specimen.

$$\varepsilon(x) = (2\varepsilon_d + 2\varepsilon_0 - 4\varepsilon_c)x^2 + (4\varepsilon_c - 3\varepsilon_0 - \ _d)x + \ _0 \quad \text{Equation 37}$$

where:

$\varepsilon(x)$ = tensile strength at depth x of the specimen;

ε_0, ε_d, and ε_c = tensile strength at the surface, bottom, and center of the specimen, respectively; and

x = relative distance from the surface of the specimen.

$$E(x) = E_d[1 + (k-1)(1-x)^n] \quad \text{Equation 38}$$

where:

$E(x)$ = elastic modulus at depth x of the specimen;

E_d = elastic modulus at the bottom of the specimen;

k = ratio of the surface modulus to the bottom modulus; and

n = power model coefficient.

Figure 89 shows a typical plot of the tensile stress applied during the VEC-DT test. The stress data was then fitted using Equation 39.

$$\sigma(t) = a_\sigma(1 - e^{-b_\sigma t}) \quad \text{Equation 39}$$

where:

$\sigma(t)$ = stress applied in the VEC-DT test at time t;

t = time; and

a_σ *and* b_σ = fitting parameters.

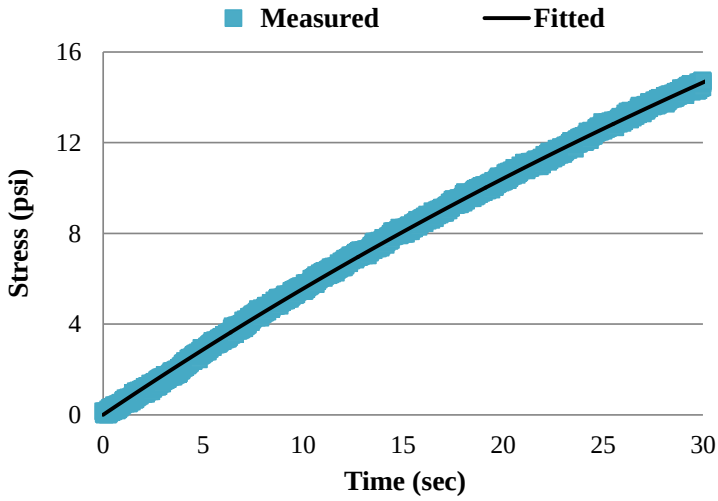

Figure 89. Measured versus fitted stress inputs in the VEC-DT test.

Using a generalized Maxwell model to simulate the viscoelastic response of the VEC-DT specimen, its creep compliance was described in Equation 40. Afterwards, the Boltzmann superposition principle (Findley et al. 1976) was applied to determine the strain response, as expressed in Equation 41. Figure 90 presents the fit of the strain outputs.

$$D(t) = \frac{1}{E_0} + \sum_{i=1}^{N} \frac{1}{E_i}(1 - e^{-t/\tau_{ci}}) \qquad \text{Equation 40}$$

where:

$D(t)$ = creep compliance of the generalized Maxwell model at time t;

E_0 = Young's modulus of the spring;

E_i = Young's modulus of the spring in the i^{th} Maxwell element;

τ_{ci} = relaxation time of the i^{th} Maxwell element; and

N = number of Maxwell elements.

$$\varepsilon(t) = \int_{0^-}^{t} D(t-s)\frac{d\sigma}{ds} \qquad \text{Equation 41}$$

$$\varepsilon(t) = a_\varepsilon - b_\varepsilon e^{-c_\varepsilon t} + d_\varepsilon e^{-e_\varepsilon t}$$

where:

$\varepsilon(t)$ = tensile strain of the specimen at time t; and

a_ε, b_ε, c_ε, d_ε, and e_ε = fitting parameters.

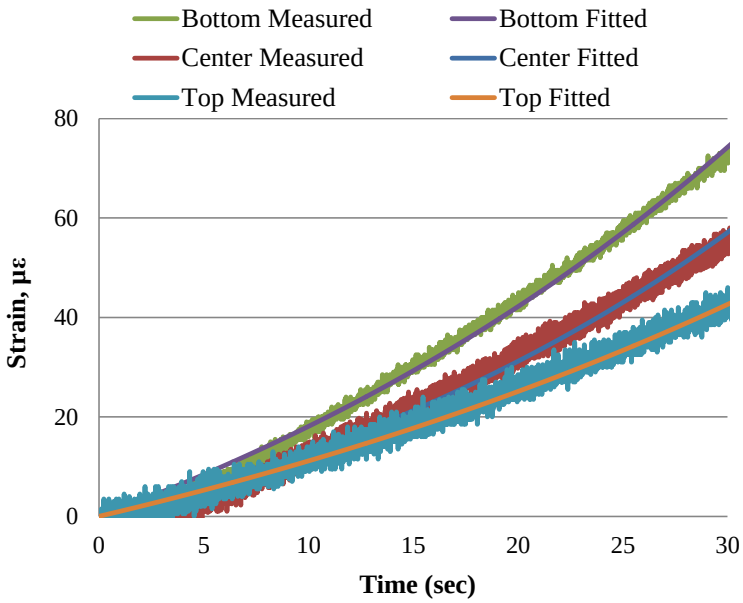

Figure 90. Measured versus fitted strain outputs in the VEC-DT test.

According to the stress-strain relationship, the internal stress of the VEC-DT specimen was found in Equation 42.

$$\sigma(x) = E(x)\varepsilon(x) \qquad \text{Equation 42}$$

where:

$\sigma(x)$ = internal stress at depth x of the specimen.

Then, the induced internal force and the position of the stiffness centroid of the VEC-DT specimen were determined, as expressed in Equation 43 and Equation 44, respectively. Due to the non-uniform field aging and mixture stiffness distribution of the field core, the stiffness centroid did not align with the geometrical centroid, and thus, the eccentricity was found in Equation 45.

$$P = bd\int_{x=0}^{x=1}\sigma(x)dx \qquad \text{Equation 43}$$

where:

b = specimen width;

d = specimen thickness; and

P = internal force of the specimen.

$$\bar{z} = \frac{bd^2}{P}\int_{x=0}^{x=1}x\sigma(x)dx \qquad \text{Equation 44}$$

where:

$\bar{z}$ = relative distance of the stiffness centroid from the specimen surface.

$$e = \frac{d}{2} - \bar{z} \qquad \text{Equation 45}$$

where:

e = eccentricity of the specimen.

The moment induced in the specimen was then determined by substituting Equation 43 and Equation 45 into Equation 46.

$$M = Pe \qquad \text{Equation 46}$$

where:

M = moment induced in the specimen.

Equation 37 through Equation 46 were derived based on the elastic solution. The viscoelastic solution was then obtained by applying the Laplace transform, as expressed in Equation 47, as well as the correspondence principle (Wineman and Rajagopal 2000). The detailed derivations are presented in Equation 48 through Equation 54.

$$\overline{f(s)} = \mathcal{L}[f(t)] = \int_0^\infty f(t)e^{-st}dt \qquad \text{Equation 47}$$

where:

$\overline{f(s)}$ = Laplace form of function *f(t)* at *s* domain;

$\mathcal{L}$ = Laplace transform function; and

f(t) = function *f* at *t* domain.

$$\overline{\sigma(s)} = \frac{a_\sigma}{s} - \frac{a_\sigma}{s + b_\sigma} \qquad \text{Equation 48}$$

where:

$\overline{\sigma(s)}$ = Laplace form of the stress inputs in the VEC-DT test.

$$\overline{\varepsilon(s)} = \frac{a_\varepsilon}{s} - \frac{b_\varepsilon}{s + c_\varepsilon} + \frac{d_\varepsilon}{s + e_\varepsilon} \qquad \text{Equation 49}$$

where:

$\overline{\varepsilon(s)}$ = Laplace form of the strain outputs in the VEC-DT test.

$$\mathcal{L}[E_x(t)] = s\overline{E_x(s)} \qquad \text{Equation 50}$$

where:

$\mathcal{L}[E_x(t)]$ = Laplace form of the specimen modulus at depth *x*.

$$\overline{P(s)} = \mathcal{L}[bd\int_{x=0}^{x=1}\sigma(x)dx] \qquad \text{Equation 51}$$

where:

$\overline{P(s)}$ = Laplace form of the internal force of the specimen.

$$\overline{\bar{z}(s)} = \mathcal{L}[\frac{bd^2}{P}\int_{x=0}^{x=1} x\sigma(x)dx] \quad \text{Equation 52}$$

where:

$\overline{\bar{z}(s)}$ = Laplace form of the relative distance of the stiffness centroid from the specimen surface.

$$\overline{e(s)} = \frac{d}{2} - \overline{\bar{z}(s)} \quad \text{Equation 53}$$

where:

$\overline{e(s)}$ = Laplace form of the eccentricity of the specimen.

$$\overline{M(s)} = \overline{P(s)}\,\overline{e(s)} \quad \text{Equation 54}$$

where:

$\overline{e(s)}$ = Laplace form of the moment induced in the specimen.

The strain induced by the moment at the surface, bottom, and center of the specimen were determined in Equation 55, Equation 56, and Equation 57, respectively.

$$\Delta\overline{\varepsilon_0(s)} = \frac{\overline{M(s)}\,\overline{\bar{z}(s)}}{Iks\overline{E_d(s)}} \quad \text{Equation 55}$$

where:

$\Delta\overline{\varepsilon_0(s)}$ = Laplace form of the strain induced by the moment at the surface of the specimen; and

I = moment of inertia.

$$\Delta\overline{\varepsilon_d(s)} = \frac{\overline{M(s)}[d - \overline{\bar{z}(s)}]}{Is\overline{E_d(s)}} \quad \text{Equation 56}$$

where:

$\Delta\overline{\varepsilon_d(s)}$ = Laplace form of the strain induced by the moment at the bottom of the specimen.

$$\Delta\overline{\varepsilon_c(s)} = \frac{\overline{M(s)}\,\overline{e(s)}}{Is\overline{E_d(s)}[1+(k-1)(\frac{1}{2})^n]} \quad \text{Equation 57}$$

where:

$\Delta\overline{\varepsilon_c(s)}$ = Laplace form of the strain induced by the moment at the center of the specimen.

Finally, the modulus distribution coefficients *k* and *n* in Equation 38 were determined by solving Equation 58 using the SOLVER application in the Microsoft Excel program.

$$\overline{\varepsilon_0(s)} + \Delta\overline{\varepsilon_0(s)} = \overline{\varepsilon_d(s)} - \Delta\overline{\varepsilon_d(s)} = \overline{\varepsilon_c(s)} - \Delta\overline{\varepsilon_c(s)} \quad \text{Equation 58}$$

Using Equation 51, the relaxation modulus at the bottom of the specimen was determined in Equation 59.

$$E_d(t) = \mathcal{L}^{-1}\left[\overline{E_d(s)}\right]$$

$$= \mathcal{L}^{-1}\left\{\frac{\overline{P(s)}}{sbd\{\overline{\varepsilon_0(s)}\left(\frac{1}{2}+\frac{k-1}{n+2}\right)+\overline{\varepsilon_d(s)}\left[\frac{1}{2}+\frac{k-1}{(n+1)(n+2)}\right]\}}\right\} \quad \text{Equation 59}$$

Then, the complex modulus at the bottom of the specimen was determined using Equation 60.

$$E_d{}^*(\omega) = i\omega\{\mathcal{L}[E_d(t)]\}_{s=i\omega} = E_{d1}(\omega) + i * E_{d2}(\omega) \quad \text{Equation 60}$$

where:

$E_d{}^*(\omega)$ = Complex modulus at the bottom of the specimen;

ω = frequency;

$E_{d1}(\omega)$ = real part of $E_d{}^*(\omega)$; and

$E_{d2}(\omega)$ = imaginary part of $E_d{}^*(\omega)$.

Finally, the magnitude of the complex modulus at the bottom of the specimen was found in Equation 61. In this study, the maximum $|E_d^*|$ value ($|E_d^*|_{max}$) and coefficients *k* and *n* in Equation 38 were used as the parameters for quantifying the mixture stiffness gradient of field cores.

$$|E_d^*| = \sqrt{E_{d1}(\omega)^2 + E_{d2}(\omega)^2} \quad \text{Equation 61}$$

where:

$|E_d^*|$ = magnitude of $E_d^*(\omega)$.

Dynamic Shear Rheometer (DSR)

The DSR test per AASHTO T 325 is commonly used to characterize the rheological properties of asphalt binders over a wide range of temperatures and frequencies. Figure 91 presents the Malvern Bohlin DSR2 equipment used in this study. During the test, a 2-mm thick sample of asphalt binder was placed between two 8 mm-diameter parallel circular plates. During the test, the bottom plate was fixed while the top plate oscillated back and forth across the sample at a given frequency to create shear in the sample. The angular rotation and the applied torque were measured, from which the test outputs including the complex shear modulus (G*) and phase angle (δ) were determined. G* represents the asphalt binder's total resistance to deformation in repeated shear, and δ refers to the time delay between the applied shear stress and the resulting shear strain. Asphalt binders with higher G* but lower δ values were stiffer and more elastic than those with lower G* but higher δ values.

Figure 91. DSR test equipment.

In this study, the DSR frequency sweep test was performed on asphalt binders extracted and recovered from the thin layers cut from the VEC-DT samples, at three different temperatures of 50°F (10°C), 77°F (25°C), and 104°F (40°C) and an angular frequency range of 0.016 to 25 Hz. During the test, the strain of the specimen was controlled at one percent to ensure the asphalt binder sample behavior was in the linear viscoelastic range.

Figure 92 and Figure 93 present the DSR frequency sweep test results in terms of G* and δ values at three different temperatures. As illustrated, the G* value increased as temperature decreased and frequency increased, while the δ results exhibited the opposite trend. For the data analysis, the G* and δ master curves were constructed by fitting the G* and δ values at each temperature and frequency to the Christensen-Anderson-Marasteanu (CAM) model (Marateanu and Anderson 1996) expressed in

Equation 62 and Equation 63, followed by horizontally shifting following the Williams-Landel-Ferry equation (Williams et al. 1955) in Equation 64. The fitting coefficients in Equation 62, Equation 63, and Equation 64 were determined by an optimization process using the SOLVER application in the Microsoft Excel program. Figure 94 presents the G* and δ master curves constructed using the software RHEA (Abatech Inc. 2011).

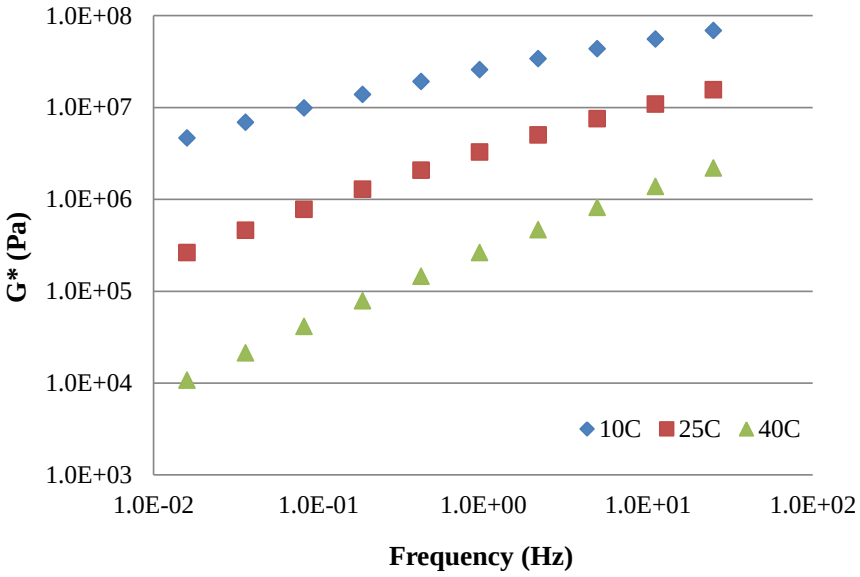

Figure 92. DSR frequency sweep test G* results.

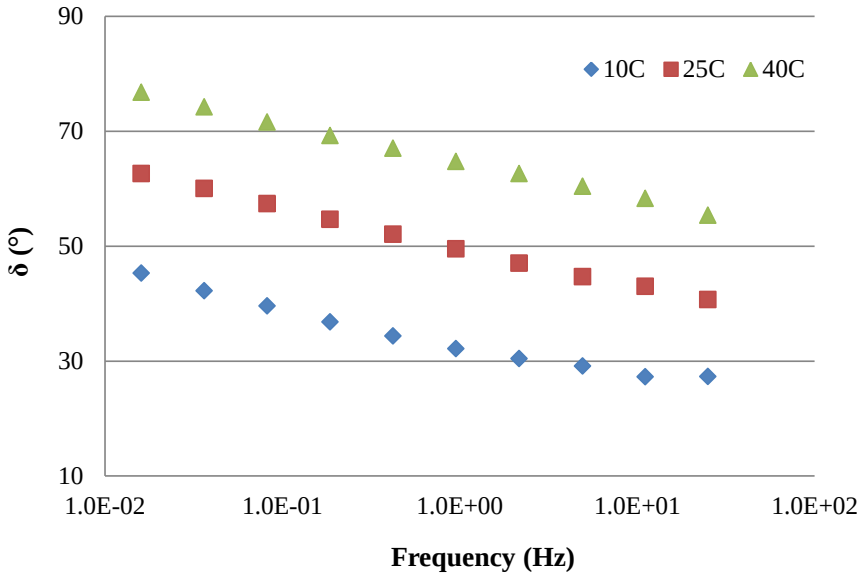

Figure 93. DSR frequency sweep test δ results.

$$G^*(f_R) = G^*_g \left[1 + (\frac{f_c}{f_r})^k\right]^{-\frac{m_e}{k}} \quad \text{Equation 62}$$

where:

$G^*(f_R)$ = G* value at reduced frequency;

G^*_g = glass modulus, assumed to be 1 GPa;

f_r = reduced frequency;

f_c = cross-over frequency; and

k and m_e = CAM Model coefficients.

$$\delta(f_R) = \frac{90 m_e}{1 + (\frac{f_r}{f_c})^k} \quad \text{Equation 63}$$

$$log\alpha(T) = \frac{-C_1(T - T_r)}{C_2 + (T - T_r)} \quad \text{Equation 64}$$

where:

$\alpha(T)$ = shift factor at temperature T;

T = test temperature;

T_r = reference temperature; and

C_1 and C_2 = shift factor coefficients.

$$f_r = f * \alpha(T) \qquad \text{Equation 65}$$

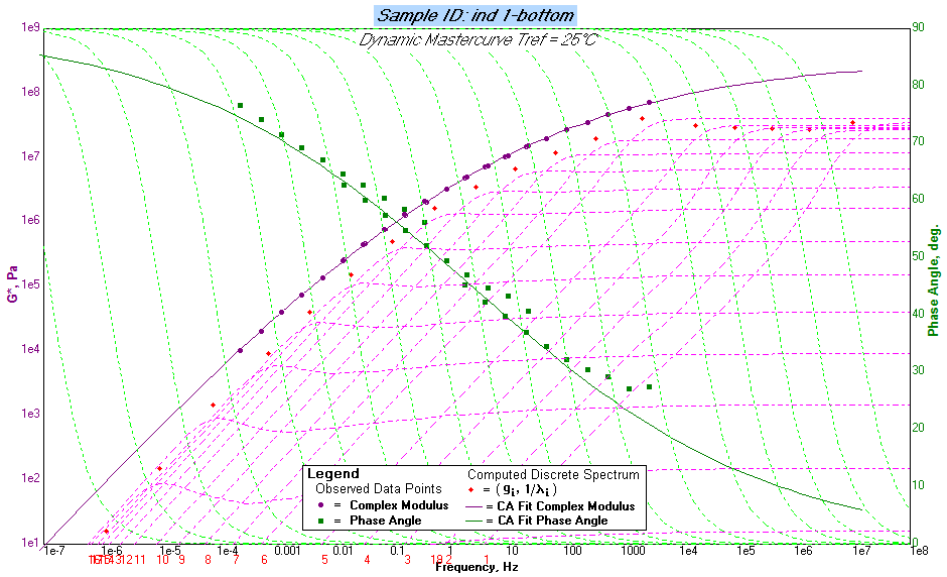

Figure 94. G* and δ master curves constructed using the software RHEA.

Using Equation 62, Equation 63, and Equation 64, the G* and δ values at 59°F (15°C) and 0.0008 Hz (0.005 rad/s) of the asphalt binder were obtained. Then, the G-R parameter, which was originally developed by Glover et al. (2005) and reformulated by Rowe (Anderson et al. 2011), was determined following Equation 66. The G-R parameter has been widely used to quantify the effects of laboratory and field on the asphalt binder rheology. Asphalt binders with higher G-R parameter values are expected to have experienced a greater level of aging than those with lower G-R parameter values. In this research study, the Glover-Rowe (G-R) parameter was determined for asphalt

binders extracted and recovered from the thin layers cut from the VEC-DT samples to discriminate their rheological properties due to the non-uniform field aging in the pavement.

$$G - R\ Parameter = \left\{\frac{G^*[\cos(\delta)]^2}{\sin(\delta)}\right\}_{T=15°C, f=0.0008Hz} \quad \text{Equation 66}$$

Fourier Transform Infrared Spectroscopy (FT-IR)

The FT-IR test has been proven to be an effective tool to determine the compositional changes occurring in asphalt binders with aging. During the process of oxidation, changes occur in the chemical bonds and molecular structure of the asphalt binder; polar oxygen-containing functional compounds, which contain infrared active carbonyl C=O bonds, are formed (Jia et al. 2014; Michalica et al. 2008). Therefore, the aging of asphalt binders can be quantified by measuring the change in the amount of carbonyl C=O bonds. In this study, the FT-IR analysis was performed on asphalt binders extracted and recovered from the thin layers cut from the VEC-DT samples in order to discriminate their chemical properties due to non-uniform field aging in the pavement. Figure 95 presents the Bruker Tensor 27 FT-IR Spectrometer used in this study.

During the test, a plastic spatula was used to apply a small amount of the molten asphalt sample (approximately 0.5 g) to the reflection surface of the prism. Different types of chemical bonds within the asphalt binders absorb lights with different infrared intensity and absorption behavior. The carbonyl area (CA) was defined as the integrated peak area from 1820 to 1650 cm-1, measured in arbitrary units, as a surrogate of asphalt oxidation level (Jemison et al. 1992). It was measured and calculated by the OPUS

software using the attenuated total reflectance method. Asphalt binders with higher CA values were expected to have experienced a greater level of aging compared to those with lower CA values.

Figure 95. FT-IR test equipment.

Test Results and Data Analysis

Table 15 summarizes the VEC-DT, DSR, and FT-IR results of the field cores obtained from four different field projects at various in-service times. For all post-construction cores tested, asphalt binders and mixtures at the surface of the pavements exhibited higher $|E_d{}^*|_{max}$, G-R parameter, and CA values than those at the bottom of the pavement structure, indicating a greater level of field aging. Detailed discussions in terms of mixture stiffness gradient and binder property gradient with pavement depth are given in the following sections.

Table 15. VEC-DT, DSR, and FT-IR Test Results

Field Project	Mixture	Field Aging (month)	Layer	AV	VEC-DT Results			G-R (kPa)	CA
					E_d*max (ksi)	k	n		
Texas I	WMA (Evotherm)	0	-	7.7%	325.0	1.00	-	29.04	0.743
		22	Top	7.1%	689.9	1.89	3.26	119.03	1.207
			Center	7.7%				77.94	1.085
			Bottom	9.6%				50.81	1.050
	WMA (Foaming)	0	-	6.5%	364.0	1.00	-	23.98	0.716
		22	Top	6.8%	659.0	1.83	3.99	134.82	1.182
			Bottom	5.5%				60.89	1.084
Iowa	HMA Low AC	0	Top	8.6%	103.6	3.86	2.78	2.56	1.027
			Center	7.0%				1.97	1.036
			Bottom	7.0%				1.44	0.932
		10	Top	6.9%	187.9	5.36	2.58	5.57	1.241
			Center	6.4%				3.55	1.116
			Bottom	11.4%				2.56	1.084
	WMA Low AC	0	Top	10.5%	73.7	5.66	2.72	2.93	0.987
			Center	9.1%				2.40	0.914
			Bottom	9.5%				2.05	0.906
		10	Top	7.6%	168.5	4.52	2.92	7.45	1.312
			Center	6.4%				5.77	1.171
			Bottom	7.2%				4.70	1.132
Indiana	HMA DMP	0	-	7.5%	458.0	1.00	-	49.35	1.101
		9	Top	6.3%	488.0	2.45	3.28	79.43	1.190
			Center	4.3%				73.58	1.154
			Bottom	5.0%				69.93	1.130
	WMA DMP	0	-	10.1%	645.0	1.00	-	48.38	1.048
		9	Top	8.0%	701.0	3.00	2.59	110.46	1.264
			Center	8.5%				89.03	1.173
			Bottom	10.0%				83.69	1.116
Florida	WMA GRN	0	-	6.7%	439.7	1.00	-	25.03	0.980
		9	Top	6.5%	519.5	2.81	3.81	69.38	1.243
			Bottom	4.5%				49.23	1.148

Mixture Stiffness Gradient

Figure 96, Figure 97, Figure 98, and Figure 99 present the mixture stiffness profiles of field cores obtained from the Texas I, Iowa, Indiana, and Florida field projects, respectively. The solid lines represent the $|E^*|_{max}$ results of construction cores and post-construction cores with various in-service times measured from the VEC-DT test, and the dashed lines represent the AV distribution of the test specimens with pavement depth.

As illustrated in Figure 96, for both WMA mixtures from the Texas I field project, the $|E^*|_{max}$ value was consistent with pavement depth (i.e., specimen thickness) for construction cores, while a different trend was observed for post-construction cores, where the $|E^*|_{max}$ value at the surface was significantly higher than that at the bottom. After 22 months of field aging in the Texas climate, the bottom modulus increased by approximately 326 ksi (average of 364 ksi for WMA with Evotherm and 287 ksi for WMA with Foaming) while the surface modulus increased by approximately 909 ksi (average of 979 ksi for WMA with Evotherm and 839 ksi for WMA with Foaming). In addition, the k value, defined as the ratio of the surface modulus to the bottom modulus, for both WMA post-construction cores was approximately 1.85. Thus, the asphalt mixtures at the surface of the pavement experienced a greater level of field aging than those at the bottom, which was likely due to the direct exposure to oxygen and solar radiation and the accumulation of elevated in-service temperatures (Glover et al. 2014). Similar to the $|E^*|_{max}$ values, the AV contents of the VEC-DT test specimens were not uniformly distributed with pavement depth. For WMA with Evotherm, the bottom layer

had a higher AV content than the top and the center layers. However, for WMA with Foaming, the top layer had a higher AV content than the bottom layer. Considering the significant effect of AV content on mixture stiffness (Yin et al. 2013), the mixture stiffness gradient in the post-construction field cores measured from the VEC-DT test was a result of the non-uniform distribution of both field aging and AV content with pavement depth.

Different from the results shown in Figure 96, an apparent field aging gradient with pavement depth was observed in Figure 97 for both HMA and WMA construction cores from the Iowa field project; the surface $|E^*|_{max}$ values were significantly higher than those at the bottom. As compared to the construction cores, the 10-month aged post-construction cores had higher $|E^*|_{max}$ values due to field aging, despite the fact that the difference was not consistent with pavement depth. After ten months of field aging in the Iowa climate, the bottom modulus increased by approximately 82 ksi (average of 84 ksi for HMA and 80 ksi for WMA) while the surface modulus increased by approximately 477 ksi (average of 608 ksi for HMA and 346 ksi for WMA). The k values for HMA and WMA post-construction cores were 5.35 and 4.95, respectively. Thus, as discussed previously, asphalt mixtures at the surface of the pavement experienced a greater level of field aging than those at the bottom. As shown in Figure 97, the AV distribution for the WMA post-construction core was fairly consistent with pavement depth. However, for the HMA post-construction core, the bottom layer had significantly a higher AV content than the top and center layers. Since a higher AV content was associated with lower mixture stiffness, the k value obtained from the VEC-

DT test for the HMA post-construction core could be artificially magnified due to the non-uniform AV distribution.

Figure 98 and Figure 99 present the mixture stiffness profiles of HMA and WMA produced at a DMP from the Indiana field project and WMA with low absorptive aggregates from the Florida field project, respectively. The trends observed for the Indiana and Florida mixtures were similar to that of the Texas I mixtures shown in Figure 96; the mixture stiffness of construction cores was consistent with pavement depth while an apparent mixture stiffness gradient was observed after aging for post-construction cores. As illustrated in Figure 98, after nine months of field aging in the Indiana climate, the surface modulus increased by approximately 738 ksi for HMA and 1,462 ksi for WMA while no change was observed for the bottom modulus. The k values of the Indiana HMA and WMA post-construction cores were 2.45 and 3.08, respectively. The higher k value for the WMA specimen as compared to the HMA counterpart was possibly due to the higher AV content, as shown in Figure 98, and therefore, more atmospheric oxygen transported to the specimen that was available to react with the asphalt binders. For the Florida mixture, after nine months of field aging, the bottom modulus increased slightly by approximately 80 ksi while the surface modulus increased by 1,020 ksi. The k value of the post-construction core was 2.81. The VEC-DT test results shown in Figure 98 and Figure 99 also indicated that asphalt mixtures at the surface of pavements experienced a greater level of field aging than those at the bottom.

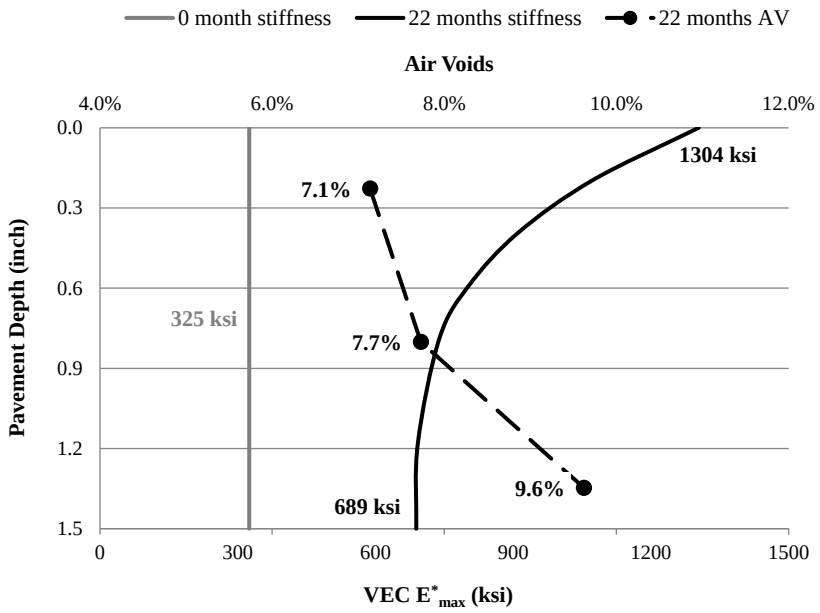

(a)

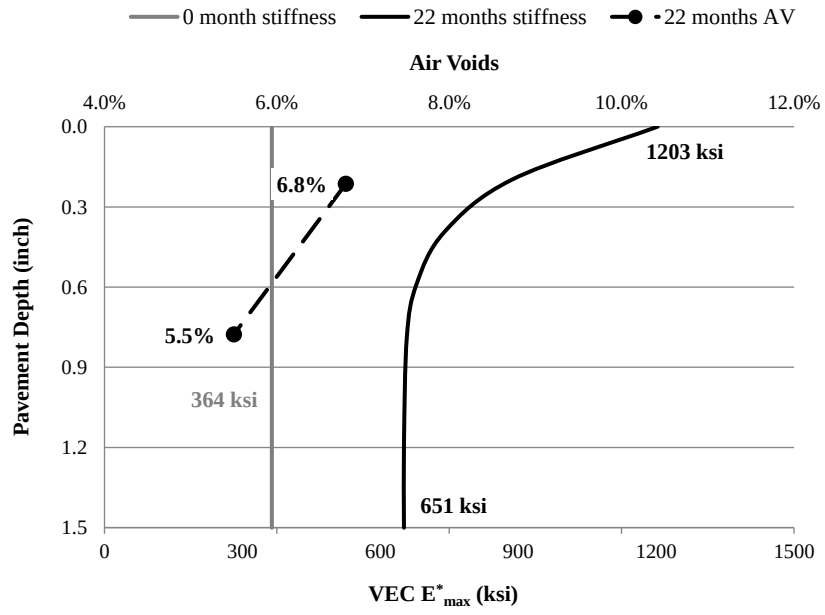

(b)

Figure 96. VEC-DT test results for Texas I field cores; (a) WMA with Evotherm, (b) WMA with Foaming.

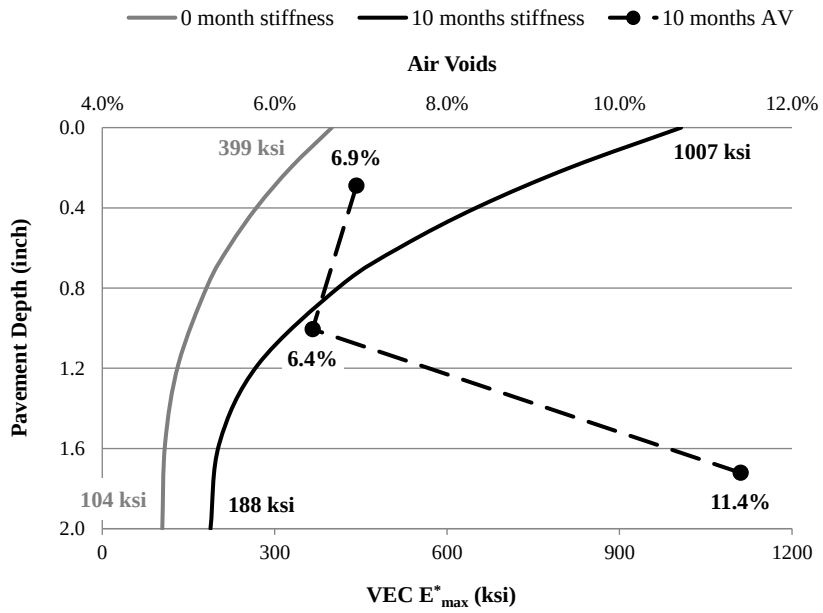

(a)

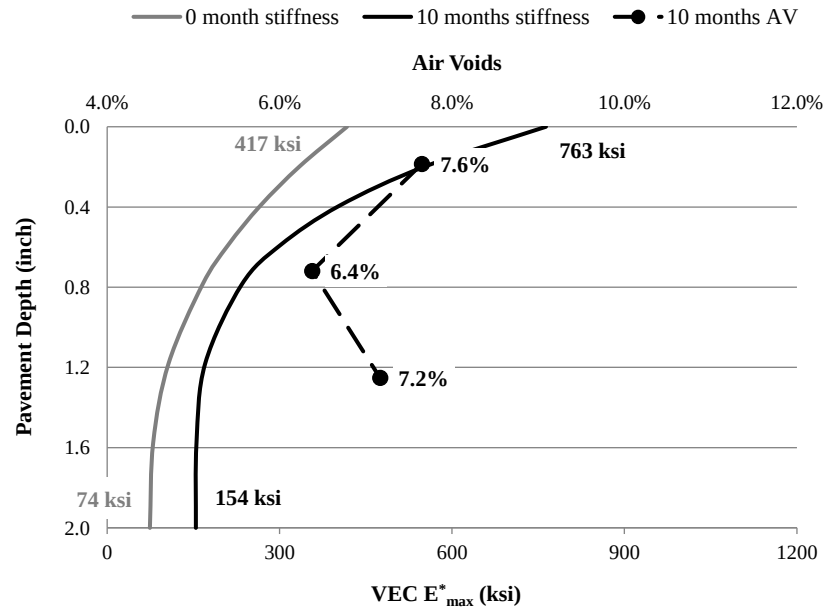

(b)

Figure 97. VEC-DT test results for Iowa field cores; (a) HMA with low absorptive aggregates, (b) WMA with low absorptive aggregates.

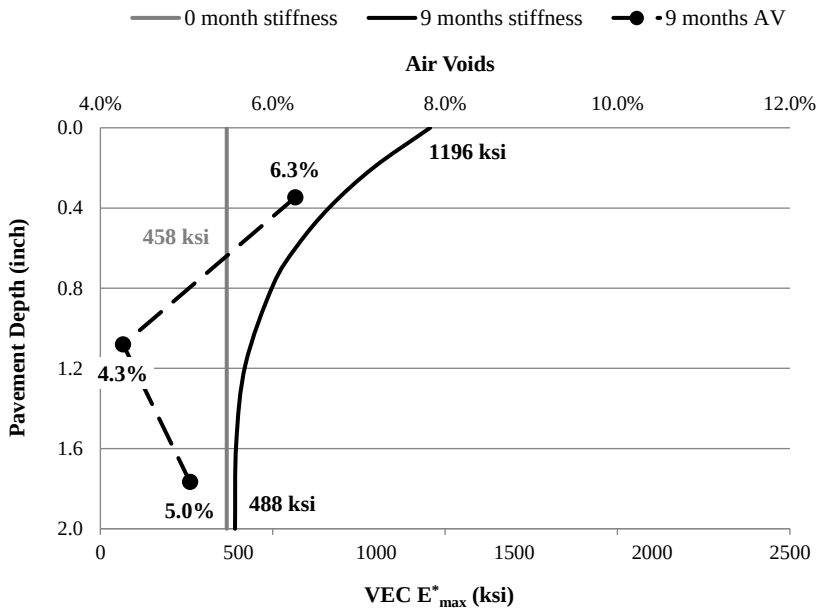

(a)

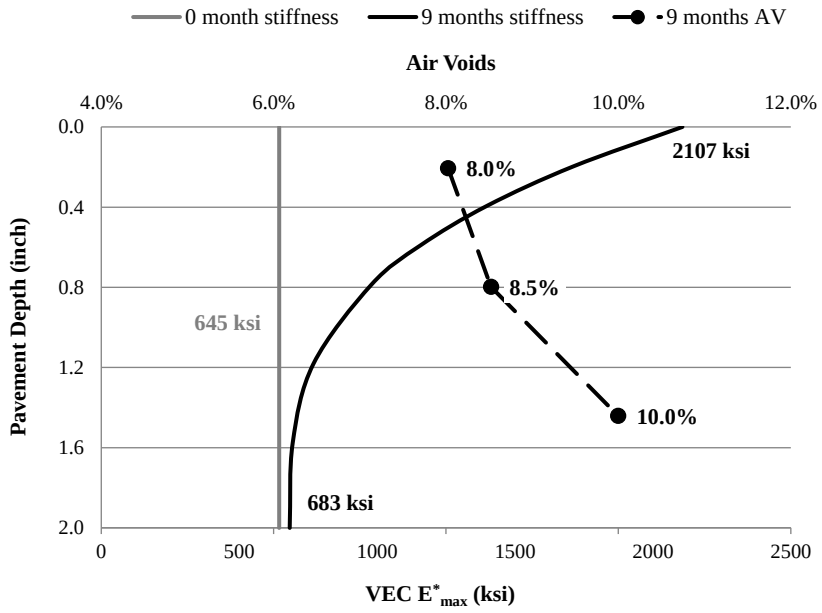

(b)

Figure 98. VEC-DT test results for Indiana field cores; (a) HMA produced at DMP, (b) WMA produced at DMP.

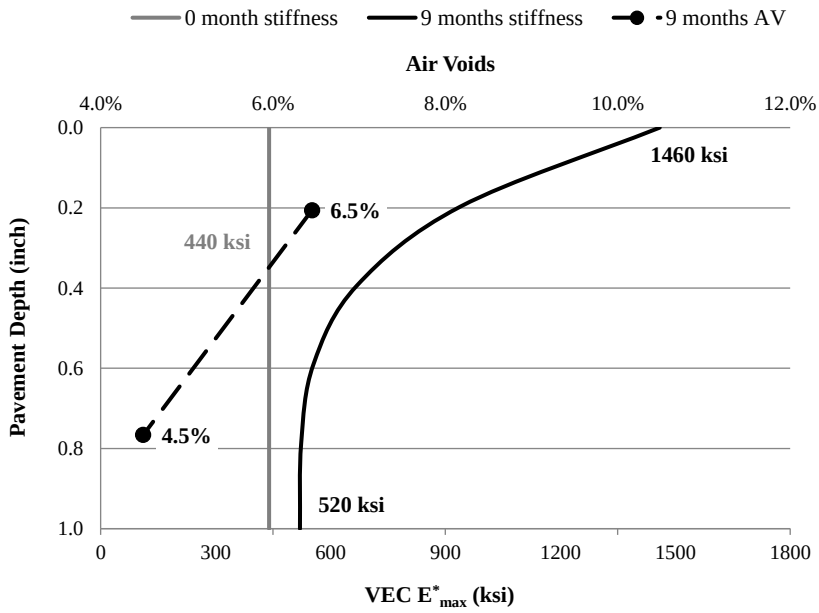

Figure 99. VEC-DT test results for Florida field cores.

Binder Property Gradient

Figure 100, Figure 101, Figure 102, and Figure 103 present the binder property profiles of the field cores obtained from the Texas I, Iowa, Indiana, and Florida field projects, respectively. The solid lines represent the DSR G-R parameter and FT-IR CA results for asphalt binders extracted and recovered from construction cores, and the dashed lines represent the results for those extracted and recovered from post-construction cores after certain in-service times in the field.

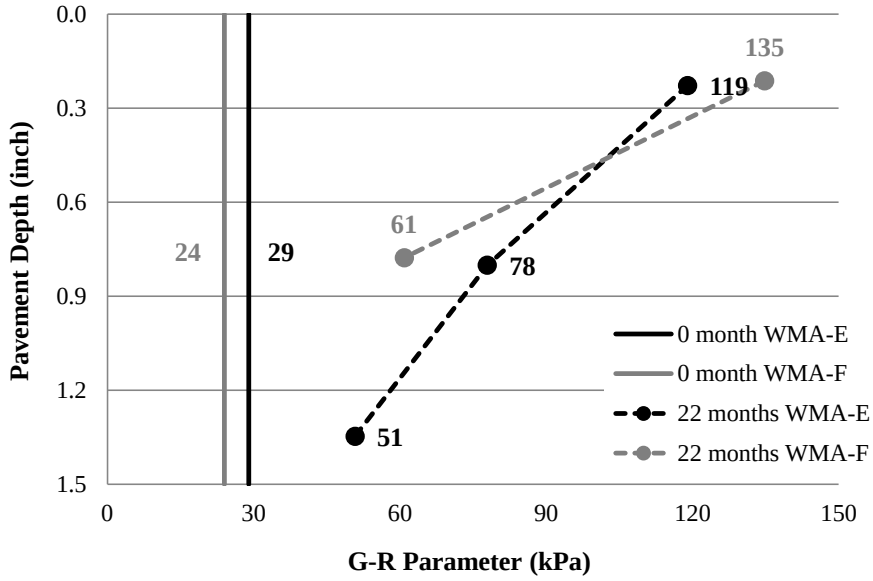

(a)

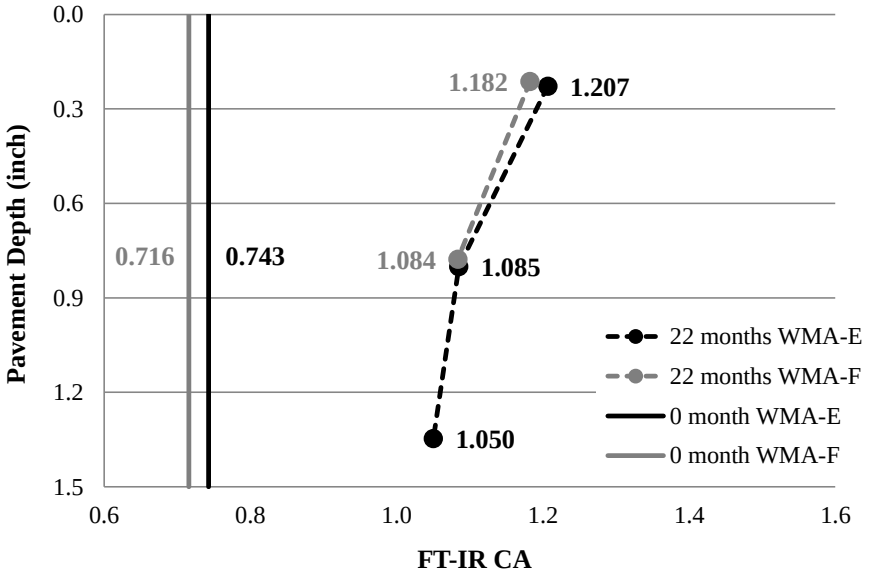

(b)

Figure 100. Binder property gradient results for Texas I field cores; (a) DSR G-R parameter, (b) FT-IR CA value.

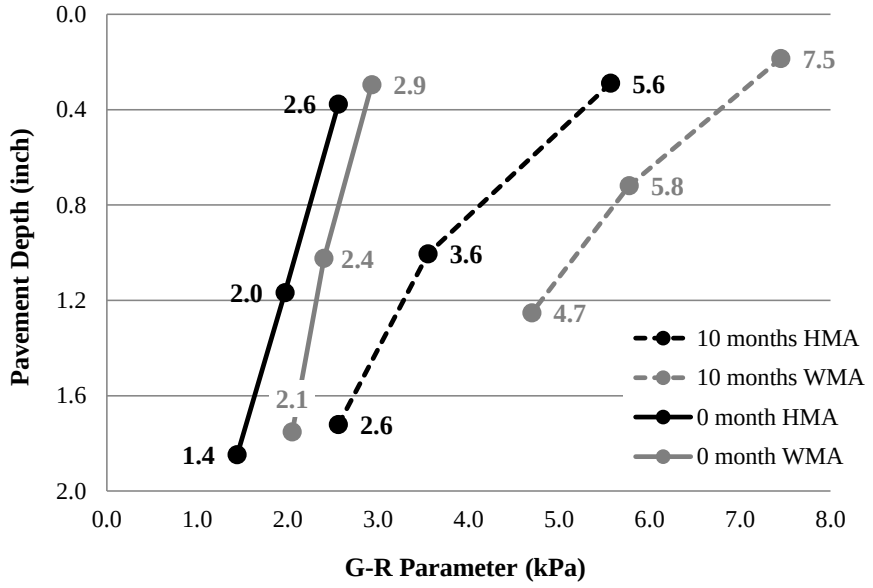

(a)

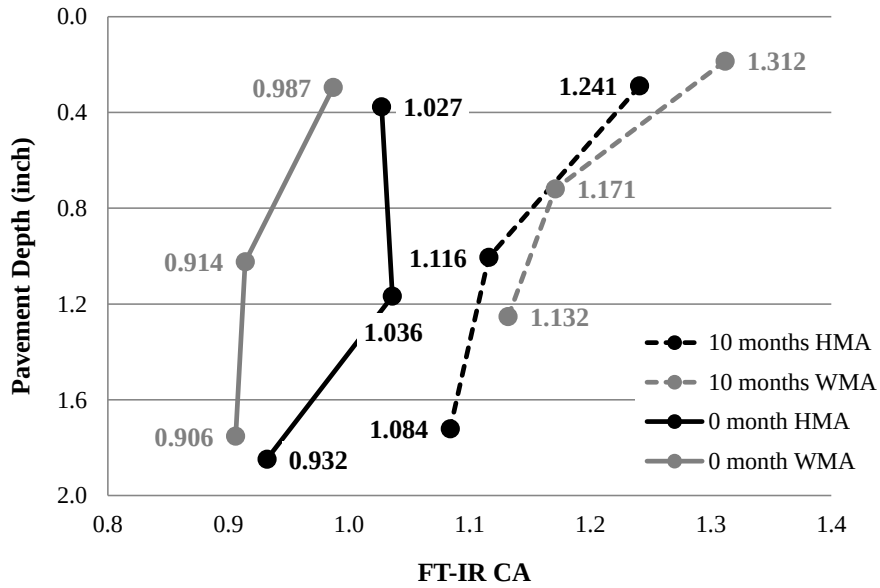

(b)

Figure 101. Binder property gradient results for Iowa field cores; (a) DSR G-R parameter, (b) FT-IR CA value.

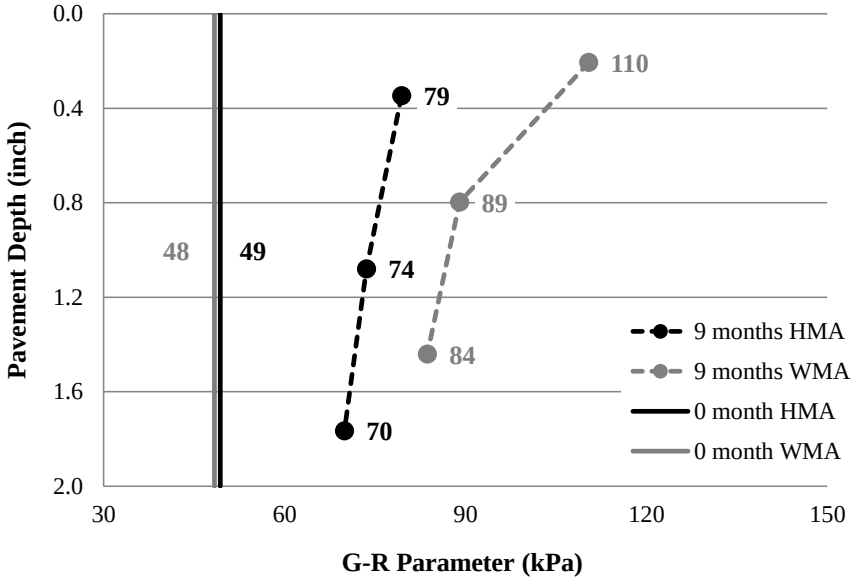

(a)

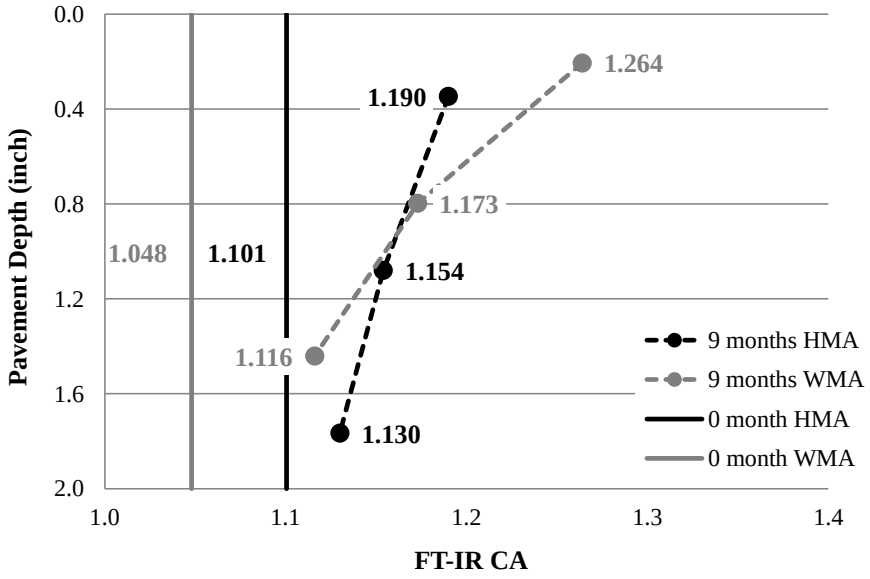

(b)

Figure 102. Binder property gradient results for Indiana field cores; (a) DSR G-R parameter, (b) FT-IR CA value.

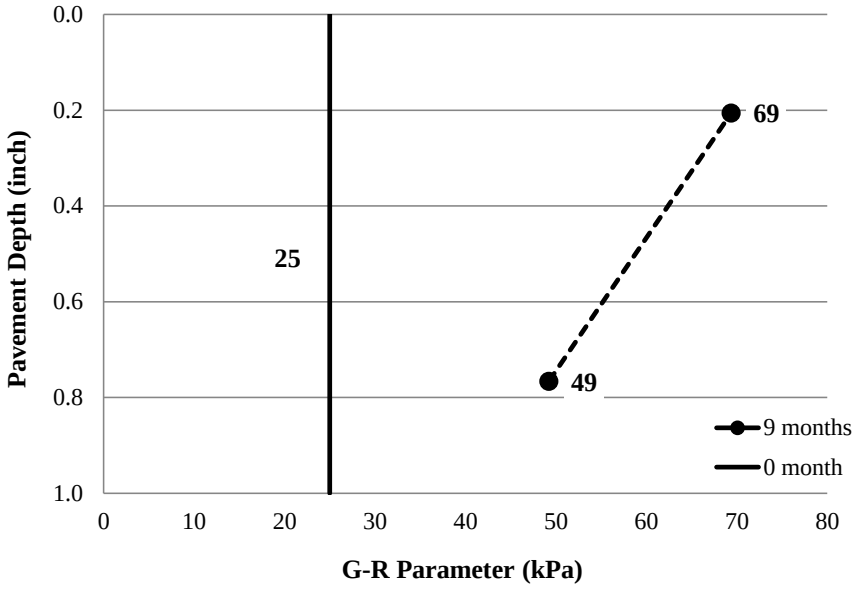

(a)

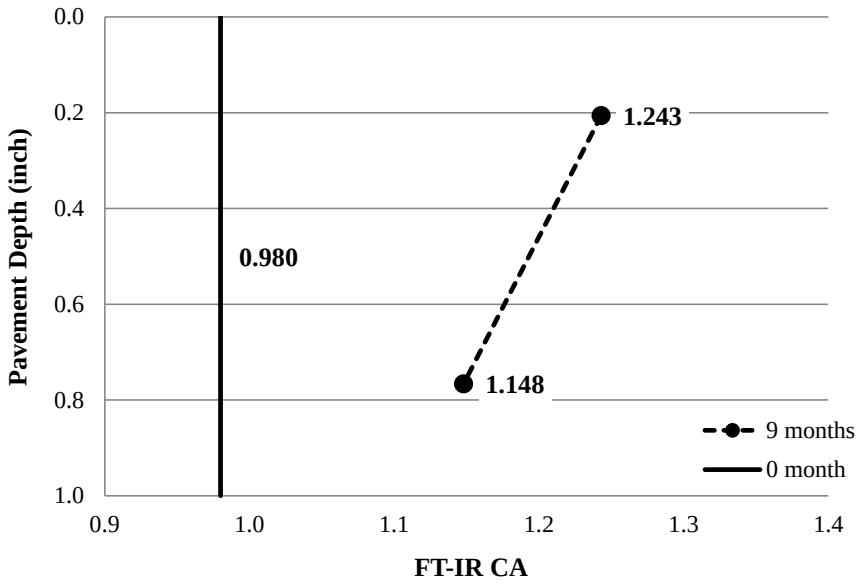

(b)

Figure 103. Binder property gradient results for Florida field cores; (a) DSR G-R parameter, (b) FT-IR CA value.

Consistent with the VEC-DT test results discussed previously, for all mixtures except those from the Iowa field project, the asphalt binder properties were consistent with pavement depth for construction cores. For the exceptional case, the asphalt binders extracted and recovered from the pavement surface exhibited higher G-R parameters and FT-IR CA values than those at the bottom. In addition, apparent binder property gradients with pavement depth were observed for all post-construction cores. Thus, the DSR and FT-IR test results for asphalt binders extracted and recovered from different pavement depths further verified the non-uniform field aging with pavement depth, and more specifically, the surface asphalt binders aged faster than those at the bottom.

Field Aging Gradient Evolution

As discussed previously in Chapter VI, the CDD and mixture property concepts were used in this study as a novel metric to quantify field aging and evaluate its effect on asphalt mixture properties. In order to explore the evolution of field aging gradient with time, two asphalt binder property ratios – DSR G-R ratio and FT-IR CA ratio – were proposed. Considering the influence on mixture stiffness from the non-uniform AV distribution within the field cores, the mixture stiffness gradient results obtained from the VEC-DT test were not evaluated.

As expressed in Equation 67 and Equation 68, the DSR G-R ratio and FT-IR CA ratio are defined as the fractions of the fitted DSR G-R parameters and FT-IR CA values by the power function expressed in Equation 38 of asphalt binders extracted and recovered from post-construction cores at a certain pavement depth over those of construction cores at the same depth. The two parameters characterize the changes in the

rheological and chemical properties, respectively of asphalt binders after the non-uniform field aging with pavement depth. Asphalt binders with higher DSR G-R ratios and FT-IR CA ratios are expected to experience a greater level of field aging than those with lower ratios. Figure 104 and Figure 105 present the evolution of DSR G-R ratio and FT-IR CA ratio with aging for field cores obtained from the Texas I, Iowa, Indiana, and Florida field projects, respectively.

$$DSR\ G-R\ Ratio = G-R_{CDD,Z}/G-R_{CDD=0,Z} \quad \text{Equation 67}$$

where:

$G\text{-}R_{CDD,Z}$ = DSR G-R parameter of asphalt binders extracted and recovered from post-construction cores at a given CDD value and pavement depth, Z (kPa); and

$G\text{-}R_{CDD=0,Z}$ = DSR G-R parameter of asphalt binders extracted and recovered from construction cores at pavement depth, Z (kPa).

$$FT-IR\ CA\ Ratio = CA_{CDD,Z}/CA_{CDD=0,Z} \quad \text{Equation 68}$$

where:

$CA_{CDD,Z}$ = FT-IR CA value of asphalt binders extracted and recovered from post-construction cores at a given CDD value and pavement depth, Z; and

$CA_{CDD=0,Z}$ = FT-IR CA value of asphalt binders extracted and recovered from construction cores at pavement depth, Z.

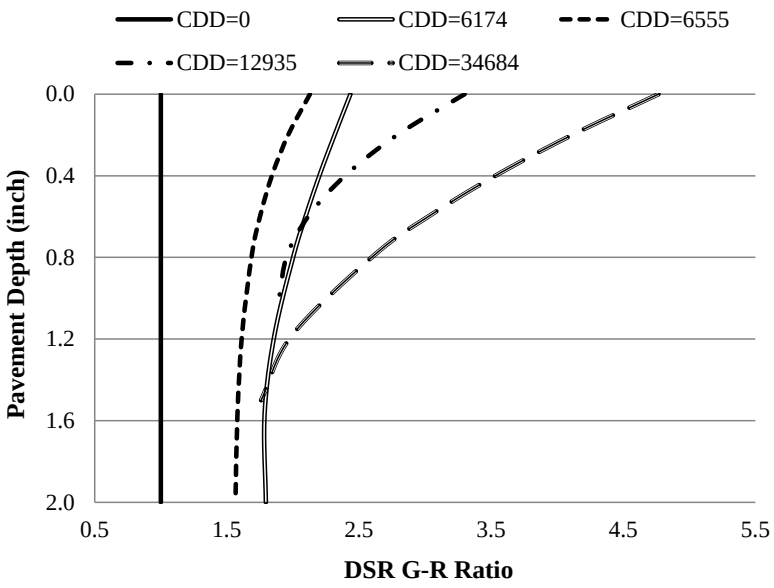

Figure 104. Evolution of DSR G-R ratio with field aging.

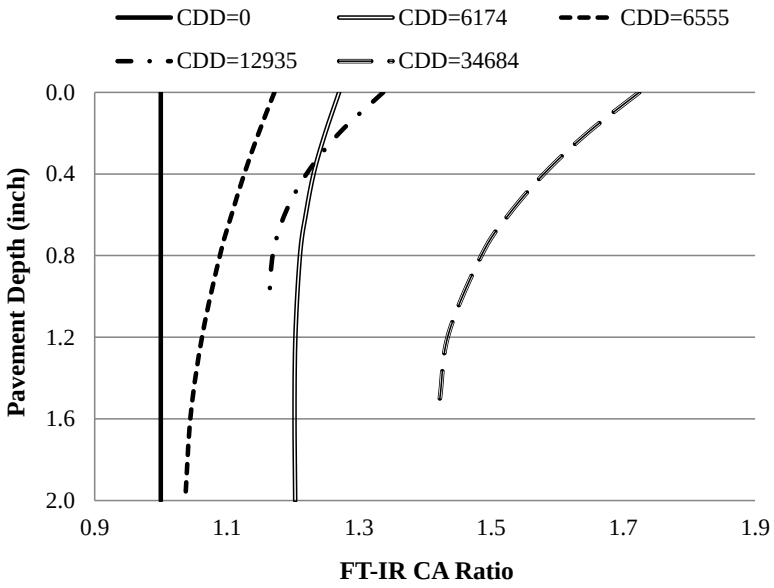

Figure 105. Evolution of FT-IR CA ratio with field aging.

As illustrated in Figure 104 and Figure 105, for most cases except “CDD=6174” (Iowa field project), the DSR G-R ratio and FT-IR CA ratio increased with CDD values, which indicated that asphalt binders had greater oxidation and reduced cracking resistance after field aging. Non-uniform field aging gradients with pavement depth were observed for all post-construction cores. Additionally, the difference between the pavement surface and bottom, as indicated by the shape of the curves in Figure 104 and Figure 105, also increased with CDD values. Thus, a significant level of non-uniform field aging was observed in the top two-inches of the pavements, and the difference in asphalt binder and mixture properties between the surface and bottom increased with the pavement in-service time and temperature.

CHAPTER VIII

CONCLUSIONS AND FUTURE RESEARCH

Economic, environmental, and engineering benefits have motivated the widespread implementation of WMA in the United States during the past decade. While WMA technologies have been successfully used as a paving material, concerns remain about the potentially increased susceptibility to rutting and moisture damage for WMA mixtures due to lower production temperatures and the use of water in the mechanical foaming process. Along with the advent of WMA, recent changes in asphalt mixture components and production parameters, including increased use of polymer modifiers, incorporation of recycled materials, and drum mix plants replacing batch mix plants, have raised the need to review the current design practices and evaluation methods for asphalt mixtures, including the effects of aging. Therefore, the main objectives of this study were to evaluate the aging characteristics of asphalt mixtures and to explore asphalt foaming technology for WMA applications.

A laboratory experiment was first performed to evaluate the performance evolution for WMA versus HMA with aging. The mixture stiffness of WMA at various aging stages obtained from two field projects was characterized to determine the critical time in the field and laboratory required for the stiffness of WMA and HMA to converge. In addition, the moisture susceptibility of WMA was compared to the HMA counterpart for each laboratory and field aging stage.

The HWTT was used in this laboratory experiment to characterize the moisture susceptibility of WMA and HMA, and several shortcomings were encountered for the traditional analysis methodology specified in AASHTO T 324. Therefore, a novel methodology was introduced to analyze the HWTT results, which avoided the bias introduced from subjective data interpolation and arbitrary selection of the test ending point. Three new parameters (LC_{SN}, LC_{ST}, and $\Delta\varepsilon^{vp}$) were proposed to quantify mixture moisture susceptibility and rutting resistance. LC_{SN} represents the maximum number of load cycles that the asphalt mixture can resist in the HWTT before stripping occurs. LC_{ST} represents the allowable additional load cycles to a common failure point that the asphalt mixture can resist after stripping occurs. Asphalt mixtures with higher LC_{SN} and LC_{ST} values are expected to have better moisture resistance than those with lower LC_{SN} and LC_{ST} values. The other parameter $\Delta\varepsilon^{vp}$ refers to the viscoplastic strain increment at a certain number of load cycles, and lower $\Delta\varepsilon^{vp}$ values are associated with better rutting resistance. The novel methodology was used as a tool throughout this study to characterize the performance of asphalt mixtures with distinct aging and foaming properties.

Next, asphalt foaming technology was explored via a comprehensive laboratory study. A non-contact test method consisting of a laser device and a digital camera was developed to measure the dynamic asphalt foaming process in terms of volume expansion and collapse and the evolution of asphalt foam bubbles. In addition, novel test methods were developed for evaluating the workability and coatability of foamed asphalt mixtures based on the SGC compaction data and the water absorption method,

respectively. The proposed test methods were then utilized to identify the effects of foaming water content and laboratory foamer type on asphalt foaming characteristics and foamed mixture properties. Finally, a mix design procedure for foamed asphalt mixtures was proposed and validated with field and laboratory data.

The aging properties of asphalt mixtures were also evaluated. Laboratory aging protocols were developed and (or) validated to simulate the asphalt aging and absorption by the aggregate that occurs during plant production and construction in the short-term and over the long-term through the initial period of performance. The impacts of various mixture components and production parameters were investigated, and those with significant effects on the aging characteristics of asphalt mixtures were identified. Finally, field cores with different in-service times obtained from several field projects were assessed using the VEC-DT, DSR, and FT-IR tests to characterize non-uniform field aging of asphalt pavements with depth.

The following sections provide the key findings, detailed conclusions, and recommendations for future research based on the results of this study.

Aging Properties

Figure 106 presents a diagram summarizing the key findings of this study in characterizing the aging properties of asphalt mixtures. Detailed conclusions are discussed as follows:

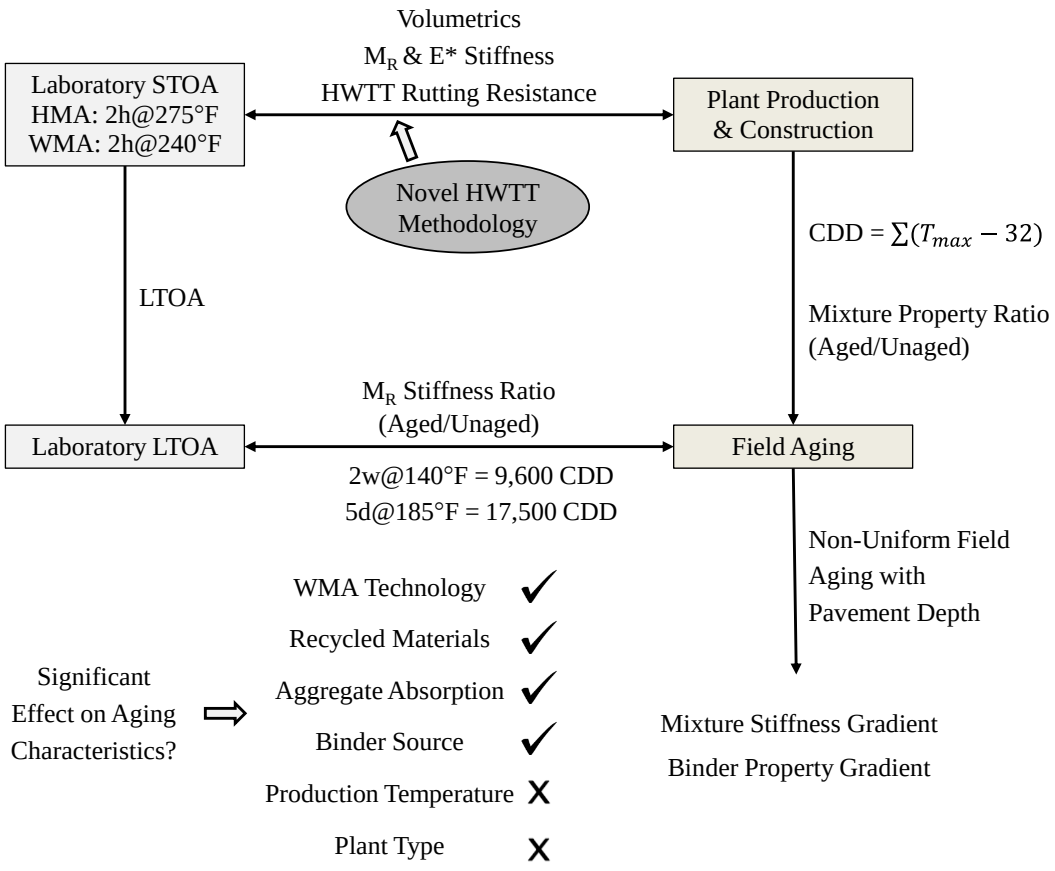

Figure 106. Summary of the aging properties for asphalt mixtures.

- The correlation between laboratory produced mixes and plant produced mixes in mixture volumetrics in terms of G_{mm}, P_{ba}, FT_{be} values indicated that laboratory STOA protocols of two hours at 275°F (135°C) for HMA and two hours at 240°F (116°C) for WMA for fabricating LMLC specimens were able to a large extent to simulate the asphalt absorption that took place during production at the plant.
- The correlations between LMLC specimens versus PMPC specimens and cores at construction in terms of M_R stiffness and E* stiffness for a wide range of

asphalt mixtures indicated that the laboratory STOA protocols for LMLC specimens were able to simulate the short-term aging during plant production and construction. The correlation between LMLC specimens and PMPC specimens for the HWTT rutting resistance parameters of ε_{SN}^{vp} values and rut depth at 5,000 load cycles also provided evidence that the laboratory STOA protocols produced representative specimens for performance testing. HWTT results for cores at construction did not correlate with those for LMLC specimens, possibly due to testing difficulties of thin lifts that required the use of plaster to fit into the HWTT molds.

- Field aging produced a significant effect in increasing stiffness and improving rutting resistance and moisture susceptibility for asphalt mixtures. The concept of CDD, proposed as a novel metric to quantify field aging, was able to account for the differences in construction dates and climates for various field projects. Asphalt pavements with higher CDD values were expected to experience a greater level of field aging due to the accumulation of elevated in-service temperatures.
- Mixture property ratios (i.e., M_R ratio and HWTT RRP ratio), defined as the fraction of mixture properties of short-term aged specimens over those of long-term aged specimens, were used to quantify the evolution of mixture stiffness and rutting resistance with field aging. An exponential function was proposed to correlate the mixture property ratios of post-construction cores versus their corresponding CDD values, and a desirable correlation was produced.

- Correlations between field aging and laboratory LTOA protocols were explored based on the mixture property ratio results for long-term aged field cores and laboratory specimens. Laboratory LTOA protocols of two weeks at 140°F (60°C) and five days at 185°F (85°C) were representative of field aging at approximately 9,600 and 17,500 CDD , respectively. Field aging at 9,600 CDD was equivalent to approximately seven months in-service in warmer climates and 12 months in-service in colder climates. As for the field aging at 17,500 CDD, approximately 12 months and 23 months in-service were required for warmer climates and colder climates, respectively.
- Laboratory test results indicated a significant effect of WMA technology on the aging characteristics of asphalt mixtures. Lower stiffness and decreased rutting resistance were observed for the short-term aged WMA mixtures as compared to their HMA counterparts, possibly due to the reduced production temperature. With field aging, mixture stiffness evolution for WMA versus HMA was classified into three different scenarios:
    - Scenario I: the stiffness of HMA cores was always higher than WMA, but the difference in stiffness between these two mixtures reduced with field aging.
    - Scenario II: HMA had higher mixture stiffness compared to WMA at the initial aging stage (i.e., cores at construction), but the WMA stiffness eventually equaled that of HMA after certain period of field aging.

- Scenario III: equivalent mixture stiffness was shown for cores at construction between HMA and WMA, but higher stiffness for post-construction cores was observed for WMA versus HMA.

For the majority of the field projects, the M_R stiffness evolution with field aging followed Scenario II. The critical in-service time when WMA equaled HMA was achieved at 23,000 CDD, which was equivalent to approximately 17 months in-service in warmer climates and 29 months in-service in colder climates. Field aging at approximately 3,000 CDD was necessary for the stiffness of WMA to equal the initial stiffness of HMA, which was equivalent to approximately two months for warmer climates and three months for colder climates.

- The inclusion of recycled materials had a significant effect on the aging characteristics of asphalt mixtures. Those with recycled materials, and often times using softer asphalt binders, had higher initial stiffness but showed a slower rate of stiffness increase with aging than the control mixtures. The greater sensitivity to aging by the control mixtures was attributed to the larger amount of virgin binders in the mixtures, which had higher oxygen diffusivity and were more susceptible to aging than the recycled binders.
- Aggregate absorption, specifically the effective binder content in the mixture, had a significant effect on the aging characteristics of asphalt mixtures. The short-term aged mixtures using high absorptive aggregates exhibited lower stiffness and decreased rutting resistance than the counterpart mixtures using low absorptive aggregates, which was attributed to the thicker effective film thickness

from volumetric compensation during the mix design process. However, the difference in mixture properties between the two mixtures reduced with field aging, due to the higher volume of effective binders in the high absorptive mixtures that was available for aging.

- Binder source had a significant effect on the short-term aging characteristics of asphalt mixtures, while its effect on the long-term aging characteristics was not studied. Different mixture performance in terms of stiffness and rutting resistance should be expected from asphalt mixtures using the same PG graded binders from different sources.
- Production temperature and plant type had no significant effect on the aging characteristics of asphalt mixtures.
- Mixture stiffness gradient and binder property gradient with pavement depth was observed for post-construction cores obtained from several field projects at various in-service times. According to the VEC-DT, DSR, and FT-IR test results, asphalt binders and mixtures at the pavement surface had higher $|E^*|_{max}$, G-R parameter, and CA values than those at the bottom, and the difference tended to increase with time. Therefore, the field aging of asphalt mixtures was not uniformly distributed with depth in the pavement structure, and more specifically, the surface of the pavement aged faster than the bottom due to the direct exposure to oxygen and solar radiation and the accumulation of elevated in-service temperatures.

Foaming Properties

Figure 107 presents a diagram summarizing the key findings of this study in characterizing the foaming properties of asphalt mixtures. Detailed conclusions are discussed as follows:

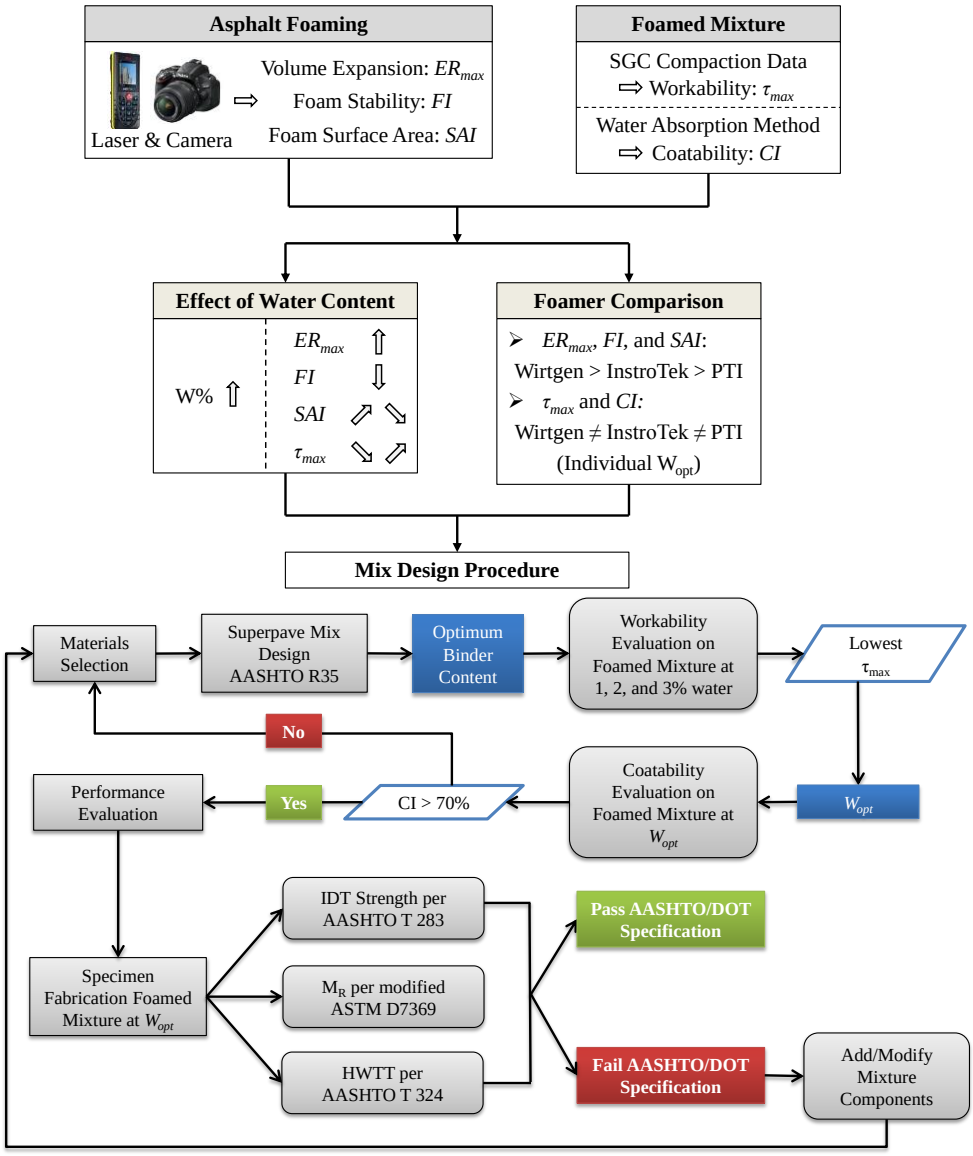

Figure 107. Summary of the foaming properties for asphalt mixtures.

- A non-contact test method consisting of a laser device and a digital camera was developed to measure the entire dynamic asphalt foaming process, and two parameters (*FI* and *SAI*) values were proposed accordingly. Compared with the traditional parameters ER_{max} and *HL*, *FI* and *SAI* values were able to characterize the asphalt volume expansion and collapse and the surface area evolution of foam bubbles over time. Foamed asphalts with higher *FI* and *SAI* values were expected to have higher volume expansion and better foam stability, and were more likely to contribute to better coating of aggregate particles during mixing.
- A test method based on the SGC compaction data was proposed for evaluating the workability of foamed asphalt mixtures. Densification of asphalt mixtures during the compaction process was considered as a function of reorientation of aggregate particles and distortion due to the flow of the asphalt binder. Thus, the shear resistance within the mixture was provided by the internal friction from the aggregates and the cohesion provided by the asphalt binder. The τ_{max} value measured during the compaction process was proposed as the workability parameter; foamed mixtures with lower τ_{max} values were considered more workable.
- A modified procedure based on the aggregate absorption method was developed for evaluating the coatability of foamed asphalt mixtures. The method was based on the assumption that a completely coated aggregate submerged in water for a short period could not absorb water since water was not able to penetrate through the asphalt film surrounding the aggregate surface. Conversely, a partially coated

aggregate was expected to have detectable water absorption since water could penetrate and be absorbed by the uncoated particle. The *CI* value was proposed as the coatability parameter; foamed mixtures with higher *CI* values were expected to have better aggregate coatability.

- Foaming water content illustrated a significant effect on asphalt foaming characteristics. Higher water contents produced foamed asphalts with higher volume expansion but less foam stability due to a faster foam collapse rate. A complex relationship was observed for the foaming water content and the surface area evolution of foamed bubbles due to the competing mechanisms between the quantity and size of foam bubbles and the foam collapse rate. In addition, a significant difference in workability and coatability was shown for foamed mixtures produced at various foaming water contents. For most cases, there was a W_{opt} value that yielded the best workability and coatability characteristics.
- Laboratory foamer type had a significant effect on asphalt foaming characteristics and foamed mixture properties. Foamed asphalts produced by the Wirtgen foamer had the greatest volume expansion and the best foam stability, followed by those produced by the InstroTek foamer and then the PTI foamer. Compared with the InstroTek foamer, the Wirtgen foamer produced more semi-stable foam bubbles, smaller in size but with larger surface area. As for the PTI foamer, only a limited amount of foam bubbles were observed during the foaming process. The difference observed in asphalt foaming characteristics for three laboratory foamers was likely due to the various conditions (i.e., pressure

and flow rate) at which asphalt foaming was produced. Although a considerable difference in workability and coatability characteristics was also observed for foamed asphalt mixtures produced by the three laboratory foamers, those produced at the W_{opt} exhibited better workability and coatability characteristics than for conventional HMA.

- A mix design procedure for foamed asphalt mixtures was developed that included consideration of asphalt foaming ability, optimization of foaming water content, and evaluation of mixture properties. The procedure was also validated with two field studies. Since adequate laboratory and field performance was achieved by the foamed mixtures, the proposed mix design procedure can be considered for implementation.

Future Research

The following suggestions for future research are made based on the results of this study. Topics related to the aging properties of asphalt mixtures are discussed first, followed by suggestions for the foaming properties of asphalt mixtures and then the improvements to HWTT test procedure.

Aging Properties

- While this study focused on the aging and foaming characteristics of asphalt mixtures over a wide range of factors; only mixture stiffness, rutting resistance, and moisture susceptibility were evaluated. Future research into the evaluation of additional mixture properties such as fatigue cracking and thermal cracking is necessary.

- There is a need for future research to continuously monitor the field aging behavior of the asphalt mixtures included in this study. It is recommended that additional sets of field cores be obtained and tested in order to validate the mixture property evolution model and to further evaluate the field aging gradient evolution in the pavement structure.
- The concept of CDD was proposed in this study to quantify field aging, and it demonstrated substantial advantages over the commonly used parameter of pavement in-service time. Additional field aging parameters including solar radiation, pavement in-service temperature, or their combination should be investigated in future research.
- Based on the limited amount of laboratory test results measured for Indiana and Florida asphalt mixtures, laboratory LTOA protocols of three days at 185°F (85°C) and two weeks at 140°F (60°C) produced an equivalent level of mixture aging. This three-day LTOA protocol might be more practical for simulating field aging in colder climates. Therefore, there is a need to further explore the LTOA protocol of three days at 185°F (85°C) with additional mixture results.

Foaming Properties

- This study evaluated the effects of foaming water content and laboratory foamer type on asphalt foaming characteristics and foamed mixture properties. For future research, it is recommended to explore additional factors, such as foaming production temperature, the presence of polymer in polymer modified binders, and foaming and anti-foaming additives.

- A mix design procedure for foamed asphalt mixtures was developed and validated in this study. Before being considered for widespread implementation, the procedure should be used on a trial basis; and the results obtained will provide increased confidence. In addition, continued field performance monitoring of the two field projects used to validate the proposed mix design procedure is suggested for future research.

Improvement to the HWTT Test

- The HWTT test was performed at 122°F (50°C) per Texas Department of Transportation specification Tex-242-F, which caused asphalt mixtures with a low high-temperature PG grade of asphalt binders to exhibit early stripping and to exceed the rut depth requirements. As a consequence, the rut depth measurements were possibly biased from the stripping of asphalt binders from the aggregates. Therefore, there is a need to establish a specification for selecting HWTT test temperature based on the prescribed virgin binder high-temperature PG grade according to the projected climate and traffic information.
- A high variability in HWTT rut depth measurements was observed when testing field cores, which was most likely due to the plaster substrate used to provide the needed height of the core specimen to fit the mold for testing. The plaster tended to weaken and disintegrate during testing due to the elevated temperature of the water bath. Therefore, improvements to the HWTT test procedure should be explored in the future to accommodate thin field cores. One potential approach is

to use molds of various heights to adjust the HWTT wheels to the desired testing height.

REFERENCES

Abatech Inc. 2011. RHEA, Blooming Glen, Pennsylvania.

Abel, F. (1978). *Foamed Asphalt Base Stabilization*, State of Colorado, Division of Highways.

Al-Qadi, I., Kern, J., Baek, J., and Doyen, M. "Short-Term Characterization and Performance of Warm Mix Asphalt." *Proc., 51st Annual Illinois Bituminous Paving Conference*.

Anderson, R. M., King, G. N., Hanson, D. I., and Blankenship, P. B. (2011). "Evaluation of the Relationship between Asphalt Binder Properties and Non-Load Related Cracking." *Journal of the Association of Asphalt Paving Technologists*, 80, 615-664.

Aschenbrener, T., and Currier, G. (1993). "Influence of Testing Variables on the Results from the Hamburg Wheel-Tracking Device." Colorado Department of Transportation, Denver, Colorado.

Aschenbrener, T., and Far, N. (1994). "Short-Term Aging of Hot Mix Asphalt." *CDOT-DTD-R-94-11*, Colorado Department of Transportation.

Asphalt Institue (1984). *Mix Design Methods for Asphalt Concrete and Other Hot-Mix Types*, Lexington, Kentucky.

Asphalt Institute (1995). *Mix Design (SP-2)*, Lexington, Kentucky.

Asphalt Institute (2001). *Superpave Mix Design*, Lexington, Kentucky.

Azari, H. (2010). *Precision Estimates of AASHTO T283: Resistance of Compacted Hot Mix Asphalt (HMA) to Moisture-Induced Damage*, National Cooperative Highway Research Program, Transportation Research Board of the National Academies.

Azari, H., and Mohseni, A. (2013). "Effect of short-term conditioning and long-term ageing on permanent deformation characteristics of asphalt mixtures." *Road Materials and Pavement Design*, 14(sup2), 79-91.

Bell, C. A., Wieder, A. J., and Fellin, M. J. (1994). *Laboratory Aging of Asphalt-Aggregate Mixtures: Field Validation*, Strategic Highway Research Program, National Academy of Sciences, Washington, D.C.

Bonaquist, R. F. (2011). *Mix Design Practices for Warm Mix Asphalt*, Transportation Research Board, Washington, D.C.

Brennen, M., Tia, M., Altschaeffl, A., and Wood, L. (1983). "Laboratory Investigation of the Use of Foamed Asphalt for Recycled Bituminous Pavements." *Transportation Research Record*(911).

Brown, S., and Scholz, T. "Development of Laboratory Protocols for the Ageing of Asphalt Mixtures." *Proc., Eurasphalt and Eurobitume Congress*.

Chipperfield, E. H., and Welch, T. R. (1967). "Studies on the Relationships between the Properties of Road Bitumens and Their Service Performance." *Journal of the Association of Asphalt Paving Technologists*, 36, 421-488.

Chollar, B. H., Zenewitz, J. A., Boone, J. G., Tran, K. T., and Anderson, D. T. (1989). "Changes Occurring in Asphalts in Drum Dryer and Batch (Pugmill) Mixing

Operations." *Transportation Research Record: Journal of the Transportation Research Board*(1228), 145-155.

Clements, T. M., Blankenship, P. B., and Mahboub, K. C. (2012). "The Effect of Loose Mix Aging on the Performance of Warm Asphalts." *Journal of the Association of Asphalt Paving Technologists*, 81, 541-565.

Daniel, J. S., Bennert, T., Kim, Y. R., and Mogawer, W. (2014). "TPF 5(230): Evaluation of Plant Produced RAP Mixtures in the Northeast." Federal Highway Administration, Washington, D.C.

DeSombre, R., Newcomb, D. E., Chadbourn, B., and Voller, V. (1998). "Parameters to Define the Laboratory Compaction Temperature Range of Hot-Mix Asphalt." *Journal of the Association of Asphalt Paving Technologists*, 67, 125-152.

Diefenderfer, S., and Hearon, A. (2008). "Laboratory Evaluation of a Warm Asphalt Technology for Use in Virginia." Virginia Transportation Research Council Charlottesville, Virginia.

Epps Martin, A., Arambula, E., Yin, F., Garcia Cucalon, L., Chowdhury, A., Lytton, R., Epps, J., Estakhri, C., and Park, E. S. (2014). *Evaluation of the Moisture Susceptibility of WMA Technologies*, Transportation Research Board, Washington, D.C.

Estakhri, C., Button, J., and Alvarez, A. E. (2010). "Field and Laboratory Investigation of Warm Mix Asphalt in Texas." Texas A&M Transportation Institute, Austin, Texas.

Estakhri, C., Cao, R., Alvarez, A., and Button, J. W. (2009). "Production, Placement, and Performance Evaluation of Warm Mix Asphalt in Texas." *ASCE Geotechnical Special Publication: Material, Design, Construction, Maintenance, and Testing of Pavement*(193), 1-8.

Estakhri, C. K. (2012). "Laboratory and Field Performance Measurements to Support the Implementation of Warm Mix Asphalt in Texas." Texas Transportation Institute, Austin, Texas.

Farrar, M., Turner, T., Planche, J.-P., Schabron, J., and Harnsberger, P. (2013). "Evolution of the Crossover Modulus with Oxidative Aging: Method to Estimate Change in Viscoelastic Properties of Asphalt Binder with Time and Depth on the Road." *Transportation Research Record: Journal of the Transportation Research Board*(2370), 76-83.

Findley, W. N., Lai, J. S., and Onaran, K. (1976). *Creep and Relaxation of Nonlinear Viscoelastic Materials* Dover Publications.

Fu, P. (2011). "Foamed Asphalt 101." <http://foam101.info/Basics/FoamedAsphalt.html>.

Glover, C. J., Davison, R. R., Domke, C. H., Ruan, Y., Juristyarini, P., Knorr, D. B., and Jung, S. H. (2005). "Development of a New Method for Assessing Asphalt Binder Durability with Field Validation." Texas Transportation Institute, Austin, Texas.

Glover, C. J., Han, R., Jin, X., Prapaitrakul, N., Cui, Y., Rose, A., Lawrence, J. J., Padigala, M., Arambula, E., and Park, E. S. (2014). "Evaluation of Binder Aging

and its Influence in Aging of Hot Mix Asphalt Concrete: Technical Report." Texas Transportation Institute, Austin, Texas.

Hajj, E., Chia, C., Sebaaly, P., Kasozi, A. M., and Gibson, S. "Properties of Foamed Warm-Mix Asphalt Incorporating Recycled Asphalt Pavement from Two Field Projects—Case Studies." *Proc., 2nd International Conference on Warm Mix Asphalt Conference*.

He, G.-p., and Wong, W.-g. (2006). "Decay Properties of the Foamed Bitumens." *Construction and building materials*, 20(10), 866-877.

Heithaus, J., and Johnson, R. "A Microviscometer Study of Road Asphalt Hardening in the Field and Laboratory." *Proc., Proceedings, Association of Asphalt Paving Technologists*, 17-34.

Houston, W. N., Mirza, M. W., Zapata, C. E., and Raghavendra, S. (2007). *Simulating the Effects of Hot Mix Asphalt Aging for Performance Testing and Pavement Structural Design*, Transportation Research Board.

Jemison, H., Burr, B., Davison, R., Bullin, J., and Glover, C. (1992). "Application and use of the ATR, FT-IR method to asphalt aging studies." *Fuel science & technology international*, 10(4-6), 795-808.

Jenkins, K. J. (2000). "Mix Design Considerations for Cold and Half-Warm Bituminous Mixes with Emphasis of Foamed Bitumen." Stellenbosch: Stellenbosch University, South Africa.

Jia, X., Huang, B., Bowers, B. F., and Zhao, S. (2014). "Infrared Spectra and Rheological Properties of Asphalt Cement Containing Waste Engine Oil Residues." *Construction and Building Materials*, 50, 683-691.

Jones, D., Wu, R., Tsai, B.-W., Barros, C., and Peterson, J. "Key Results from a Comprehensive Accelerated Loading, Laboratory, and Field Testing Study on Warm-Mix Asphalt In California." *Proc., Proceedings 2nd International Conference on Warm-Mix Asphalt*.

Kari, J. "Effect of Construction Practices on the Asphalt Properties in the Mix." *Proc., Canadian Technical Asphalt Association* 310-334.

Kekevi, B., Berber, H., and Yıldırım, H. (2012). "Synthesis and Characterization of Silicone-Based Surfactants as Anti-Foaming Agents." *Journal of Surfactants and Detergents*, 15(1), 73-81.

Kemp, G. R., and Predoehl, N. H. "A Comparison of Field and Laboratory Environments on Asphalt Durability." *Proc., Journal of the Association of Asphalt Paving Technologists*, 492-537.

Koohi, Y., Lawrence, J. J., Luo, R., and Lytton, R. L. (2011). "Complex Stiffness Gradient Estimation of Field-Aged Asphalt Concrete Layers Using the Direct Tension Test." *Journal of Materials in Civil Engineering*, 24(7), 832-841.

Kuennen, T. (2004). "Warm Mixes are a Hot Topic." *Better Roads*, 74(6).

Lund, J. W., and Wilson, J. E. (1984). "Evaluation of Asphalt Aging in Hot Mix Plants." *Journal of the Association of Asphalt Paving Technologists*, 53, 1-18.

Lund, J. W., and Wilson, J. E. (1986). "Field Validation of Asphalt Aging in Hot Mix Plants." *Journal of the Association of Asphalt Paving Technologists*, 55, 92-119.

Luo, R., and Lytton, R. L. (2009). "Characterization of the Tensile Viscoelastic Properties of an Undamaged Asphalt Mixture." *Journal of Transportation Engineering*.

Luo, X., Gu, F., and Lytton, R. (2015). "Prediction of Field Aging Gradient in Asphalt Pavements." *Transportation Research Record: Journal of the Transportation Research Board*, No. 2507.

Marateanu, M., and Anderson, D. (1996). "Time-Temperature Dependency of Asphalt Binders - An Improved Model." *Journal of the Association of Asphalt Paving Technologists*, 65, 408-448.

Michalica, P., Daucik, P., and Zanzotto, L. (2008). "Monitoring of Compositional Changes Occurring During the Oxidative Aging of Two Selected Asphalts from Different Sources." *Petroleum & Coal*, 50(2), 1-10.

Mogawer, W., Austerman, A., and Bahia, H. (2011). "Evaluating the Effect of Warm-Mix Asphalt Technologies on Moisture Characteristics of Asphalt Binders and Mixtures." *Transportation Research Record: Journal of the Transportation Research Board*(2209), 52-60.

Mogawer, W., Bennert, T., Daniel, J. S., Bonaquist, R., Austerman, A., and Booshehrian, A. (2012). "Performance Characteristics of Plant Produced High RAP Mixtures." *Road Materials and Pavement Design*, 13(sup1), 183-208.

Morian, N., Hajj, E., Glover, C., and Sebaaly, P. (2011). "Oxidative Aging of Asphalt Binders in Hot-Mix Asphalt Mixtures." *Transportation Research Record: Journal of the Transportation Research Board*(2207), 107-116.

Namutebi, M. (2011). "Some Aspects of Foamed Bitumen Technology." Royal Institute of Technology.

Newcomb, D. (2007). "Introduction to Warm-Mix Asphalt." National Asphalt Pavement Association, Lanham, Minnesota.

Newcomb, D. E., Arambula, E., Yin, F., Zhang, J., Bhasin, A., Li, W., and Arega, Z. (2015). *Properties of Foamed Asphalt for Warm Mix Asphalt Applications*, Transportation Research Board.

Rashwan, M. H., and Williams, R. C. (2011). "An Evaluation of WMA Additives and RAP on Performance Properties of Asphalt Mixtures." *91st Annual Meeting of the Transportation Research Board* Washington, D.C., USA, 12-4469.

Rolt, J. "Top-Down Cracking: Myth or Reality." *Proc., The World Bank Regional Seminar on Innovative Road Rehabilitation and Recycling Technologies*, 24-26.

Rondon, H. A., Reyes, F. A., Flintsch, G. W., and Mogrovejo, D. E. "Environmental Effects on Hot-Mix Asphalt Dynamic Mechanical Properties: Case Study in Bogota, Colombia." *Proc., Transportation Research Board 91st Annual Meeting*.

Safaei, F., Lee, J.-s., Nascimento, L. A. H. d., Hintz, C., and Kim, Y. R. (2014). "Implications of Warm-Mix Asphalt on Long-Term Oxidative Ageing and Fatigue Performance of Asphalt Binders and Mixtures." *Road Materials and Pavement Design*, 15(sup1), 45-61.

Sharp, K., and Malone, S. (2013). *Evaluation Protocol for Warm Mix Asphalt*, Austroads, Australia.

Solaimanian, M., Harvey, J., Tahmoressi, M., and Tandon, V. "Test Methods to Predict Moisture Sensitivity of Hot-Mix Asphalt Pavements." *Proc., Transportation Research Board National Seminar*, 77-110.

Tarbox, S., and Daniel, J. S. (2012). "Effects of Long Term Oven Aging on RAP Mixtures." *Transportation Research Record: Journal of the Transportation Research Board*, 1504, 1-15.

Terrel, R. L., and Holen, D. J. "Performance of Asphalt Concrete Pavement Mixtures Produced by the Drum Mixer Process." *Proc., Association of Asphalt Paving Technologists* 169-198.

Topal, A., and Sengoz, B. "Effect of SBS Polymer Modified Bitumen on the Ageing Properties of Asphalt." *Proc., 4th Eurasphalt and Eurobitume Congress*.

Traxler, R. "Relation between Asphalt Composition and Hardening by Volatilization and Oxidation." *Proc., Association of Asphalt Paving Technologists*, 359-372.

Tseng, K.-H., and Lytton, R. L. (1989). "Prediction of Permanent Deformation in Flexible Pavement Materials." *American Society for Testing and Materials*, 1016.

Velasquez, R., Cuciniello, G., Swiertz, D., Bonaquist, R., and Bahia, H. "Methods to Evaluate Aggregate Coating for Asphalt Mixtures Produced at WMA Temperatures." *Proc., 57th Annual Conference of the Canadian Technical Asphalt Association* Canadian Technical Asphalt Association, 225-238.

West, R., Rodezno, C., Julian, G., and Prowell, B. (2014). *Engineering Properties and Field Performance of Warm Mix Asphalt Technologies*, Transportation Research Board.

Williams, M. L., Landel, R. F., and Ferry, J. D. (1955). "The Temperature Dependence of Relaxation Mechanisms in Amorphous Polymers and Other Glass-Forming Liquids." *Journal of the American Chemical society*, 77(14), 3701-3707.

Wineman, A. S., and Rajagopal, K. R. (2000). *Mechanical Response of Polymers: An Introduction*, Cambridge University Press.

Xiao, F., Shivaprasad, P. V., and Amirkhanian, S. N. (2012). "Low-Volume Road WMA Mixtures: Moisture Susceptibility of Mixtures Containing Coal Ash and Roofing Shingle with Moist Aggregate." *Journal of Materials in Civil Engineering*, 24(1), 48-56.

Yin, F., Arambula, E., and Newcomb, D. (2015). "Effect of Water Content on Binder Foaming Characteristics and Foamed Mixture Properties." *Transportation Research Record: Journal of Transportation Research Board*, 2506.

Yin, F., Garcia Cucalon, L., Epps Martin, A., Arambula, E., Chowdhury, A., and Park, E. S. (2013). "Laboratory Conditioning Protocols for Warm-Mix Asphalt." *Journal of the Association of Asphalt Paving Technologists*, 82, 177-212.

Zhao, D., Lei, M., and Yao, Z. (2009). "Evaluation of Polymer-Modified Hot-Mix Asphalt: Laboratory Characterization." *Journal of Materials in Civil Engineering*, 21(4), 163-170.